The Fumarases of *Schistosoma mansoni*: A Novel Drug Target?

Adam Muslem George Burgess

2023

A thesis submitted to the Department of Life Sciences (Aberystwyth University), for the degree of Doctor of Philosophy

Acknowledgements

I would like to thank Professor Karl Hoffmann whose guidance, support, care and patience (of that he has needed plenty!) has brought this PhD to fruition and been invaluable in its completion. I would also like to thank Dr. Iain Chalmers, my secondary supervisor, who brought me into the world of schisto all those years ago when I was a budding scientist in immunology lectures. Thank you both for your support and supervision through all of my projects taken at Aberystwyth.

I would like to offer a broad thank you to the wider Hoffmann group and the staff who have supported our research activity. Without the efforts to maintain the lifecycle and the wealth of research knowledge shared I would not have gotten anywhere. I would especially like to thank Jess whose constant joy, kindness and tireless work deserves more appreciation than can be written in a line.

To Tom Gasan. You trained me in the lab and have always been a kind a patient friend. Thank you for checking in on me over the years and listening to a rant, or two, or three… I am glad we were able to reconnect properly at York and I can't wait to see what the future brings for both of us!

To Jo Forde-Thomas. Without your help and work I don't think this thesis would have been completed. Your knowledge and support have especially guided me through the final stages of this work (although it's always been helpful!) and even just being there to discuss other problems and venting have been a huge help. You've earned all the Port in Portugal!

To Helen Whiteland. You've been a great friend and you've always brought different perspectives and ways of thinking. Everyone needs a friend like you to remind them of what's necessary and what's not and to keep you grounded (also your dog Archie has been of immense comfort through trying times but that definitely is not the main reason for this long thanks!).

To Lisa, Ben, Greg, Holly C and Merl. Thank you all for your patience, encouragement and for lending an ear when times have been tough. I haven't always been in the best of moods or the easiest of friends, but your patience and understanding has meant the world. Thank you for all the coffee, tea, cakes, and other treats we shared over the years.

To the Aberystwyth crew. Luke, Hannah, Sam, Cynan, Ryan, Owain, Rhys and Maldwyn words cannot express how important you guys have been over the last two years. You guys have always been there to listen, to help me blow off steam, to just sit and enjoy free time and, more recently, to build good habits and regular activity. From D&D to watching the football to going hard in the gym. These kinds of friendships remain the strongest!

To the FunFunGroup. Jamie, Beth, Rob, Mike and Hannah. The lockdown years were probably the hardest through this whole process. You guys helped me when I felt at my lowest and most lonely. Jamie and Rob for years you two have been a constant rock in my corner just letting me vent and offering me sage advice and wisdom.

To Betty, Rich, Thomas, Holly T, Liam and Will. True friendships are those where you can pick up where you left off even after years of not seeing each other. We may only see each other a few times a year but when we do it's as if no time has passed. Thank you for many years of joy and many more to come.

To my family. It may sometimes be difficult but without your support throughout the years I would have never been the man I am today.

To others… There is so much more I could say and so many more people I could thank but I only have so much space and the will to write more (after tens of thousands of words!). Ultimately the work within this thesis is attributed to one person. But behind every person there are friends, family and influences that make it all possible.

One final thanks to Aberystwyth. My Home.

Mandatory Layout of Declaration/Statements

Word Count of thesis: DECLARATION	41,228
This work has not previously been accepted in substance for any degree and is not being concurrently submitted in candidature for any degree.	
Candidate name	Adam Muslem George Burgess
Student ID Number	140106930
Signature	
Date	30/05/2024

STATEMENT 1

This thesis is the result of my own investigations, except where otherwise stated. Where **correction services** have been used, the extent and nature of the correction is clearly marked in a footnote(s).

Other sources are acknowledged by footnotes giving explicit references. A bibliography is appended.

Signature	
Date	30/05/2024

[*this refers to the extent to which the text has been corrected by others]

STATEMENT 2

I hereby give consent for my thesis, if accepted, to be available for photo copying and for inter-library loan, and for the title and summary to be made available to outside organisations.

Signature	
Date	30/05/2024

NB: *Candidates on whose behalf a bar on access (hard copy) has been approved by the University should use the following version of Statement 2:*

I hereby give consent for my thesis, if accepted, to be available for photocopying and for inter-library loans after expiry of a bar on access approved by Aberystwyth University.

Signature	
Date	30/05/2024

Abstract:

Schistosomiasis is a neglected tropical disease (NTD) that affects the world's poorest people in tropical and sub-tropical regions caused by trematodes of the genus *Schistosoma*. Praziquantel is the only drug used in the field for treatment and there are concerns of drug resistance emerging. Fumarases are enzymes involved in cellular metabolism and DNA repair. Two biologically distinct classes exist which share no sequence homology. *S. mansoni* possesses two genes $SmFH_I$ (class I) and $SmFH_{II}$ (class II) and humans only possess a class II.

Homolog searches reveal that Lophotrochozoa are the only metazoan clade to have maintained two classes of fumarase. There have also been two losses of class I in Chordata and Ecdysozoa. Class II was only lost in Cestoda and Monogenea. Phylogenetic analyses reveal the evolutionary relationships within each class of fumarase. Localisation prediction tools reveal that $SmFH_I$ possesses a mitochondrial targeting peptide while $SmFH_{II}$ does not, suggesting a division of labour between these two enzymes. Mining of expression data from DNA-microarray and RNA-seq meta-analysis reveals relatively high expression of both fumarases across the human-infecting lifecycle stages. Expression in human-infective lifecycle is elucidated through qRT-PCR and reveals relatively high expression of both genes except for 24-hour schistosomula expression of *Smfh*$_I$. ScRNA-seq of adult worms shows high expression across different cell types.

Using RNAi it is revealed that the targeting of both fumarases elicits a phenotypic response of motility loss in male and female adult worms, however knockdown data is inconclusive for females. There isn't a significant rise or loss of the non-targeted fumarase when compared with the control.

Using computer aided drug design (CADD), a homology model of $SmFH_I$ is made based on the crystal structure of *Leishmania major* class I fumarase LmFH-2. This model is used for *in silico* docking experiments against a library of 300,000 compounds. A selection of 18 compounds from those identified as hits in CADD as well as a class II fumarase inhibitor identified in the literature are screened against schistosomula. Compounds identified as a hit in these screens are then screened against adult worms for 72-hours and cytotoxicity is calculated. Neither of the compounds identified were found to be cytotoxic to human cell lines. Neither of the compounds were found to be particularly potent. Methods to improve the potency and delivery of potential mitochondrial inhibitors are discussed.

Common Abbreviations:

$SmFH_I$	*Schistosoma mansoni* class I fumarase enzyme
$SmFH_{II}$	*Schistosoma mansoni* class II fumarase enzyme
$Smfh_I$	*Schistosoma mansoni* class I fumarase gene
$Smfh_{II}$	*Schistosoma mansoni* class II fumarase gene
bp	base pair
Ct	cycle threshold
DNA	deoxyribonucleic acid
cDNA	complimentary DNA
gDNA	genomic DNA
RNA	ribonucleic acid
DMEM	Dulbecco's modified eagles medium
BME	Basal Medium Eagle
FBS	Foetal bovine serum
PCR	polymerase chain reaction
qRT-PCR	quantitative reverse-transcription PCR
CADD	Computer Aided Drug Discovery
v/v	volume per volume
Fe-S	Iron-sulphur cluster
mTP	Mitochondrial targeting peptide
HLRCC	Hereditary leiomyomatosis and renal cell carcinoma
fumA	*Escherichia coli* class I fumarase for aerobic conditions
fumB	*E. coli* class I fumarase for anaerobic conditions
fumC	*E. coli* class II fumarase for temperature stress conditions
LmFH-2	*Leishmania major* cytosolic class I fumarase
RNAi	RNA interference
siRNA	small interfering RNA
dsRNA	double stranded RNA

Contents

Figures

Tables

1. Introduction

1.1 Fumarases

1.1.1 The classes of fumarase

Fumarases, also known as fumarate hydratases, are enzymes that facilitate the reversible conversion of fumarate to *S*-malate by hydration or dehydration of the two substrates respectively (Figure 1.) (Mann and Woolf, 1930; Woods et al., 1988). Two biologically distinct enzyme classes are capable of catalysing this reaction and these are referred to as class I and class II fumarases.

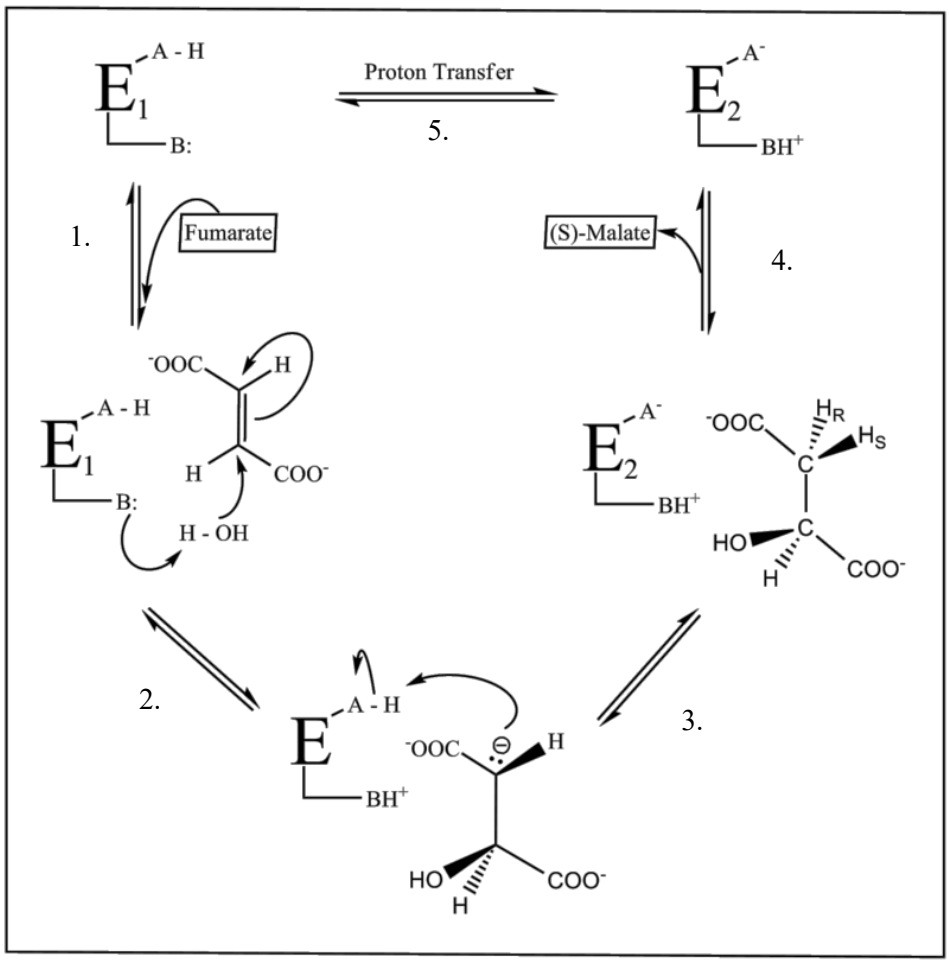

Figure 1.1. The reversible conversion of fumarate to *S*-malate. Enzyme labelled E. Enzymatic residues that interact with substrates are labelled A and B. 1. Fumarase is in an

internally neutralised state (E_1) where A possesses a hydrogen and B possesses two electrons. E_1 accepts a proton from H_2O and the covalent double bond between carbons 2 and 3 in fumarate accepts the hydroxide (OH^-). This leaves a negative charge on the substrate and residue B with the addition of a proton becomes positively charged. 2. The substrate accepts a proton from residue A. 3. Fumarase is now in a zwitterionic state (dipolar) where A possesses a negative charge and B possesses a positive charge (E_2) 4. *S*-malate is released from the enzyme. 5. E_2 is returned to an internally neutral state E_1 by the transfer of the proton from B to A. This reaction can occur in the reverse direction.

The class I fumarases form homo-dimeric enzyme complexes that consist of 60 kDa monomers and are heat sensitive (Woods et al., 1988). Class I fumarases are reliant on a [4Fe-4S] cluster for enzymatic activity. When this cluster is oxidised to [3Fe-4S], enzymatic activity for class I fumarasescease as demonstrated in a purified *E. coli* class I (Flint et al., 1992). These enzymes possess two active sites, one in each monomer that becomes activated following dimerisation. This conformation is likely adopted as it facilitates the formation of a positively charged cavity, which allows the negative charged substrates to enter and interact with the bioactive Fum1 complex (Feliciano et al., 2016). *Escherichia coli* class I fumarases are also oxygen sensitive *in vitro*, where it was demonstrated that exposure to air for 30 seconds resulted in the loss of ~70% activity followed by a further reduction of residual activity to 10% after 2 minutes (van Vugt-Lussenburg et al., 2013). FumA, one of the two *E. coli* class I fumarases is still active under aerobic conditions *in vivo*, however (Woods et al., 1988). It has been demonstrated that class I fumarases are essential for the anaerobic growth of *E. coli* on D-tartrate during D-tartrate fermentation. When anaerobic *E. coli* class I fumarase, FumB, was deleted, colonies were unable to grow on D-tartrate plates (Kim et al., 2007).

The class II fumarases are homo-tetrameric enzymes thatconsist of 50 kDa monomers (Wu and Tzagoloff, 1987). Class II fumarases are lyases and are structurally similar to aspartate

ammonia-lyase, an enzyme that converts L-aspartate to fumarate (Woods et al., 1986). Class II fumarases possess a signature sequence motif containing a flexible catalytic SS-loop (GSSxxPxKxNPxxxE) which binds and manipulates the substrate. These loops are common amongst fumarase/aspartase protein family members (Ajalla Aleixo et al., 2019; Cardoso et al., 2021; Woods et al., 1986). Unlike class I fumarases, class II enzymes are thermostable and insensitive to oxygen disruption; in the case of *E. coli* which possesses a single class II fumarase (FumC), expression increases when the bacteria is under heat stress (Woods et al., 1988). Class II fumarases are prevalent in Eukaryotic organisms (Akiba et al., 1984; Edwards and Hopkinson, 1979; Kobayashi and Tuboi, 1983; O'Hare and Doonan, 1985; Tolley and Craig, 1975) with a wealth of research into their importance for human (Ruecker et al., 2017; Ryder et al., 2018; Tomlinson et al., 2002; Toro et al., 2003) and plant (Pracharoenwattana et al., 2010, 2010; Saunders et al., 2022) metabolism and health. Enzymes from this protein family are not reliant on an iron sulphur cluster for their function, activity is instead facilitated by interactions between the substrate and residues within the active site (Ajalla Aleixo et al., 2019; Cardoso et al., 2021). Fumarases are found within multiple cellular compartments and are involved in several metabolic cycles that are crucial for the survival of cells and the maintenance of stable cellular conditions (Leshets et al., 2018).

1.1.2 Fumarases in the mitochondria

Fumarases are a crucial component of the tricarboxylic acid (TCA)-cycle (also described as the Krebs cycle), a metabolic cycle that takes place within the mitochondrial matrix and generates precursors for the electron transport chain for cellular respiration (Gasmi et al., 2021; Krebs, 1940; Krebs and Johnson, 1980; Martínez-Reyes and Chandel, 2020). In this cycle acetate in the form of acetyl-CoA and water are consumed to generate carbon dioxide and the reduction of NAD^+ to NADH (Alberts et al., 2002a). The cycle consists of 8 enzymes and results in a net yield of three NADH molecules, one $FADH_2$ and one molecule of GTP

(Figure 1.2) (Chinopoulos, 2013). The NADH and $FADH_2$ are utilised in the electron transport chain to generate an electrochemical gradient across the inner mitochondrial membrane (Alberts et al., 2002a). The electrochemical gradient drives the production of adenosine triphosphate (ATP), the molecule that provides energy for most cellular processes, through the oxidative phosphorylation of ATP-synthase (Anraku, 1988). The TCA-cycle can operate aerobically and anaerobically with the majority of enzymes capable of reversible reactions (with the exception of citrate synthase and the α-ketoglutarate dehydrogenase complex (Chinopoulos, 2013).

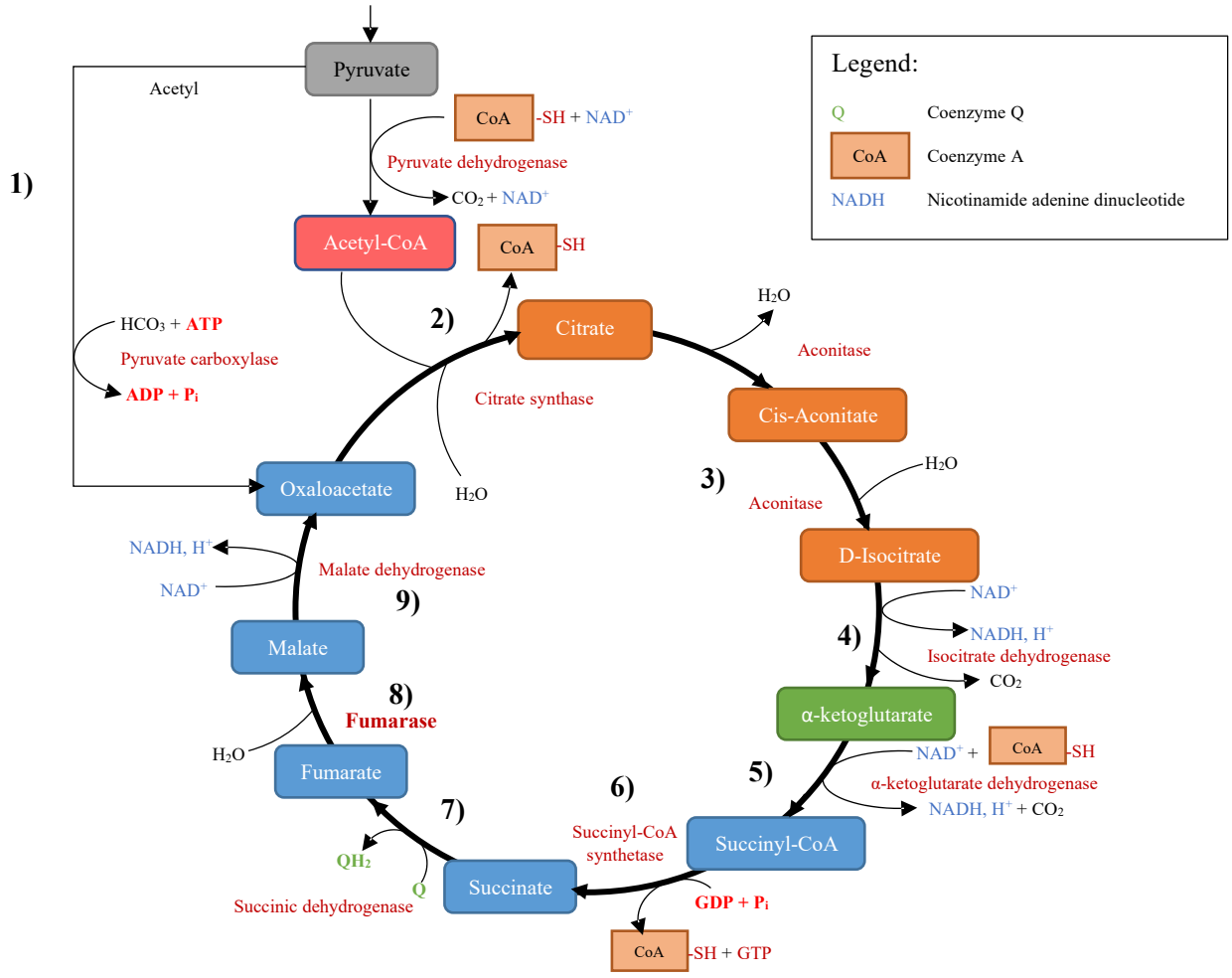

Figure 1.2. The Tricarboxylic Acid (TCA) cycle. 1) Pyruvate from the glycolysis pathway is converted to Acetyle-CoA by Pyruvate dehydrogenase with the addition of CoA and NAD^+ in

a process called gluconeogenesis. This produces CO_2 and NADH in the process. Some pyruvate is converted to oxaloacetate by pyruvate carboxylase. **2)** Acetyl-CoA reacts with oxaloacetate and H_2O through the activity of citrate synthase, liberating CoA in the process. This is the first step in the TCA-cycle. **3)** Citrate is dehydrated by aconitase 1 forming cis-aconitate, which is then hydrated in the presence of aconitase 2 to form D-isocitrate. **4)** Isocitrate dehydrogenase converts D-isocitrate to α-ketoglutarate using NAD+ as a proton acceptor, generating NADH and CO_2 in the process. **5)** α-ketoglutarate dehydrogenase, an enzyme complex, catalyzes the reaction between α-ketoglutarate, NAD+ and CoA to form Succinyl-CoA, NADH and CO_2. **6)** Succinyl-CoA synthetase converts succinyl-CoA to succinate utilising guanine diphosphate (GDP) and inorganic phosphate, generating guanine triphosphate (GTP) and liberating CoA in the process. **7)** Succinic dehydrogenase, a mitochondrial membrane protein complex oxidises succinate to form fumarate. **8)** Fumarate is hydrated to form malate facilitated by fumarase. **9)** Malate dehydrogenase dehydrates malate with NAD+ to form oxaloacetate.

Fumarases are one of the eight crucial enzymes involved in the TCA cycle and are crucial for its function (Figure 1.2 stage 8) (Leshets et al., 2018). The mutation of fumarase genes resulting in structural changes to the enzyme and deficiencies in the enzyme is found to be responsible for a range of metabolic disorders (Bayley et al., 2008; Ruecker et al., 2017, 2017; Ryder et al., 2018) and human cancers (Lorenzato et al., 2008; Tomlinson et al., 2002; Toro et al., 2003). A variety of mechanisms and possible causes for this have been researched.

It has been suggested that metabolic disorders caused by a non-functional fumarase gene could be as a result of fumarate accumulation in the cell(Blatnik et al., 2008; Kinch et al., 2011; Ruecker et al., 2017; Ternette et al., 2013; Xiao et al., 2012). Fumarate is capable of modifying cysteines through the nucleophilic addition of fumarate. This results in the formation of *S*-(2-succinyl)-cysteine and can lead to the rapid disruption of enzymatic function due to

conformation changes and residue disruption (Alderson et al., 2006). Studies investigating fumarase deficient mice identified 94 proteins that are affected by succination including 13 that are active within the mitochondria (Ternette et al., 2013). Notably, aconitase 2 involved in the conversion of citrate to isocitrate within the TCA cycle (Figure 1.2 stage 3) showed dose-dependent inhibition. LC-MS mass spectrometry was used to determine that an increase in succination occurs in aconitase 2, changing the conformation of this protein and resulting in the chelation of the iron-sulphur cluster responsible for enzymatic activity. Increases in succination because of fumarase deficiency has also been demonstrated to be lethal towards *Mycobacterium tuberculosis*. An *M. tuberculosis* mutant strain was generated where dual control genetic switch (Kim et al., 2013) was used to induce knockdown of the fumarase gene (Ruecker et al., 2017). The bacteria that possessed this mutation were unable to survive both *in vitro* and within chronic and acute mouse infections due to succination of proteins. This further highlights the importance of fumarase for the continued metabolic activity of organisms and in turn their survival.

1.1.3 Fumarases in the cytosol

Fumarases also perform crucial functions within the cytosol of eukaryotic cells spanning single-cell yeast (Wu and Tzagoloff, 1987) to metazoan mammals such as humans (Edwards and Hopkinson, 1979; Tolley and Craig, 1975) and rats (Kobayashi and Tuboi, 1983). Although fumarases are canonically associated with the TCA cycle and are broadly considered to be active within the mitochondria (section 1.1.2), studies investigating hepatic cells of mammals, birds, reptiles and fish found the quantities of fumarase enzymes found in the cytosol and mitochondria were similar (Akiba et al., 1984). Fumarate is generated as a by-product of two metabolic cycles that are active within the cytosol, the urea cycle (also known as the ornithine cycle) (Adam et al., 2013) and the purine biosynthesis pathway (Bulusu et al., 2011) (Figure 1.3.). In both cases, fumarate is produced as a by-product that is scavenged by

cytosolic fumarases. The malate produced in this reaction is utilised in other metabolic cycles, the most prevalent of which is the TCA-cycle(Bulusu et al., 2011).

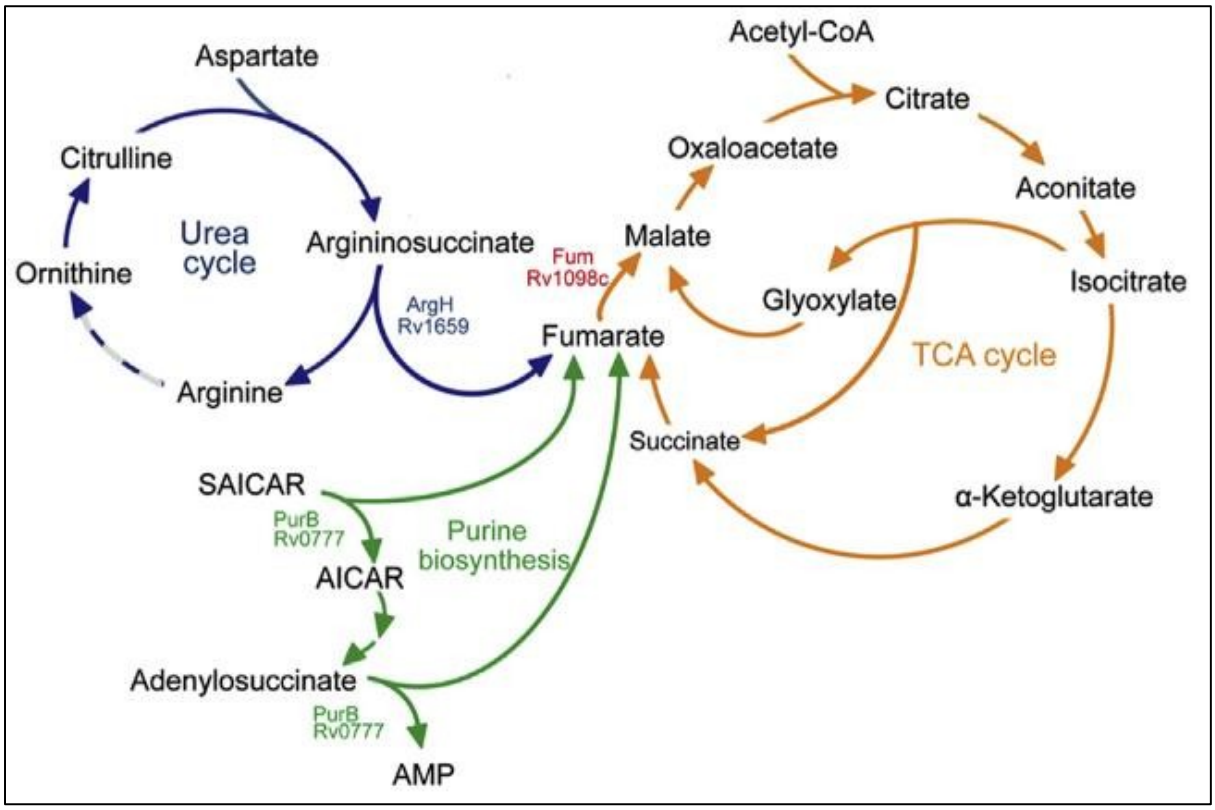

Figure 1.3. Routes of fumarate synthesis within the cell. Fumarate is generated within the TCA cycle (gold) by succinate dehydrogenase prior to being converted to *S*-malate by mitochondrial fumarase. Within the cytosolic compartments fumarate is generated as a by-product of the urea cycle (blue) when arginosuccinate is converted to arginine by arginosuccinate lyase. Fumarate is produced as a by-product of purine biosynthesis (green) in the cytosol when adenylosuccinate lyase catalyses the conversion of Phosphoribosylaminoimidazolesuccinocarboxamide (SAICAR) to 5-Aminoimidazole-4-carboxamide ribonucleotide (AICAR). (Ruecker et al., 2017)

As described briefly in 1.1.2 fumarase deficiencies are associated with cancers, more specifically they are responsible for hereditary leiomyomatosis and renal cell cancer (HLRCC) caused by the heterozygous germline mutation in the human fumarase gene (Lorenzato et al., 2008; Menko et al., 2014; Toro et al., 2003). Research has suggested that succination of proteins in fumarase knockdown models could contribute to the formation of HLRCC (Ternette et al., 2013) and succinated proteins have been identified in cancerous cells (Kinch et al., 2011). Recent research suggests that alternatively, fumarases are directly involved in the DNA-damage repair response to double strand breaks (Yogev et al., 2010; Yogev and Pines, 2011). Yeast strains that lack cytosolic fumarases were found to accumulate more double strand breaks to nuclear DNA when exposed to ionizing radiation (IR) than wild type yeast (Yogev et al., 2010). When colonies lacking cytosolic fumarase were supplemented with fumarate, they were found to recover when compared to those lacking a fumarate supplement. This suggests that fumarate assists in the DNA damage repair response of yeast and is facilitated by the enzymatic activity of cytosolic fumarases. This study also demonstrated the movement of cytosolic fumarases to the nucleus following DNA damage. Following IR exposure HeLa cells were left to recover for 6, 12 and 24 hours. These cells were immune stained with anti-fumarase antibodies and DAPI for staining DNA. Over the course of 24-hours the amount of fumarase present in the nucleus increased. Experiments performed by Jiang et al. (2015) demonstrated that fumarase was directly involved in a DNA repair pathway in human cells exposed to IR. It was found that the local generation of fumarate in the nucleus lead to non-homologous end joining DNA repair. From metabolic cycles to the DNA-damage repair response, fumarases possess an important role in the cellular function of Eukaryotic organisms, but could they present an interesting target for schistosome drug discovery?

1.2 Schistosomiasis

1.2.1 Platyhelminthes

The phylum Platyhelminthes (flat worms) belongs to the basal Spiralian clade Platytrochozoa (Struck et al., 2014). However, they are often grouped with the Lophotrochozoa, which includes the Annelida (segmented worms) and the Mollusca (molluscs) (Paps et al., 2009). Platyhelminthes is traditionally divided into four classes: Turbellaria, Trematoda, Monogenea and Cestoda (Laumer et al., 2015). The majority of Turbellaria are free-living species that largely reside in marine and freshwater environments, however, some species are found in warm, humid terrestrial environments (Collins, 2017). Turbellaria have long been known to be paraphyletic. Phylogenetic studies using transcriptomic alignments have divided this group into new classifications allowing for better understanding of the evolutionary relationships between free-living and parasitic platyhelminths (Egger et al., 2015). Trematoda, Cestoda and Monogenea consist of solely parasitic species that infect a vertebrate host (Laumer et al., 2015). In modern phylogeny, these parasites are classed as Neodermata, characterised by the transition from a larval epidermis to a syncytial (single multinucleated cell) epidermis called the tegument (Littlewood et al., 1999). This parasitic adaptation has arguably been utilised most successfully by the class Trematoda that occupy a range of host environments in their adult lifecycle stages (Collins, 2017). The four host environments these parasites occupy are: the bile ducts, which are occupied by the liver flukes (e.g. *Fasciola*, *Clonorchis* and *Opisthorchis*), the intestines, occupied by intestinal flukes (e.g. *Fasciolopsis*), the lungs occupied by lung flukes (e.g. *Paragonimus*) and the blood flukes (e.g. *Schistosoma*) that reside in venules surrounding organs (Doughty, 1996). The most significant of these parasites to human health are the liver flukes as food-borne diseases and the blood flukes as water-borne diseases (Vos et al., 2012). Blood flukes of the genus *Schistosoma* are responsible for schistosomiasis in humans and many animal species.

Schistosomiasis of humans is predominantly caused by three species: *Schistosoma mansoni*, *Schistosoma haematobium* and *Schistosoma japonicum* (WHO, 2016). Less common human-infecting species include *Schistosoma mekongi*, *Schistosoma guineensis*, *Schistosoma intercalatum* (WHO, 2016) and *Schistosoma malayensis* (Latif et al., 2013). The disease pathology differs between the species of schistosome. Urinary and urogenital schistosomiasis develops predominantly in people infected with *S. haematobium* (Barsoum, 2013) while intestinal and hepatosplenic schistosomiasis is predominantly caused by *S. mansoni* and *S. japonicum* (Elbaz and Esmat, 2013). Urinary and urogenital schistosomiasis results in genital itching and vaginal discharge (Kjetland et al., 2008), post-coital bleeding, genital ulceration (Poggensee et al., 2000) and genitopelvic discomfort (Leutscher et al., 2008). Chronic infections with *S. haematobium* can result in lesions and ulcerations in the bladder and urinary tract that can lead to blockages that can affect kidney function and lead to secondary infections (Barsoum, 2013). Additionally the urinary/urogenital disease has been associated with bladder cancers (Mostafa et al., 1999) and increased risk of contracting HIV (Hotez et al., 2009). Intestinal/hepatosplenic schistosomiasis is often associated with abdominal pain, blood in stool and diarrhoea; however, infections with low numbers of worms can be asymptomatic (Boros, 1989). Chronic infections can lead to the highly debilitating symptoms. These symptoms are associated with the deposition of eggs that become trapped in tissues as they attempt migration to the lumen (Elbaz and Esmat, 2013). The accumulation of eggs in the intestines, spleen, kidneys and most numerous in the liver, leads to host immune responses that include granuloma formation and Symmers' clay-pipestem fibrosis which affects the hepatic portal tract (Cheever and Andrade, 1967; Coutinho, 1990; Mohamed-Ali et al., 1999). These morbid symptoms are highly associated with hepatosplenomegaly (Boros, 1989; Elbaz and Esmat, 2013) and portal hypertension (Cheever and Andrade, 1967) respectively.

1.2.2 The Schistosome Lifecycle

Schistosomiasis, historically known as bilharzia, is a neglected tropical disease (NTD) that affects some of the world's poorest populations with conservative estimates suggesting 252 million people were infected in 2015 (GBD 2015 Disease and Injury Incidence and Prevalence Collaborators, 2016). Schistosomiasis is found in tropical and sub-tropical regions with sub-Saharan Africa showing the highest prevalence followed by the Middle East, South America and South-East Asia (Utzinger et al., 2011). A handful of human vaccines are under different stages of clinical trials (see Molehin, 2020) but none have yet been approved for use in the field. For decades this disease has had major socio-economic and medical implications on communities due to the effects of morbidity (Umeh et al., 2004). The measure of morbidity caused by the disease is often quoted in the measurement of disability adjusted life years (DALYs), a measurement of disease burden based on years lost to ill-health. An estimated 1.1-3.1 million DALYs has been estimated to have been lost every year since 1990 (GBD 2015 Disease and Injury Incidence and Prevalence Collaborators, 2016).

All trematodes possess complex lifecycles that incorporate both free-living and parasitic stages. These lifecycles incorporate more than one host and thus, are described as being digenetic. The intermediate host acts as a reservoir for the asexual proliferation of parasite numbers whereas the definitive host facilitates sexual reproduction (Collins, 2017). Schistosomes parasitise two hosts in their lifecycle, a snail intermediate host and a mammalian definitive host. Within the definitive host, an adult schistosome will reside in the mesenteric venules or the venous plexuses of the bladder, dependent on the species (Figure 1.4.10), and deposits eggs into the lumen or the bladder respectively where they are released in the stool or urine. When the stool or urine meets warm freshwater, the eggs hatch miracidia, the snail infective stage (Figure 1.4.2). The conditions of the water in which the eggs are deposited can determine whether the eggs will hatch or not. The egg requires the external water to be of a

lower osmolarity than the inside of the egg. This has been demonstrated where eggs that are exposed to saline water do not hatch (Samuelson et al., 1984). Additionally, in studies using artificial pond water at 22°C, 70 ± 15% of miracidia hatched within 10 minutes with an increase in the hatching rate at 34°C shown by fewer intact eggs after 40 minutes (Samuelson et al., 1984). After exiting the eggshell, the miracidium swims through the freshwater environment using cilia in search of an appropriate snail host. Different species of *Schistosoma* will infect different intermediate hosts. Of the three most significant schistosome species, *S. mansoni* infects *Biomphalaria*, *S. haematobium* infects *Bulinus* and *S. japonicum* infects *Oncomelania* snail species (Clumpp and Slootweg, 1997). Within the natural habitat of these parasites, there are numerous obstacles to overcome such as finding the correct host species of snail in a vast body of water and potential interfering particles and small molecules that can be found in muddy environments. It has been shown that *S. mansoni* miracidia respond non-specifically to all snail excreted substances, regardless of species origin (Chernin, 1970). However, studies on *S. japonicum* miracidia have shown they will selectively infect *Oncomelania* snails over *Biomphalaria* (Haas et al., 1991). Further studies on miracidia of *S. mansoni* and *S. haematobium* have demonstrated these parasites are able to detect a range of complex macromolecules excreted by snail hosts. This may act as a more specific means of targeting host species (Haberl et al., 1995). Following the location of an appropriate snail host, the miracidium attempts infection by penetrating the tegument of the snail host, which is triggered by the detection of components secreted by the snail (Chernin, 1972).

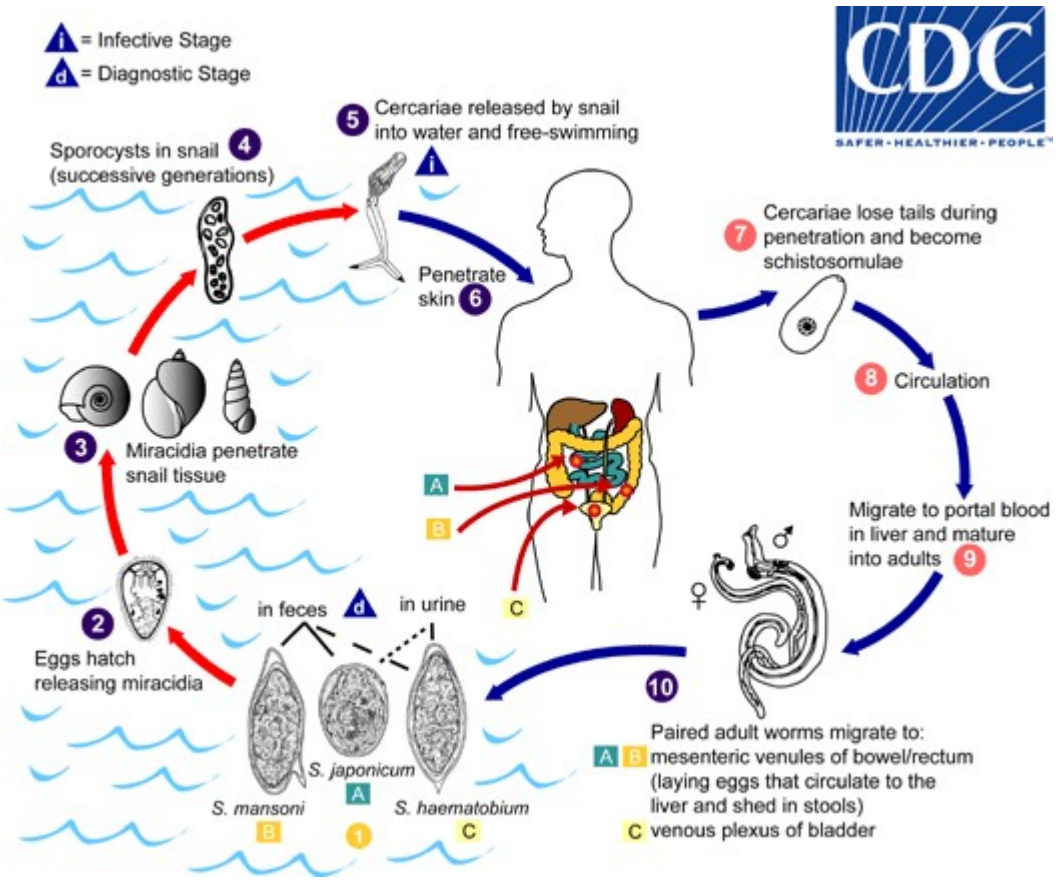

Figure 1.4. The lifecycle of *Schistosoma* species *S. mansoni*, *S. japonicum* and *S. haematobium*. 1) Eggs are released into fresh water from faeces (*S. mansoni* and *S. mansoni*) or in urine (*S. haematobium*). 2) Miracidia are released from the eggs and seek out a snail host using their ciliated tegument to move through the water. 3) Miracidia penetrate intermediate snail host *S. mansoni* infects *Biomphalaria* species, *S. haematobium* infects *Bulinus* species and *S. japonicum* infects *Oncomelania* species. 4) Ciliary coat is shed after penetration of the snail and the miracidia transforms into a sporocyst. Mother sporocysts asexually reproduce more sporocysts. Daughter sporocysts later shed from the mother sporocysts. 5) Cercaria are generated by the daughter sporocyst and are shed from the snail host into fresh water. 6) Cercariae penetrate the skin of the definitive host. 7) Cercariae lose tails during skin penetration and develop into schistosomulae, which 8) enter the circulatory system. Schistosomulae migrate through the lungs and heart during development. 9) Schistosomulae migrate to the portal vein in the liver where they mature into adult worms. Male worms clasp female worms

prior to final migration. 10) Paired adult worms migrate to the mesenteric venules of the bowel/rectum (*S. mansoni* and *S. japonicum*) or the venus plexus of the bladder (*S. haematobium*) and eggs are shed in sexual reproduction.

After penetrating the snail, the miracidium sheds its ciliary coat and transforms into a sporocyst, an asexually reproducing lifecycle stage (Voge and Seidel, 1972) (Figure 1.4.3 and 4). The mother sporocyst develops from the miracidia approximately two weeks after infection and occupies regions of the snail near the surface including the head-foot, mantle and tentacles (Olivier and Mao, 1949). Mother sporocysts contain a large number of germinal cells which can be seen developing into daughter sporocyst embryos within the brood chamber after 5 to six days post infection of the intermediate host (Meuleman et al., 1980). Approximately ten to eleven days post infection, the daughter sporocysts begin to shed from the mother sporocyst and after fifteen to sixteen days can be seen in the connective tissues between the lobes of the snail digestive gland (Meuleman, 1971). The daughter sporocyst is responsible for the generation or cercariae, however, it has also been found that daughter sporocysts can halt production of cercariae and instead produce additional daughter sporocysts (Jourdane et al., 1980).

Cercariae, the infective stage of the definitive host, are released from the daughter sporocyst in a process called shedding. Cercariae that are shed exit through the snail tissue and into the freshwater environment inhabited by the snails (Figure 1.4.5). Shedding behaviours, such as time of shedding, can vary between the parasite species/host snail and can vary during different seasons (Wolmarans et al., 2002). After shedding, the cercariae undergo an initial phase of active swimming to reach the surface of the water before undergoing passive phases of non-movement and short bursts of active phases to maintain their position in the water column (Haas et al., 1994). With no further stimulation, cercariae tend to remain inactive for long periods of time with the occasional short burst of activity. Here they remain distributed

throughout the water column until stimulated by changes in light such as a shadow passing over the water. This results in the cercaria migrating to the water surface (Haas et al., 1994). When cercariae come into contact with the skin of a mammalian host, they begin penetration of the skin. Detection of the mammalian host can be achieved through thermal cues (Cohen et al., 1980) and chemical signals (Haas et al., 1997). Once attached to the surface of the skin, the cercariae move through the epidermis and dermis until they reach a lymphatic of blood vessel (McKerrow and Salter, 2002). Penetration is achieved through the degradation of host proteins including keratin (Tzeng et al., 1983), elastins (Gazzinelli and Pellegrino, 1964; Salter et al., 2000) and collagens (Miller and Wilson, 1978). Cercariae excretory/secretory (E/S) products including enzymes (Tzeng et al., 1983; Hansell et al., 2008; Sanin and Mountford, 2015), anti-inflammatory factors (Ramaswamy et al., 1995) and prostaglandins (Ramaswamy et al., 2000; Angeli et al., 2001) aid in the parasites' penetration of the skin and the subsequent modulation of immune components to aid infection and establishment of disease. Many cercariae perish during their migration to the vascular system where they can be found stuck in the host's skin (Clegg and Smithers, 1968; Miller and Wilson, 1978).

During host penetration, the cercariae lose their forked tails and develop into schistosomula where the remaining head region begins to develop a heptalaminate surface membrane following the loss of the glycocalyx (Hockley and McLaren, 1973). The schistosomulum passes through the skin through enzymatic degradation before entering the circulatory system of the host. From here schistosomula migrate to the lungs where they remain for 3-4 days. In the lungs, many schistosomula end their migration where they enter the alveoli and are unable to continue their migration. Schistosomula that remain in the circulatory system then migrate to the liver primarily via the hepatic artery; in order to reach this organ, they can take several rounds of circulation through the host vasculature. Schistosomula can also enter the liver via gastric arteries, small intestine via the gastroduodenal artery or the spleen and

pancreas via the splenic artery. However, once in the liver, schistosomula cross the capillary networks and eventually migrate to the hepatic portal system (Nation et al., 2020).

Within the hepatic portal system, schistosomula are unable to pass through the sinusoids and return to the systemic blood flow (Wilson et al., 1978). Here, schistosomula attach to the blood vessels through the use of ventral suckers and are positioned facing the blood flow (coming from the intestines) (Bloch, 1980). From here, the schistosomula consume blood and rapidly mature, doubling in size every 2-3 days for two weeks (van Oordt et al., 1988). Once matured, adult male worms will find a mate and the pair begin migration, in the case of *S. mansoni*, to the mesenteric venules where they begin egg production.

S. mansoni paired worms begin producing eggs up to a rate of 350 per day. Eggs migrate to the intestines where they are passed in faeces. Approximately two thirds of eggs produced are unsuccessful in their passage and remain stuck in tissues of the definitive host (Cheever et al., 1994). During the migration to the intestines, eggs can become lost in systemic organs or the blood flow where they can become trapped in the liver. When trapped in tissues, eggs elicit an immune response leading to inflammation and the formation of granulomas when immune cells such as macrophages, Th2 cells, eosinophils, basophils and neutrophils (Schwartz and Fallon, 2018). The formation of granulomas leads to the greatest morbidities seen in cases of schistosomiasis. In chronic infections where individuals are infected with many worm pairs, the accumulation of granulomas leads to the dramatic expansion of the liver described as hepatosplenomegaly. This can often affect school-aged children in endemic areas where they have experienced repeat reinfection by schistosomes (Wilson et al., 2011).

1.2.3 Schistosomiasis control

Current methods for the control of schistosomiasis rely on the mass drug administration (MDA) of the drug Praziquantel (Kura et al., 2020). This drug has been used for the treatment of schistosomiasis for over 40 years and remains an effective treatment for all species of

human-infecting *Schistosoma* (Fukushige et al., 2021). An alternative drug, Oxamniquine, has also been used for the treatment of *S. mansoni*, however, it is not effective at clearing infections from other species of schistosome and is a more expensive drug to produce leading to praziquantel being a preferred option (da Silva et al., 2017). Although there are ongoing clinical trials of vaccines, there are currently no vaccines deployed for use in endemic areas (Molehin, 2020). Due to the use of a single drug, there are fears of resistance emerging. Research into new drug candidates and drug targets is therefore considered an important effort towards the ongoing control of this disease.

1.2.4 Platyhelminth respiration

The respiration of platyhelminths has been largely studied in parasitic species, however, aspects of respiration appear to be shared between different groups (Tielens and van Hellemond, 2005). Free-living stages of the parasitic lifecycle such as the miracidium or cercaria will often survive within aquatic environments where they rely solely on endogenous glycogen reserves and only take up oxygen from the environment for aerobic respiration. With no way to replenish lost energy, they will quickly perish once their energy reserves have diminished (Tielens and van Hellemond, 2005). Once inside the host, the parasitic worm switches to the consumption of nutrients from the host environment where resources are plentiful and energy is no longer a limiting factor (Tielens and van Hellemond, 2005). Studies investigating different species have suggested a variety of specialised metabolic pathways that have evolved for the survival in a range of different host environments.

Fasciola hepatica is a digenean parasite predominantly of livestock that enters the definitive host by consumption of metacercariae encysted on grass (Mas-Coma et al., 2005). When fully matured, this liver fluke occupies the bile duct of its mammalian host where it feeds on tissue and blood from the bile through its oral sucker (Mas-Coma et al., 2005; Tielens and van Hellemond, 2005). *F. hepatica* has been used as a model for the study of parasitic

platyhelminth metabolism and respiration; findings have highlighted that this organism, likely due to its environmental context (Moss, 1970), has a greater dependence upon anaerobic metabolism to generate its energy (Lloyd, 1986). Despite the possession of a full repertoire of enzymes, such as the TCA-cycle and electron transport chain enzymes, capable of carrying out aerobic respiration, the lack of oxygen availability in the bile duct renders the worm incapable of respiring by oxidative phosphorylation (Lloyd, 1986). The majority of anaerobically respiring organisms generate ATP through the glycolysis pathway, an ancient pathway that generates pyruvate later used in the TCA-cycle, and two molecules of ATP (Romano and Conway, 1996). By utilising a partially reversed TCA-cycle, *F. hepatica* is able to generate a larger quantity of ATP. Unlike *F. hepatica*, adult schistosomes are surrounded by an oxygen rich environment in the blood of their definitive host giving rise to the possibility of a more active aerobic respiration.

1.2.5 Schistosome respiration

S. mansoni transition from aerobic metabolism of glycogen stores in cercariae to anaerobic metabolism in the early stages of definitive host development (Van Oordt et al., 1989). Physiological changes to the cercariae undergone following transformation through the hosts skin includes a utilisation of glycolytic energy production to generate ATP as opposed to oxidative phosphorylation. Experiments undertaken on adult worms where radiolabelled glucose was used in media suggested that the adults produce a third of their energy aerobically with two thirds derived from glycolysis (van Oordt et al., 1985). Early studies exploring the transcript abundance of metabolic markers shed further light on the share of aerobic and anaerobic pathways in different lifecycle stages (Skelly et al., 1995, 1993). Analysis of the TCA-cycle enzyme malate dehydrogenase and the electron transport chain subunit 1 of cytochrome oxidase (Skelly et al., 1993) found that there was lower expression of these genes than anaerobic markers. However, expression still occurred at relatively high quantities (Skelly

et al., 1995). The importance of aerobic respiration in schistosomes may provide avenues of target-based investigations. Research exploring reactive oxygen species (ROS) has been demonstrated to affect aerobic metabolism (Drapier and Hibbs, 1986; Stamler et al., 1992) and studies have explored their effects on schistosomes (see James, 1995).

Enzymes containing [4Fe-4S] clusters are highly enriched within aerobic respiratory pathways. ROS, like nitric oxide (NO), have been shown to inactivate many proteins that contain [4Fe-4S] clusters such as aconitase in the TCA-cycle and succinate dehydrogenase (Drapier and Hibbs, 1986; Stamler et al., 1992). The production of NO occurs in numerous cells and tissues and has been demonstrated to inhibit the growth and development of many parasitic pathogens of medical importance including protozoans and helminths (See review: James, 1995). Additionally, NO has been shown to have anti-schistosomal properties. In a study by Ahmed et al. (1997) observing the effects of NO on schistosomula, parasites were either mechanically transformed by vortex and incubated for 3-hours, harvested from the lungs of infected mice 1 week post-infection, or 2.5 weeks post-infection from the liver. Schistosomula were exposed to NO through the use of donor molecule diethylenetriamine nitric oxide adduct (DETA/NO), which has an NO generating half-life of 20 hours. Parasites were incubated for 48 hours and mortality was evaluated through microscopy. It was found that incubation of 0.5 mM DETA/NO with 3-hour schistosomula led to death in over 95% of individuals. The 2.5 week schistosomula showed fewer deaths (just under 50%) with the lung-stage parasites showing the fewest deaths (under 10%). Further experiments were conducted in which the DETA/NO concentration was increased to 1 mM; this demonstrated a larger percentage killed in all three groups. However, it remained true that lung stage parasites showed the fewest deaths. This suggests that as the parasites move to the lungs they shift towards anaerobic respiration to avoid the highly damaging effects of NO within a highly aerobic environment. This demonstrates a way in which schistosomes are able to evade the

natural defences of their hosts to establish a successful infection. To demonstrate that disruption of aerobic respiration was the likely cause of this killing, further experiments were conducted in which schistosomula were exposed to inhibitors of the TCA-cycle and electron transport chain (Ahmed et al., 1997). The inhibitors used were: fluoroacetate, an inhibitor of aconitase; sodium azide, an inhibitor of electron transport of cytochromes a/a_3; oligomycin B, which inhibits mitochondrial ATPase; antimycin A, an inhibitor of cytochrome *b* and *c*; 2,4-dinitrophenol, which uncouples oxidative phosphorylation; rotenone, which inhibits electron transport within the NADH-ubiquinone complex; and 2-deoxy-D-glucose, which inhibits glycolysis. The inhibitors were all capable of inhibiting mammalian cell respiration. The quantity for maximal killing of 3-hour schistosomula was identified by a titration of compounds and once identified, this quantity was used to dose 1-week and 2.5-weeks schistosomula. All inhibitors demonstrated a high mortality of schistosomula in the 3-hour and 2.5-weeks parasites and low killing % in lung stage schistosomula. This suggests that the respiration of schistosomes shifts at different lifecycle stages, likely mediated by the presence of host-defences that are more able to inhibit the aerobic pathways of migrating parasites. It is interesting that although there are fewer deaths of 2.5 weeks liver-stage schistosomula in NO exposure compared to 3-hour parasites, the % killed following exposure to inhibitors increases in some cases two-fold (antimycin and azide). It was found that schistosomula at 3-hour and 2.5 weeks showed a loss of motility when exposed to inhibitors at two- to 5-fold lower doses than the killing dose. This suggests that the metabolic requirements lean more towards aerobic respiration, potentially for motility. NO inhibition of schistosomes is not only limited to *S. mansoni* as it has been demonstrated that *S. japonicum* is able to parasitise rats, an accidental host, when NO production has been inhibited (Shen et al., 2017). Experiments have been performed exploring the killing of *S. mansoni* sporocysts by parasite-resistant *B. glabrata* (Hahn et al., 2001). It was found that parasite-resistant snails possessed haemocytes that

produced NO which effectively killed sporocysts. This was demonstrated through cell-mediated cytotoxicity assays in which haemocytes extracted from the haemolymph of resistant snails were plated in 96-well plates and sporocysts were added. Through the inhibition of nitric oxide synthase and the use of NO scavengers, the researchers were able to demonstrate a reduction in sporocysts killing when compared to assays with just haemocytes. There were, however, still many deaths of sporocysts (up to 60%) in some assays containing NOS inhibitors. This suggests that NO may just be a contributing factor to the killing of sporocysts in resistant snails and further components produced by the haemocytes of resistant snails contribute to the resistance.

Adult worm respiration and the importance of metabolic pathways have been explored using compounds with known targets. The drug closantel is a broad anthelmintic drug used predominantly to treat cattle and livestock. It has antiparasitic effects on adult and juvenile *F. hepatica* and *Fasciola gigantica* as well as several blood feeding nematodes (Guerrero, 1984). Closantel has been shown to affect mitochondrial activity in *F. hepatica* (Vanden Bossche, 1990). Experiments performed on adult *S. mansoni* worms dosed with closantel have been performed to provide insight into the contribution of aerobic respiration to parasite survival (Bossche, 1985). Worm pairs were dosed with 10 μM closantel and were compared with untreated control. The motility and lactic acid production (measurement of anaerobic respiration) were measured and compared with the untreated controls. It was found that although anaerobic respiration remained closely in line with controls over the course of 4 hours, the motility of the worms rapidly declined to a total loss of motility after 2 hours. This study suggests that although anaerobic respiration remains uninhibited, the motility of the adult worms appears to be reliant on aerobic respiration.

1.3. Aims of this project

The current literature surrounding fumarases is largely focused on human fumarases and their relevance to human diseases. As such the vast majority of research is focused on class II fumarases; where research on class I fumarases have been conducted, it has mainly been focused on non-metazoan (e.g. Protozoan and bacteria) examples. Much of the focus of metabolic cycles in schistosomes and their relevance for target identification was performed in the late 20th century. Since then new tools have become available and the generations of the *S. mansoni* genome offers an opportunity to investigate fumarases in this neglected tropical parasite **(**Berriman et al., 2009). Within this genome, two genes have been identified that transcribe predicted fumarases, one a class I and the other a class II. The presence of two genes, one of which there is no homolog in humans, presents a unique opportunity for the potential targeting of a crucial metabolic enzyme. This study would also be the first of its kind to study a metazoan class I fumarase. The characterisation of these enzymes was progressed through the following research objectives:

1. **Characterise the fumarases of *S. mansoni* using a range of available bioinformatic tools and qPCR techniques.** Confirmation that these genes exist within the *S. mansoni* genome was achieved through the whole gene amplification from cDNA and sequencing of the PCR products. Amino acid sequences were used to identify homologs of class I and class II fumarases and were used to construct phylogenetic trees to analyse the evolutionary relationship of these homologs between different species. Available datasets including DNA microarray, RNAseq and single cell transcriptomes of different lifecycle stages were interrogated to understand the expression profiles of these genes across lifecycle stages and different cell populations. Quantitative real-time PCR was used to consolidate expression profiles and compare expression between human-infective lifecycle stages and between the two schistosome fumarase genes. The

localisation of the two genes and their potential roles as mitochondrial, cytosolic or both was explored using mitochondrial targeting peptide prediction tools.

2. **Functional genomics of fumarases explored through RNA interference (RNAi).** Using two RNAi techniques (small interfering and double stranded RNA), the knockdown of one and both *S. mansoni* fumarases was explored and phenotypic effects were assessed. For the purposes of long-term RNAi, different culturing techniques were optimised to ensure optimal health of adult worms over the course of 21 days for double stranded RNAi. Knockdown analysis of RNAi experiments was also determined to explore how the silencing of one gene affects the expression of the other.
3. **Computer aided drug discovery and compound screening using putative and known inhibitors of fumarases.** Homology models of the *S. mansoni* class I fumarase was created and used for *in silico* docking experiments to identify putative small-molecule inhibitors of class I fumarases. In tandem, the literature was explored to identify inhibitors of class II fumarases. Informed by RNAi experiments these screens were performed on schistosomula and adult worms of *S. mansoni*.

2 Materials and methods

2.1 Common buffers and solutions

2.1.1 General laboratory solutions

Phosphate buffered saline (PBS)

- NaCl (137 mM)
- KCl (2.68 mM)
- Na_2HPO_4 (8.10 mM)
- KH_2PO_4 (1.47 mM)
- pH 7.4

High Salt Lysogeny Broth (HSLB) Purchased as a ready mixed powder (Sigma Aldrich) The mix is dissolved at 25 g/L and autoclaved at 121°C for 15 minutes.

- Casein enzymic hydrolysate (10 g/L)
- Sodium chloride (10 g/L)
- Yeast extract (5 g/L)

HSLB-Agar plates

- 8 g of HSLB
- 4 g of High melt Agar (10 g/L; Sigma Aldrich)
- 400 mL of distilled H_2O

Autoclaved at 121°C for 15 minutes. Antibiotic was added once the mixture had cooled (Ampicillin 100 µg/mL, Kanamycin 50 µg/mL) and plates were poured and allowed to set. Once set, plates were sealed and stored at 4°C.

2.1.2 Parasite handling and life cycle maintenance

- Sodium pentobarbital with heparin

Mice were euthanised using 0.1 ml/10g of body weight sodium pentobarbital (JM Loveridge, 10mg/ml solution) with heparin added (100 U/ml, H3149, Sigma Aldrich)

Perfusion media:

- 10U/ml Heparin (H3149-50K, Sigma-Aldrich)
- High glucose (4500 mg/l) Dulbecco's Modified Eagle Medium (DMEM) (11594416, Fisher Scientific)

Adult worm culture media (general)

- DMEM (Fisher Scientific)
- 2% Antibiotic-Antimycotic (100X: Penicillin (100 units/ml), Streptomycin, (0.1 mg/ml)
- 10% v/v heat inactivated Foetal Bovine Serum (FBS) (11573397, Fisher Scientific)
- 2 mM L-glutamine (11539876, Fischer Scientific).

Percoll gradient

- 16 ml DMEM (Fisher Scientific)
- 24 ml GE Healthcare™ Percoll™ Centrifugation Media (10607095, Fischer Scientific)
- 2% Antibiotic-Antimycotic (100X) (Fisher Scientific)

M169 media

- 0.5 g Glucose
- 0.5 g Lactalbumin hydrolysate (61300-500G, Sigma-Aldrich)
- 43.25 mL of distilled H_2O
- 250 µl of hypoxanthine (1 mM) (H9636-1G, Sigma-Aldrich)
- 500 µl serotonin (1 mM) (H9523-100MG, Sigma-Aldrich)
- 500 µl hydrocortisone (1 mM) (H0888, Sigma-Aldrich)

- 500 µl 3,3”,5-triiodo-l-thyronine sodium (0.2 mM)
- 5 ml MEM vitamins (100 x) (M6895, Sigma-Aldrich) was added. M169 media was thoroughly mixed prior to syringe filter sterilisation using 0.22 µm filter.

Basch Media

- Basal Medium Eagle (BME) (11514476, Fisher scientific)
- 15.6 mM HEPES solution (H0887, Merck)
- 10% v/v M169 media
- 10% v/v Schneider’s insect media (S0146, Merck)
- 2% Antibiotic-Antimycotic (100X) (Fisher Scientific)
- 5% v/v FBS (Fisher Scientific).

AC Media 169

- Basch Media
- 200 µM Ascorbic Acid (A92902-25G, Sigma-Aldrich)
- 0.2% v/v Chemically Defined Lipid Concentrate (11548846, ThermoFisher).

Lepple water (10X):

- Distilled H_2O
- 5 mM $CaCl_2$
- 5 mM $MgSO_4$
- 0.25 mM K_2SO_4
- 5 mM $NaHCO_3$

Saline solution (2X)

- 291 mM NaCl dissolved in distilled H_2O.

Lugol's iodine

- 80 mM I_2
- 240 mM KI
- In distilled H_2O

2.1.3 Human cell culture and MTT

Human Caucasian hepatocyte carcinoma (HepG2) media

- 86 ml BME (Sigma-Aldrich)
- 10 ml FBS (Fisher Scientific)
- 1 ml MEM Non-essential Amino Acid Solution (100 x, M7145, Sigma-Aldrich)
- 1 ml L-glutamine (200 mM stock, 25030081, Invitrogen)
- 1 ml Antibiotic-Antimycotic Solution (100 x) (Sigma-Aldrich)
- 0.25 µg/ml Amphotericin B (11570486, Fisher Scientific)

MTT reagent (12 mM)

- 250mg 3-(4,5-dimethylthiazol-2-yl)-2,5-diphenyltetrazolium bromide (MTT, M2128, Sigma-Aldrich)
- 50.3ml 1 x PBS
- Filter sterilised using a 0.45µm acrodise syringe filter prior to aliquoting and storage at -20°C.

2.2 Maintenance of the *S. mansoni* life cycle

The NMRI (National Medical Research Institute) Puerto Rican strain (NMRI, Naval Medical Research Institute) of *S. mansoni* was used for all experiments and lifecycle maintenance. Vertebrate lifecycle stages were cultivated through the outbred Tuck Ordinary (HsdOla:TO, Envigo, UK) *Mus musculus* strain (Harlan, UK). Snail-specific lifecycle stages

were cultivated in two strains of *Biomphalaria glabrata*: the NMRI albino strain and an outbred strain (Geyer et al., 2017). All procedures were performed on animals in accordance with the UK Home Office (HO) guidelines (Scientific Procedures Act, 1986; PPL 40/3700 and P3B8C46FD) as well as the European Union Animals Directive 2010/63/EU and were approved by the Aberystwyth University's Animal Welfare and Ethical Review Body (AWERB).

2.2.1 Snail infection with *S. mansoni* miracidia for mixed and single-sex cercariae

B. glabrata with a shell diameter of ~0.5-1.0 cm were selected for infection with miracidia (Lee and Lewert, 1956) and immersed in 1x Lepple water. Infected mouse livers (section: 2.3.4) were homogenised in 2x saline solution to obtain *S. mansoni* eggs. Homogenates were passed through a 0.45 μm filter to remove liver material and retain the eggs, which were then transferred to a 500 mL volumetric flask. Eggs were incubated in 1x Lepple water under bright light for up to 1 hour. The bulb of the flask was covered in foil to block light and concentrate miracidia in the neck of the flask. Miracidia were collected from the neck using a Pasteur pipette and counted prior to infecting 100 snails/in 300 mL Lepple water tanks with ~12 miracidia per snail. Tanks were placed in the dark for 24 hours before being returned to normal ambient lighting.

For the generation of single-sex cercariae, individual *B. glabrata* (~0.5-1.0 cm shell diameter) were infected with a single miracidium in the well of a 12-well plate (Janse et al., 2018). Individual miracidium were separated under dissection microscope and placed into plate wells. Wells were topped up with ~2 mL 1x Lepple water and placed into the dark for 24 hours. After 24 hours, snails were placed into a small tank under ambient light.

2.2.2 Shedding of *S. mansoni* cercariae and mouse infection

Infected *B. glabrata* were moved into the dark 5 weeks post-infection (section: 2.3.1). *S. mansoni* cercariae were shed from infected snails by immersing snails in a small quantity of

1x Lepple water and exposed to direct light for up to 1 hour. Cercariae from different snail infections were pooled and 3x aliquots of 50 µL were killed and stained using Lugol's iodine for counting. The mean number of parasites in the aliquots was calculated to determine the concentration of the parasites. The volume required for ~180 cercariae was determined for use in mouse infection. Cercariae not used for mouse infection or generation of schistosomula by mechanical transformation (section: 2.3.3) were stored on ice for >45 minutes prior to centrifugation at 500 xg, 4°C for 5 minutes and stored appropriately for RNA extraction or generation of soluble antigen preparations. Mice were percutaneously infected through the tail with ~180 cercariae for 45 minutes. In the event of severe suffering of the animal, they were euthanised via Schedule 1 HO method (according to PPL P3B8C46FD).

Single miracidium-infected *B. glabrata* were treated and shed as described above, however, the snails were shed in 12-well plates in 1 mL of Lepple water under direct light for up to 1 hour. Wells were assessed to determine which snails were shedding cercariae under a dissection microscope. Snails that shed cercariae were placed into individual pots of 1x Lepple water for maintenance. Snails that did not shed were placed back into a small tank together and shed in successive weeks. If the snails were not shedding after 3 weeks, they were euthenised (in 70% ethanol). Cercariae from shedding snails were quantified by the mean of 3x 50µL aliquots and the volume for ~50 cercariae were calculated. Aliquots of approximately 50 cercariae were taken for use in qRT-PCR sex identification of the single-sex cercariae (section: 2.5.4). For the infection of mice, ~180 cercariae were used for percutaneous infection as described above. Following confirmation of single-sex immature adult worms (section: 2.2.4), single-sex cercariae were used to superinfect mice with ~750 cercariae (according to PPL P3B8C46FD).

2.2.3 Mechanical transformation of cercariae into schistosomula

Cercariae shed from infected *B. glabrata* (section 2.2.2) were left on ice for >45 minutes and pelleted by centrifugation at 300 xg, 4°C, 5 minutes with half brake applied. Excess Lepple water was removed using a serological pipette and all water was dispensed into beaker containing presept granules (12378667 Fisher Scientific) to kill any loose parasites. Multiple pellets were combined using a Pasteur pipette and culture media without FCS added to achieve a final volume of ~8-10 mL. Cercariae were vortexed twice for 45 seconds and placed on ice for a minute in between. The tails of the cercariae were then sheered by successive passage of the parasites through a 0.23-gauge needle and syringe at least 20 times. A 50 µL aliquot was then taken and assessed on a petri dish under dissecting microscope to determine if the transformation was successful, if intact cercariae remained the process was repeated. Transformed schistosomula were then transferred to a single percoll gradient using a serological pipette and centrifuged at 400 xg, 4°C, 10 minutes to separate the sheared tails. The supernatant was removed and the pellet was washed 3 times using Basch media without FCS and centrifugation at 400 xg, 4°C, 2 minutes in between and removing the supernatant between each wash. Basch media was then added to the pellet and the density of parasites was calculated using 3x 50 µL aliquots under a dissection microscope.

2.2.4 Recovery of adult worms

Mice infected with *S. mansoni* cercariae (section: 2.2.2) were sacrificed 7 weeks post-infection by intraperitoneal injection with a lethal dose of sodium pentobarbital (100 µl/10 g body weight). Once the ocular reflex was lost, the abdomen and rib cage were opened to expose the heart and hepatic portal vein which was then severed for hepatic-portal vein perfusion (Duvall and DeWitt, 1967). 30 mL of perfusion media, pre-heated to 37°C, was injected into the left ventricle of the heart using an 18 gauge needle and syringe. Adult worms were flushed out through the opened hepatic portal vein and collected in an inverted conical flask, and livers

were removed for use in the infection of *B. glabrata* (section 2.2.2). Perfused worms were allowed to settle to the base of the flask before the supernatant was removed using a serological pipette and washed with DMEM (37°C) at least once to remove contaminating mouse blood/tissue. Male and female worms were counted under a dissection microscope and processed further depending on the experiment performed.

For single-sex infections, livers were assessed to ensure no granulomas were present and worms were assessed under dissection microscope to ensure there were no members of the opposite sex within the infection. If only single-sex immature worms were present within the infection, the snails used in this infection were subsequently shed for superinfections (section: 2.2.2). After 7 weeks of superinfection with single-sex cercariae, mice were perfused as described above to generate a large quantity of male or female immature worms.

2.2.5 Assessment of adult worm health using WHO-TDR scoring matrix

Worm scoring was carried out using the WHO-TDR method described in Ramirez et al. (2007). Briefly, motility and health of the worms was assessed based on a numerical scoring system between 0-4 where each number was assigned to a motility description. The criteria were as follows: 4 = normal activity, full body movement and coiling; 3 = full body movement however activity is slowed; 2 = minimal activity with movement only at the head and/or tail of the worm, no movement of the body; 1 = total loss of activity throughout the worms body, movement in the gut still present; 0 = total loss of motility, no gut movement present. Worm motility was assessed under a microscope for 1-2 minutes. For long-term culture (2.2.6) and RNAi (2.6.4), 5 worm pairs were scored using this matrix for each replicate. Mean worm motility was calculated to observe trends in worm motility over the course of experiments as performed in Ramirez et al. (2007).

2.2.6 Long-term culture of adult worms

Adult worms were cultured in modified Basch Media, AC Media 169 (2.1.2) for 21 days. AC Media 169 was compared with three other culture media in a long-term pilot study of culturing 5 adult worm pairs. The other media tested over the course of a 28-day period were standard adult worm media, standard adult worm media with the addition of 200 µM ascorbic acid and a formulation of AC Media 169 using cholesterol lipid concentrate 250x (12531018, Gibco) at 0.2% v/v. The formulation of AC Media 169 described in section 2.2.2 was ultimately used in downstream experiments requiring long term culture of adult worms.

Five adult worm pairs were cultured in AC Media 169 for up to 21 days and medium was replaced every other day for long-term culture. These techniques were used in long-term RNAi experiments (Chapter 2.7.4). Health of the worms was assessed using WHO-TDR scoring matrix.

2.3 Bioinformatics and *in silico* procedures

2.3.1 Domain confirmation of $SmFH_I$ (class I fumarase) and $SmFH_{II}$ (class II fumarase)

Predicted amino acid sequences of Smp_126020 ($SmFH_I$) and Smp_158240 ($SmFH_{II}$) were downloaded from WormBase ParaSite during late 2019 (Parasite WormBase Version: WS271) from the *S. mansoni* genome (Version 7: Smansoni_v7, PRJEA36577). Domain searches were carried out using the Interpro database that incorporated databases such as Pfam (Punta et al., 2012) and PANTHER database (Thomas et al., 2022). $SmFH_I$ and $SmFH_{II}$ were aligned to profile hidden Markov models (HMM) (Eddy, 2011) of class I and class II fumarases respectively to ensure that the predicted amino acid sequences contained domains associated with the protein family. This approach was used with additional fumarases identified in this study to confirm that they belonged to the family. If enzymes did not contain the characteristic domains of class I or class II fumarases they were not used in further analysis or considered a fumarase.

2.3.2 $SmFH_I$ and $SmFH_{II}$ homolog searches

2.3.2.1 Naming system of phyla

Systematic biology is a dynamic field where nomenclature and groupings of clades based on molecular data can change based on novel discoveries. It is important to outline the naming systems used in this study for phylogenetic purposes.

It was decided that the metazoan naming system would follow the molecular based naming system derived from ribosomal RNA studies since the late 1980s (Adoutte et al., 2000; Bourlat et al., 2008; Field et al., 1988; Giribet, 2008; Paps et al., 2009). This system combines molluscs, annelids and platyhelminths into a single clade, lophotrochozoa that diverges from ecdysozoa. In line with using contemporary phylogenomic naming systems it was also decided to separate the traditionally grouped turbellaria into their modern groups (Egger et al., 2015). In the case of this study this described *Schmidtea mediterranea* as a tricladida and *Macrostomum lignano* as a macrostomorpha.

2.3.2.2 Basic Local Alignment Search Tool

Using the amino acid sequences of $SmFH_I$ and $SmFH_{II}$ and known representative class I (*Leishmania major* and *E. coli*) and class II (*Homo sapiens*, *E. coli*, *Arabidopsis thaliana*), a Basic Local Alignment Search Tool (BLAST) search was performed using peptide libraries (BLASTp). Searches were carried out against the ParaSite Wormbase database (parasite.wormbase.org). BLASTp searches against the NCBI (blast.ncbi.nlm.gov) non-redundant protein database were also performed for the identification of fumarases belonging to other phyla. Major phyla were searched extensively for both classes of fumarase, and iterative searches were conducted using the results of previous BLAST searches. Amino acids derived from BLASTp searches were considered homologs if they possessed high sequence similarity (cutoff *E* value of $1e^{-5}$ or lower) to at least one of the representative fumarases used in searches. For clades investigated with few representative species (e.g. Fungi and plants for

class I) representatives of these species were used in additional searches. Final confirmation that amino acid sequences were fumarases and didn't belong to closely related enzyme family members (e.g. Aspartase for class II), amino acid sequences were searched against the Pfam and PANTHER databases (2.3.1) to confirm they possessed the correct domains associated with class I and class II fumarases. If they did not possess these domains, they were removed from further analysis.

2.3.3 Mitochondrial targeting peptide (mTP) searches

TargetP 2.0 (Armenteros et al., 2019) web server (https://services.healthtech.dtu.dk/services/TargetP-2.0/) and MitoFates 1.2 (Fukasawa et al., 2015) web server (https://mitf.cbrc.pj.aist.go.jp/MitoFates/cgi-bin/top.cgi) were used to predict mitochondrial targeting peptides (mTPs) on fumarase homologs identified in BLAST searches (2.3.2). TargetP was developed through machine learning where the program was trained using protein data from UniProt containing different signal and targeting peptides in addition to a negative dataset with proteins known to not have any signalling peptides. Details on how the algorithm was developed and features involved in its determination can be found in the Armenteros et al. (2019) paper. MitoFates is similarly trained using datasets including an older version of TargetP in addition to the plant mitochondrial and plastid targeting database Predotar (Small et al., 2004). The training data also incorporated species-specific N-terminal cleavage data from *Saccharomyces cerevisiae*, *Arabidopsis thaliana* and *Oryza sativa*. Details regarding training of the model can be found in the Fukasawa et al. (2015) paper. In the case of both tools an mTP prediction >0.5 was considered to show an mTP.

2.3.4 Multiple sequence alignments

MUSCLE alignment tool (www.ebi.ac.uk/Tools/msa/muscle/; Edgar, 2004) was utilised to align class I and class II fumarase sequences for a range of downstream investigations. In all cases sequences were arranged in a FASTA format and uploaded to the

MUSCLE alignment tool. Outputs were in the ClustalW format and alignments were downloaded for downstream analysis.

2.4.4.1 Concatenation of homolog sequences and phylogenetic tree

FASTA amino acid sequences of class I and class II fumarase homologs were uploaded to MUSCLE for alignment. Multiple sequence alignments were then uploaded to the Gblocks server (version 0.91b, molevol.cmima.csic.es) to identify conserved regions (Castresana, 2000). Aligned sequences were visualised using Jalview v2.10 (Waterhouse et al., 2009) and non-conserved regions were removed. Concatenated sequences were visually inspected to determine whether further concatenation was required before use in phylogenetic analysis.

2.4.4.2 Multiple sequence alignments for homology modeling

For the construction of the homology model of SmFH $_{I}$, multiple sequence alignments were carried out using MUSCLE (EBI), where the amino acid sequence for SmFH$_{I}$ (ParasiteWormbase) was aligned with the X-ray crystal structure of *Leishmania major* class I fumarase LmFH-2 (PDB: 5l2R). Alignments were checked to ensure all residues crucial for class I fumarase active site formation and dimerisation were present within *Smfh$_{I}$* as described by Feliciano et al. (2016). This alignment was visualised using ESPript 3.0 and edited to show crucial amino acids for class I fumarase dimerisation and enzymatic function. Multiple sequence alignments were then used for the construction of homology models of SmFH (2.7.2).

2.3.5 Gene expression in *S. mansoni* lifecycle stages

2.3.5.1 DNA microarray analysis

A Transcriptome DNA microarray database (Fitzpatrick et al., 2009) consisting of 37,632 elements was interrogated by nucleotide BLAST (BLASTn). Transcription patterns of *Smfh$_{I}$* and *Smfh$_{II}$* across 10 lifecycle stages were determined (cercariae, 3-hour schistosomula,

24-hour schistosomula, 72-hour schistosomula, 6 day schistosomula, 21 day worm, 35 day worm, 49 day mixed-sex worms, 49 day male worm and 49 day female worm). Nucleotide sequences from WormBase ParaSite (parasite.wormbase.org) of *Smfh*$_I$ and *Smfh*$_{II}$ were used in BLASTn searches against an internal Aberystwyth Microarray search engine to identify contigs that aligned with 50mers used in the microarray experiment. The contig that showed the greatest sequence similarity to *Smfh* $_I$ and *Smfh* $_{II}$ was used to search the database and generate histograms from the lifecycle expression based on mean fluorescence intensity (normalised $\log_2$ AF647 intensity).

2.3.5.2 RNA-seq data analysis

Meta-analysis of RNA-seq studies (Lu and Berriman, 2018) were interrogated using an online server (v7test.schisto.xyz). *Smfh* $_I$ and *Smfh* $_{II}$ were searched against this database and expression data was mined from outputs. The human-infective lifecycle stages was the focus of this study and data was incorporated from cercaria, 3-hour schistosomula, 24 hour schistosomula (Protasio et al., 2012), 3 week, 4 week, 5 week and 6 week worms originating from a mixed-sex infection and 6 week worms from single-sex infections (Lu et al., 2016). All lifecycle stages beyond the 24-hour schistosomula were separated into male and female. These data were visualised as histograms showing the normalised expression units as determined by Lu and Berriman (2018).

2.3.5.3 Single-cell transcriptome analysis

Single-cell transcriptome data of adult male, female and immature female worms were interrogated using the SchistoCyte Atlas servers (Wendt et al., 2021). Gene IDs were (Smp_126020 and Smp_158240) entered into the search engine site (https://www.collinslab.org/schistocyte/). Plots were generated showing the normalised relative expression within individual cells and tissue types by the search engine. Data were analysed and normalised using the Seurat workflow (Satija et al., 2015).

2.3.6 Phylogenetic analysis

Following concatenation of multiple sequence alignments 2.3.4.1, sequences were used to generate phylogenetic trees by two methods, maximum likelihood and Bayesian inference.

2.3.6.1 Maximum-likelihood

Concatenated alignments were uploaded to MEGA X (Kumar et al., 2018). Alignments were viewed in MEGA to confirm they were converted correctly to the MEGA formatting prior to phylogenetic analysis. The maximum likelihood method and JTT (Jones et al., 1992) matrix-based model were used to determine the evolutionary history of class I and class II fumarases. Bootstrap consensus trees (Felsenstein, 1985) were inferred from 1000 replicates (class I fumarases) and 2500 replicates (class II fumarases). Two trees were generated in this analysis, the 'original tree' which represented the tree with the highest log likelihood determined by these methods showing percentage of trees that contained the branches. The second tree was the bootstrap consensus tree where branches with less than 50% likelihood were discarded. Bootstrap values were used as support for Bayesian inference branches if shared between the two trees.

2.3.6.2 Bayesian inference

Concatenated fumarase sequences were converted to NEXUS files using Mesquite v3.51 (www.mesuiteproject.org). NEXUS files were run using MrBayes v3.2.7 (Huelsenbeck and Ronquist, 2001). Parameters for Bayesian inference trees were as follows; class I fumarases: generations = 3,000,000, burninfrac = 0.25, sample freq = 1000. Class II fumarases: generations = 1,000,000, burninfrac = 0.25, sample freq = 1000.

2.3.6.3 Consensus tree

Bayesian inference trees generated in 2.3.6.2 were visualised using FigTree v1.4.4 (tree.bio.ed.ac.uk). Trees were rooted at *E. coli* fumarases and trees were edited to show

probability scores at the nodes. Bootstrap consensus scores were added to branches that were supported in both types of phylogenetic analyses. Where branches were not shared with the Bootstrap tree, an (X) was labelled next to the probability score.

2.3.7 Computer Aided Drug Discovery (CADD)

2.3.7.1 Homology modelling

Protein models of $SmFH_I$ were made using software MOE 2014.09 (Chemical Computing Group LLC). This program was used heavily in the model creation and visualisation of docking. The crystal structure of LmFH-2 was downloaded from PDB and used to coordinate the homology model in the MOE workspace. Homology modelling was performed using a combination of segment-matching and the insertion/deletion of regions (Dolan et al., 2012). Segment-matching methods indicate that oligopeptides of six amino acids (hexamers) that are present in a protein can be classed in 100 structural classes (Unger et al., 1989). Using the segment-matching approach, atomic positions were derived from the target template PDB: 5L2R as a guide to identify matching segments for the construction of the 3D model.

The amino acid sequence for $Smfh_I$ was uploaded to MOE and alignments with 5L2R were adjusted based on the alignment generated in 2.7.1. Induced fit modelling based on PDB coordinates was performed in the presence of crystalisation solvents, metal cofactors, water molecules and substrates to improve the fit of the model. Water molecules and crystallisation solvents were later removed from the model. Ten models of *Smfh* were created using the knowledge-based loop searching method and side chain rotamer selection method. Following this a Cartesian average model was generated. MOE structure preparation tool was used to construct missing loops in the protein model and steric clashes were removed using energy minimization tool AMBER94 force field.

Visual inspection of the final model was carried out to ensure reasonable conformation

before being subjected to stereochemical quality control using several tools: RAMPAGE (Ramachandran Plot Analysis) (Lovell et al., 2003), ProSA-web (Protein Structure Analysis) (Wiederstein and Sippl, 2007), and Verify-3D (Bowie et al., 1991).

Homology models were successfully generated and formatted for use in Maestro v10.1 for *in silico* docking experiments to identify putative inhibitors of $SmFH_I$.

2.3.7.2 *In silico* docking

The homology model of *Smfh*$_I$ was uploaded to Glide docking software within Maestro v10.1 (released in 2014). Preparation of the docking site for investigation and selection of the compound library to be screened were prepared prior to the experiments. The Specs library (www.specs.net) containing 300,000 commercially available compounds was selected for screening and downloaded in an sdf format compatible with Glide. An appropriate docking site on the homology model was then selected. The active site cavity described in X-ray crystallography studies (Feliciano et al., 2016; Feliciano and Drennan, 2019) was selected as a site to block substrate interactions and access to the active site. Ala-337, Gly-336 and His-335 were selected as a centroid for the docking grid due to their presence within the active site cavity and proximity to the active site. The docking grid around the active site cavity was used for docking experiments.

Virtual screening of compounds from the Specs library were carried out following a standard pipeline with increasing stringency to identify compounds with the best predicted binding. Docking simulations consisted of each compound being virtually docked in the designated docking site and predictions of binding modes were carried out using different algorithms. These algorithms determine how well the compounds bind with the docking site in different positions and rank them based on energy (kcal/mol). The lower this value, the higher its affinity to binding to the target. Firstly high-throughput virtual screening (HTVS) was performed. This step is capable of screening millions of compounds by performing docking

experiments at a rate of 2 seconds/compound with limited sampling and repeats. After this initial screen 222,000 compounds from the original 300,000 remained. The Glide standard precision (SP) sampling method was applied to the remaining compounds and performs a more exhausting sampling process taking 10 seconds/compound. Compounds that were predicted to dock using SP were then examined using the extra precision (XP) docking protocol in Glide, which utilises an anchor-and-grow sampling approach to ensure the highest accuracy in the Glide pipeline and remove false positives generated through the previous steps. This is the most stringent approach on Glide and takes 2 minutes/compound. Compounds identified in this pipeline were then rescored using two additional programs, FlexX (LeadIT v2.1.3) and PLANTS (Korb et al., 2009). FlexX works by considering the target as rigid but the compound as flexible. The program changes the conformation of the compound within the target site and rapidly generates a geometric prediction of the protein-compound complex. PLANTS treats the compound as flexible and the target site as both rigid and flexible. Empirical scoring functions described in Korb et al. (2009) are used to score the interactions. Compounds that were hits in XP, FlexX and PLANTS were considered putative inhibitors of $SmFH_I$.

2.3.8 ChEMBL database search

The ChEMBL database is a manually curated database of compounds that possess bioactive and drug-like properties (Davies et al., 2015). This database collates data related to chemical properties, bioactivity and target predictions/identities for different compounds. This database can be searched using targets to identify literature and compounds known to target homologs of a searched sequence. $SmFH_I$ and $SmFH_{II}$ were BLASTp searched against this database and compounds identified using this database were used in downstream drug screening.

2.4 Polymerase Chain Reaction (PCR)

2.4.1 Total RNA extraction and cDNA synthesis

Two kits, Direct-zol RNA MiniPrep Kit (Zymo Research) and MasterPure™ Complete DNA and RNA Purification Kit (Lucigen), were used for the extraction of total RNA of *S. mansoni* lifecycle stages.

Direct-zol: For adult worms, either 10 worms of individual sex or 5 worm pairs (male and female) were used. For the extraction of cercariae or schistosomulae, a minimum of 100,000 parasites per sample were used. Parasite material was frozen at -80°C in the presence of TRIzol (ThermoFisher) of a volume sufficient to immerse the material (typically 500-1000µL). Adult worm material was homogenized using a TissueLyser LT (Qiagen) for 2x 5 minutes at 50 Hz. Cercariae and schistosomula were homogenized on ice with a hand-held tissue homogenizer (Qiagen) for 6X 20 second bursts at setting 3. Samples were centrifuged at 10,000 xg for 10 minutes to remove insoluble material. Total RNA was extracted following manufacturer's instructions.

MasterPure™: For adult worms, one or two worms (either single sex or mixed) were used per-extraction. For cercariae or schistosomula >3000 parasites were used per-extraction. Parasite material was immediately frozen at -80°C after all medium was removed from samples. Samples were thawed for extraction and lysed using proteinase K as described in the manufacturer's instructions under the section for tissue samples. Total nucleic acid was extracted prior to DNase I treatment for 1 hour (5µl of 1U/µl diluted up to 200µl using 1x DNase buffer per sample. See instruction manual). DNA-free RNA was liberated by ethanol precipitation overnight at -20°C (see instruction manual for details). RNA pellet was resuspended in 30µl of double distilled H_2O. Concentration of total RNA extracted by both methods was quantified using a Nanodrop-2000 spectrophotometer (ThermoFisher Scientific, Wilmington DE, USA).

Total RNA extracted from parasite material was used as a template for synthesising cDNA by reverse transcription using the SensiFAST cDNA synthesis kit (Bioline). Briefly, 100 ng-1 µg of RNA was added to 4 µL of 5xTransAmp Buffer and 1 µL of Reverse Transcriptase in a total reaction volume of 20 µL (nuclease-free H_2O used). Reverse transcriptase negative reactions were also prepared to identify gDNA contamination. Primer annealing occurred at 25°C for 10 minutes followed by the reverse transcription step at 42°C for 15 minutes. Finally, the reaction was inactivated by heating the reaction mix to 85°C for 5 minutes. The cDNA product was then diluted up to 100 µL with nuclease free H_2O and stored at -20°C. All cDNA used for the same analysis were synthesised using the same concentration of RNA template and were therefore considered comparable concentrations following dilution.

2.4.2 gDNA extraction

To identify the sex of cercariae being shed from mono-miracidial infection (section 2.3.1), aliquots of 50 cercariae were taken from individual snail sheds (section 2.2.2). Cercariae were placed on ice for up to an hour and spun down at 500 xg for 5 minutes. Lepple water was removed and dispensed into 70% EtOH. Parasites were then frozen at -80°C until extraction. gDNA was extracted using the ISOLATE II Genomic DNA Kit (Bioline) following manufacturer's instructions.

2.4.3 PCR amplification

2.4.3.1 Design of full-length *Smfh$_I$* and *Smfh$_{II}$* primers

Primers were designed to amplify the full-length coding sequence (CDS) predictions of *Smfh$_I$* (smp_126020) and*Smfh$_{II}$* (smp_158240) from start to STOP codon, excluding any 5′ and 3′ untranslated region (UTR) (See table 2.1). The full-length products were expected to be 1713 bp (*Smfh$_I$*) and 1467 bp (*Smfh$_{II}$*). Primers were designed using the Sigma Aldrich custom oligo ordering system.

Table 2.1 Full-length *Smfh$_I$* and *Smfh$_{II}$* Primers

	Name/Target	5´-to 3´- sequence	Tm°C
Forwards	*smfh$_I$* (FL) FW	ATGAATGTTAAATTAATGTCAGCTCAAG	63.10
Reverse	*smfh$_I$* (FL) RV	CTATTCTACTTGCCATTCCTTAAAGAAA	63.40
Forward	*smfh$_{II}$* (FL) FW	ATGTTAGAAACAGATTCACAACGTTTAC	63.10
Reverse	*smfh$_{II}$* (FL) RV	TCATTTGTTGTTATGAGGAAAGGC	64.80

2.4.3.2 Optimising annealing temperature

Mixed-sex adult worm cDNA was synthesised and tested for gDNA contamination (section 2.4.2) and used for PCR amplification using BioMix™ (Bioline). Manufacturer's instructions were followed including standard PCR reaction with minor modifications (Table 2.2). Annealing temperatures were tested in a gradient (56°C-62°C) for SmFH $_I$ and SmFH $_{II}$ primer sets. The optimum temperature for both sets of primers was discovered (60°C) for the full-length product of both primer sets (Table 2.1).

Table 2.2 Standard protocol for BioMixTM (Bioline)

Template cDNA	**Biomix**	**Forward Primer**	**Reverse Primer**	**Final Volume**
4 µL	12.5 µL	0.5 µL	0.5 µL	25 µL
1 cycle		**35 cycles**		**1 cycle**
Denaturation	**Denaturation**	**Annealing**	**Extension**	**Extension**
95°C 2 min	95°C 30 sec	T°C 30 sec	72°C 30 sec/Kb	72°C 2 min

2.4.4 DNA Electrophoresis

Visualisation of appropriately sized amplicons of PCR products was separated by gel electrophoresis. 10 µL of PCR product was mixed thoroughly with 2 µL of 6x DNA loading

dye (ThermoFisher) or TriTrack DNA Loading Dye (6x) (ThermiFisher). Samples were loaded onto a 1% w/v agarose gel containing 1/20,000 of SybrSafe (Invitrogen). Electrophoresis was carried out using a Bio-Rad Powerpac 300 electrophoresis power pack at 80-100V for 20-40 minutes. DNA bands were visualised under ultraviolet light using a BIOSpectrum Multi Imaging Unit (UVP) and corresponding software.

2.4.5 Cloning and sequencing of *Smfh$_I$* and *Smfh$_{II}$*

2.4.5.1 T/A Ligation into pGEMT-easy

Amplified DNA that showed a single band of appropriate Kb size when compared with a ladder (section 2.4.4) were used for T/A ligation into pGEM®-T easy vector plasmid (Promega). A standard pGEM®-T easy reaction consisted of:

- 3 µL of *Smfh$_I$* or *Smfh$_{II}$* PCR product
- 5 µL of 2X Rapid Ligation Buffer
- 1 µL pGEM®-T easy Vector (50 ng)
- 1 µL T4 DNA Ligase (3 Weiss units/µL)

Reactions were incubated overnight (12-17 hours) at 4°C and were either used directly for transformation into *E. coli* or stored at -20°C.

2.4.5.2 Transformation of vector into Escherichia coli α-select bronze efficiency cells

Smfh$_I$/pGEM®-T easy and *Smfh $_{II}$*/pGEM®-T easy constructs were transformed into α-select chemically competent *E. coli* Bronze efficiency cells (Bioline) by heat-shock. *E. coli* were thawed on ice for 10 minutes. 5µL of ligated plasmid was added to 50µL of thawed bacteria suspension and agitated before incubation on ice for 30 minutes. Heat shock was carried out on a heat block set to 42°C for 30 seconds before placing on ice for 2 minutes. Transformation reaction was then diluted with 900µL of SOC media and placed in a shaking incubator for 60 minutes at 37°C and 250rpm.

Transformants were grown overnight on HSLB agar plates containing 100 µg/mL ampicillin. Blue/white screening was carried out to identify colonies containing plasmids (conferring ampicillin resistance) by the addition of 100 µL of 100 mM Isopropyl-β-D-1-thiogalactopyranoside (IPTG) and 50 µL X-Gal at 20 mg/mL to the agar plates. Colonies that contained a desired vector were white and a representative number of colonies were picked (>4). Each picked colony was added to 5-10 mL of HSLB with 100 µg/mL ampicillin and grown at 37°C o/n. Additionally, colonies were picked for use in colony PCR (section 2.4.6.1). For long-term storage of cells, glycerol stocks consisting of 150 µL of 100% glycerol mixed with 850 µL of the cell mixture were prepared and stored at -80°C.

Remaining cultures were used in the extraction of pGEM ®-T easy constructs using a mini-prep plasmid purification kit (Bioline). All centrifugation was carried out at 11,000 xg. Up to 5 mL of cells were pelleted for 1 minute using 1 mL of the culture per centrifugation. Cell pellets were lysed for 5 minutes in 250 µL lysis buffer and terminated with the addition of 350 µL neutralisation buffer. Lysate waspelleted for 5 minutes and supernatant was transferred to spin columns provided. DNA was bound to the column and washed with 600 µL of wash buffer and finally eluted in 30 µL of nuclease free water.

2.4.6 Verification of insert sequence

2.4.6.1 Colony PCR

E. coli colonies that demonstrated uptake of pGEM®-T easy plasmids with an insert by blue/white screening (section 2.4.5.2) were picked and re-suspended in nuclease free water. This mixture was used as the template DNA for PCR reactions following BioMix ™ (bioline) instructions (described in section 2.4.3.2). Inserts were assessed using full length *Smfh* $_I$ and *Smfh*$_{II}$ primers depending on the expected insert. PCR products were visualised using gel electrophoresis (section 2.4.4). Colonies that showed a PCR product of expected size were then used in plasmid extractions (section 2.4.5.2)

2.4.6.2 In house sequencing

Sequencing was carried out at the IBERS Sanger sequencing facility, Aberystwyth University. Briefly, 250ng of pGEM®-T easy plasmid containing *Smfh I* or *Smfh II* inserts were prepared in a total volume of 10 µL using nuclease free water. 2 µL of sequencing primers (10 mM stock concentration) were added to the mixture for a total volume of 12 µL. For pGEM®-T easy plasmid sequencing, T7 (forward sequencing) and M13 (reverse sequencing) primers were used. DNA was sequenced using an ABI 3100 DNA analyser by capillary array sequencing (IBERS, Aberystwyth University). Sequencing data was analysed using FinchTV v1.4.0 (Geospiza, Inc.; Seattle, WA, USA; available at: http://www.geospiza.com). Sequencing results were checked for quality of sequencing (clear and defined peaks) and nonessential sequences such as the plasmid sequence or sequencing primer sequences were removed. Due to the length of the sequences (*Smfh I*: 1713 bp; *Smfh II*: 1467 bp), forward and reverse sequencing results were used to determine whether the entire sequence was present within the plasmid. Multiple sequence alignments of the forward and reverse sequencing results were compared with the predicted CDS of *Smfh I* and *Smfh II* (parasite.wormbase.org) using Clustal Omega (ebi.ac.uk).

2.5 Quantitative Reverse Transcription-PCR (qRT-PCR)

2.5.1 Primer design

The sequences confirmed by laboratory cloning of *Smfh I* and *Smfh II* were used for the design of qRT-PCR primers (Table 2.3). Both *Smfh I* and S*mfh II* showed predicted alternative splices by the genome. *Smfh I* showed two predicted splice variants with exon 5 being present in all variants. A constant region was selected for primer design that would generate a PCR product of 154 bp (Table 2.3). For *Smfh II* there were three predicted alternate splice variants. Exons 4 and 5 were present in all three and primers were designed that spanned both of the exons that was 238 bp in length (Table 2.3).

Table 2.3 Primers used in qRT-PCR

Target genes				
	Oligonucleotide Primers	**Tm°C**	**Size bp**	**Efficiency %**
smfh$_I$	FW: 5′-GCCTGACTATTTACGTAATCACCCA-3′	65.60	154	103[1]
	RV: 5′- CAGCATAATCATACTTCCTCCGG-3′	65.40		
smfh$_{II}$	FW: 5′- TTGGACAAGAACTGAGTGGA-3′	60.90	238	103[1]
	RV: 5′- GCTGGTTTGAAAATGAGATCTAC-3′	60.60		
Housekeeping genes				
SmRGBD	FW: 5′- CGGCTTTAACTCGCCTACAC-3′	63.60	186	103[1]
	RV: 5′- CATTCGACGGTTGTTCACAC-3′	64.10		
SmTscD	FW: 5′ - GCCAACAAATTTCGTGGTCT-3′	63.80	228	104[1]
	RV: 5′ - TTCACCATTTCGGTCGTACA-3′	63.90		
SmAT1	FW: 5′ - CTTCGAACCAGCAAATCAGA - 3′	62.90	158	99
	RV: 5′ – GACACCAATCCACAAACTGG - 3′	62.90		

2.5.2 Confirmation of on-target annealing

cDNA synthesised from mixed-sex adult worm total RNA (2.2.1) and used in a BioMix (Bioline) PCR reaction (section 2.4) with annealing temperature gradients (58°C-62°C) for *smfh$_I$* and *smfh$_{II}$* primer pairs to ensure the optimum annealing temperature was around 60°C. The PCR products were visualised on an agarose gel alongside a 100 bp ladder (GeneRuler 100 bp DNA Ladder, ThermoFisher). If the products were of the correct size, PCR products were ligated into pGEM ®-T easy vectors and transformed into α-select Bronze efficiency *E. coli* (section 2.5.5.2). Plasmids were then extracted from overnight cultures and used for in-house sequencing ensuring amplification of the expected regions (section 2.5.6.2).

2.5.3 qRT-PCR reactions

cDNA was synthesised from 500 ng total RNA of 10 lifecycle stages associated with the human infection: cercariae, schistosomula (24 hour), 3 week, 5 week, 6 week and 7 week worms, 7 week male and female worms from a mixed sex infection and 7 week male and females from a single sex infection (section 2.5.1). All qRT-PCR reactions were prepared in duplicate in 96-well MicroAmp PCR plates and carried out using a StepOnePlus Real-Time thermal cycler (Applied Biosystems). Reaction mixtures contained 2 µL of lifecycle cDNA in a total volume of 10 µL which included 5 µL of SensiFAST™ SYBR® Hi-ROX Kit (Bioline, London, UK), 0.2 µL of each forward and reverse primer (10 mM stock) and 2.6 µL of nuclease free water. Negative controls consisting of the same reaction mix for each primer set used with 2 µL of nuclease free water instead of template DNA. The PCR reaction consisted of: 95°C for 20 seconds; 35 cycles of: 95°C for 1 seconds, 60°C for 20 seconds. Melt curve analysis of PCR products were conducted to determine the amplification of a single PCR product which consisted of 95°C for 15 seconds, 60°C for 60 seconds and increased to 95°C in 0.3°C increments.

2.5.4 qRT-PCR results analysis

2.5.4.1 Amplification efficiency

Amplification efficiency of *smfh*$_I$ and *smfh*$_{II}$ primer pairs was calculated prior to transcript abundance experiments. To calculate efficiency, lifecycle expression data from Fitzpatrick et al.,(2009) was analysed to identify a suitable lifecycle stage that was predicted to express *smfh*$_I$ and *smfh*$_{II}$. Mixed-sex 7 week adult worms cDNA was used as a template and five serial 10-fold dilutions were made from the template that was generated from 500 ng of RNA.

Results were analysed using the StepOne Software v.2.1 (Applied Biosystems) using the comparative *Ct* method ($\Delta\Delta Ct$) where the fluorescence threshold value was selected within

the exponential phase of the amplification curve for each primer pair. *Ct* value was determined by the cycle in which the fluorescent signal exceeded the given threshold. The mean of *Ct* values of each template dilution were determined across triplicates and plotted against $\log_{(\text{dilution factor})}$ to generate a line of best fit (y = mx+c). Amplification efficiency (E) was calculated using the following equations:

$$\boldsymbol{E = (10^{\frac{-1}{m}}) - 1}$$

2.5.4.2 Geometric mean analysis

Data were analysed using the Geometric mean method/Vandesompele method (Vandesompele et al., 2002) and described in (Cardoso et al., 2021). Briefly, the Δ*Ct* was determined using the equation:

$$\boldsymbol{\Delta Ct = Calibrator\ Ct - Sample\ Ct}$$

Where the *Calibrator Ct* was selected as the highest mean *Ct* (Hellemans et al., 2007). Using the Δ*Ct*, relative quantities (RQ) of target and housekeeping genes were determined using the equation:

$$\boldsymbol{RQ = E^{\Delta Ct}}$$

Where E denotes the primer efficiencies of primer pairs. Finally, relative gene expression was determined using the equation:

$$\boldsymbol{Relative\ Gene\ Expression = \frac{RQ_{GOI}}{GeoMean[RQ_{SmRGBD}, RQ_{SmTscD}]}}$$

Where GOI stands for gene of interest (*Smfh* $_I$ and *Smfh* $_{II}$). Histograms were generated from these results showing the relative gene expression ± Standard deviation.

2.6 RNA interference (RNAi)

2.6.1 Cloning vector for synthesis of double stranded RNA

Primers were designed over target genes (*Smfh*I and *Smfh*II) spanning up to 700 bp (table 2.4). Similarly, primers were designed for the amplification of firefly luciferase (table 2.4). *Smfh*$_I$ and *Smfh*$_{II}$ primers were used to amplify inserts from mixed adult worm cDNA (2.4.1) and luciferase was amplified from the Luciferase-pcDNA3 plasmid containing firefly luciferase (addgene #18964; Safran et al., 2006).

Table 2.4 Primers used for the amplification of pJC53.2 inserts for use in dsRNA synthesis

	Name/Target	5´-to 3´- sequence	Tm°C	Product (bp)	Size
Forward	*Smfh*$_I$ (dsRNA) FW	AGTCGCTCCACTGGATCT	60.0	543	
Reverse	*Smfh*$_I$ (dsRNA) RV	GTTATTCTTCCAAGAATCTGCC	60.5		
Forward	*Smfh*$_{II}$ (dsRNA) FW	TTGGACAAGAACTGAGTGA	56.7	607	
Reverse	*Smfh*$_{II}$ (dsRNA) RV	GCAAAACAACGTGTCGAA	61.0		
Forward	Luc (dsRNA) FW	CCAGGGATTTCAGTCGATG	63.1	536	
Reverse	Luc (dsRNA) RV	TGATACCTGGCAGATGGAA	61.7		

A cloning vector for double stranded RNA (dsRNA), pJC53.2 (addgene #26536; (Collins et al., 2010)) was used (figure 2.1). To prepare the vector for inserts, plasmids were digested using Eam1105I (ThermoFisher: FD0244), a restriction enzyme that recognises GACNNN^NNGTC. This digestion leaves overhanging T bases, which can be used for ligation (Figure 2.2). Digestion reaction consisted of:

- 1µg pJC52.3
- 1µl Eam1105I
- 2µl FastDigest Buffer
- to 20µl with DEPC treated water

Reactions were then incubated at 37°C for 60 minutes. Following digestion, plasmids were ligated using un-purified PCR products consisting of:

- 4µl un-purified PCR product
- 150ng pJC53.2 (digested)
- to 10µl with H2O
- 10µl 2x Rapid Ligation Buffer
- 1µl t4 DNA Ligase (NEB)

Ligation reactions were incubated at 4°C overnight. Ligated plasmids were then transformed into α-select bronze (Bioline) (2.4.5.2). Cells were grown on agarose plates containing Ampicillin 100µg/ml, Kanamycin 50µg/ml. Colonies were picked and a colony PCR was performed (2.4.6.1) using T7 high-melt primers (GGATCC-TAATACGACTCACTATAGGG), which amplify both ends of the insert due to identical sequences on pJC53.2. Cells showing successful amplification were grown overnight and extracted plasmids were sequenced.

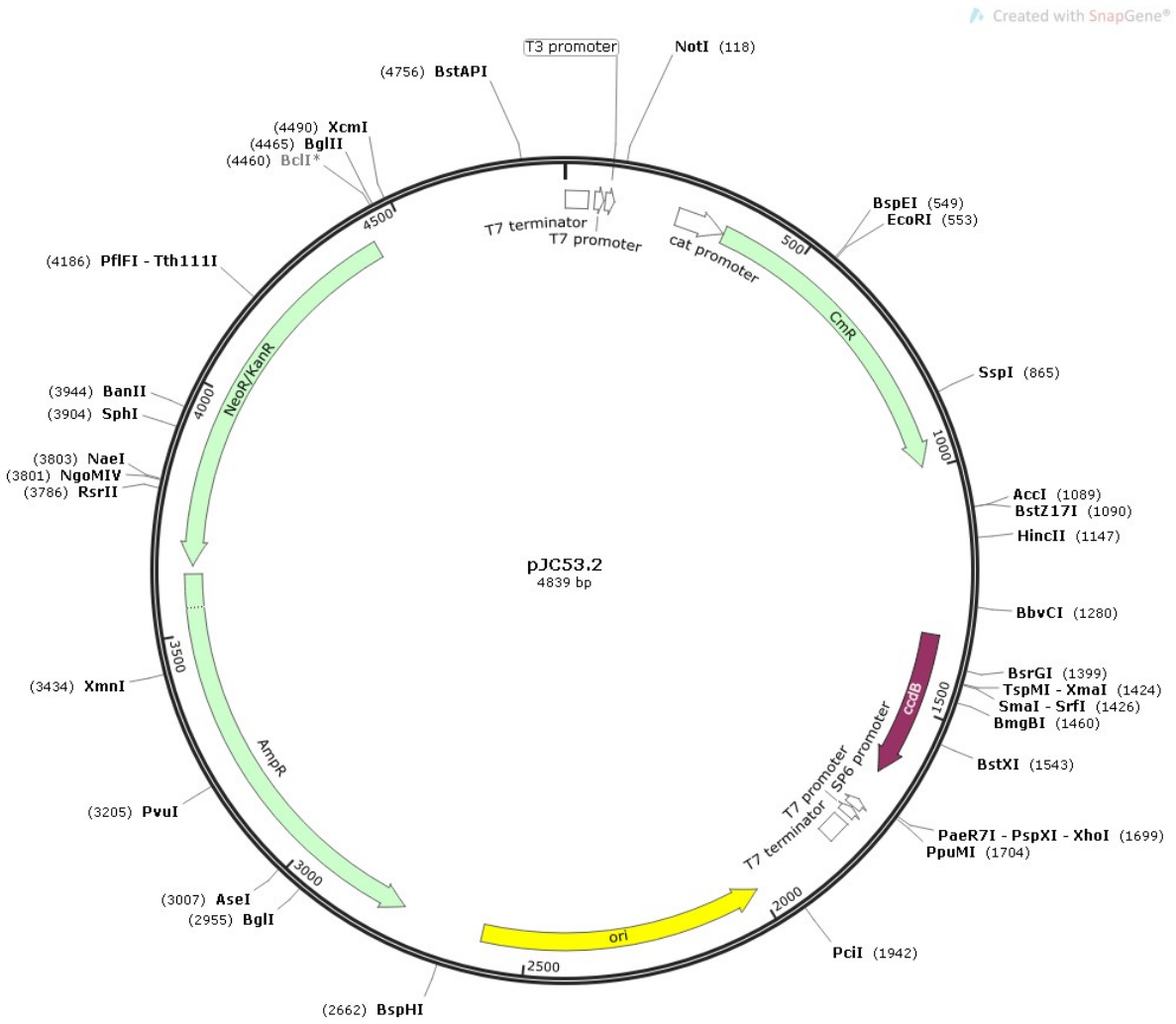

Figure 2.1 pJC53.2 plasmid map for double-stranded RNA synthesis. Main features include ori (origin of replication), T7 terminator, SP6 promoter, ccdB (toxin protein), CmR (chloramphenicol resistance), cat promoter, T7 promoter, NeoR/KanR (neomycin/kanamycin resistance). Other features on the outside of the map denote restriction sites.

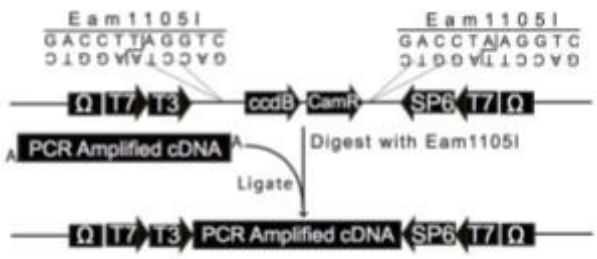

Figure 2.2 Digestion and ligation of pJC53.2. Eam1105I recognises GACNNN^NNGTC leaving T-overhangs and removing the genes for ccdB and CamR. PCR products of the cDNA of target genes is then ligated into the plasmids using T4 DNA Ligase.

2.6.2 dsRNA synthesis

Fumarase and luciferase inserts in pJC53.2 plasmids were amplified using PCR to generate template for *in vitro* transcription. The following PCR reaction was used to amplify inserts:

Components:

- 12.5µl Biomix reaction mix
- 12.1µl Nuclease Free H_2O
- 0.2µl 100µM high-melt T7 primer (GGATCCTAATACGACTCACT-ATAGGG)
- 0.2µl pJC53.2-based plasmid

PCR cycle conditions:

- Stage 1
    - 1 x: 2 mins 95°C
- Stage 2
    - 39x: 30 secs 95°C, 30 secs 55°C, 1 min 72°C
- Stage 3
    - 1x: 2 mins 72°C

Resulting PCR products were used for *in vitro* transcription in the following reaction mixture:

- 10µl unpurified PCR product
- 10µl High-yield transcription buffer
- 5µl rNTPs (100 mM, Promega)
    - rATP
    - rCTP
    - rGTP
    - rUTP
- 10µl T7 polymerase (100 µg/ml)
- 1µl Pyrophosphatase, Inorganic (*E. coli*) (NEB)
- 49µl DEPC-treated water

In vitro transcription reactions were left overnight at 37°C. Reactions were then precipitated by the addition of 50µl Sodium Acetate (pH 5.5) and 750µl 100% ethanol. Precipitation was carried out for a minimum of 17 hours at -20°C. Following precipitation, RNA was centrifuged at 10,000 Xg and all supernatant was removed. 300 µl of DEPC treated water was added to the RNA pellet and quantity was evaluated a Nanodrop-2000 spectrophotometer (ThermoFisher Scientific, Wilmington DE, USA). dsRNA was diluted to 1µg/µl as a working solution for RNAi experiments.

2.6.4 Double Stranded RNAi of adult *S. mansoni*

Adult worms were separated into groups of five male and female pairs and placed into 6-well culturing plates. Worm pairs were cultured in 3 ml of AC Media 169. Treatments of 30 µg/mL dsRNA of *Smfh*, *Smfh*$_{II}$ and a treatment containing 30 µg/mL of *Smfh* and *Smfh*$_{II}$ dsRNA was carried out in triplicate. Additionally triplicate controls were also carried out

consisting of 30 µg/mL Luciferase dsRNA and 60 µg/mL dsRNA Luciferase. Culturing lasted for 21 days and media exchanges were carried out as described in table 2.5. After 14 days, two males and two females were removed from each treatment for RNA extraction and downstream knockdown confirmation using the MasterPure™ kit (2.4.1).

Table 1.5 Schedule for dsRNAi experiment over 21 days.

D1	**D2**	**D3**	**D4**	**D5**	**D6**	**D7**
Media/dsRNA	Media/dsRNA	Media/dsRNA		Media/dsRNA		Media/dsRNA
D8	**D9**	**D10**	**D11**	**D12**	**D13**	**D14**
	Media/dsRNA		Media/dsRNA		Media/dsRNA	Remove worms for qPCR
D15	**D16**	**D17**	**D18**	**D19**	**D20**	**D21**
	Media/dsRNA		Media/dsRNA		Media/dsRNA	End of experiment

2.7 Compound screening

2.7.1 Compound preparation and storage

Compounds identified in CADD were purchased from Specs as a dry powder. Compounds were resuspended in dimethyl sulfoxide (DMSO) at a stock concentration of 10mM upon delivery and aliquoted into smaller volumes. All stocks were stored at -20°C prior to use. Positive controls for compound screens included praziquantel (P4668, Sigma-Aldrich, UK) and auranofin (A6733, Sigma-Aldrich, UK) which were resuspended and stored under the same conditions as Specs compounds.

2.7.2 Synthesis of 2,3-dicarboxyaziridine

A single compound was identified using ChEMBL (2.3.8) against class II fumarases. Commercial sources of the compound, 2,3-dicarboxyaziridine, were not viable as they were either no longer in stock or costs were beyond the budget for this project. Colleagues at the University of Dundee were able to synthesise the compound as described by Legters et al. (1991) and outlined in Figure 2.3. Powdered stocks of this compound were in excess of 50mg and stocks were prepared as previously described in 2.8.1.

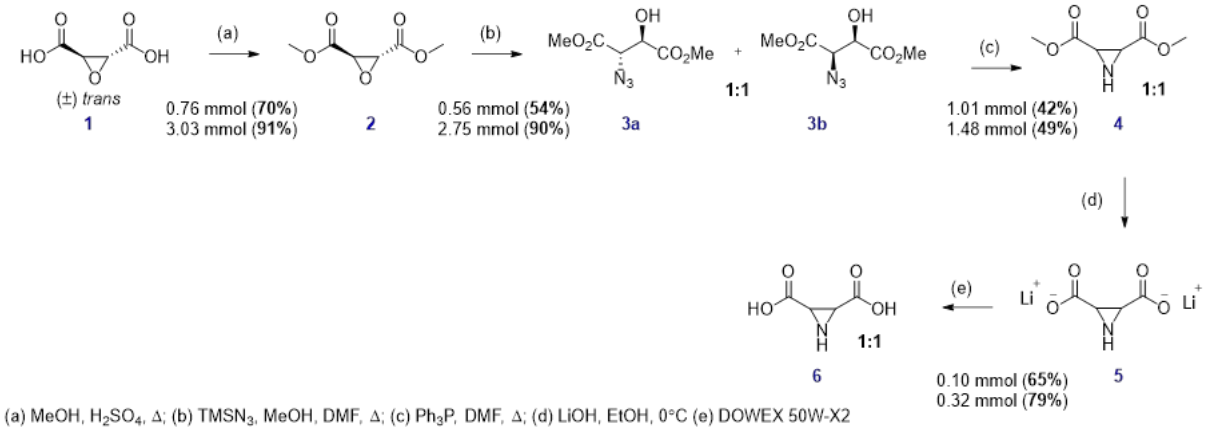

Figure 2.3 Synthesis of 2,3-dicarboxyaziridine. Esterification of commercially available (+/-)-trans-Oxirane-2,3-dicarboxylic acid (1) under acidic conditions in methanol yielded methyl ester (2). A ring opening of the epoxide moiety in compound (2) using trimethylsilyl azide yielded the azido alcohol compounds (3a and 3b), which was then reacted with triphenylphosphine in dimethylformamide to afford the ring closure aziridine motif in compound 4. The subsequent synthetic step was a saponification reaction on compound (4) using lithium hydroxide, and the final step involved the ion-exchange resin using DOWEX 50W-X2 to access 2,3-dicarboxyaziridine (6).

2.7.3 Schistosomula compound screens

Schistosomula compound screens using putative inhibitors of fumarases were carried out using the in-house Roboworm platform, which automatically assesses the motility and morphology of larval parasites by Bayesian analysis (Paveley and Bickle, 2013). Assays were carried out in a 384 Perkin Elmer black-walled plate (6007460, Greiner bio-one) where parasites were distributed across the plate by a WellMate (Thermo Scientific, UK). The WellMate was flushed with ethanol, ddH_2O and wash Basch. 20µl of full Basch mediawas then dispensed into all wells in preparation for the addition of compounds.

Compounds were prepared in 96-well V-bottom plates (master drug plate, 651161, Greiner bio-one) and dilutions were prepared from 10mM stocks so that a final concentration in the screens would result in the following concentrations: 0.625µM, 1.25µM, 2.5µM, 5µM, 10µM, 25µM and 50µM. 0.5µl of compound dilutions were added to the 384-well plates according to a standard layout for drug plates where the two last columns are reserved for positive (auranofin and praziquantel) and negative (DMSO) controls. In plates where Specs compounds were screened in combination with 2,3-dicarboxyaziridine, addition of compound was repeated at the same concentrations. All these pipetting steps were performed using the Roboworm platform written into the Biomek software (v3.3). This program has a compound resuspension protocol written into it to ensure that the compound is fully resuspended in the Basch media prior to the addition of schistosomula.

Schistosomula were added to the 384-well plate at a density of 120 parasites/60µl full Basch media using the WellMate. Plates were then incubated for 72-hours or 120-hours at 37°C in a humidified atmosphere containing 5 % CO_2.

Schistosomula scoring based on ‘motility’ and ‘phenotype’ were determined from images taken using ImageXpress Micro XL (Molecular devices) high-content imaging machine. 5 images were taken over a 6-second period using a 4x objective lens to image each

well in its entirety and this assessed the movement of the schistosomula (motility). A second round of imaging then took place using the 10x objective lens at 4 non-overlapping positions to assess characteristics of the parasites for example: shape, size and granularity (phenotype). Phenotype images were combined to provide a higher resolution image of the entire well. Images were exported to a custom-built analysis package written using the software package Pipeline pilot. Analysis of phenotype and motility assigns a numerical value to these characteristics independent of each other that can be used to score the health of parasites in the well compared with positive and negative controls. The calculation of Z ′ factor score of 0.3 was achieved using a DMSO negative control and an Auranofin positive control. Auranofin provides a predictable phenotype wherein the parasites showed uniform tegument disassociation and total loss of motility. Z ′ factor scores of 0.3 or above for phenotype and motility is considered a successful screen and any plate with a Z ′ factor score below 0.3 is discarded. A compound is considered a 'hit' when phenotype scores less than -0.15 and motility scores less than -0.35.

2.7.4 Adult worm screens

Compound screens were carried out on single worm pairs in 1ml adult worm medium. Worms were distributed into clear-walled 48-well plates prior to the addition of compound. Compounds that showed consistent hits in schistosomula screens (2.7.3) were used in adult worm screens. Worms were dosed at a 100µM, 50µM and 25µM in 10µl of DMSO (1% of volume for the screens). These were compared with 1% DMSO controls. Worms were scored for motility using the WHO-TDR method (2.2.5). Individual scores for males and females were plotted using GraphPad Prism 8.14.

The IC50 of compounds tested on adult worms was calculated using GraphPad Prism 8.14. Concentrations were $\log_{10}$ transformed and scores were transformed to percentage of the DMSO controls.

2.7.5 Human cell cytotoxicity

2.7.5.1 HepG2 cell culture

Compounds used in live parasite screens were assessed for cytotoxicity against human cell-line HepG2 (85011430, Sigma Aldrich) using MTT assays. Stocks of HepG2 cells cryopreserved at a density of 1 x 10^6 cells/ml were defrosted at 37°C and transferred to a 15ml Falcon tube where ~5ml of pre-warmed HepG2 media was added to them. Cells were centrifuged at room temperature for 2 minutes at 1,200 rpm and supernatant was poured off. 1ml of pre warmed media was added to the pellet to resuspend before cell viability was assessed by Trypan Blue. 10µl of cell suspension was mixed with 10µl Trypan Blue solution and pipetted into a dual chambered counting slide for the BIORAD TC-10 Automated cell counter. Cell suspension was then diluted up to 10ml and transferred to a T75 cell culture flask.

Cells were passaged at 70-80% confluency. Medium was poured off and cells were washed twice with 1X PBS for 2 minutes. Cells were incubated for 5 minutes at 37°C with 3ml Trypsin EDTA with gentle agitation every 2 minutes to detach cells. Equivalent volumes of HepG2 media were added to trypsinised cells to halt Trypsin EDTA activity. Cells were centrifuged as described above and resuspended in 1ml of media prior to cell counting. Cells with >80% viability were used in MTT assays.

2.7.5.1 MTT assay

Cells were distributed on black-walled 96-well clear bottomed plates at a density of 20,000/50µl media per well. Cells were assessed for even distribution across the bottom of the plate using an inverted microscope and gentle agitation was applied as needed. Seeded plates were incubated in a humidified incubator at 37°C and 5% CO_2 for 24 hours.

HepG2 cells were dosed with 100, 75, 50, 25, 10, 5µM (in 1% DMSO) for each test compound and % cell viability was assessed against 1% DMSO negative controls and 1% Triton X-100 (Sigma-Aldrich) positive control. Following compound addition, the plate was

returned to the incubator for a further 20 hours before the addition of 10µl of 12mM MTT reagent was added to each well. The plate was incubated for 4 hours prior to removing all media by blotting under a laminar flow hood. 100µl of 1:1 DMSO:isopropanol solution was added to each well before incubating for a further 10 minutes. Absorbance of each well was then assessed using a FLUOstar Omega (BMG-Labtech) measured at 570nm and corrected for using blank wells. Dose response curves were generated using GraphPad 8.4.

3. Bioinformatic Characterisation and transcriptional profiling of the Schistosome Fumarases

3.1 Introduction

The aim of this project is to provide the first detailed description of *Smfh* $_{I}$ and *Smfh* $_{II}$, specifically predicting the roles they play within *S. mansoni* (i.e. individual or compensatory functions), determining if they are essential to the survival/behaviour of the parasite and whether they exhibit characteristics suitable for progression as druggable anti-schistosomal targets. The description of fumarases across different kingdoms has identified crucial roles in cellular respiration and the production of ATP (Alberts et al., 2002) as well as a role in the DNA damage repair response of eukaryotes (Yogev et al., 2010). Based on these investigations, it is likely that schistosome fumarases also possess important functions in the lifecycle and survival of this pathogen. Given the biological distinctiveness between the two enzymes, there is a real opportunity for developing interventions that specifically inhibit only one enzyme if desired. It is not, however, understood if these two enzymes possess features that predict individual functions in mitochondrial or cytosolic compartments or if they, perhaps, provide compensatory functions in both compartments. The later scenario is similar to the single fumarase of mammals (a class II fumarase) in which this enzyme operates across both mitochondrial and cytosolic compartments. It is also unknown whether these enzymes are transcribed and translated within the human-infective stages of *S. mansoni*, a requirement for promoting these proteins as next-generation anti-schistosomal drug targets. Through the interrogation of databases and the use of molecular techniques for validation, it is now possible to detail the temporal and spatial transcription of *Smfh* and *Smfh* $_{II}$ across the schistosome lifecycle. Using phylogenetic approaches, it is also possible to understand the relationship of these distinct enzymes and to highlight where class I fumarases were lost during animal evolution.

3.2 Aims and Objectives

The aims of this chapter are to predict the roles of *Smfh I* and *Smfh II*, understand their evolutionary relationship to other species' fumarases including humans and to fully-describe the transcription of these enzymes across several human-infective lifecycle stages. Five objectives will be used to achieve these aims:

- Identify $SmFH_I$ and $SmFH_{II}$ homologues across a range of organisms representing model species and found within major phylogenetic clades using BLASTp analyses of distinct nucleic acid databases.
- Estimate evolutionary relationships of class I and class II fumarases amongst different groups of organisms.
- Predict the likely intracellular localisation of $SmFH_I$ and $SmFH_{II}$, alongside orthologs derived from BLASTp analyses, using available tools.
- Detail the temporal expression of both *Smfh I* and *Smfh II* in *S. mansoni* intra-mammalian lifecycle stages using historical DNA microarray and RNAseq databases as well as quantitative, reverse transcription PCR analyses.
- Describe the spatial expression of both *Smfh I* and *Smfh II* in adult male and females from a mixed-sex infection and females from a single-sex infection using available scRNA-Seq data.

3.3 Results

3.3.1 Identification of fumarases

Fumarases of *S. mansoni* were identified in BLASTp searches (2.3.2.2 and described in Cardoso, *et al*., 2021) of the most recent version of the genome (Buddenborg, et al., 2021). The two genes, *smp_126020* and *smp_158240*, were viewed using WormBase ParaSite and amino acid sequences were mined from this database. Using online domain databases Pfam and PANTHER, based on Hidden Markov Models (HMM), the predicted amino acid sequences encoded by both genes were assessed for the presence of specific protein domains. *Smp_126020* possessed two domains in the Pfam database; Fe-S hydro-lyase (InterPro: IPR004646) and a second Fe-S hydro-lyase (InterPro: IPR004647) and a single domain in the PANTHER database Fumarate Hydratase-Related (PANTHER: PTHR30389) (Figure 3.1.A). These domains belong to class I fumarases and the smp_126020 gene was, therefore, named *Smfh$_I$*. *Smp_158240* possessed two domains in the Pfam database Fumarate-Lyase (InterPro: IPR022761) and Fumarase C, C-Terminus (InterPro: IRP008948) and a single domain in the PANTHER database Fumarate Hydratase, Class II (PANTHER: PTHR11444:SF22) (Figure 3.1.B). These domains belong to class II fumarases and the *smp_158240* was named *Smfh$_{II}$*.

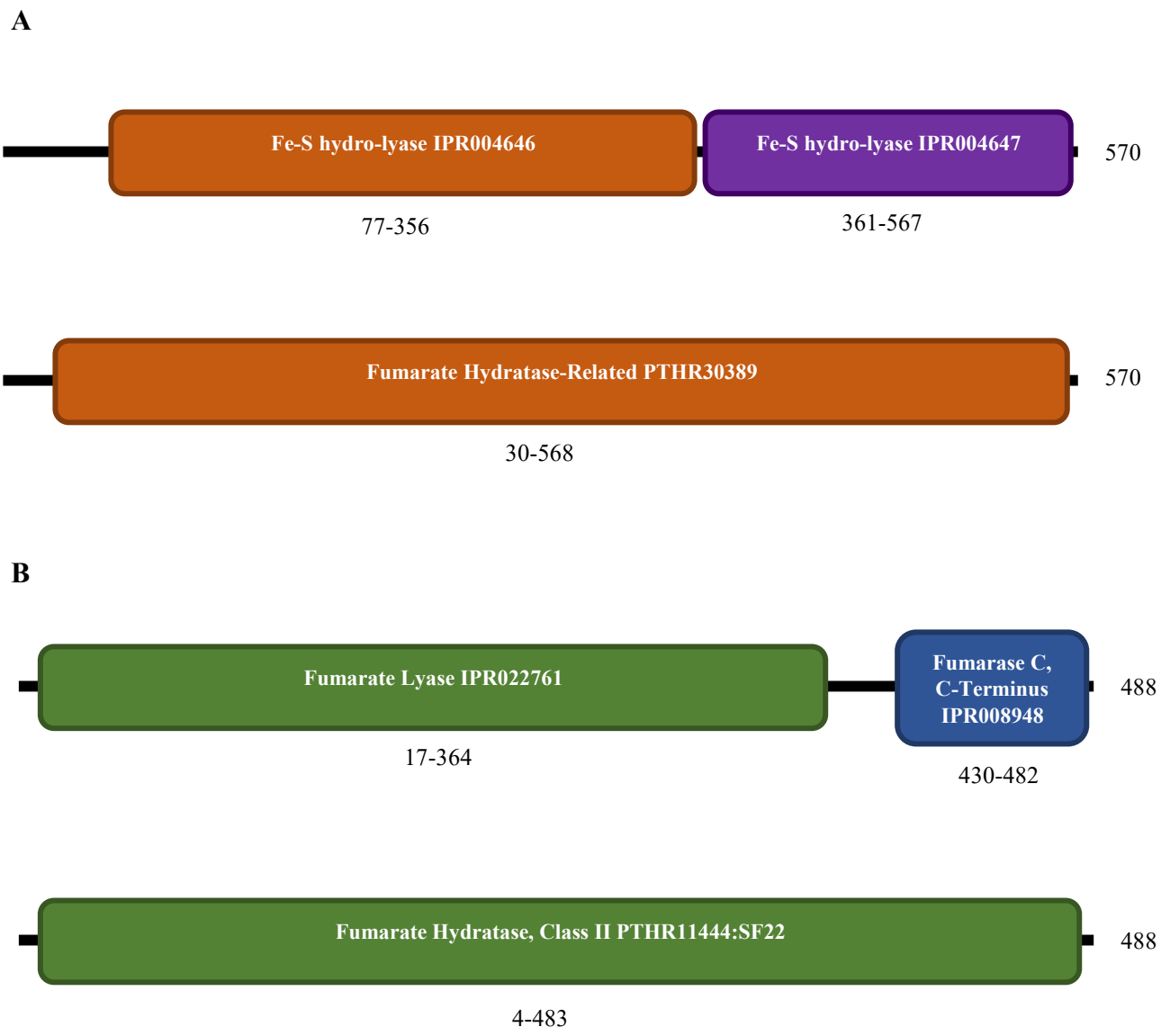

Figure 3.1. Domain searches for Smp_126020 and Smp_158240 against Pfam and PANTHER databases. Searches using predicted amino acid sequence of (A) Smp_126020 found domains associated with class I fumarases (Pfam: IPR004646 and IPR004647; PANTHER: PTHR30389). For (B) Smp_158240 domains associated with class II fumarases were found (Pfam: IPR022761 and IPR008948; PANTHER: PTHR11444:SF22).

In order to identify fumarase homologues in other species, amino acid sequences for $SmFH_I$ and $SmFH_{II}$ as well as known representatives of each class (See 2.4.2) were used during BLASTp analyses of peptide databases. Search results were considered fumarases if they showed high similarity to one of the sequences used (cutoff $E = \leq 1e^{-5}$). Search results were also additionally confirmed as fumarases by submitting them to the Interpro database where they were discarded if they did not possess the characteristic domains of class I or class II fumarases (Figure 3.1).

Class I fumarases were identified in all schistosome species, however, downstream analyses within the *Schistosoma* were restricted to *S. mansoni*, *S. japonicum, S. haematobium, Schistosoma curassoni* and *Schistosoma bovis* (Table 3.1) as major representatives of human- (*S. mansoni*, *S. japonicum* and *S. haematobium*) and livestock- (*S. curassoni* and *S. bovis*) infecting schistosomes. These searches additionally identified class I fumarases in other trematode species including *F. hepatica, Opisthorchis viverrini, Opisthorchis felineus, Fasciolopsis buski* and *Clonorchis sinensis*. Expansion of searches to other platyhelminth classes identified class I fumarase genes in the Cestoda (e.g. *Echinococcus granulosus, Taenia solium, Mesocestoides corti, Hymenolepis nana* and *H. diminuta*), the Monogenea (e.g. *Gyrodactylus salaris* and *Gyrodactylus bullatarudis*) as well as free-living species (*Schmidtea mediterranea* and *Macrostomum lignano*). Searches were expanded to identify class I fumarases in other species of Lophotrochozoa (Annelida, Gastropoda and Cepholopoda) (Table 3.1). Here, class I fumarases were found extensively throughout the Gastropoda including the *S. mansoni* and *S. haematobium* intermediate hosts, *Biomphalaria glabrata* and *Bulinus truncatus*. Additional Gastropoda species (e.g. sea slugs: *Aplysia californica* and *Elysia chlorotica*; the sea snails: *Haliotis rufescens* and *Patella vulgata*; fresh water snail *Pomacea canaliculata*) also contained class I fumarases. Searching more widely across the Lophotrochazoan revealed class I fumarases in the Cephalopoda (e.g. *Octopus sinensis* and

Octopus bimaculoides) and the Annelida, (e.g. *Helobdella robusta, Owenia fusiformis* and *Dimorphilus gyrociliatus*). While searches were conducted on other metazoan phyla (Chordata, Nematoda and Arthropoda), class I fumarases were only found in the genomes of metazoans belonging to Lophotrochozoa. Further searches were conducted on further Eukaryotic phyla. Searches of protozoan species identified class I fumarases in Euglenozoan and Apicomplexan species. Among the important human and zoonotic parasites found within the Euglenozoa, several (e.g. *Leishmania major, Leishmania infantum,* and *Trypanosoma cruzi*) possessed two class I fumarases (perhaps paralogs) whereas others (e.g. *T. brucei brucei* and *T. brucei gambiense*) only possessed a single class I fumarase. Within the Apicomplexans, *Eimeria tanella, Toxoplasma gondii* (GT1), *Plasmodium falciparum* (3D7), *Plasmodium vivax* (India VII) and *Plasmodium malariae* all possessed a single class I fumarase. Of note, *Plasmodium ovale curtisi* was the only Apicomplexan species found to contain two class I fumarases. Within the Fungi, the only species that possessed class I fumarases were *Beauveria bassiana* (D1-5) (containing two copies) and *Batrachochytrium salamandrivorans* (only one copy). Similarly, very few Plantae species contained class I fumarases. Here, this enzyme's presence was restricted to species of green algae (*Volvox reticuliferus, Volvox africanus, Chlamydomonas schloesseri* and *Chlamydomonas reinhardtii*) and species of the class Magnoliopsida (*Cichorium endivia*; two copies and *Ricinus communis*; one copy). Well-characterised class I fumarases were also found in the representative Gram-negative bacterium *Escherichia coli* (fumA and fumB), supporting previous work. Despite exhaustive searching, class I fumarases were not found in any Ecdysozoa or Chordata species.

Replicating the search for class II fumarases in the same species as above was next performed (Table 3.2). Here, class II fumarases were found in Trematoda and free-living classes Tricladida and Macrostomorpha, but were noticeably absent in species belonging to the Cestoda and Monogenea. Searches within the other Lophotrochozoa found class II fumarases

in all Gastropoda, Cephalopoda and Annelida species. Interestingly, *B. glabrata* possessed two class II fumarases. While Ecdysozoan species did not possess class I fumarases, the class II enzymes were clearly present in Nematoda- (e.g. *Ascaris suum, Ascaris lumbricoides, Heligmosomoides polygyrus, Toxocara canis, Trichuris trichiura, Truchuris suis* and *Trichuris muris*) as well as Arthropoda- (e.g. *Drosophila melanogaster* and *Bombus impatiens*) species. The Plantae species, previously shown to harbour class I fumarases (Table 3.1), also contained class II fumarases, with the exception of those found in *Volvox*. An additional plant species, *Arabidopsis thaliana,* was found to possess two class II fumarases. Within the Fungi, both *Beauveria bassiana* (D1-5) and *Batrachochytrium salamandrivorans* possessed two class II enzymes (in addition to possessing class I fumarases). In contrast, Saccharomycetes species (e.g. *Saccharomyces cerevisiae, Candida dubliniensis* and *Scheffersomyces stipites*) were found only to possess class II fumarases. While searches of the Chordata did not reveal class I fumarases, all species (represented here as *Mus musculus, Rattus rattus, Homo sapiens, Gorilla gorilla, Pan troglodytes* and *Pan paniscus*) possessed class II exemplars.

Table 3.1 Class I fumarases identified in BLASTp searches.

Species	*Gene ID*	*Class*	*Phylum/Superphylum*
Schistosoma mansoni	smp_126020	Trematoda	Lophotrochozoa
Schistosoma japonicum	EWB00_002951	Trematoda	Lophotrochozoa
Schistosoma haematobium	MS3_0020466	Trematoda	Lophotrochozoa
Schistosoma curassoni	SCUD_0001110801-mRNA-1	Trematoda	Lophotrochozoa
Schistosoma bovis	DC041_0003001	Trematoda	Lophotrochozoa
Fasciola hepatica	D915_003140	Trematoda	Lophotrochozoa
Opisthorchis viverrini	T265_13772	Trematoda	Lophotrochozoa

Species	*Gene ID*	*Class*	*Phylum/Superphylum*
Opistorchis felineus	CRM22_000726	Trematoda	Lophotrochozoa
Clonorchis sinensis	CSKR_102014	Trematoda	Lophotrochozoa
Fasciolopsis buski	FBUS_01081	Trematoda	Lophotrochozoa
Clonorchis siniensis	GAA32985.1 (NCBI)	Trematoda	Lophotrochozoa
Echinococcus granulosus	EGR_05306	Cestoda	Lophotrochozoa
Taenia solium	TsM_000704600	Cestoda	Lophotrochozoa
Hymenolepis nana	HNAJ_0001042001	Cestoda	Lophotrochozoa
Hymenolepis diminuta	WMSIL1_LOCUS11771	Cestoda	Lophotrochozoa
Mesocestoides corti	MCU_006550	Cestoda	Lophotrochozoa
Gyrodactylus salaris	genemark-scf7180006947481-processed-gene-0.2	Monogenea	Lophotrochozoa
Gyrodactylus bullatarudis	Gbulla1a006699	Monogenea	Lophotrochozoa
Schmidtea mediterranea	SMESG000009591	Tricladida	Lophotrochozoa
Macrostomum lignano	BOX15_Mlig007570g1	Macrostomorpha	Lophotrochozoa
Biomphalaria glabarata	KAI8737748	Gastropoda	Lophotrochozoa
Bulinus truncatus	KAH9499440	Gastropoda	Lophotrochozoa
Aplysia californica	XP_012940821	Gastropoda	Lophotrochozoa
Pomacea canaliculata	C0Q70_03768	Gastropoda	Lophotrochozoa
Halioris rufescens	XP_046328799	Gastropoda	Lophotrochozoa
Elysia chlorotica	RUS82196	Gastropoda	Lophotrochozoa
Patella vulgata	XP_050412557	Gastropoda	Lophotrochozoa
Helobdella robusta	HELRODRAFT_103347	Annelida	Lophotrochozoa
Owenia fusiformis	CAH1775949	Annelida	Lophotrochozoa
Dimorphilus gyrociliatus	CAD5115263	Annelida	Lophotrochozoa
Octopus sinensis	XP_029651698	Cepholopoda	Lophotrochozoa
Octopus bimaculoides	XP_014785547	Cepholopoda	Lophotrochozoa
Leishmania major (mitochondrial)	XP_001683549	Kinetoplastea	Euglenozoa

Species	*Gene ID*	*Class*	*Phylum/Superphylum*
Leishmania major (cytosolic)	XP_003722278	Kinetoplastea	Euglenozoa
Leishmania infantum (A)	ABF20401	Kinetoplastea	Euglenozoa
Leishmania infantum (B)	ABF20376	Kinetoplastea	Euglenozoa
Trypanosoma brucei brucei	XP_844042	Kinetoplastea	Euglenozoa
Trypanosoma brucei gambiense	XP_011772442	Kinetoplastea	Euglenozoa
Trypanosoma cruzi (Mitochondrial)	KAF5223411	Kinetoplastea	Euglenozoa
Trypanosoma cruzi (Cytosolic)	KAF8293098	Kinetoplastea	Euglenozoa
Eimeria tanella	XP_013233133	Conoidasida	Apicomplexa
Toxoplasma gondii (GT1)	EPR57093	Conoidasida	Apicomplexa
Plasmodium ovale curtisi (A)	SBS86366	Aconoidasida	Apicomplexa
Plasmodium ovale curtisi (B)	SBS82255	Aconoidasida	Apicomplexa
Plasmodium falciparum (3D7)	XP_001352143	Aconoidasida	Apicomplexa
Plasmodium vivax (India VII)	KMZ81105	Aconoidasida	Apicomplexa
Plasmodium malariae	XP_028860858	Aconoidasida	Apicomplexa
Beauveria bassiana D1-5 (A)	KGQ13153	Sordariomycetes	Ascomycota
Beauversia bassiana D1-5 (B)	KGQ11123	Sordariomycetes	Ascomycota
Batrachochytrium salamandrivorans	KAH9261591	Chytridiomycetes	Chytridiomycota

Species	*Gene ID*	*Class*	*Phylum/Superphylum*
Volvox reticuliferus	GIL74129	Chlorophyceae	Chlorophyta
Volvox africanus	GIL54355	Chlorophyceae	Chlorophyta
Chlamydomonas schloesseri	KAG2437600	Chlorophyceae	Chlorophyta
Chlamydomonas reinhardtii	XP_001696634	Chlorophyceae	Chlorophyta
Cichorium endivia (A)	KAI3489196	Magnoliopsida	Magnoliophyta
Cichorium endivia (B)	KAI3490666	Magnoliopsida	Magnoliophyta
Ricinus communis	EEF26711	Magnoliopsida	Magnoliophyta
Escherichia coli (fumA, aerobic)	WP_219381586	Gammaproteobacteria	
Escherichia coli (fumB, anaerobic)	HBB8954962	Gammaproteobacteria	

Table 3.2 Class II fumarases identified in BLASTp searches.

Species	*Gene ID*	*Class*	*Phylum/Superphylum*
Schistosoma mansoni	smp_158240	Trematoda	Lophotrochozoa
Schistosoma japonicum	EWB00_004437	Trematoda	Lophotrochozoa
Schistosoma haematobium	MS3_0013262	Trematoda	Lophotrochozoa
Schistosoma curassoni	SCUD_0001850201	Trematoda	Lophotrochozoa
Schistosoma bovis	DC041_0004449	Trematoda	Lophotrochozoa
Schmidtea mediterranea	SMU15040147 (SmedGD)	Trematoda	Lophotrochozoa
Fasciola hepatica	D915_008240	Trematoda	Lophotrochozoa
Opistorchis felineus	CRM22_000716	Trematoda	Lophotrochozoa
Opisthorchis viverrini	T265_06847	Trematoda	Lophotrochozoa
Clonorchis sinensis	CSKR_110661	Trematoda	Lophotrochozoa
Fasciolopsis buski	FBUS_05632	Trematoda	Lophotrochozoa
Schmidtea mediterranea	SMESG000048275	Trepaxonemata	Lophotrochozoa

Species	*Gene ID*	*Class*	*Phylum/Superphylum*
Macrostomum lignano	BOX15_Mlig006789g1	Macrostomorpha	Lophotrochozoa
Helobdella robusta (A)	XP_009019568	Annelida	Lophotrochozoa
Helobdella robusta (B)	XP_009028699	Annelida	Lophotrochozoa
Owenia fusiformis	CAH1792902	Annelida	Lophotrochozoa
Dimorphilus gyrociliatus	CAD5119317	Annelida	Lophotrochozoa
Biomphalaria glabrata (A)	KAI8735230	Gastropoda	Lophotrochozoa
Biomphalaria glabrata (B)	KAI8784507	Gastropoda	Lophotrochozoa
Bulinus truncatus	KAH9500882	Gastropoda	Lophotrochozoa
Haliotis rufescens	XP_048259799	Gastropoda	Lophotrochozoa
Aplysia californica	XP_005106113	Gastropoda	Lophotrochozoa
Elysia chlorotica	RUS73264	Gastropoda	Lophotrochozoa
Pomacea canaliculata	XP_025105270	Gastropoda	Lophotrochozoa
Patella vulgata	XP_050406911	Gastropoda	Lophotrochozoa
Octopus sinensis	XP_029644594	Cepholopoda	Lophotrochozoa
Octopus bimaculoides	XP_014786186	Cepholopoda	Lophotrochozoa
Ascaris suum	AgR038_g048_t01	Nematoda	Ecdysozoa
Ascaris lumbricoides	ALUE_0001532201	Nematoda	Ecdysozoa
Heligmosomoides polygyrus	HPOL_0002172101	Nematoda	Ecdysozoa
Toxocara canis	Tcan_02753	Nematoda	Ecdysozoa
Trichuris trichiura	TTRE_0000116001	Nematoda	Ecdysozoa
Trichuris suis	M514_11547	Nematoda	Ecdysozoa
Trichinella muris	TMUE_3000011916	Nematoda	Ecdysozoa
Drosophila melanogaster	NP_572339	Arthropoda	Ecdysozoa
Bombus impatiens	XP_012249960	Arthropoda	Ecdysozoa
Chlamydomonas schloesseri	KAG2447238	Chlorophyceae	Chlorophyta
Chlamydomonas reinhardtii	XP_042928374	Chlorophyceae	Chlorophyta

Species	*Gene ID*	*Class*	*Phylum/Superphylum*
Cichorium endivia	KAI3514683	Magnoliopsida	
Arabidopsis thaliana (A)	NP_001078075	Magnoliopsida	
Arabidopsis thaliana (B)	NP_199908	Magnoliopsida	
Escherichia coli (fumC)	WP_096860542	Gammaproteobacteria	
Batrachochytrium salamandrivorans (A)	KAH6594584	Chytridiomycetes	
Batrachochytrium salamandrivorans (B)	KAH6562383	Chytridiomycetes	
Beauveria bassiana D1-5 (A)	KGQ02326	Sordariomycetes	Ascomycota
Beauveria bassiana D1-5 (B)	KGQ13152	Sordariomycetes	Ascomycota
Saccharomyces cerevisiae (YJM470)	AJW21490	Saccharomycetes	Ascomycota
Candida dubliniensis (CD36)	XP_002422013	Saccharomycetes	Ascomycota
Scheffersomyces stipitis (CBS 6054)	XP_001386687	Saccharomycetes	Ascomycota
Mus musculus	NP_034339	Mammalia	Chordata
Rattus rattus	XP_032770898	Mammalia	Chordata
Homo sapiens	NP_000134	Mammalia	Chordata
Gorilla gorilla	XP_004028710	Mammalia	Chordata
Pan troglodytes	NP_001267172	Mammalia	Chordata
Pan paniscus	XP_003824573	Mammalia	Chordata

3.3.2 Phylogenetics of class I and class II fumarases

Phylograms were generated using the sequences identified in 3.3.1. No sequence homology was found between SmFH $_{I}$ and SmFH $_{II}$ as similarly discovered by Woods, *et al.* (1988) (data not shown), therefore further analysis of class I and class II enzymes were performed independently of one another. Maximum likelihood trees for both class I and class II fumarases can be found in the appendix (Supplementary figure. 1 and 2).

Bayesian inference trees of class I fumarases were generated with posterior probability values indicated alongside bootstrap percentage values derived from maximum likelihood trees in brackets (Figure 3.2). The class I fumarases of Trematoda formed a single clade (Figure 3.2 labelled clade 1) where the schistsome species grouped together (Bayesian inference: 0.99, maximum likelihood: 100%) more closely than the other species analysed (*F. hepatica*, *F. buski*, *C. sinensis*, *O. viverrini* and *O. felineus*) (Bayesian inference: 0.96, maximum likelihood: 90%). This clade was separate to other platyhelminth phyla (Bayesian inference: 0.94, maximum likelihood: 65%; Figure 3.2 labelled clade 2). A separate clade was found on the Bayesian inference tree (Posterior probability: 0.63) containing the species of Cestoda (*M. corti*, *T. solium*, *E. granulosus*, *H. diminuta* and *H. nana*) species of Monogenea (*G. salaris* and *G. bullatarudis*) and all apicomplexan species analysed (Figure 3.2 labelled clade 3). This was unsupported by maximum likelihood trees where the Cestoda species clustered more basal to the trematode (Bootstrap: 99%). The cestodes formed a more basal clade in Bayesian inference trees (Probability: 0.68; Figure 3.2.3) and the Monogenea form a clade with the apicomplexa (Figure 3.2.2). Apicomplexa form two clades, one containing *Eimeria tanella*, *Toxoplasma gondii* and the *Plasmodium* species (*P. ovale* (A & B), *P. malariae*, *P. falciparum* and *P. vivax* (India VII)) and the other containing *Leishmania* (*L. major* and *L. infantum*) and *Trypanosoma* (*T. cruzi* and *T. brucei*) (Bayesian inference: 0.76; maximum likelihood: 32%) (Figure 3.2.2). In Bayesian inference trees, *Helobdella robusta* and *Batrachochytrium*

salamandrivorans formed a clade together (Probability: 0.81) and *Schmidtea mediterranea* formed a clade on its own (Probability: 0.57). *Macrostomum lignano* and species of algae (*Volvox reticuliferus*, *Volvox africanus*, *Chlamydomonas schloesseri* and *Chlamydomonas reinhardtii*) formed a clade together (Bayesian inference: 0.64; Maximum likelihood: 6%) (Figure 3.2 labelled clade 4). The majority of Lophotrochozoan formed a clade (Figure 3.2 labelled clade 5) in the Bayesian inference tree (Probability: 0.79) consisting of: *Dimorphilus gyrociliatus*, *Octopus sinensis*, *Octopus bimaculoides*, *Pomacea canaliculata, B. glabrata*, *Bulinus truncatus*, *Aplysia californica*, *Elysia chlorotica*, *Patella vulgata* and *Haliotis rufescens*. *Owenia fusiformis* formed its own clade in Bayesian inference trees (Probability: 0.56) as did *Ricinus communis* (Probability: 0.99). The remaining species included the two *E. coli* class I enzymes which clustered together (Bayesian inference: 1; maximum likelihood: 100%). The two enzymes of *Beuveria bassiana* also clustered together (Bayesian inference: 1; maximum likelihood: 64%). The two enzymes identified for *Cichorium endivia* formed separate clades from each other (*C. endivia* (A) Bayesian inference: 1; maximum likelihood: 86%; *C. endivia* (B) Bayesian inference: 1; maximum likelihood: X)

Figure 3.2. Phylogenetic relationships of class I fumarases. Phylogenetic trees were generated usin probability support values are indicated at nodes with maximum likelihood support values within brackets as branch. (X) is indicated if relationship was not supported by the maximum likelihood tree. Phylogram rooted **1** consists of trematoda species. **Clade 2** consists of monogenean and apicomplexan species. **Clade 3** consists species of *Volvox*, *Chlamydamonas* and *M. lignano*. **Clade 5** consists of the majority of lophotrochozoan spec

Bayesian inference trees of class II fumarases were generated with support bootstrap values from maximum likelihood trees (Figure 3.3). Like class I, Trematoda class IIs formed a single clade (Bayesian inference: 1; maximum likelihood: 99%) consisting of two nested clades (Figure 3.3 labelled clade 1); one containing the schistosome species (Bayesian inference: 1, maximum likelihood: 99%) and the other consisting of *F. hepatica*, *F. buski*, *C. sinensis*, *O. viverrini* and *O. felineus* (Bayesian inference: 0.88, maximum likelihood: 55%). *S. mediterranea* formed a more basal clade to the trematoda (Bayesian inference: 0.88; maximum likelihood: 64%) with *M. lignano* also forming an individual clade more basal to *S. mediterranea* (Bayesian inference: 0.99, maximum likelihood: 50%). In the Bayesian inference tree, the platyhelminths formed a separate clade to the majority of other class II fumarases including Lophotrochozoa (probability: 1). *Chlamydomonas* species (*C. schloesseri* and *C. reinhardtii*) formed the most basal clade of this large cluster only in the Bayesian inference tree (probability: 0.94). Mammalian class II (*Mus muculus*, *Rattus rattus*, *Homo sapiens*, *Gorilla gorilla*, *Pan troglodytes* and *Pan paniscus*) formed a clade in the Bayesian inference tree (probability: 1) (Figure 3.3 labelled clade 2). The adjacent branch to the mammalian clade in the Bayesian inference tree (probability: 95) contained six clades. The first of these clades consisted of Annelida species (*H. robusta* and *D. gyrociliatus*), gastropoda (*P. vulgate*) and Cepholopoda (*O. sinensis* and *O. bimaculoides*) (Bayesian inference: 0.72; maximum likelihood: X) (Figure 3.2.B. labelled clade 3). A clade containing Gastropoda species (*B. glabrata* (A and B), *B. truncates*, *E. chlorotica* and *A. californica*) was adjacent to clade 3 and the relationships in this clade were supported by maximum likelihood (Figure 3.3 labelled clade 4). Two Gastropoda species (*H. rufescens* and *P. canaliculata*) each formed their own independent clades adjacent to clades 3 and 4. A clade consisting of arthropoda (*D.*

melanogaster and *B. impatiens*) and *Trichuris* species (*T. trichiura*, *T. suis* and *T. muris*) was present in Bayesian inference but not maximum likelihood (probability: 0.54) adjacent to clades 3 and 4 (Figure 3.3 labelled clade 5). Adjacent to clades 3, 4 and 5 in the Bayesian inference tree was a branch consisting of two clades (probability: 0.79). The first clade consisted of class II enzymes belonging to species of plant (*Arabidopsis thaliana* (mitochondrial and cytosolic) and *C. endivia*), species of yeast (*S. cerevisiae*, *C. dubliniensis* and *S. stipites*) and a single Annelida (*O. fusiformis*) (Bayesian inference: 0.79, maximum likelihood: X; Figure 3.3 labelled clade 6). The adjacent clade to clade 6 consisted of Nematoda (*Ascaris suum*, *Ascaris lumbricoides*, *Toxocara canis* and *Heligmosimoides polygyrus*) (Bayesian inference: 0.94, maximum likelihood: X), none of these branches were supported in the maximum likelihood tree except for *Ascaris* species (Bayesian inference: 1, maximum likelihood: 100; Figure 3.3 labelled clade 7). The remaining class II enzymes of *B. bassiana* A (Bayesian inference: 1, maximum likelihood: 99) and B (Bayesian likelihood: 1, maximum likelihood: 100) formed their own individual clades before the root of the tree consisting of the fumC of *E. coli*.

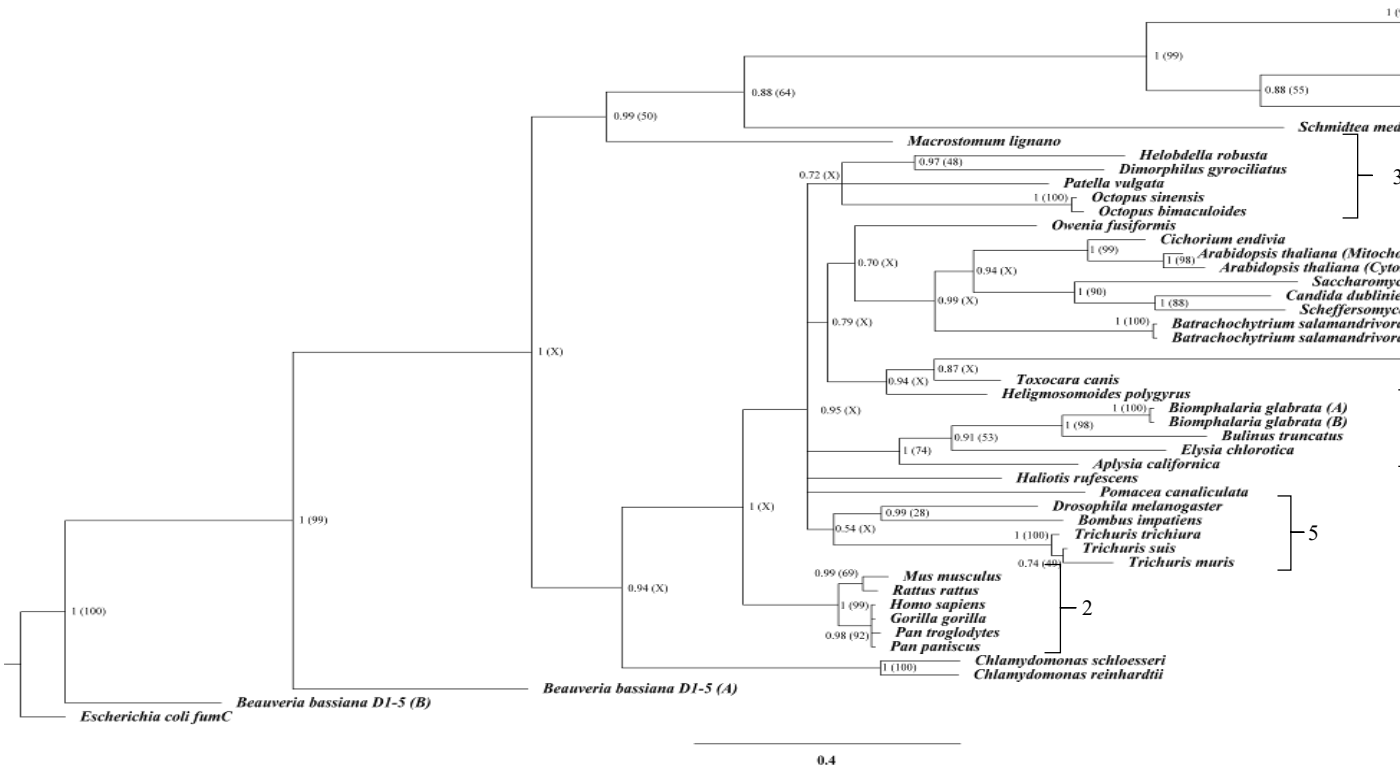

Figure 3.3. Phylogenetic relationships of class II fumarases. Phylogenetic trees were generated using MrB
in Figure 3.2. Phylogram rooted at the *E.coli* fumC. **Clade 1** consists of trematoda with *S. mediterranea* and
consists of mammalia. **Clade 3** consists of *H. robusta*, *D. gyrociliatus*, *P. vulgate*, *O. sinensis* and *O. bimacu*
gastropoda. **Clade 5** consists of arthropoda species and species of *Trichuris*. **Clade 6** consists of plant, yeast
of nematoda species of *Ascaris*, *T. canis* and *H. polygyrus*.

3.3.3 Predicting the intracellular localisation of SmFH$_{I}$ and SmFH$_{II}$

Using localisation prediction web server TargetP-2.0 (Emanuelsson et al., 2007) and MitoFates 1.2 (Fukasawa, *et al*., 2015), amino acid sequences of class I and class II fumarases of Eukaryotic species were assessed for their probability of containing a mitochondrial signal peptide (Table 3.3). Schistosome fumarases showed varying predictions. *S. mansoni* (*fh* TargetP: 0.516, MitoFates: 0.760) and *S. japonicum* (*fh*TargetP: 0.809, MitoFates: 0.894) predicted *fh$_{I}$* to localise to the mitochondria while their respective *fh $_{II}$* showed no localisation prediction in either prediction tool. All other species of schistosome analysed didn't predict targeting peptides for either fumarase gene. The class I gene of all other trematode species in this dataset, except for *O. viverrini*, were predicted to localise to the mitochondria (*F. hepatica* TargetP: 0.921, MitoFates: 0.704; *C. sinensis* TargetP: 0.532, MitoFates: 0.862; *F. buski* TargetP: 0.960, MitoFates: 0.828; *O. felineus* TargetP: 0.975, MitoFates: 0.996). *O. viverrini* predicted no localisation for both genes.

S. mediterranea, predicted no localisation for both genes when analysed by TargetP. However, MitoFates predicted localisation to the mitochondria for the class I fumarase (MitoFates: 0.544). *M. lignano* mitochondrial targeting was predicted for both class I (TargetP: 0.857, MitoFates: 0.632) and class II (TargetP: 0.982, MitoFates: 0.522).

Monogenean and cestode species, which lack a class II gene, all predicted mitochondrial targeting for their respective class I genes except for *G. bullatarudis* which predicted no targeting peptide.

Annelid species *H. robusta* (TargetP: 0.952, MitoFates: 0.990) and *D. gyrociliatus* (TargetP: 0.966, MitoFates: 0.999) both predicted mitochondrial targeting for their class I fumarase but class II fumarases showed no peptide prediction. Both class I and class II genes of *O. fusiformis* predicted no localisation. The *S. mansoni* intermediate host *B. glabrata* was predicted to have mitochondrial localisation in the class I fumarase (TargetP: 0.865, MitoFates:

0.797) but no target predictions in either of its class II fumarases. The *S. haematobium* intermediate host *B. truncatus* similarly showed no class II localisation, however, the class I gene was only predicted to localise to the mitochondria by TargetP (0.843) *A. californica* similarly only predicted localisation to the mitochondria in the class I fumarase when using TargetP (0.737), its class II fumarase did not predict localisation. *H. rufescens* fumarases were predicted to localise to the mitochondria for both class I (TargetP: 0.958, MitoFates: 0.549) and class II (TargetP: 0.910, MitoFates: 0.561). *E. chlorotica* (TargetP: 0.993, MitoFates: 0.977), *P. vulgate* (TargetP: 0.990, MitoFates: 0.649), *O. sinensis* (TargetP: 0.961, MitoFates: 0.924) and *O. bimaculoides* (TargetP: 0.986, MitoFates: 0.981) all predicted localisation in the class I fumarase but not the class II. *P. canaliculata* predicted mitochondrial targeting in the class I fumarase (TargetP: 0.970, MitoFates: 0.884) and in the class II fumarase but only in the MitoFates analysis (0.732).

The class I fumarase of *E. tenella* predicted mitochondrial targeting (TargetP: 0.718, MitoFates: 0.825) and did not possess a class II gene. Although *T. gondii* also lacked a class II gene the prediction for its class I did not predict targeting to the mitochondria by either prediction tool. All species of *Plasmodium* lacked a class II however their class I genes did not predict localisation to the mitochondria with the exception of one of the class I genes belonging to *P. ovale curtisi* (A TargetP: 0.693, A MitoFates: 0.550) and *P. vivax* which only showed mitochondrial targeting predictions in MitoFates (0.644). None of the class I genes of *Leishmania* predicted localisation to the mitochondria. The only species of *Trypanosoma* to predict mitochondrial localisation was *T. cruzi* where one of the class I genes (A) was predicted localisation (TargetP: 0.565, MitoFates: 0.568).

Ascomycota species *Beauveria bassiana* was found to possess two class I and two class II genes. None of the genes were predicted to possess a targeting peptide. Chytrid species *B. salamandrivorans* possessed a class I fumarase (TargetP: 0.946, MitoFates: No mTP) and two

class II fumarases (A TargetP: 0.997, MitoFates: 0.668; B TargetP: 0.996, MitoFates: 0.632) all of which were predicted to localise to the mitochondria however, the class I fumarase was not predicted to by MitoFates. Yeast species possessed only class II fumarases, however, *S. cerevisiae* was the only species to predict localisation to the mitochondria (TargetP: 0.589, MitoFates: 0.996).

Algae species *V. reticuliferus* (TargetP: 0.868, MitoFates: 0.899) and *V. africanus* (TargetP: 0.929, MitoFates: 0.930) both possessed only a class I gene that was predicted to localise to the mitochondria. *C. schloesseri* (TargetP: 0.809, MitoFates: 0.809) and *C. reindhartii* (TargetP: 0.835, MitoFates: 0.698) class I fumarases were predicted to localise to the mitochondria but their class II fumarases did not. *C. endivia* possessed two genes for class I, which showed no prediction of localisation, and a single class II gene that was predicted to localise to the mitochondria (TargetP: 0.695, MitoFates: 0.832). *R. communis* only possessed a class I fumarase however this was not predicted to localise to the mitochondria. *A. thaliana* possessed two class II fumarases, one was predicted to localise to the mitochondria (A TargetP: 0.978, MitoFates: 0.978) and the other showed no localisation prediction.

All nematode species including genus *Ascaris, Heligmosimoides, Toxocara* and *Trichuris* only possessed class II fumerases. Only *T. canis* (MitoFates: 0.779) and *T. muris* (TargetP: 0.695) were predicted mitochondrial localisation but in both cases there wasn't consensus between the two prediction tools.Insects included in this dataset, *D. melanogaster* and *B. impatiens*, possessed only class II genes. *D. melanogaster* class II (TargetP: 0.897, MitoFates: 0.523) was predicted to localise to the mitochondria but *B. impatiens* had no localisation prediction.

All species of mammal included in this dataset only possessed class II genes and all of them showed mitochondrial localisation prediction in both prediction tools with probabilities >0.9 in all cases (Table 3.3).

Table 3.3. TargetP-2.0 and MitoFates 1.2 outputs for FH_I and FH_{II} identified in BLASTp searches.

Species	FH_I	FH_{II}
Schistosoma mansoni	TargetP: 0.516 MitoFates: 0.760	TargetP: No mTP MitoFates: No mTP
Schistosoma haematobium	TargetP: No mTP MitoFates: No mTP	TargetP: No mTP MitoFates: No mTP
Schistosoma japonicum	TargetP: 0.809 MitoFates: 0.894	TargetP: No mTP MitoFates: No mTP
Schistosoma curassoni	TargetP: No mTP MitoFates: No mTP	TargetP: No mTP MitoFates: No mTP
Schistosoma bovis	TargetP: No mTP MitoFates: No mTP	TargetP: No mTP MitoFates: No mTP
Fasciola hepatica	TargetP: 0.921 MitoFates: 0.704	TargetP: No mTP MitoFates: No mTP
Clonorchis sinensis	TargetP: 0.532 MitoFates: 0.862	TargetP: No mTP MitoFates: No mTP
Fasciolopsis buski	TargetP: 0.960 MitoFates: 0.828	TargetP: No mTP MitoFates: No mTP
Opistorchis felineus	TargetP: 0.975 MitoFates: 0.996	TargetP: No mTP MitoFates: No mTP
Opistorchis viverrini	TargetP: No mTP MitoFates: No mTP	TargetP: No mTP MitoFates: No mTP
Schmidtea mediterranea	TargetP: No mTP MitoFates: 0.544	TargetP: No mTP MitoFates: No mTP
Macrostomum lignano	TargetP: 0.857 MitoFates: 0.632	TargetP: 0.982 MitoFates: 0.522
Gyrodactylus salaris	TargetP: 0.843	NA

Species	**FH$_I$**	**FH$_{II}$**
	MitoFates: 0.755	
Gyrodactylus bullatarudis	TargetP: No mTP MitoFates: No mTP	NA
Mesocestoides corti	TargetP: 0.965 MitoFates: 0.974	NA
Taenia solium	TargetP: 0.997 MitoFates: 0.991	NA
Echinococcus granulosus	TargetP: 0.987 MitoFates: 0.971	NA
Hymenolepis diminuta	TargetP: 0.998 MitoFates: 0.999	NA
Hymenolepis nana	TargetP: 0.872 MitoFates: 0.637	NA
Helobdella robusta	TargetP: 0.952 MitoFates: 0.990	TargetP: No mTP A and B MitoFates: No mTP A and B
Owenia fusiformis	TargetP: No mTP MitoFates: No mTP	TargetP: No mTP MitoFates: No mTP
Dimorphilus gyrociliatus	TargetP: 0.966 MitoFates: 0.999	TargetP: No mTP MitoFates: No mTP
Biomphalaria glabrata	TargetP 0.865 MitoFates: 0.797	TargetP: No mTP A and B MitoFates: No mTP A and B
Bulinus truncatus	TargetP: 0.843 MitoFates: No mTP	TargetP: No mTP MitoFates: No mTP
Haliotis rufescens	TargetP: 0.958 MitoFates: 0.549	TargetP: 0.910 MitoFates: 0.561
Aplysia californica	TargetP: 0.737 MitoFates: No mTP	TargetP: No mTP MitoFates: No mTP
Elysia chlorotica	TargetP: 0.993 MitoFates: 0.977	TargetP: No mTP MitoFates: No mTP

Species	**FH$_I$**	**FH$_{II}$**
Pomacea canaliculata	TargetP: 0.969 MitoFates: 0.884	TargetP: No mTP MitoFates: 0.732
Patella vulgata	TargetP: 0.990 MitoFates: 0.649	TargetP: No mTP MitoFates: No mTP
Octopus sinensis	TargetP: 0.961 MitoFates: 0.924	TargetP: No mTP MitoFates: No mTP
Octopus bimaculoides	TargetP: 0.986 MitoFates: 0.981	TargetP: No mTP MitoFates: No mTP
Eimeria tenella	TargetP: 0.718 MitoFates: 0.825	NA
Toxoplasma gondii	TargetP: No mTP MitoFates: No mTP	NA
Plasmodium ovale curtisi	TargetP: A 0.693, B No mTP) MitoFates: A 0.550, B No MTP	NA
Plasmodium falciparum 3D7	TargetP: No mTP MitoFates: No mTP	NA
Plasmodium vivax India VII	TargetP: No mTP MitoFates: 0.644	NA
Plasmodium malariae	TargetP: No mTP MitoFates: No mTP	NA
Leishmania major	TargetP: No mTP A and B MitoFates: No mTP A and B	NA
Leishmania infantum	TargetP: No mTP A and B MitoFates: No mTP A and B	NA
Trypanosoma cruzi	TargetP: A 0.565, B (No mTP) MitoFates: A 0.568, B No mTP	NA
Trypanosoma brucei brucei	TargetP: No mTP MitoFates: No mTP	NA
Trypanosoma brucei gambiense	TargetP: No mTP	NA

Species	**FH_I**	**FH_{II}**
	MitoFates: No mTP	
Beauveria bassiana D1-5	TargetP: No mTP A and B MitoFates: No mTP A and B	TargetP: No mTP A and B MitoFates: No mTP A and B
Batrachochytrium salamandrivorans	TargetP: 0.946 MitoFates: No mTP	TargetP: A 0.997, B 0.996 MitoFates: A 0.668, B 0.632
Saccharomyces cerevisiae	NA	TargetP: 0.589 MitoFates: 0.996
Candida dubliniensis (CD36)	NA	TargetP: No mTP MitoFates: No mTP
Scheffersomyces stipitis	NA	TargetP: No mTP MitoFates: No mTP
Volvox reticuliferus	TargetP: 0.869 MitoFates: 0.899	NA
Volvox africanus	TargetP: 0.930 MitoFates: 0.930	NA
Chlamydomonas schloesseri	TargetP: 0.809 MitoFates: 0.809	TargetP: No mTP MitoFates: No mTP
Chlamydomonas reinhardtii	TargetP: 0.835 MitoFates: 0.698	TargetP: No mTP MitoFates: No mTP
Cichorium endivia	TargetP: No mTP A and B MitoFates: No mTP A and B	TargetP: 0.695 MitoFates: 0.832
Ricinus communis	TargetP: No mTP MitoFates: No mTP	NA
Arabidopsis thaliana	NA	TargetP: A 0.978, B No mTP MitoFates: A 0.978, B No mTP
Ascaris suum	NA	TargetP: SP 0.817 No mTP MitoFates: No mTP
Ascaris lumbricoides	NA	TargetP: No mTP MitoFates: No mTP

Species	**FH$_I$**	**FH$_{II}$**
Heligmosomoides polygyrus	NA	TargetP: No mTP MitoFates: No mTP
Toxocara canis	NA	TargetP: No mTP MitoFates: 0.779
Trichuris trichiura	NA	TargetP: No mTP MitoFates: No mTP
Trichuris suis	NA	TargetP: No mTP MitoFates: No mTP
Trichuris muris	NA	TargetP: 0.695 MitoFates: No mTP
Drosophila melanogaster	NA	TargetP: 0.897 MitoFates: 0.523
Bombus impatiens	NA	TargetP: No mTP MitoFates: No mTP
Mus musculus	NA	TargetP: 0.976 MitoFates: 1
Rattus rattus	NA	TargetP: 0.931 MitoFates: 0.937
Homo sapiens	NA	TargetP: 0.991 MitoFates: 1
Gorilla	NA	TargetP: 0.985 MitoFates: 0.999
Pan troglodytes	NA	TargetP: 0.991 MitoFates: 1
Pan paniscus	NA	TargetP: 0.988 MitoFates: 1

3.3.4 DNA microarray and RNA-seq estimates of *Smfh*$_I$ and *Smfh*$_{II}$ abundances

Gene expression profiles across 10 lifecycle stages were obtained from a published *S. mansoni* DNA microarray study (Fitzpatrick et al., 2009). Searches against the database were carried out (see 2.4.5) and a single probe was found to align to the 3'UTR of *Smfh* $_I$ (CONTIG2341 *E* = e-108; Figure 3.4.A) and a single probe aligned to exon 5 of *Smfh* (CONTIG9371 *E* = 0.0; Figure 3.4.B).

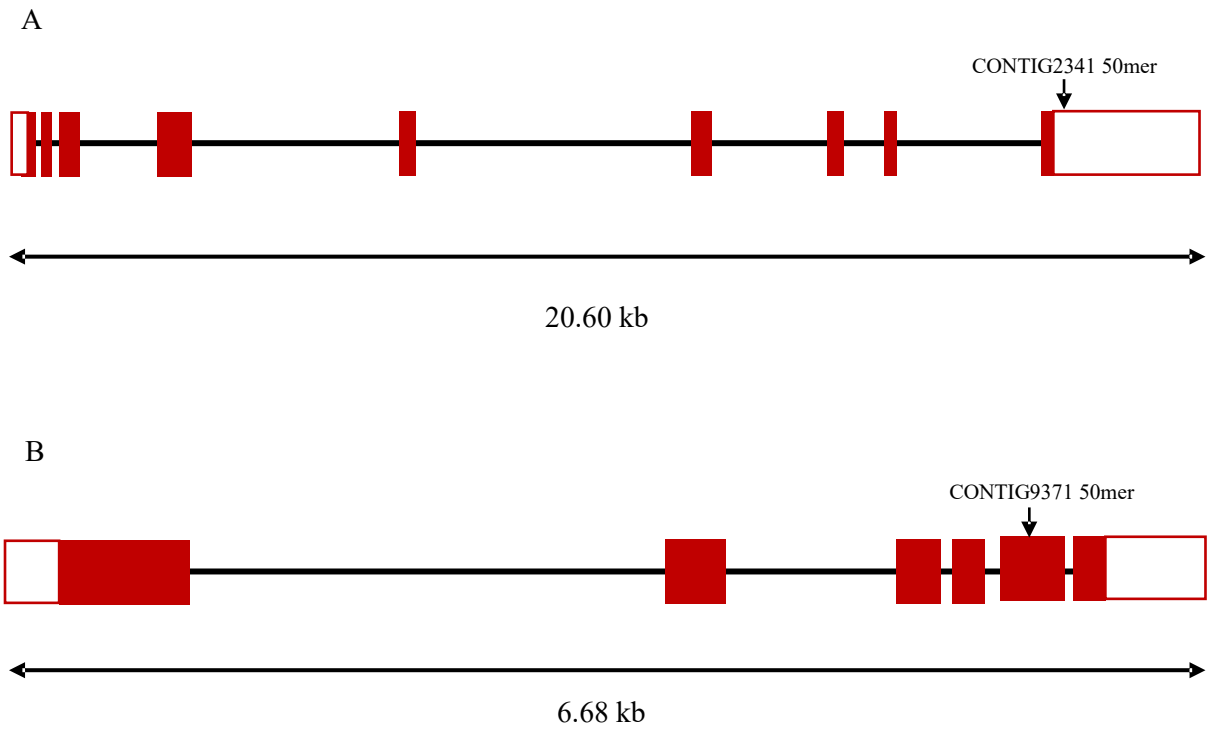

Figure 3.4. Exon maps of schistosome fumarases with location of DNA microarray 50mer. Exons (red box) and untranslated regions (UTR; white box) are shown. (A) *Smfh* $_I$ has 9 exons and the 50mer associated with CONTIG2341 (*E* = e-108) maps to a region in the 3′UTR. (B) *Smfh*$_{II}$ has 6 exons and the 50mer associated with CONTIG9371 (*E* = 0.0) maps to exon 5.

Histograms representing the normalised mean fluorescence intensity of *Smfh* $_I$ (Figure 3.5.A) and *Smfh* $_{II}$ (Figure 3.5.B) were generated and demonstrated that both fumarases were expressed throughout the lifecycle with *Smfh* $_{II}$ showing a higher overall expression profile.

Highest expression of *Smfh I* was shown in the 3-week worm, 5-week worm and 7-week worm (Figure 3.5.A). *Smfh II* showed highest expression in the human lifecycle stages in the schistosomula and adult worm stages (Figure 3.5.B).

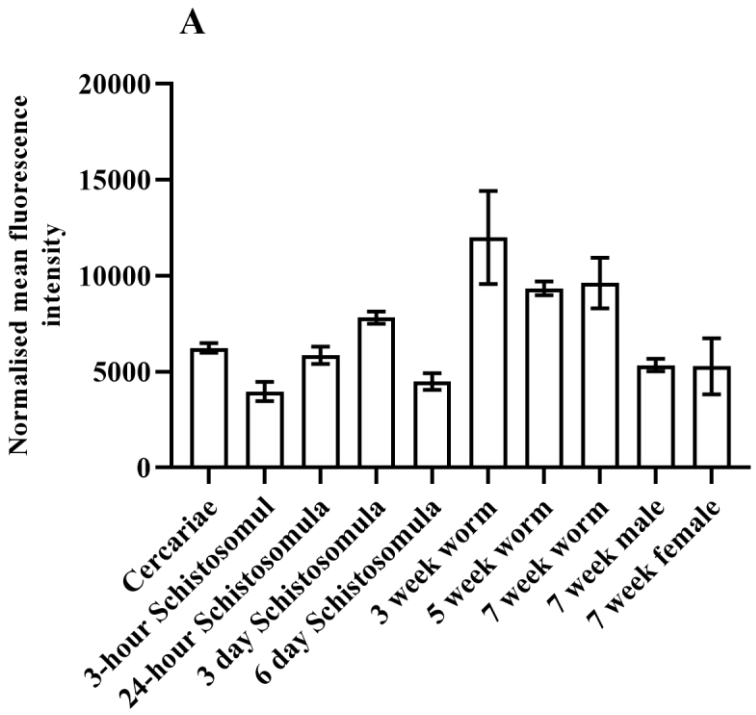

Lifestages compared	Significance
3-week worm vs Cercariae	P<0.05
3-week worm vs 3-hour Schistosomula	P<0.005
3-week worm vs 24-hour Schistosomula	P<0.05
3-week worm vs 7-week male	P<0.005
3-week worm vs 7-week female	P<0.05
5-week worm vs 3-hour Schistosomula	P<0.05
7-week worm vs 3-hour Schistosomula	P<0.05
7-week worm vs 6-day Schistosomula	P<0.05

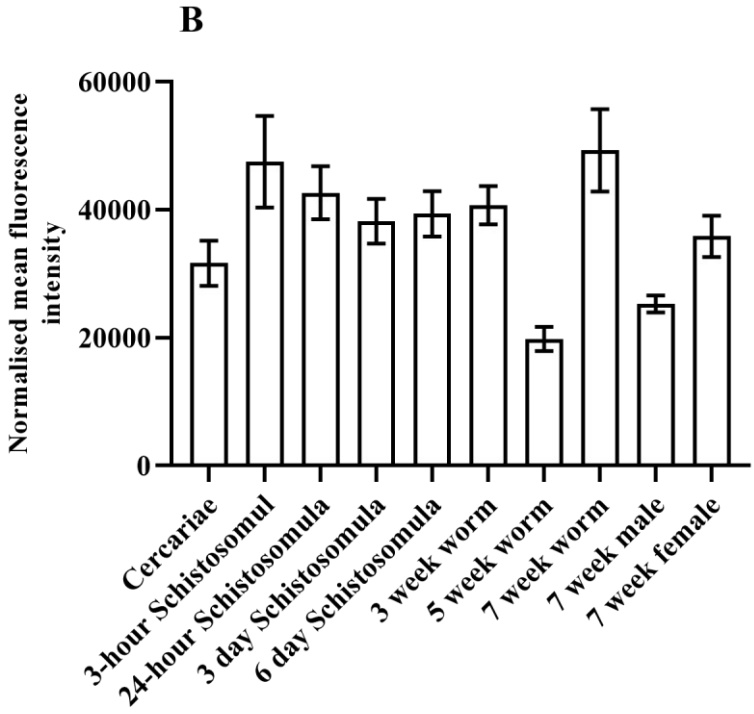

Lifestages compared	Significance
3-hour vs 5-week worm	P<0.005
3-hour vs 7-week male	P<0.05
24-hour vs 5-week worm	P<0.05
7-week worm vs 5-week worm	P<0.005
7-week worm vs 7-week worm male	P<0.05

Figure 3.5. DNA microarray analysis of *Smfh*$_I$ and *Smfh*$_{II}$ expression across intra-mammalian lifecycle stages. Histograms represent normalised mean fluorescent intensities + standard deviation (N=3 replicates per lifecycle stage except for 7 week adult female where N=2). Tables below histograms show significant differences between mean fluorescence intensities (One-way ANOVA, Tukey's test for multiple comparison). **(A)** of *Smfh*$_I$ (Smp_126020) transcript abundance derived from CONTIG2341. **(B)** of *Smfh*$_{II}$ (Smp_158240) transcript abundance derived from CONTIG9371. CONTIGs acquired from datasets produced by Fitzpatrick, *et al.* (2009).

RNA-seq data for 13 human-infective lifecycle stages were mined from datasets curated by Lu and Berriman (2018) from previously published RNAseq data. Histograms were generated using normalised expression data (NE) and showed relatively high expression across these lifecycle stages for both genes (Figure 3.6). For *Smfh*$_{I}$, the highest expression was seen in cercariae (NE: 36.07) and 6 week female worms from a mixed sex infection (NE: 36.96) while lowest expression was observed in 24 hour schistosomula (NE: 17.07) (Figure 3.6.A.). For *Smfh*$_{II}$, the highest expression was seen in 3-hour schistosomula (NE: 45.06) and lowest expression was seen in 24-hour schistosomula (NE: 18.90) and 6 week male worms from a mixed sex infection (NE: 18.61) (Figure 3.6.B).

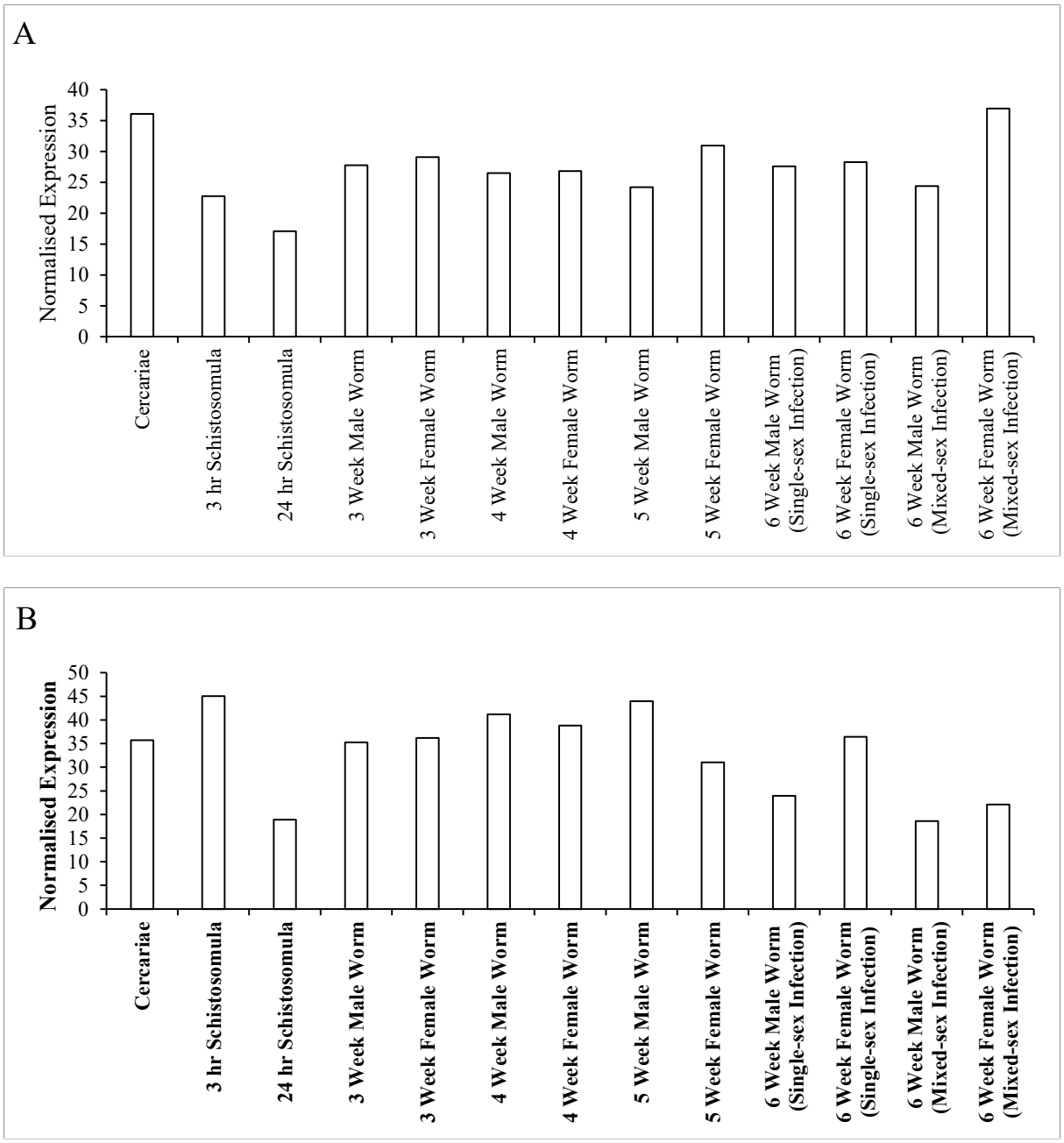

Figure 3.6. RNA-seq meta-analysis data for *Smfh I* and *Smfh II* expression across intra-mammalian lifecycle stages. Histograms represent normalised expression values of (A) *Smfh*$_{I}$ and (B) *Smfh*$_{II}$. Data acquired from Lu and Berriman (2018).

3.3.5 PCR amplification of *Smfh*$_{I}$ and *Smfh*$_{II}$ and sequence confirmation

Confirmation of *Smfh*$_{I}$ and *Smfh*$_{II}$ coding sequences were required for downstream studies (e.g. confirmatory gene expression studies, 3.3.6 and RNAi-mediated knockdown studies, 4.3.1 and 4.3.3). Therefore, PCR primers (2.3.1) were designed to amplify the entire

predicted coding sequence of *Smfh I* and *Smfh II*; amplifications were initiated from mixed-sex, 7-week adult worm cDNA (2.2.1). PCR products were electrophoresed on a 1% agarose gel and stained with SYBR-safe DNA gel stain prior to imaging (Figure 3.7). *Smfh*generated three bands, one bright band was the size of the predicted CDS (WormBase ParaSite = 1713 bp) between 1500 and 2000 bp, two smaller bands at a lower intensity were present also at 500 bp and 250 bp. *Smfh II* amplification produced a single bright band at the predicted size of the CDS (WormBase ParaSite = 1467 bp) at just below the 1500 bp mark.

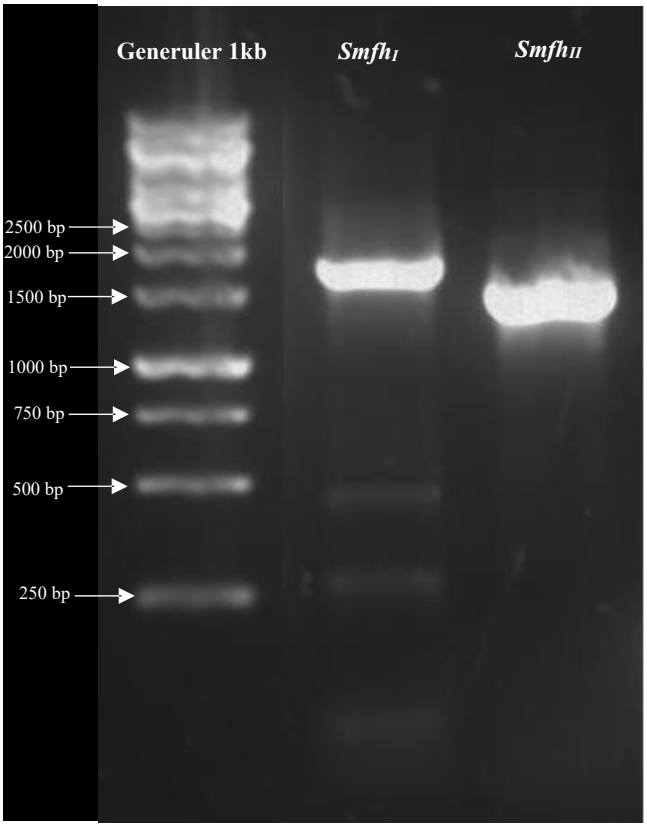

Figure 3.7 Full-length coding sequences of *Smfh I* and *Smfh II* were successfully amplified from mixed-sex adult worm cDNA. *Smfh* amplification produced a bright band between 1500 bp and 2000 bp and two bands at a lower intensity at 500 bp and 250 bp. *Smfh II* amplification produced a single bright band at ~1500 bp.

PCR products were ligated into pGEM-T easy vectors (Promega) and sequenced using T7 (TAATACGACTCACTATAGGG) and SP6 (ATTTAGGTGACACTATAG) sequencing primers (Sigma-Aldrich). DNA sequencing results were aligned with coding sequence (CDS) for *Smfh I* and *Smfh II*. Forward and reverse sequencing reactions using T7 (forward) and SP6 (reverse) primers found vector inserts aligned with 100% identity for *Smfh I* and *Smfh II*. No inserts were identified for *Smfh I* at the smaller band sizes seen in Figure 3.8.

3.3.6 Quantification of *Smfh I* and *Smfh II* abundances in intra-mammalian associated lifecycle stages by qRT-PCR.

To provide confirmatory evidence that both *Smfh I* and *Smfh II* are being expressed in the *S. mansoni* NMRI strain kept at Aberystwyth University and to additionally generate temporal data in support or refute of the DNA microarray/RNA-seq historical data, qRT-PCR analyses were next performed performed. Central to these experiments was the propagation of key lifecycle stages and cDNA derived from them.

3.3.6.1 Lifecycle stage cDNA preparation

While the generation of parasite material, derived from mixed-sex or single-sex infections, was generally described in 2.2.1, the detailed assessment of single-sex parasite material was performed according to Janse *et al.* (2018). Mono-miracidial infected *B. glabrata* were shed 5-weeks post-infection for 4-weeks to determine whether infection had occurred or not. Dead snails were removed during this period and of the 20 remaining snails, half were found to be uninfected and were euthenised (Figure 3.9.A). Shed cercaria were next sexed by quantitative PCR according to previous methodologies comparing the ΔCT between ITS2 (found in both sexes) and a W1 repeat (found only in females) (Grevelding *et al.*, 1997). Of the ten snails shedding cercaria, half produced males and half produced females (Figure 3.9.B)

where ΔCT of each reaction can be seen in Figure 3.9.C.). Male and female cercaria were used to infect mice for a period of 7 weeks to produce adult worms from a single-sex infection.

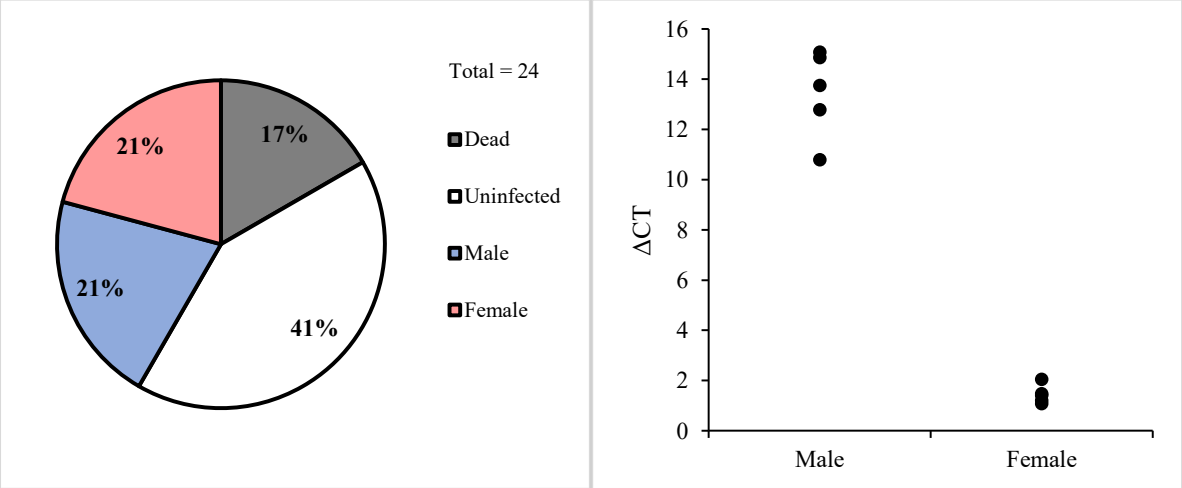

SNAIL NUMBER	ITS2	W1	ΔCT DIFFERENCE[1]	SEX (M/F)
A6	15.91389	30.77144	14.85756	M
A8	16.50273	31.5756	15.07286	M
A9	17.01869	18.09512	1.076433	F
A12	16.3594	30.10283	13.74343	M
A13	14.7104	16.17505	1.464645	F
A15	16.24552	18.29351	2.047992	F
A16	16.71078	17.90818	1.197405	F
A17	16.19124	17.60209	1.410846	F
A18	15.61935	28.39515	12.7758	M
A19	15.95359	26.74778	10.79419	M

Figure 3.8. Male and female cercaria were generated from mono-miracidial infected *B. glabrata*. Top left panel shows total snails infected with a single miracidium were shed 5-weeks post infection. Snails were shed weekly for 4-weeks to determine if they were successfully infected or not. Snails that died during this period were removed. Uninfected snails were euthenised after this period. Top right panel shows qPCR of the gDNA of cercaria shed from infected snails with ITS-2 and W1 repeats were used to distinguish male and female snails

where a ΔCT >10 (table in bottom panel) was indicative of male cercaria and <4 was indicative of female cercaria.

In addition to these single sex adult male and female samples, cDNA from 13 other lifecycle stages (egg, miracidia, sporocyst, cercaria, 24-hour schistosomula, 3-week worm, 5-week worm, 6-week worm, 7-week worm, 7-week male (mixed sex infection), 7-week female (mixed sex infection), 7-week male (single sex infection), 7-week female (single sex infection)) was generated from extracted RNA as described (2.4.1). The reaction was also performed in the absence of reverse transcriptase to confirm the absence of genomic DNA. Both reverse transcriptase positive and negative reactions were used as templates for PCR with primers specific for *SmAT1* (alpha tubulin; Smp_090120) (table 2.3). PCR reactions were electrophoresed on a 1% w/v agarose gel and amplicons were only observed in reverse transcriptase positive reactions (Figure 3.10). Being now validated, the cDNA lifecycle stages associated with the mammalian host (cercaria, 24-hour schistosomula, 3-week worm, 5-week worm, 6-week worm, 7-week worm, 7-week male (mixed sex infection), 7-week female (mixed sex infection), 7-week male (single sex infection), 7-week female (single sex infection) were subsequently used for qRT-PCR quantification of $Smfh_I$ and $Smfh_{II}$.

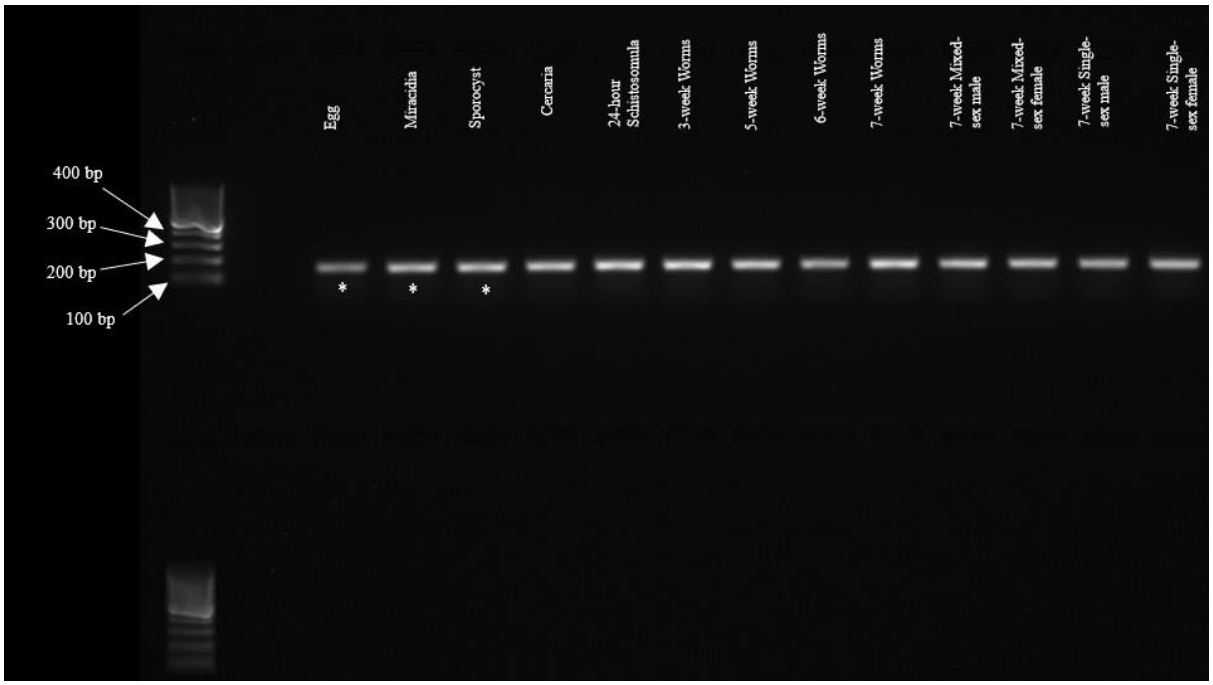

Figure 3.9. cDNA synthesis of 13 *S. mansoni* life-stages confirmed by PCR using primers to detect *SmAT1*. 1% w/v agarose gel containing SYBR Safe DNA gel stain with GeneRuler 100 bp DNA Ladder. Lifecycle RNA used included: Egg, miracidia, sporocyst, cercaria, 24 hour schistosomula, 3 week worm, 5 week worm, 6 week worm, 7 week worm, 7 week male (mixed sex infection), 7 week female (mixed sex infection), 7 week male (single sex infection), 7 week female (single sex infection). Top track shows reverse transcriptase positive reactions and bottom track shows reverse transcriptase negative reactions. **(***) Indicates samples not used for assessing $Smfh_I$ and $Smfh_{II}$ abundances**.**

3.3.6.2 Selection of housekeeping genes and primer efficiencies

As *SmAT1* may not be the most appropriate house-keeping marker to use in temporal analyses of $Smfh_I$ and $Smfh_{II}$ abundance (Haeberlein, *et al.*, 2019), new candidates were sought. Here, using criteria defined by Haeberlein, *et al.* (2019), new candidates were selected (Smp_190770, Smp_151720, Smp_058790, Smp_026090 and Smp_153590) based on their low (and mostly equal) expression across human-infective lifecycle stages (Lu and Berriman,

2018). PCR primers were designed for these candidates and PCR was performed using mixed-sex 7-week worm cDNA (primers targeting *SmAT1* served as an amplification positive control). All PCR primer pairs amplified products of the correct size (Figure 3.11 and Table 3.4) and all products were subsequently verified by DNA sequencing. House-keeping candidates were subsequently triaged according to primer efficiencies with values between 90% and 110% being sought. Of the five primer sets tested, two produced efficiency values that met agreed community standards (Silveira et al., 2021): Smp_026090 (*SmRGBD*) and Smp_153590 (*SmTscD*). The calculated efficiencies of these two primer sets as well as for those amplifying cDNA fragments of $Smfh_I$ and $Smfh_{II}$ used in qRT-PCR analyses are included in Table 3.4.

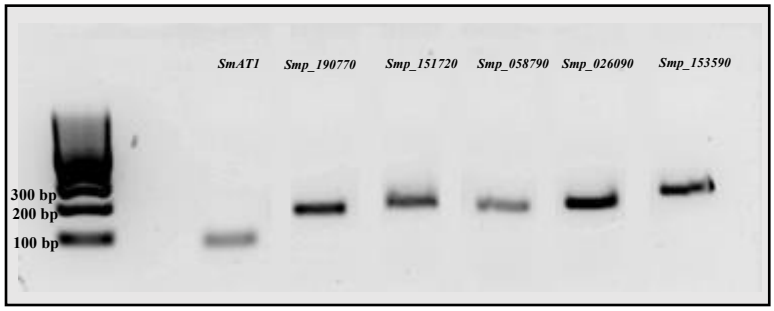

Figure 3.10. PCR of housekeeping candidates using mixed sex adult cDNA. SmAT1, Smp_190770, Smp_151720, Smp_058790, Smp_026090, Smp_153590. All lanes showed amplicons of expected size.

Table 3.4. Oligonucleotide primers used for qRT-PCR analysis of *Smfh$_I$* and *Smfh$_{II}$* abundance.

Target	Primer Sequences	Size (bp)	Efficiencies (%)
Smfh$_I$	5′ GCC TGA CTA TTT ACG TAA TCA CCC A 3′	154	103.9100684
	5′ CAG CAT AAT CAT ACT TCC TCC GG 3′		
Smfh$_{II}$	5′ TTG GAC AAG AAC TGA GTG GA 3′	238	104.3140638
	5′ GCT GGT TTG AAA ATG AGA TCT AC 3′		
SmRGBD	5′ CGG CTT TAA CTC GCC TAC AC 3′	186	103.3262288
	5′ CAT TCG ACG GTT GTT CAC AC 3′		
SmTscD	5′ GCC AAC AAA TTT CGT GGT CT 3′	228	104.2471381
	5′ TTC ACC ATT TCG GTC GTA CA 3′		

3.3.6.3 Quantitative reverse-transcription Polymerase Chain Reaction

Having now validated cDNAs and confirmed the choice of appropriate house-keeping candidates, *Smfh$_I$* and *Smfh$_I$* expression profiles were produced across the human-infective lifecycle stages (Figure 3.12). In *Smfh $_I$* the highest expression can be seen within the cercaria and 24-hour schistosomula, which were both significantly higher than the other lifecycle stages measured. Expression is similar between 3-, 5-, 6- and 7-week worms. The expression between male and female 7-week worms as well as between male and female worms derived from a single-sex infection was not significantly different (Figure 3.12.A). *Smfh$_I$* shows highest expression in 5-week worms, which was significantly higher than all other lifecycle stages (Figure 3.12.B). Lowest expression was seen in 24-hour schistosomula, which was significantly lower than all other lifecycle stages (Figure 3.12.B). There is relatively high expression in all other lifecycle stages. Male and female 7-week worms show similar expression profiles, however, 7-week female worms from a single-sex infection have a slightly higher expression profile when compared to females from a mixed-sex infection. (Figure

3.12.B). Overall *Smfh*$_{II}$ shows higher relative expression across all lifecycle stages when compared with *Smfh*$_{I}$ (Figure 3.12).

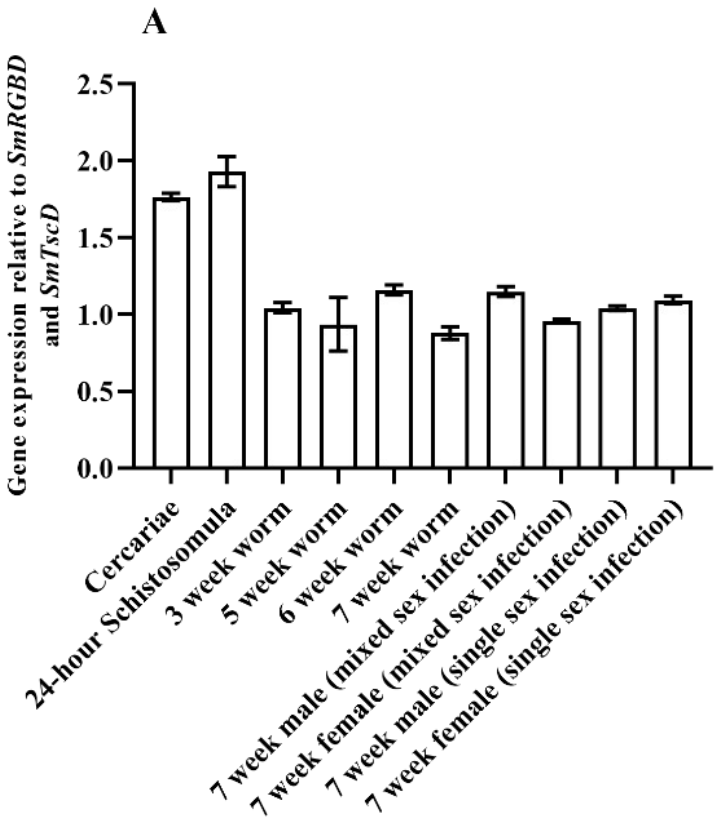

Lifestages	Significance
Cercariae vs 3-week worm	P<0.0005
Cercariae vs 5-week worm	P<0.0005
Cercariae vs 6-week worm	P<0.005
Cercariae vs 7-week worm	P<0.0001
Cercariae vs 7-week male (MS)	P<0.005
Cercariae vs 7-week female (MS)	P<0.0005
Cercariae vs 7-week male (SS)	P<0.0001
Cercariae vs 7-week female (SS)	P<0.0005
24-hour schistosomula vs 3-week worm	P<0.0001
24-hour schistosomula vs 5-week worm	P<0.0001
24-hour schistosomula vs 6-week worm	P<0.0005
24-hour schistosomula vs 7-week worm	P<0.0001
24-hour schistosomula vs 7-week male (MS)	P<0.0005
24-hour schistosomula vs 7-week female (MS)	P<0.0001
24-hour schistosomula vs 7-week male (SS)	P<0.0001
24-hour schistosomula vs 7-week female (SS)	P<0.0005

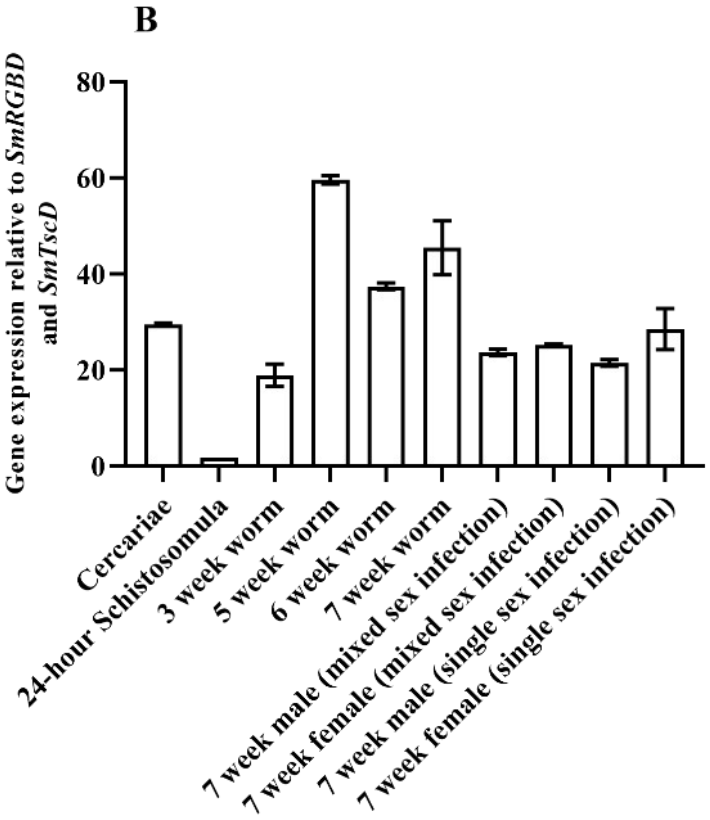

Lifestages	Significance
Cercariae vs 24-hour schistosomula	P<0.001
3-week worm vs 24-hour schistosomula	P<0.05
5-week worm vs Cercariae	P<0.0005
5-week worm vs 24-hour schistosomula	P<0.0001
5-week worm vs 3-week worm	P<0.0001
5-week worm vs 6-week worm	P<0.0005
5-week worm vs 7-week worm	P<0.05
5-week worm vs 7-week male (MS)	P<0.0001
5-week worm vs 7-week female (MS)	P<0.0001
5-week worm vs 7-week male (SS)	P<0.0001
5-week worm vs 7-week female (SS)	P<0.0001
6-week worm vs 24-hour schistosomula	P<0.0001
6-week worm vs 3-week worm	P<0.01
6-week worm vs 7-week male (MS)	P<0.05
6-week worm vs 7-week male (SS)	P<0.05
7-week worm vs 24-hour schistosomula	P<0.0001
7-week worm vs 3-week worm	P<0.005
7-week worm vs 7-week male (MS)	P<0.005
7-week worm vs 7-week female (MS)	P<0.005
7-week worm vs 7-week male (SS)	P<0.001
7-week worm vs 7-week female (SS)	P<0.05
7-week worm male (MS) vs 24-hour schistomula	P<0.005

7-week worm female (MS) vs 24-hour schistomula	P<0.005
7-week worm male (SS) vs 24-hour schistomula	P<0.005
7-week worm female (SS) vs 24-hour schistomula	P<0.0005

Figure 3.11. *Smfh$_I$* and *Smfh$_{II}$* abundance across the *S. mansoni* lifecycle. Quantitative reverse transcription PCR (qRT-PCR) of *Smfh$_I$* (**A**) and *Smfh$_{II}$* (**B**) gene expression in cercariae, 24-hour schistosomula, 3 Week worm, 5 Week worm, 6 Week worm, 7 Week worm, 7 Week male worm, 7 Week female worm, 7 Week male worm (single sex infection) and 7 week female worm (single sex infection). Histogram represents the mean ± Standard Deviation of relative *Smfh$_I$* and *Smfh$_{II}$* gene expression compared to the geometric mean of two reference genes *SmRGBD* (Smp_026090) and *SmTscD* (Smp_153590). Statistical significance show in tables below the histograms (One-way ANOVA, Tukey's test for multiple comparison)

3.3.7 Spatial distribution of *Smfh$_I$* and *Smfh$_{II}$* in *S. mansoni*

Detailing spatial (i.e. cell/tissue) contexts related to fumarase localisation aids in the interpretation of temporal data generated by DNA microarray (Figure 3.5), RNA-Seq (Figure 3.6) and qRT-PCR (Figure 3.12) analyses. Therefore, single-cell RNA-Seq (scRNA-Seq) data of mature adult male, mature adult female and virgin female (produced in an identical manner to the single-sex infection females in 3.3.6) *S. mansoni* (Wendt, *et* al. 2020) were mined for *Smfh$_I$* and *Smfh$_{II}$* localisation (Figure 3.13). Transcripts encoding both of these enzymes were abundantly found in all cell types identified in the study, regardless of sex or developmental state (e.g. female).

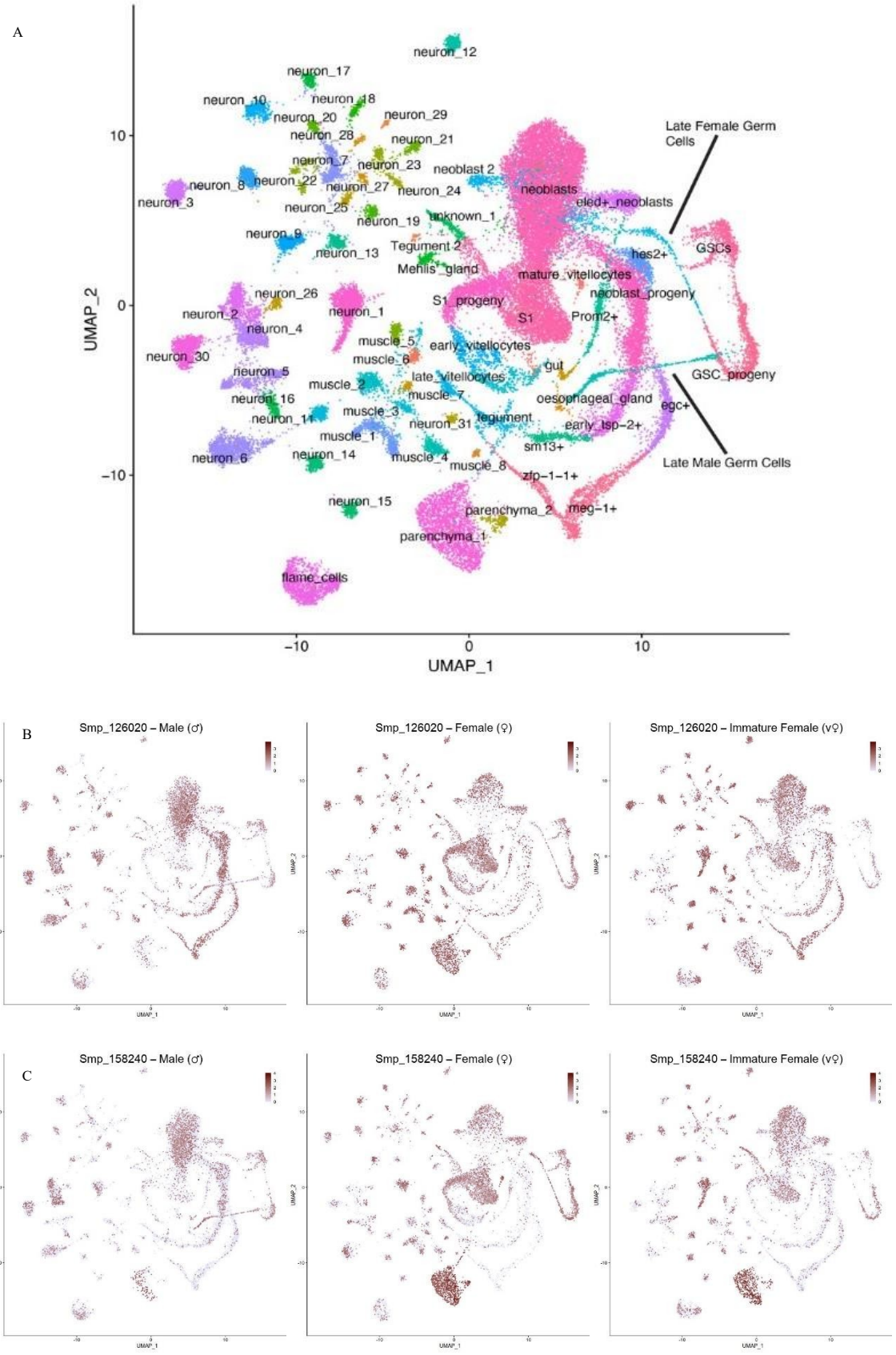
A
neuron_12
neuron_17
neuron_10
neuron_18
neuron_20
neuron_29
neuron_28
neuron_21
neuron_7
neuron_23
neoblast 2
neuron_8
neuron_22
neuron_27
neuron_24
neoblasts
neuron_3
eled+_neoblasts
neuron_25
neuron_19
unknown_1
neuron_9
Tegument 2
neuron_13
hes2+
GSCs
Late Female Germ Cells
Mehlis' gland
mature_vitellocytes
neuron_26
neoblast_progeny
S1_progeny
neuron_2
neuron_1
S1
Prom2+
neuron_4
muscle_5
early_vitellocytes
neuron_30
muscle_6
gut
neuron_5
late_vitellocytes
GSC_progeny
muscle_2
muscle_7
oesophageal_gland
egc+
neuron_16
muscle_3
tegument
neuron_11
neuron_31
early_tsp-2+
muscle_1
sm13+
neuron_6
neuron_14
muscle_4
muscle_8
Late Male Germ Cells
zfp-1-1+
neuron_15
parenchyma_2
meg-1+
parenchyma_1
flame_cells
UMAP_2
UMAP_1
10
0
−10
B
Smp_126020 – Male (♂)
Smp_126020 – Female (♀)
Smp_126020 – Immature Female (v♀)
C
Smp_158240 – Male (♂)
Smp_158240 – Female (♀)
Smp_158240 – Immature Female (v♀)

Figure 3.12. Single-Cell RNA sequencing (scRNA-seq) of adult *S. mansoni* show uniform expression across all cell types. (A) Uniform manifold approximation projection (UMAP) view of 68 identifiable cell clusters (Wendt, *et al.*, 2020). (B) UMAP plots of *Smfh I* (smp_126020) in male and female worms derived from a mixed-sex infection and females from a single-sex infection (Immature female). (C) UMAP plots of *Smfh II* (smp_158240) in the same lifecycle stages as B.

3.4 Discussion

3.4.1 The distribution of fumarases

3.4.1.1 Iron-Sulphur clusters

Since the discovery of fumarase genes in *E. coli* (Woods, et al. 1988), Fe-S cluster containing Class I fumarases have often been described as the prokaryotic type. *Smfh I* was identified in this research project as the first instance where a class I enzyme was found in a metazoan parasite. Further searches conducted in this study have detailed the extent to which class I fumarases permeate throughout the metazoan and indeed other Eukaryotic organisms such as plants, fungi, and protozoa. When considering Fe-S cluster containing proteins, historically they have been largely overlooked, until recently, often due to the difficulties of distinguishing them from other inorganic substances via absorbance (Beinhert, 2000). There is also the problem in that these proteins have inherent labilities to both temperature and oxidisation, which has contributed to the difficulty of studying these enzymes due to the requirement of maintaining controlled environments (Beinhert, 2000). The combination of these factors has led many to postulate that these proteins were often phased out of Eukaryotic metabolic pathways by natural selection (Rouault, 2019). With the description of more genomes and the refining of techniques, these proteins have been explored more extensively and a plethora have been identified in Eukaryotic and Prokaryotic species alike.

By the 1990s, the majority of Fe-S containing proteins had been identified in bacteria

such as *E. coli* (e.g. Johnson et al., 2005). During this time only a handful of proteins in the TCA cycle had been identified in mammalian cells including succinate dehydrogenase and mitochondrial aconitase (Kennedy et al., 1983; Beinert and Kennedy, 1993). In subsequent decades it has been found that many Fe-S proteins exist and are active throughout eukaryotic cells with functions within many different cellular compartments. The majority of these genes originate from the nuclear genome and have been found to be processed within the mitochondria for the attachment of Fe-S clusters.

De novo biosynthesis pathways for Fe-S clusters have been studied extensively in *S. cerevisiae* (Lill, et al., 2012). In summary, proteins enter the mitochondrial matrix for the addition of Fe-S clusters and then either are transported to other mitochondrial compartments or are exported to the cytosol via transporters. Additional Fe-S biosynthesis pathways have also been studied in mammalian cells (Rouault and Maio, 2017) and in trypanosomes (Pena-Diaz and Lukes, 2018). The widespread utilisation of mitochondria by Eukaryotes supports the hypothesis that not only are mitochondria the powerhouse of the cell, but they are also the source of iron metabolism as well as the formation of crucial Fe-S clusters required for the catalytic activity of many crucial enzymes (Lill et al., 1999). Even in amitochondrial organisms, Fe-S biosynthesis pathways are performed by the proto-mitochondrial organelles hydrogenosomes and mitosomes for homologous proteins (Tovar, et al., 2003). Only one Eukaryotic exception to mitochondrial/proto-mitochondrial Fe-S biosynthesis has been discovered. Namely the genus *Monocercomonoides,* consisting of flagellated protozoa, which lacks mitochondria (Krankowska, et al., 2016). Instead of sharing the same pathways and genes utilised by other Eukaryotic organisms to create Fe-S clusters within proteins, they utilise the same sulphur mobilisation pathway found in bacteria. This provides evidence that some Eukaryotes can survive without mitochondria and the iron-metabolising pathways that are found within them. However, the vast majority of single-cell Eukaryotes and all multicellular

Eukaryotes, to our knowledge, require the mitochondrial pathway. As determined in this study, and similar to many other Fe-S containing proteins, class I fumarases are far more abundant in eukaryotes than once thought.

3.4.1.2 Class I lost independently in Chordata and Ecdysozoa

When looking at the distribution of fumarases across different species, there is strong evidence for two independent losses of class I fumarases and one loss of class II fumarases. Within the superphyla Chordata (represented by mammals in the discussion below but including all organisms with a notochord) and Ecdysozoa (represented by insects and nematodes), no class I fumarases were identified during BLASTp searches. Evolutionarily, these two groups are more distant from each other than Ecdysozoa are from Lophotrochozoa (Adoutte et al., 2000) suggesting that their loss of class I fumarases is independent and not due to a common ancestor. What could cause this loss if not the formerly postulated lability of the class I enzymes?

Mammals possess a high demand for iron. For example, the human body contains between 3 and 5 grams of iron (Wang and Pantopoulos, 2011); the majority of which is utilised by haemoglobin in erythrocytes or myoglobin in muscles in the form of haem. Other organs such as the liver, bone marrow and macrophages in the spleen also account for a large amount of the iron. It is estimated that enzymes which utilise iron for their catalytic properties only account for a total of ~8 mg of iron (Pantopoulos et al., 2012). The production of haem in mammalian cells is also a key regulator of the TCA-cycle (Fiorito et al., 2021). It has been shown that production of haem in and its export from the mitochondria results in a reduction in activity of the TCA-cycle and oxidative phosphorylation. Some haem containing proteins, such as cytochrome c oxidase, operate within the electron transport chain and are, therefore, crucial for cellular respiration (Kim et al., 2012). With iron being such a crucial element for mammalian survival, entire mechanisms have evolved for iron homeostasis and scavenging.

Although many iron-sulphur cluster enzymes are utilised by mammalian cells in crucial metabolic cycles, with the evolution of two fumarase classes, there may have been an evolutionary advantage towards the loss of an iron-sulphur cluster gene when iron demands were increasing in other areas. This may have allowed for a reduction in iron demands and an increase in the availability of iron elsewhere allowing oxygen transport systems to become more complex. This hypothesis may explain the losses of class I within Chordata, however would reducing iron burdens explain the independent loss found in Ecdysozoa?

Insects show different iron homeostasis mechanisms to mammals (Gorman, 2023). When compared with mammals, insects have evolved a tracheal system for the delivery of oxygen throughout the body. Additionally, they rely largely on a copper-based protein, hemocyanin, for oxygen coupling (Burmester and Hankeln, 2007). There are however, some intracellular haemoglobins present within the fat body and tracheal system of some insects such as *Drosophila* (Burmester and Hankeln, 2007). Despite this, the quantities of iron required for haemoglobin in insects is dwarfed to that needed by mammals. This would suggest that insects, containing smaller reserves of iron, do not have sufficient biosynthetic mechanism to sustainably create Fe-containing metabolic enzymes (including Fe-S clusters). Concerning iron-sulphur cluster formation, much of the machinery is shared between insects and mammals and as with mammals; insects have a repertoire of enzymes requiring iron for catalytic activity (Dietz et al., 2021; Marelja et al., 2018). The closely related nematodes, consisting of free-living and parasitic worms, possess many similarities to their arthropod cousins. Both nematodes and arthropods shed their skins in a process called Ecdysis, the origin of the name Ecdysozoa, as they grow (Valentine and Collins, 2000). One major difference between these groups of animals, however, is the lack of a circulatory system in nematodes (Basyoni and Rizk, 2016). Both groups of organisms lack a class I fumarase despite variations in iron homeostasis between species. For example some species lack a *de novo* haem synthesis

pathway such as *C. elegans* (Rao et al., 2005) and *Loa loa* (Desjardins et al., 2013). Overall, it is not possible to hypothesise what caused the loss of class I fumarases in Ecdysozoa based on current research. It would be an interesting line of inquiry to explore the extent by which iron-sulphur enzymes differ between Ecdysozoa, Chordata and other superphyla and to understand to a greater extent the iron demands these species possess.

3.4.1.3 Class I and class II fumarases are found across Lophotrochozoa

Lophotrochozoa maintained both classes of fumarase except for the Cestoda, which possessed only class I. Evolutionarily, the same kinds of selection pressures that may have resulted in the losses of class I in the Chordata and Ecdysozoa do not appear to have happened in Lophotrocozoa. Regarding Lophotrochozoa, there has been little research into iron metabolism and iron dependencies. What is clear, however, is that the retention of class I fumarases within metazoan is more common than past studies, largely based on mammalian models, have suggested. But what evolutionary pressure could lead to the loss of a class II fumarase in the Cestoda?

The loss of class II fumarases in cestodes could be as a result of the wider streamlining of genomes found in these species. Compared with *S. mansoni,* the genomes of *E. multilocularis, E. granulosus, T. solium* and *H. microstomata* are a third of the size, in large part due to the lack of repeats (Tsai et al., 2013). Although the size of these genomes is reduced, they possess a comparable complement of protein coding genes to that of *S. mansoni* with the addition of novel gene products that may be involved in tegumental formation and cell adhesion. When looking at the proteins involved in metabolic cycles, both cestodes and *S. mansoni* possess a more streamlined set of pathways (Tsai et al., 2013). Despite the loss of a class II fumarase, cestodes otherwise possess a full complement of genes encoding other TCA-associated enzymes, as well as their class I fumarase required for oxidative phosphorylation. It has been noted that a reverse TCA-cycle is utilised by cestodes for the purposes of anaerobic

energy production (see Fioravanti and Vandock, 2009). Fumarase has been studied in this process where it converts malate to fumarate (McKelvey and Fioravanti, 1985). Due to the importance of so-called aerobic metabolic enzymes for this process the streamlining of these cycles does not account for the loss of class II fumarases in cestodes. It was found by Tsai *et al*. (2013) that there was a greater loss enzymes associated with arginine and proline metabolism when compared to *S. mansoni*, *H. sapiens* and *M. musculus*. The urea cycle is a component of these metabolic pathways, and it has been found that in many parasitic helminths including cestodes that streamlining of the urea cycle has occurred (Janssens and Bryant, 1969). In this study all cestode species assessed using two mitochondrial target prediction tools were predicted to possess an mTP in FH_I (Table 3.3). It is possible that as a result of the loss/streamlining of the urea cycle, the class II fumarases were also lost.

Within the definitive host, schistosomes occupy an iron-rich environment within the blood vessels. Consuming erythrocytes leads to the formation of haemozoin in the gut lumen of worms. Iron-rich haemozoin is formed through the aggregation and detoxification of haem, which in excess is toxic (Oliveira et al., 2005). Iron was found to be sequestered in the gastrodermal lumen of *S. mansoni* and *S. japonicum* when studied by plasma spectrometric analysis (Mussie and Bennett, 1982). This is largely in the form of haem, haematin (Corrêa Soares et al., 2007) and the iron storage protein ferritin within somatic tissues (Dietzel et al., 1992) and the vitelline cells of eggs (Schüßler et al., 1995). Of the two genes encoding ferritin, *Fer-1* and *Fer-2*, the former is expressed 15-fold more highly in adult female worms than male worms while *Fer-2* is equally expressed (Schüßler et al., 1995). Iron has been found to be crucial in the development of schistosome eggs, where it is important for the stabilisation of cross-linked proteins in the formation of the eggshell (Jones et al., 2007). With an overabundance of haem and a need to detoxify it, the presence of Fe-S cluster proteins and the biosynthetic pathways responsible for their formation, could act as contributors to iron

homeostasis within the parasite in its definitive hosts. Due to its abundant supply, there may also be no pressure to conserve or restrict iron utilisation allowing for the retention of two fumarase enzymes. This explanation does not account for other species possessing both classes, however. Further research and understanding of the evolutionary differences between metazoan species with regards to their fumarase gene retention is needed. What could the role of these two enzymes have within the parasite and are they crucial for the survival within the definitive host?

3.4.2 Evolutionary Relationship of Fumarases

Phylogenetic trees were generated from a database of representative class I and class II fumarases and rooted with Prokaryotic members represented by *E. coli* fumA and fumB for class I and fumC for class II. The two fumarase classes share no significant sequence similarity and come from two evolutionary distinct groups of proteins (Woods, *et al.*, 1988).

3.4.2.1 Class I Fumarases derived from Parasitic Platyhelminths and Parasitic Protozoa form a distinct clade

Broadly speaking, class I fumarases cluster according to the taxonomic groupings of organisms, with schistosomes forming a clade with other trematodes, lophotrochozoans forming a clade etc. but curiously the parasitic protozoa including species of *Plasmodium*, *Leishmania*, *Trypanosoma*, *Toxoplasma* and *Eimeria* form a broader clade with the parasitic helminths. This was not shared in both the Bayesian inference tree and maximum likelihood trees, however. This clade of parasitic class I fumarases are more closely related than the parasitic platyhelminths are to other free living platyhelminth species *S. mediterranea* and *M. lignano*. All of these species share a parasitic lifestyle with all but the monogeneans being endo-parasites.

The only exception to the lophotrochazoan class I cluster is *H. robusta*, which clusters with fungal class I *B. salamandrivorans* and more basally with *S. mediterranea*. Broadly

speaking the few fungal Class I genes identified cluster most closely to *E. coli* fumA and fumB. Plant and algal class I did not form a distinct clade with each other. This could be improved using more representative species to better elucidate the evolutionary relationship between these groups. However, this is outside the scope of this project.

3.4.2.2 Platyhelminth Class II fumarases form a Distinct Clade

Phylogenetic analyses of class II fumarases found trematodes formed a clade that was more basally linked with free living platyhelminths *S. mediterranea* and *M. lignano*. All other class II fumarases with the exception of the two *B. bassiana* and *E. coli* fumC formed a large clade. Other lophotrochazoan species were found to be separate from platyhelminths but didn't form a clear clade with each other as seen in the Class I analysis. Lophotrochozoan class II are within a clade that includes the Ecdysozoan nematodes and insects as well as plant species and yeasts. This clade is separated from mammalian fumarases which form a distinct clade.

Evolutionarily the class II fumarase of *S. mansoni* is distant from the human orthologue suggesting that these proteins show some differences. Broadly speaking the most interesting aspect of the evolution of these genes is how some species have independently lost a fumarase class while others have maintained both. To understand why this might be this study explored the literature and investigated the amino acid sequences of these proteins to better understand the relationship between these two classes.

3.4.3 The Role of Fumarases in *Schistosoma mansoni*

Fumarases are crucial to metabolic cycles (TCA-cycle, Urea cycle) and are involved in the DNA damage repair response. With two genes present in *S. mansoni,* it is important to elucidate whether these genes carry out the same roles within the organism or whether there is a division of labour. Although *S. mansoni* possesses a full repertoire of aerobic metabolism enzymes, is this mode of energy metabolism even necessary for the survival of the parasite in the definitive host?

3.4.3.1 Energy Metabolism in Schistosomes

Energy metabolism in mammals is well understood (Figure 3.14). ATP and other molecules necessary for energy production can be produced by a variety of pathways including glucose oxidation (glycolysis), the TCA-cycle and oxidative phosphorylation and fatty acid metabolism during β-oxidation. This repertoire of metabolic pathways allows for mammals to utilise energy from a variety of sources and a range of diets. In humans, diets can be adapted and shifted to lean towards certain metabolic pathways in the management of disease or for the purposes of weight loss or gain (Arai, 2014). Diet has been explored in the management of fumarase deficiency in infants (Ryder et al., 2018). A high fat diet in an infant patient was found to greatly reduce some of the phenotypes of fumarase deficiency likely due to β-oxidation driving the electron transport chain and producing NADH and $FADH_2$. As a result, the TCA-cycle can be bypassed leading to milder clinical pathology. When comparing the metabolic pathways of humans and schistosomes, helminths have evolved streamlined pathways (Tsai et al., 2013)

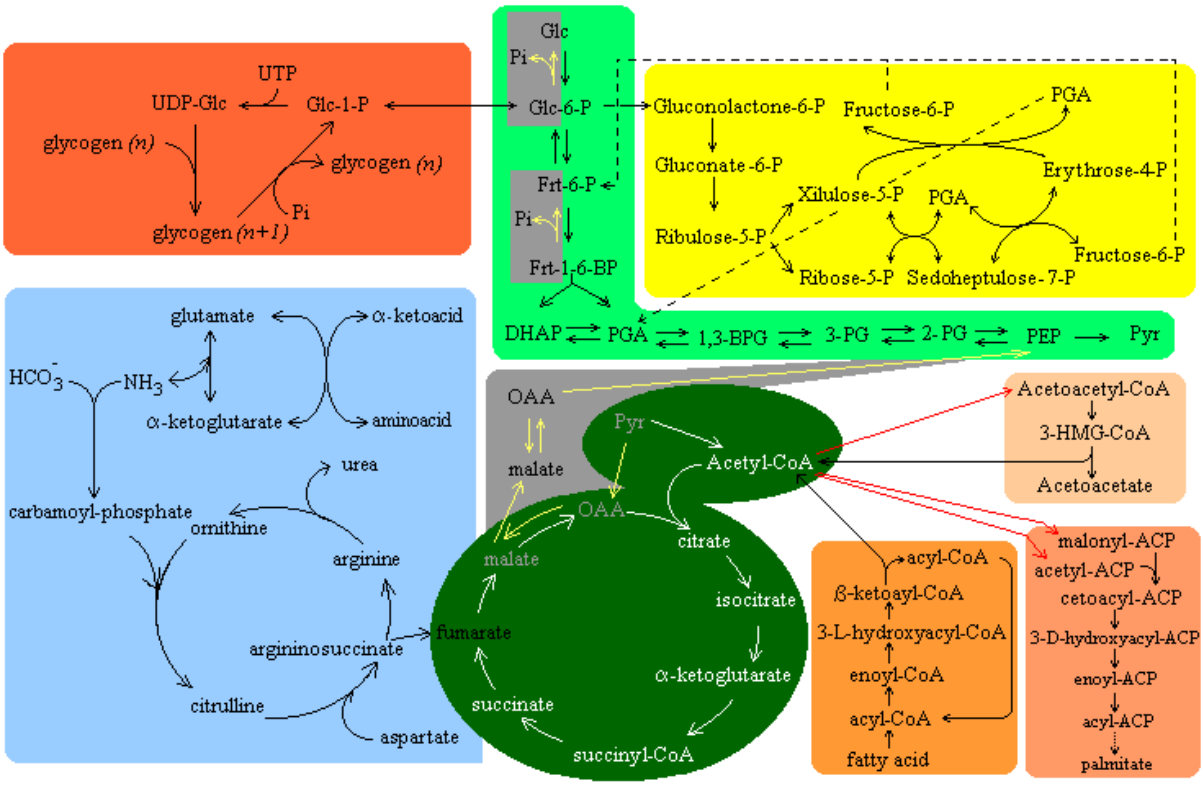

Figure 3.13. The major metabolic pathways for mammalian energy production. Taken from (Silva, 2023).

While the genome of *S. mansoni* is streamlined (like cestodes), these parasites maintain a full repertoire of genes coding for glycolysis and the TCA pathway, a partial Urea cycle (lacking argininosuccinate synthase and ornithine transcarbamylase) and the β-oxidation pathway (Tsai, *et al*., 2013). An in-depth study investigating fatty acid metabolism in *S. mansoni*, both bioinformatically and experimentally through lipidomics, demonstrated that the parasite does not possess genes coding for functional enzymes in this pathway (Bexkens et al., 2019). This particular study demonstrated that the only pathways for energy metabolism in *S. mansoni* is through glycolysis and the TCA-cycle and that any fatty acids utilised by the parasite were scavenged from the host. As fumarases are a key enzyme within the TCA-cycle, they are likely to be essential for schistosome survival due to the lack of alternative pathways providing other routes for oxidative phosphorylation. The metabolism of different schistosome lifecycle stages has been previously investigated (Bruce, *et al.*, 1969; Skelly, *et al*., 1993;

Skelly and Shoemaker, 1995), providing some insights into both aerobic and anaerobic respiration. Understanding the importance of the TCA-cycle in human-infective lifecycle stages can provide insight into the roles of both fumarases in the parasite lifecycle.

The free-swimming cercariae utilise glycogen stores and aerobic respiration in host-seeking behaviour as they are shed from their snail hosts (Bruce et al., 1969). It has been found that the expression of genes (malate dehydrogenase and COX1 of cytochrome oxidase) corresponding with aerobic respiration are highly expressed in the tails of cercaria when compared with the head and subsequent schistosomula following penetration of the definitive host (Skelly et al., 1993). As the parasite develops into an adult male or female, expression of malate dehydrogenase and COX1 was found to rise to a level suggesting adult schistosomes utilise aerobic respiration for energy production to a greater extent to schistosomula. RNA-seq studies by Protasio, *et al*., (2012) confirmed on a whole transcriptome level that expression of genes associated with aerobic metabolism are higher in cercaria and adults than they are in schistosomula. Experiments on adult *S. mansoni* worms treated with closantel, an anthelmintic that disrupts oxidative phosphorylation, suggest that disruption of this pathway results in detrimental phenotypes (Bossche, 1985). Although lactic acid, a by-product of glycolysis in anaerobic conditions, was detected in closantel-treated worms, these worms lost all motility within 3-hours. It is likely that immobile worms would not be able to maintain their location within the mesenteric venules demonstrating the importance of aerobic respiration, to the survival of these worms *in vivo*.

3.4.3.2 DNA Damage Repair

Cytosolic fumarases are stereotypically associated with the Urea cycle and processing fumarate following the conversion of argininosuccinate to arginine. With an incomplete Urea cycle in *S. mansoni* and the ability to convert argininosuccinate to arginine, why was there not also a loss of class II fumarases as seen in Cestodes?

Fumarase deficiency caused by a homozygous mutation in the fumarase gene in humans leads to a metabolic disorder characterised by brain malformations, severe intellectual disabilities and seizures; as sufferers age, these phenotypes become more prevalent (Bayley et al., 2008; Kerrigan et al., 2000). Fumarase deficiency also leads to hereditary leiomyomatosis and renal cell carcinoma (HLRCC) where the complete loss of fumarase activity leads to tumorigenesis (Tomlinson et al., 2002). The leading model for tumorigenesis proposes that fumarate accumulation causes inhibition of PHD 1, 2 and 3 (α ketoglutarate dependent hydroxylases). This, in turn, initiates a cascade in which the α subunit of hypoxia-inducible transcription factor is stabilised leading to high quantities of the active protein. A consequence of this cascade leads to glucose metabolism and angiogenesis, both of which are essential for tumorigenesis (Pollard et al., 2005). Although the role of Fumarase as a tumour suppressor has been well-established (see Leshets, *et al*., 2018), the mechanism seems to be more complex than previously thought.

Fumarases have been found to be involved in the DNA damage repair response where their activity has been found to mitigate damage and repair double strand breaks (DSB). Experiments on yeast colonies exposed to ionizing radiation showed that fumarase activity mitigates against the damage caused by ionizing radiation and improved colony recovery when compared with knockout strains (Yogev, *et al*., 2010). Curiously, when fumaric acid was added to the damaged colonies, recovery was improved; this did not occur with malic acid, suggesting that the production of fumarate aids in the DSB repair response (Yogev et al., 2010). Overexpression of fumarase was found in both wild type yeast and HeLa cells with subsequent fluorescent microscopy of extracted nuclei demonstrating localisation of fumarase. Further studies have linked cytosolic fumarase with histone methylation where fumarase interacts with histone variant H2A.Z at DSB sites. The generation of fumarate at these sites inhibits the histone demethylase enzyme KDM2B resulting in increased accumulation of enzymes

involved in non-homologous end-joining DNA repair, which in turn can lead to the survival of cells (Jiang et al., 2015). Both *S. cerevisiae* and humans possess only class II fumarases, which perform both a mitochondrial and a nuclear/cytosolic function. However, what occurs in organisms containing both class I and class II fumarases or in organisms that only possess a class I fumarase?

In the model organism *E. coli,* studies have investigated how their repertoire of fumarases respond to DNA damage. *E. coli* strains with knockout of fumA (Class I aerobic), fumB (Class I anaerobic) and fumC (Class II heat stable) were exposed to ionizing radiation or methanesulfonate for up to 45 minutes to induce DNA damage (Silas *et al.*, 2021). Results of these experiments suggested that, when lacking fumA or fumB, more damage occurred; however lacking fumC was comparable to that of wild type. It was found that in a double knockout of fumA and fumB the *E. coli* show comparable survival to wild type strains when exposed to ionizing radiation. Overexpression of fumC occurs in the double knockout strain under DNA damage conditions and possibly a similar DSB repair response to that of *S. cerevisiae* occurs. Using strains of yeast that exclusively expressed fumarase in the mitochondria, fumA, fumB and fumC were transfected into these cells to assess their ability respond to DNA damage. In these experiments it was found that only cells transfected with fumA and fumB showed protection against ionizing radiation, while those transfected with fumC showed comparable damage to that of the controls. Among the plethora of enzymes that contain Fe-S clusters, many are involved in in DNA repair such as DNA polymerase, XPD and RTEL1 (Fuss *et al.,* 2015; Netz *et al.*, 2012). Interestingly, recent studies have identified a novel way that fumarases support DNA-damage repair in yeast by protecting the cysteine desulphurase, Nfs1p, an enzyme crucial in the formation of Fe-S clusters in mitochondria (Yip et al., 2021). This study found that overexpression of Nfs1p protected *S. cerevisiae* from DNA-damage likely due to its contribution to the production of DNA-repair enzymes. Succination, a

reaction in which fumarate modifies cysteines, can cause permanent modification of proteins leading to inactivation (Blatnik, *et al.*, 2008). Fumarase has been found to directly interact with Nfs1p, generating a non-modifying environment where succination in prevented by the conversion of fumarate to malate. With the function of Nfs1p protected, the generation of Fe-S clusters is in turn protected. What is clear is that fumarase is involved in the DNA-damage repair response through a multitude of pathways and mechanisms that are yet to be fully explored and understood. Through direct interactions with enzymes in the nucleus and mitochondria to their importance in preserving an environment conducive to enzymatic activity, fumarases are crucial for the functionality of all organisms. As the study of the involvement of class I fumarases in the DNA-damage repair response is still ongoing, there may be further direct involvements yet to be uncovered with the presence of Fe-S clusters and their importance in DNA-damage repair. To this end, the potential localisation of schistosome fumarases was next explored.

3.4.3.3 Localisation of S. mansoni Fumarases Suggests a Division of Labour

mTPs are a signal that directs the transport of proteins into the mitochondria (Friedl *et al.*, 2020). $SmFH_I$ was predicted to possess an mTP, while $SmFH_{II}$ did not (Table 3.3). When looking at other organisms and how their fumarases have evolved, there is often a division of labour in eukaryotes possessing both fumarase I and fumarase II enzymes. For example, *A. thaliana* (Pracharoenwattana, *et al.*, 2010) and *L. major* (Feliciano, *et al.*, 2012) both posses two separate fumarase genes. In the case of *A. thaliana* there are two class II fumarases, one which possesses a mTP and localises to the mitochondria and the other does not possess a mTP and localises to the cytosol. In the case of *L. major* the same occurs, however, it possesses two class I fumarases. In studies of *L. major,* the fumarase containing a mTP was found to exclusively localise to the mitochondria with no cytosolic overlap with the other gene, demonstrating a division of labour between these enzymes (Feliciano et al., 2012). Despite the

practical identification of the mTP in *L. major* mitochondrial enzyme (XP_001683549) neither TargetP nor MitoFates were able to predict a mTP (Table 3.3). With sequence confirmations for the genes in question, it is unlikely to be due to inaccuracies in genome predictions however, inaccuracies cannot be discounted for other species analysed. Nematode class II were only predicted to have an mTP in *T. muris* (TargetP: 0.695, MitoFates: No mTP) and *T. canis* (TargetP: No mTP, MitoFates: 0.779). However, neither had the consensus of both mTP prediction tools (Table 3.3). All mammalian class II fumarases were predicted to possess mTPs by both prediction tools (Table 3.3). In schistosomes only *S. mansoni* and *S. japonicum* were predicted to possess a mTP in the class I fumarase and no mTP in the class II fumarase. This wasn't the case for other schistosome species analysed and further analysis of these genes is required to confirm their sequences experimentally. It is possible in the case of *S. haematobium*, *S. bovis* and *S. currasoni* that the genome predictions are incorrect, however, without experimental confirmation this cannot be determined.

These data suggest that SmFH$_{I}$ would be responsible for TCA-cycle roles while SmFH$_{II}$ would perform the cytosolic and DNA-damage repair roles. The division of labour for these genes could indicate a vulnerability in the *S. mansoni* metabolic machinery. With the TCA-cycle and oxidative phosphorylation crucial for adult worm motility, disruption of SmFH$_{I}$ could lead to the death of the worm. As humans lack a class I fumarase, developing a drug discovery strategy around SmFH$_{I}$ is appealing. Additionally, SmFH$_{II}$ is evolutionarily distant from that of humans (Figure 3.3), offering a potential secondary area for drug discovery by exploiting these differences. Unfortunately, this study did not attempt to confirm by fluorescent microscopy that SmFH$_{I}$ localised to the mitochondria, however, this would be a crucial area of future research to demonstrate this division of labour. Until this data can be generated, temporal and spatial transcriptional profiling can provide some evidence useful in predicting roles of these two enzymes in *S. mansoni*.

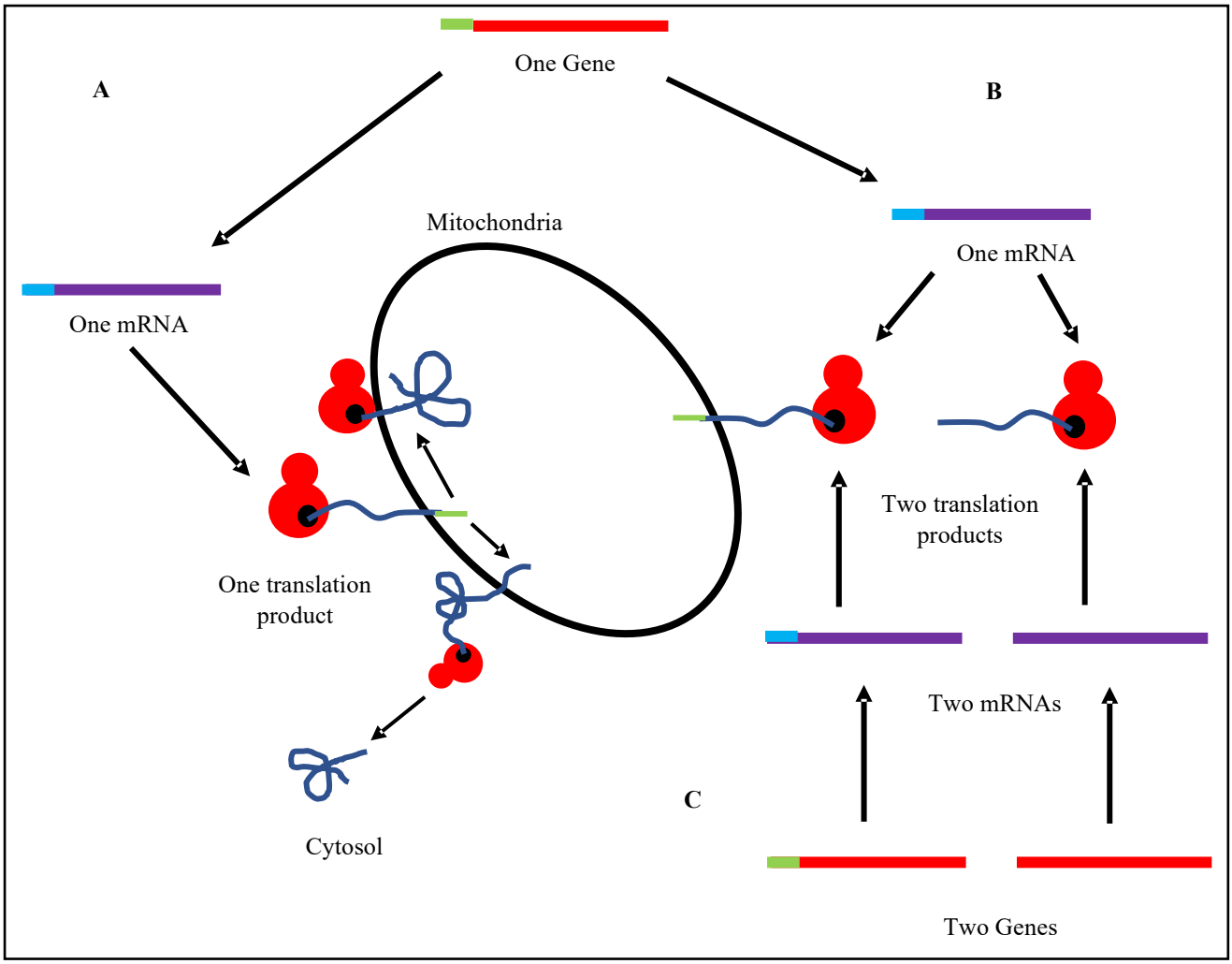

Figure 3.14. Routes to mitochondrial and cytosolic fumarases. (A) *S. cerevisiae* produces a single mRNA, which is translated into an amino acid product containing a mTP; this product undergoes two possible fates. The protein either folds when fully inside the mitochondria or folds outside of the mitochondria. In both cases the mTP is cleaved and leads to a mitochondrial or cytosolic fumarase respectively. (B) Mammalian fumarases are generated as a single mRNA where two translation products occur; one with and one without a mTP. These fold into cytosolic and mitochondrial fumarases within their respective cellular compartment. (C) In species that possess two genes, one with and one without a mTP, each gene produces an mRNA and produce two translation products. This mode of fumarase production can occur in species with two class I fumarases (*L. major*, *T. cruzi*) or two class II fumarases (*A. thaliana*).

3.4.4 Fumarase Expression in the Human-infective Lifecycle Stages

For this study, historical DNA microarray and RNA-seq data were analysed to obtain *Smfh$_I$* and *Smfh$_{II}$* profiles. Although there were differences in the profiles generated by each method, both fumarases were predicted to be relatively highly expressed in all of the lifecycle stages analysed.

3.4.4.1 Discrepancies in Different Methods

The DNA microarray showed relatively high expression of both genes across human infective lifecycle stages; the major difference between the two was seen in the fluorescence intensities of the two genes. The expression range of *SmfhI* ranged from ~4,000-12,000 mean fluorescence intensity units while *Smfh$_{II}$* ranged from ~20,000-50,000. The difference between lifecycle stages is around 5 times greater in *Smfh$_{II}$*. When looking at examples of fumarase quantities in other species, this difference in abundance could be explained by the functions of these two genes and their respective roles within the cell. Studies in *S. cerevisiae* have found that the mitochondrial isoform accounts for 30% of the total fumarase while the remaining 70% was found in the post-ribosomal supernatant fraction corresponding with the cytosol (Wu and Tzagoloff, 1987). Other studies have suggested as much as 80-90% of fumarase is in the cytosol of *S. cerevisiae* despite the majority of activity (~70%) taking place within the mitochondria (Sass et al., 2001). Similarly, the proposed cytosolic fumarase, *Smfh$_{II}$*, shows a higher relative expression than its mitochondrial partner *Smfh$_I$* according to DNA microarray estimates.

RNA-seq data generated from a meta-analysis of various RNA-seq studies was used to generate expression profiles of schistosome fumarases. Data corresponding to human-infective lifecycle stages similarly suggested that both fumarases showed relatively high expression across all lifecycle stages. There were some differences between which lifecycle stages showed the highest expression. Cercariae and 6-week adult female worms from a mixed sex infection showed the highest normalised expression in the RNA-seq profile of *Smfh$_I$* while DNA

microarray showed the highest fluorescence intensity in 3-week worms (Figure 3.5 and Figure 3.6). The major difference between the two however, is the difference between *Smfh*$_{I}$ and *Smfh*$_{II}$. In the RNA-seq analysis both fumarases have very similar normalised expression in contrast with the greater expression of *Smfh* $_{II}$ shown by DNA microarray. The ways in which these techniques quantify expression differ and both have their pros and cons.

DNA microarrays have been utilised since the 90s for large-scale studies of gene expression. This technique is a powerful tool for the interrogation of thousands of genes simultaneously and has been utilised for the greater understanding of the differences in gene expression between cancerous and normal tissues (Golub et al., 1999) and identifying differences between strains of organism showing resistance phenotypes (Passador-Gurgel et al., 2007). DNA sequences corresponding with a short sequence of a gene, oligos, are covalently attached to a glass slide. Fluorescently labelled cDNA from an organism or tissue is hybridised to the oligo-containing slide which is then washed to remove non-specific hybridization and quantified for fluorescence. Relative fluorescence of these spots is measured by subjecting these features to excitation and comparing them to background (Hoffmann and Fitzpatrick, 2005). Fitzpatrick et al. (2009) performed microarray analysis of 35,437 oligos of 50 base pairs each over 15 lifecycle stages. mRNA levels were measured by proxy through the generation of cDNA of these lifecycle stages. Other studies have pointed out the limitations of DNA microarrays including the potential for background hybridization interfering with measurements (Zhao et al., 2014). Oligos used for *Smfh* $_{I}$ and *Smfh*$_{II}$ were searched against the genome of *S. mansoni* to identify potential non-specific hybridisation partners, however, the only significant hits corresponded to *Smfh* $_{I}$ and *Smfh* $_{II}$ respectively. Other issues can include the fluorescence limits of these techniques. Although a large quantity of oligos is bound to the DNA microarray, highly abundant genes can cause it to reach saturation. RNA-seq is a technique that utilises next generation sequencing of cDNA libraries generated from isolated

RNA. These readings are aligned to reference genomes and provide a direct expression profile, which is not affected by non-specific hybridization and can account for splice variation and potential sequence differences (Zhao et al., 2014). Many of the schistosome studies using RNA-seq were performed independently of each other exploring expression in a handful of lifecycle stages (Anderson et al., 2015; Lu et al., 2016; Protasio et al., 2012; Wang et al., 2013). Downstream normalisation was performed in the meta-analysis to determine expression profiles (Lu and Berriman, 2018). The striking difference between these two datasets needed to be resolved as both provided a different representation of the potential relationship between these genes.

3.4.4.2 Quantitative PCR Reveals Higher Expression of *Smfh$_{II}$*

Quantitative PCR of *Smfh$_{I}$* and *Smfh$_{II}$* relative to housekeeping genes of low abundance *SmRGBD* and *SmTscD* demonstrated that the human-infective lifecycle stages show relatively high abundance of schistosome fumarases. In early human infection expression of *Smfh$_{I}$* is the highest with cercariae and 24-hour schistosomula showing the highest expression. From 3 weeks onwards the expression profiles of worms are very similar. This would seem to contradict the greater reliance of adult worms on aerobic activity when compared with schistosomula. However, fumarase is not the only indicator of aerobic respiration and likely not the best as these enzymes possess a variety of functions within the cell. The expression of *Smfh$_{II}$* is highest in the 5-week worm, a lifecycle stage where mature adult worms are emerging. The lowest expression is seen in the 24-hour schistosomula at similar levels to that of *Smfh$_{I}$*. Generally speaking, however, the differences in expression between the two genes is more comparable to that of DNA microarray and supports they hypothesis of activity within two cellular compartments with *Smfh$_{II}$* being expressed at a much higher level.

3.4.4.3 Fumarases are Expressed Abundantly in Adult Cells

Recent single-cell RNA-seq data can be used to visualise where genes are expressed most highly in different tissue and cell types. Using the online database SchistoCyte Atlas (https://www.collinslab.org/schistocyte/) data corresponding with different genes can be explored in adult male, mature female and immature female worms (Wendt et al., 2020). Both fumarases were highly expressed across the different cell clusters likely due to their importance in DNA repair and metabolic functions. It was noted that some cells within the clusters showed low enrichment of transcripts, a feature common in these techniques where dropout of expression is observed (Qiu, 2020).

3.4. Conclusion

Fumarases have an interesting evolutionary history that would appear to be linked heavily to the roles these enzymes possess within all organisms but also in the evolutionary requirements of certain groups. This study has explored the presence of class I and class II fumarases in the animal kingdom and beyond. Through greater understanding of the evolution of these genes a possible explanation for the loss of class I fumarases has been proposed due to the higher iron demands of these animals following the evolution of an iron-dependent circulatory system and demands for this element being lowered by the loss of an iron-dependent enzyme. It has also identified the independent loss of class I in Ecdysozoa, however, there is limited information in the literature to explain why this could have occurred. The loss of class I fumarases was found to have occurred in cestodes and could be linked to the streamlining of metabolic pathways seen in many parasitic helminths. Similarly, losses were seen in monogeneans and the class I fumarases of monogeneans and cestodes are closely related.

Further investigations of fumarases revealed that both class I and class II fumarases are capable of mitochondrial and cytosolic functions in different species. It is common for species with two fumarase genes to have one dedicated to the mitochondria and the other dedicated to

the cytosol. Through prediction tools it is postulated that $SmFH_I$ is targeted to the mitochondria while $SmFH_{II}$ is targeted to the cytosol. This would indicate a division of labour between these two enzymes in the parasite and an opportunity to selectively target mitochondrial functions of the parasite with compounds that would have limited activity on the human class II fumarase. Literature was explored to identify the potential importance of aerobic activity in *S. mansoni* and there have been several studies investigating aerobic marker proteins suggesting that adult worms express these genes relatively highly. Additionally, the disruption of oxidative phosphorylation of adult worms with closantel leads to the loss of motility and a phenotype to look for in downstream experiments seeking to disrupt the aerobic metabolic pathway.

Expression profiles from DNA microarray, RNA-seq and qPCR. All profiles showed high expression of both genes across the human-infective lifecycle stages of *S. mansoni*. DNA microarray and qRT-PCR both showed that *Smfh II* was expressed at a much higher level than *SmfhI*, a feature seen in the levels of mitochondrial and cytosolic fumarases. This further suggested that $SmFH_I$ is a mitochondrial fumarase and $SmFH_{II}$ cytosolic fumarase. Finally, the expression of these genes in adult worm cells was shown to be high across all different cell types due to the importance of these enzymes in metabolism and DNA-damage repair.

To understand the importance of these genes in the survival of *S. mansoni* and to further understand the relationship between these two genes, RNAi-mediated functional genomics investigations of SmFHI and SmFHII was next performed.

4. Functional Genomics of *Smfh$_I$* and *Smfh$_{II}$*

4.1 Introduction

This project has established the evolutionary history of the class I and class II fumarases while investigating the potential roles of SmFH $_I$ and SmFH $_{II}$ in the human infective lifecycle stages of *S. mansoni*. So far, this has largely been speculative and based on the interrogation of availably datasets, the use of bioinformatic techniques and through experimental confirmation of expression profiles. It is crucial however, to demonstrate the importance of these genes for the parasite's survival through direct interventions. RNA interference (RNAi) is a technique where mRNA is suppressed or silenced and can lead to the prevention of translation of new enzymes. The phenotypes induced from this direct intervention can be observed in the live parasite. These techniques have been applied to *S. mansoni* both using small interfering (si) RNAs (Krautz-Peterson, et al., 2010) and double stranded (ds) RNAs (Štefanić, et al., 2010). Through the use of these techniques for both genes individually and in combination it is possible to explore the importance of these genes for the survival of *S. mansoni*.

4.2 Aims and Objectives

The aim of this chapter is to elucidate the importance of SmFH $_I$ and SmFH $_{II}$ in the survival of *S. mansoni* and to understand the effect of knocking down these genes in the adult worm. The objectives used to achieve these aims are as follows:

- Long-term culturing techniques for *S. mansoni* adult worms were optimised for use in downstream dsRNA experiments. This was the first time this has been performed within the Hoffmann Lab and allows for the possibility of exploring long-term effects of knockdown.

- siRNA experiments were performed on adult worms to explore whether this widely used technique would produce a knockdown in adult worms.
- dsRNA experiments were carried out for the disruption of *Smfh* $_{I}$, *Smfh* $_{II}$ and both in tandem to understand the effect of knocking down these genes.

4.3 Results

4.3.1 RNAi of *S. mansoni* Adult Worms Using siRNA

Experiments were carried out using siRNAs designed by Merck using their custom siRNA platform. 5 worm pairs were electroporated at 125 V with 5 µg of siRNA and cultured for 7 days in standard worm medium. Each day WHO-TDR scores were taken. Knockdown was assessed after 48 hours by quantitative reverse-transcription PCR. Male and female worms were processed for RNA, however, female RNA was too deteriorated and sufficient cDNA could not be made for knockdown assessment.

Worm scoring found no difference in motility or appearance between worms treated with *siSmfh* $_{I}$, *siSmfh* $_{II}$ or *siLuciferase* (Figure 4.1). In male worm knockdown assessments of siRNA treated worms, all treatments were assessed for their expression of *Smfh* $_{I}$, *Smfh* $_{II}$ and SmAT1 as a reference gene. For *Smfh* $_{I}$ expression, when compared with *siLuciferase* treated worms a knockdown of the gene was seen in *siSmfh* $_{I}$ treatment of 27.16% and an increase of expression was seen in *siSmfh*$_{I}$ treated worms of 12.79% (Fig.4.2). When looking at the expression *Smfh*$_{II}$, an increase of 28.29% was seen in *siSmfh*$_{I}$ treated worms while a knockdown of 27.96% was seen in *siSmfh*$_{II}$ treated worms when compared with *siLuciferase* treatment (Figure 4.2). Experiments were carried out using siRNAs designed by Merck using their custom siRNA platform. 5 worm pairs were electroporated at 125V with 5µg of siRNA and cultured for 7 days in standard worm medium. Each day WHO-TDR scores were taken. Knockdown was assessed after 48 hours.

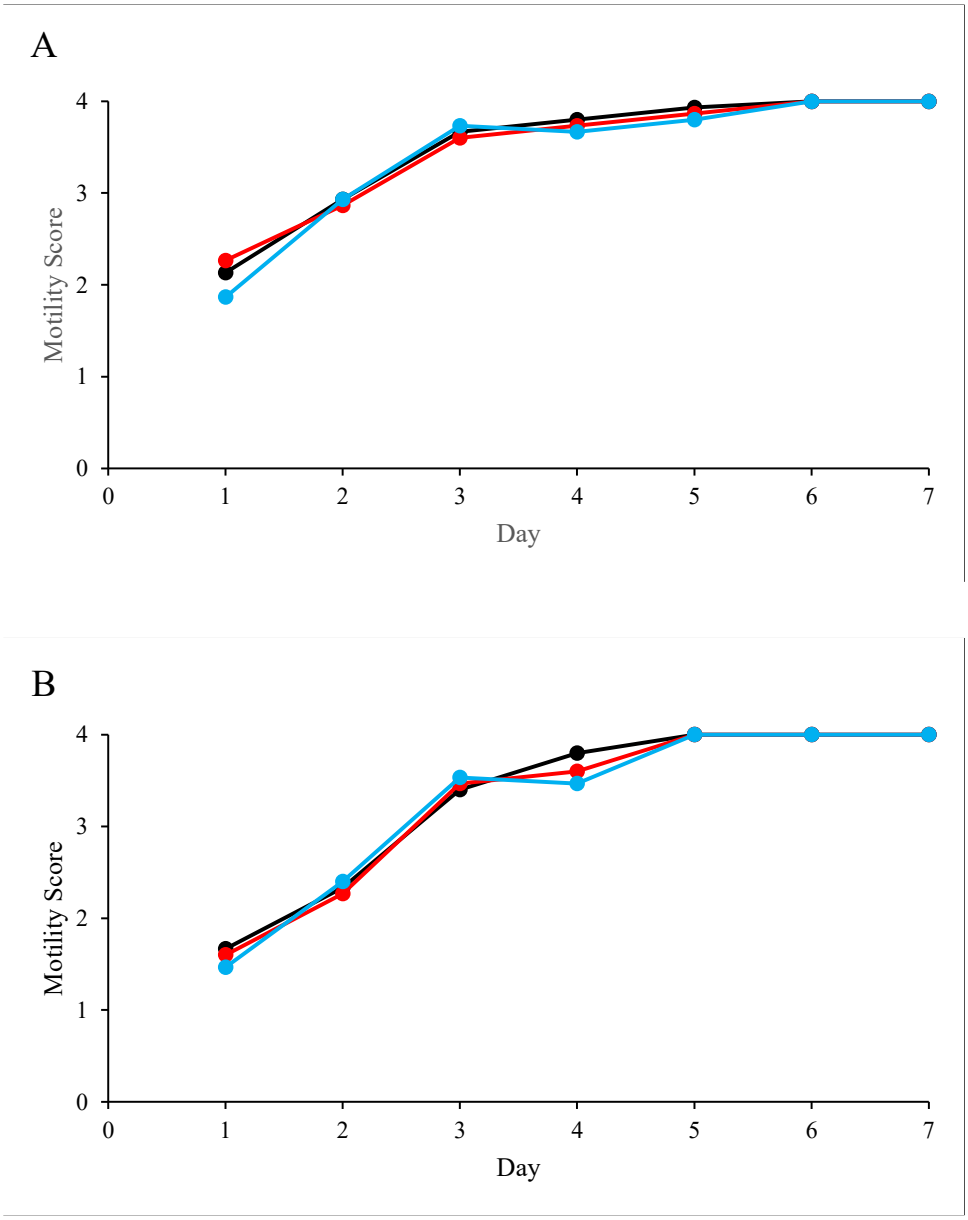

Figure 4.1. Motility of adult worms targeted with small interfering RNAs. RNA interference with siRNAs targeting *Smfh* $_{I}$ (●) and *Smfh* $_{II}$ (●) shows no difference in motility when compared with controls treated with *siLuciferase* (●). Scoring of worms began 24-hours post-electroporation and was carried out for 7 days. Each treatment possessed three replicates of the electroporations consisting of 5 worm pairs. Worms scored by WHO-TDR matrix and plots show the trend in motility over time based on the mean score. A) Male worms. (N = 15) B) Female worms (N = 15).

Worm scoring found no difference in motility or appearance between worms treated with *siSmfh$_I$*, *siSmfh$_{II}$* or *siLuciferase* (Figure 4.1). Male worm RNA was converted to cDNA to assess knockdown by real-time PCR. Primers for *Smfh$_I$*, *Smfh$_{II}$* and *SmAt1* (See 2.5.1) were used in these experiments with *smAt1* acting as the housekeeping gene. Data were assessed using the Pfaffl method with a single housekeeping gene (Pfaffl, 2001). Worms treated with *siSmfh$_I$* were found to have a knockdown in the expression of *Smfh$_I$* of 27.16% (P = 0.63; one-way ANOVA) (Figure 4.2.A) and an increase in expression of *Smfh$_{II}$* of 28.29% (P = 0.49; one-way ANOVA) (Figure 4.2.B) when compared with *siLuciferase* treated worms. Worms treated with *sismfh$_{II}$* showed an increase of 12.79% (P = 0.89; one-way ANOVA) in the expression of *smfh$_I$* when compared to *siLuciferase* control. A knockdown of 49.92% (P = 0.28; one-way ANOVA) was seen in *Smfh $_{II}$* was found in worms treated with *siSmfh $_{II}$* when compared with *siLuciferase* treated controls. None of these changes in expression were found to be statistically significant and remained inconclusive. With no phenotype change observed over a 7-day period and inconclusive knockdown data, it was decided a different approach would be taken for RNAi consisting of longer term culture and the addition of double-stranded RNA (dsRNA) to culture media over time.

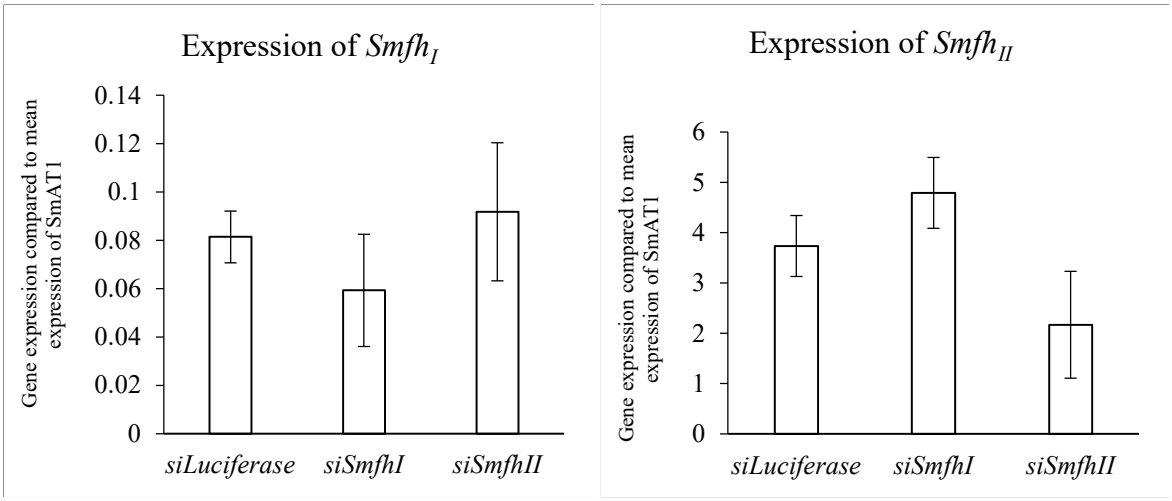

Figure 4.2. Knockdown assessments of schistosome fumarases in adult male *S. mansoni* using siRNAs. Assessments of knockdown were carried out using qRT-PCR procedures using *smAt1* primers as a housekeeping gene. Worms were processed for RNA 48 hours post electroporation. Left panel shows expression of *Smfh*in male worms electroporated with *siLuciferase*, *siSmfh$_I$* and *siSmfh$_{II}$*. Expression levels show a knockdown of 27.16% (P = 0.63; one-way ANOVA) of *Smfh$_I$* when treated with *siSmfh$_I$* when compared to *siLuciferase* and an increase in expression of *Smfh $_{II}$* by 12.79% (P = 0.89; one-way ANOVA) when treated with *siSmfh$_{II}$*. Right panel shows expression of *Smfh$_{II}$* in male worms electroporated with *siLuciferase*, *siSmfh$_I$* and *siSmfh $_{II}$*. Expression of *Smfh $_{II}$* increased by 28.29% (P = 0.49; one-way ANOVA) in males electroporated with *siSmfh $_I$* and a knockdown of 49.92% (P = 0.28; one-way ANOVA) when treated with *siSmfh$_{II}$*.

4.3.3 RNAi of *S. mansoni* Adult Worms Using dsRNA

4.3.3.1 Long-Term Culturing of *S. mansoni* Adults

RNAi experiments carried out over 28 days have been performed for large-scale experiments for the identification of novel therapeutic targets in *S. mansoni* (Wang et al., 2020). Culture techniques in this study were published by Wang et al. (2019) and incorporated the use of medium containing cholesterol, ascorbic acid and erythrocytes. One issue encountered was

the source of cholesterol, a purified low-density lipoprotein (LDL) mixture, from a USA based company Rocky Mountain Biologicals. Importing biological materials for the purposes of culture techniques proved to be difficult with regulatory barriers. It was therefore necessary to source alternative LDL media supplements and test them in a long-term culture pilot study to determine the best replacement.

Five worm pairs were cultured for 28 days in four different culture media (see 2.2.2 for media ingredients). Briefly, the four media used in the long-term culture pilot study included two control media: standard adult worm culture medium used in typical worm culture post-perfusion and adult worm culture medium with the addition of 200 µM ascorbic acid. The two test media were more similar to the so-called ABC (Ascorbic acid, Blood, Cholesterol) media used by Wang et al. (2019). These media consisted of Basch media (see 2.2.2) with the addition of 200µM ascorbic acid and 0.2% v/v bovine cholesterol concentrate (RMBIO) as a source of LDL. In this study 250 x Cholesterol Lipid Concentrate (250 x CLC) (Gibco 12531018) and Chemically Defined Lipid Concentrate (CDLC) (Gibco, 11905031) were tested as sources of LDL. Worm motility was scored every two days with each condition measured in triplicate on two separate occasions. Combined histograms showing the percentage of worm scores is shown in Figure 4.3.

WHO-TDR scores of male worms (Figure 4.3.A) showed all worms across treatments remained motile and in healthy condition for the first 8 days. After this, however, all media showed changes in the worm scores across replicates. The most rapid decline was seen in standard worm media where motility and worm condition decreased rapidly and some worms were found to be dead or highly immotile after 28 days. WM+C showed a similar decline, however worm motility was slightly higher than that of WM. Overall CDLC+C had the healthiest worms after 28 days with motility remaining in the 3-4 score range. It was noted that a decline was seen after 22 days in this condition however this was only slight. Similarly in

female worms CDLC+C showed the highest scores over the 28 day period and also a decline in mean motility after day 22. Up to day 8 all worm scores were high across treatment conditions. However, similar to male worms a rapid decline was seen in WM and WM+C. Following these results long-term RNAi experiments were designed to run for 21 days based on observations of decline following 22 days in culture and would be performed using CDLC+C media, named AC media, to ensure the healthiest conditions for adult worms.

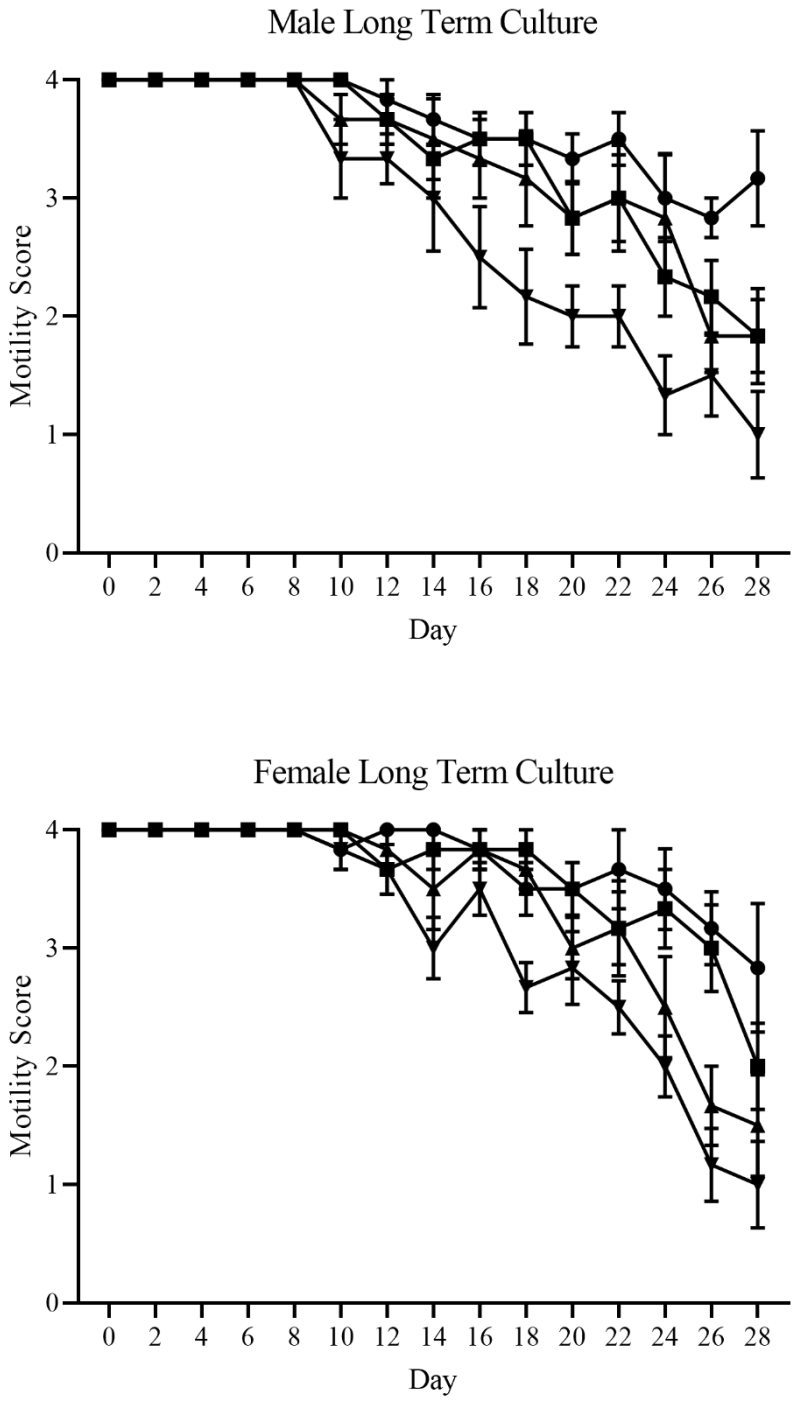

Figure 4.3. Long-term culture of adult worm pairs over 28-days shows health is improved by the addition of lipid supplement and ascorbic acid. Adult worms were cultured in four media. WM (▼, Standard worm culture medium), WM+C (▲, standard worm culture medium with the addition of 200 µM ascorbic acid), CDLC+C (●, BM169, 200 µM ascorbic acid and 0.2% v/v chemically defined lipid concentrate) and 250 x CLC+C (■, BM169, 200 µM ascorbic

acid and 0.2% v/v 250 x cholesterol lipid concentrate). Motility scores were assessed using WHO-TDR method and were plotted as mean score over time with standard deviation of scores shown as error bars. 30 male worms and 30 female worms were used in these analyses.

4.3.3.2 Generation of Double-Stranded RNA

Protocols from Wang *et al*. (2020) were adapted for the generation of dsRNA (2.6.2). Sequences ranging between 500-750 bp were cloned into pJC53.2 vectors for *Smfh*, *Smfh$_{II}$* and firefly Luciferase (2.6.1). Sequencing confirmed the presence of these inserts in the plasmid and miniprepped plasmids were used as templates for *in vitro* transcriptions.

Working stocks of 1 µg/µl were required for RNAi experiments and repeatable production of 2-3 µg/µl of dsRNA was produced using the reaction mixture described in chapter 2.6.2. Products of *in* vitro transcription were run on a 1% w/v agarose gel containing 1:10,000 Sybr-safe gel stain which resulted in bright bands at the correct sizes outlined in table 2.6. Working stocks were made by diluting *in vitro* transcription products to 1µg/µl. Working stocks were used in downstream RNAi experiments.

4.3.3.3 RNAi Using dsRNA

Experiments were performed under conditions determined in section 4.3.3.1. DsRNA addition was modified from large-scale RNAi experiments (Wang et al., 2020). Briefly, adult worms were cultured in 6-well plates in 3 ml of AC media. DsRNA was added at a concentration of 30 µg/ml with a negative control consisting of dsLuciferase (30 µg/ml and 60 µg/ml for double knockdown). For the first 3 days of the experiment media was exchanged daily and fresh dsRNA was applied. Following day 3, media was exchanged every other day with dsRNA applied with each media exchange. Motility of worms was assessed using WHO-TDR method prior to each media exchange. Long-term RNAi experiments were carried out twice with 3 replicates of each condition in each experiment. After 14 days two worm pairs were removed from each replicate for knockdown assessment.

Worm motility of luciferase controls showed relatively high scoring over 21 days. Both male (Figure 4.4.A) and female (Figure 4.4.B) worms both treated with *dsSmfh* $_{I}$ and *dsSmfh* $_{II}$ individually didn't show any difference in motility from negative controls. However, double knockdown showed a rapid decline in motility from day 7 onward.

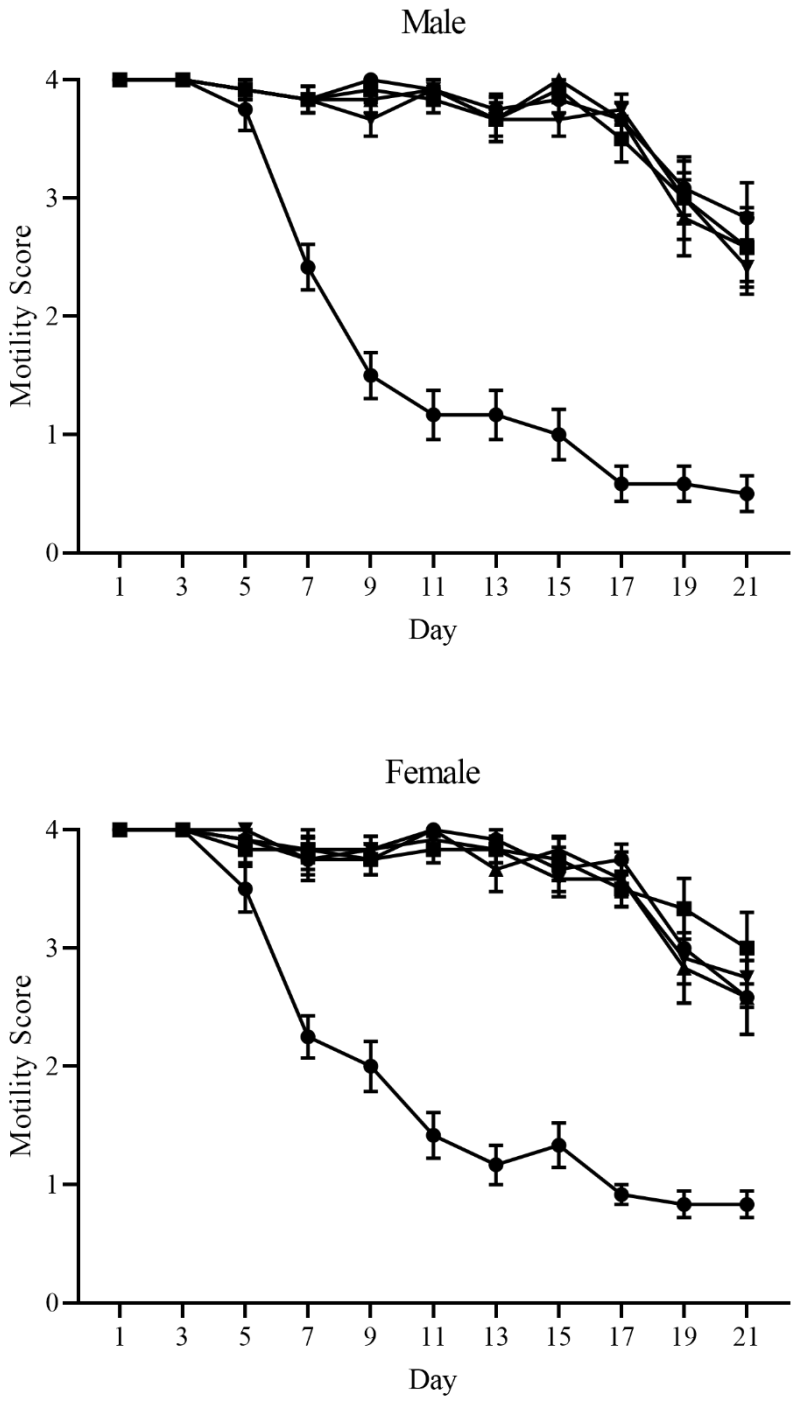

Figure 4.4. RNAi of adult male and female worms using dsRNA over 21 days. Y axis: Worms were scored using WHO-TDR scoring matrix (0-4). Charts show data from two separate knockdown experiments combined for male (top panel) and female (bottom panel) worms. Points represent mean worm score (N = 30 up to day 13, N = 20 after day 13 due to

knockdown assessment). Error bars represent standard deviation. Double knockdown (●), *dsSmfh*$_I$ (▲), *siSmfh*$_{II}$ (♦), *siLuciferase* 30µg/ml (■), *siLuciferase* 60µg/ml (○).

Knockdown of fumarase genes was assessed after 14 days of RNAi. Worms treated with 30 µg/ml and 60 µg/ml of *dsLuciferase* were combined for knockdown assessment. *Smfh*$_I$ expression in male worms (Figure 4.4.A) was found to be significantly knocked down ($P<0.05$, One-way ANOVA) in both double knockdown and in treatment with *dsSmfh*$_I$. Expression of *Smfh*$_I$ in worms treated with *dsSmfh*$_{II}$ was not significantly different from that of luciferase. Expression of *Smfh*$_{II}$ was found to be significantly knocked down in male worms (Figure 4.4.B) in both double knockdown ($P<0.05$) and treatment with *dsSmfh*$_{II}$ ($P<0.01$). No significant difference was seen in the expression of *Smfh*$_{II}$ in males treated with *dsSmfh*$_I$. In female worms no significant knockdown was found in the expression of *Smfh*$_I$ ($P>0.05$) or *Smfh*$_{II}$ ($P>0.05$) in all treatments assessed.

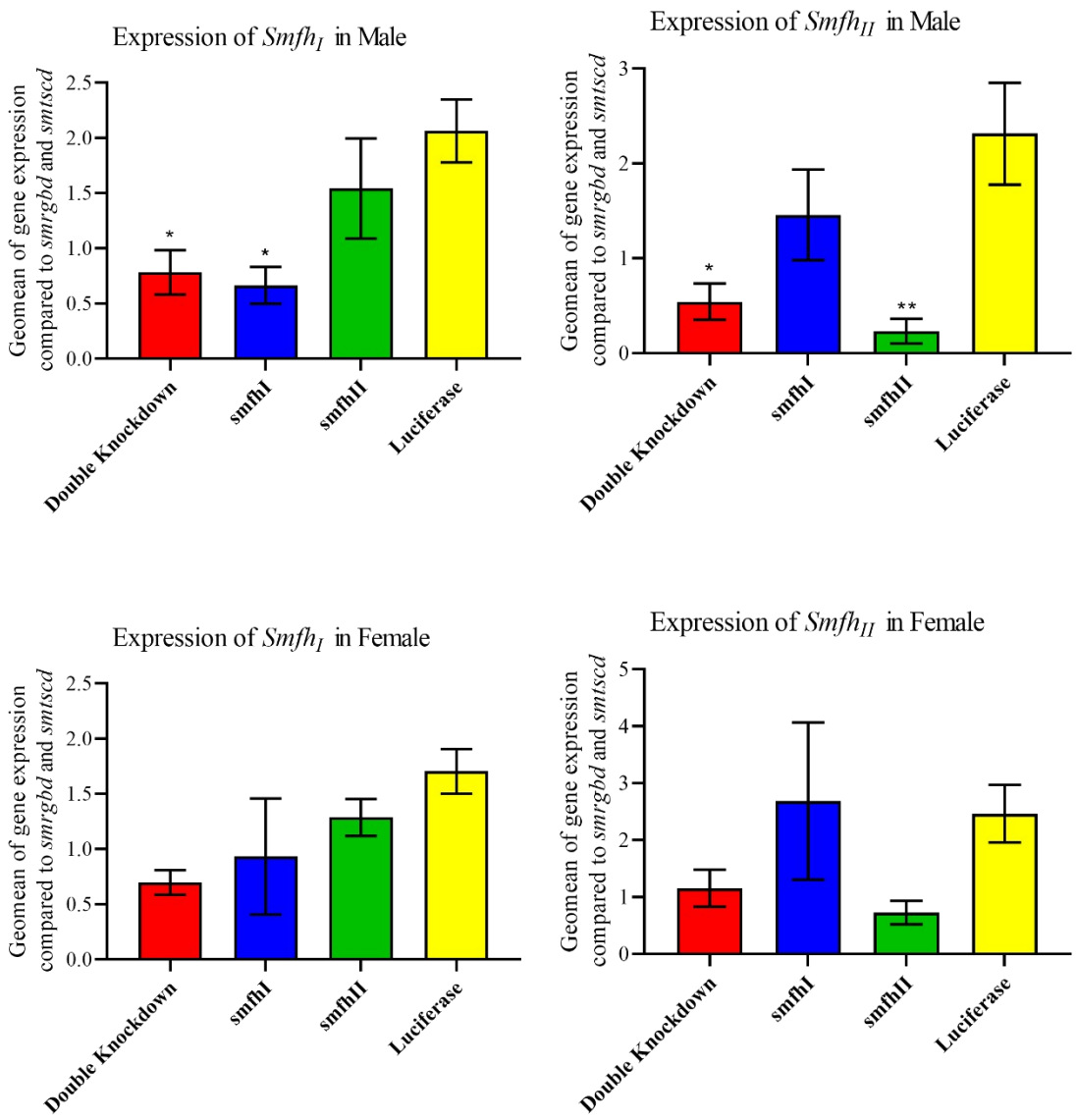

Figure 4.5. Knockdown assessment of *Smfh* $_I$ and *Smfh* $_{II}$ of worms treated with double stranded RNAs show significant knockdown of genes in male worms. Worms were taken for assessment at 14 days to assess knockdown of genes. Worms were sampled from each experimental replicate. Knockdown is shown as the geomean of $Smfh_I$ and $Smfh_{II}$ compared to two housekeeping genes (*SmRGBD* and *SmTscD*). Top left panel shows expression of *Smfh*$_I$ in male worms in all treatments of dsRNA. Top right panel shows expression of *Smfh* $_{II}$ in male worms in all treatments of dsRNA. Bottom left panel shows expression of *Smfh* $_I$ in female worms in all treatments of dsRNA. Bottom right panel shows expression of *Smfh* $_{II}$ in female worms in all treatments of dsRNA.

4.4 Discussion

4.4.1 siRNA experiments suggest changes in expression profiles are dependent on treatment despite no phenotype

RNAi gene silencing has been applied to the characterising of many schistosome targets and their potential for drug targeting using both siRNAs (e.g. Geyer et al., 2011; Hulme et al., 2022) and dsRNAs (e.g. Krautz-Peterson et al., 2010; Wang et al., 2020). When trying to understand the effect of silencing a target it is crucial to also have an awareness of what phenotypes may be exhibited in the organism when successful disruption occurs. In the case of metabolic disruption and more specifically aerobic metabolic inactivity in adult *S. mansoni*, there are historic papers that have shown a loss of motility when the electron transport chain is targeted by closantel (Bossche, 1985). The maintenance of the TCA-cycle is crucial for the electron transport chain to function (Gasmi et al., 2021). Observations in motility loss would suggest a disruption of this pathway.

RNAi using siRNAs targeting schistosome fumarases showed no motility difference to luciferase controls when assessed using WHO-TDR over the course of 7-days. There were differences in the knockdown assessments of male worms, however none of these differences were found to be significant. In the case of both $Smfh_I$ and $Smfh_{II}$ knockdowns, the expression of the other fumarase showed a higher mean expression than luciferase. Although expression differences were not found to be statistically significant, they may be indicative of a compensatory mechanism in fumarase genes.

Genetic compensation to knockout or knockdown of genes have been observed in studies of model organisms (see: El-Brolosy and Stainier, 2017; Tautz, 1992). Compensation of fumarases was briefly discussed in studies exploring the DNA-damage repair mechanism of class I fumarases where yeast were transfected with *E. coli* fumarases and the loss of cytosolic fumarases were suggested to be compensated for by increase in expression of mitochondrial

fumarases (Silas et al., 2021). To the knowledge of this study, no other papers have explored the genetic redundancy/compensatory effect of mitochondrial and cytosolic fumarases to each other. In large part this is due to the fact that most model organisms possess either a single fumarase gene or two highly conserved fumarase genes for both roles (see: Yogev et al., 2011). In many ways, *S. mansoni* presents a unique model for exploring whether genetic redundancy can be observed due to the presence of two distinct fumarases that are predicted to target two separate cellular compartments. With the publishing of data improving long-term *in vitro* culture of adult worms (Wang et al., 2019) and the large-scale RNAi studies using dsRNA (Wang et al., 2020) efforts were refocused to utilise this technique to observe phenotypes of fumarase knockdown over longer time-scales.

4.4.2 RNAi with dsRNA demonstrates knockdown of both fumarases induces motility loss

The long-term knockdown of schistosome fumarases suggests the two genes compensate for one another. In both male and female worms, motility loss was only seen in worms where both genes were targeted (Figure 4.4). When investigating the large-scale RNAi data produced by Wang et al. (2020) both *Smfh* $_{I}$ and *Smfh* $_{II}$ were targeted individually. The study similarly observed no change in motility over the course of 28 days. However, a double knockdown was not performed. This study is therefore the first to show that the knockdown of both *S. mansoni* fumarases induces rapid motility loss after 8 days in culture. Although the knockdown of female worms was inconclusive, male worms were found to show significant knockdowns in both genes when both genes were targeted (Figure 4.5 A and B). It is apparent from these data that there is genetic redundancy in schistosome fumarases.

In higher organisms genetic redundancies are common across genomes (Brookfield, 1997). In *S. mansoni* there are examples of possible genetic redundancies in the identification of many small-scale duplications across the genome (Wang et al., 2017). Many of these duplications occur within protein families likely to be involved in immune evasion such as the

tegumental venom allergen-like proteins (Chalmers and Hoffmann, 2012). In the case of the fumarases, however, these genes are not duplications but are rather two distinct enzymes with overlapping functions. It has been suggested that one of the evolutionary models whereby redundancy can occur stably is when two genes have an overlap in function yet also possess independent roles (Nowak et al., 1997). Although siRNA knockdown data suggested a possible increase in the other fumarase that was not targeted, these data were inconclusive and were not seen in the dsRNA knockdowns.

Metabolites pass between the cytosol and mitochondria regularly (Passarella et al., 2021). The inner mitochondrial membrane is quite restrictive requiring transporters for ions and molecules to move in and out, the outer mitochondrial membrane is highly permeable (Giacomello et al., 2020; Rosencrans et al., 2021). In the case of fumarate (Atlante et al., 1985) and malate (Rognstad and Katz, 1973) this trend is no different and can occur rapidly. Fumarate as a signalling molecule is involved in innate immune system functions such as the suppression of B-cell activation (Cheng et al., 2022) and the release of mtDNA (Zecchini et al., 2023). Fumarate production originating from the mitochondria can induce these signalling pathways (Cheng et al., 2022). Malate also moves between the mitochondria and cytosol. In the aerobic TCA-cycle fumarate is converted to malate, however malate can also be produced from the conversion of pyruvate to malate via malic enzymes (Saz and Hubbard, 1957). It is possible that the movement of fumarate and malate between the cytosol and mitochondria and the employment of other enzymes, including the second fumarase possessed by *S. mansoni*, could maintain the cellular roles of fumarases in the TCA-cycle. Further research is required to investigate the enzymatic activity of the two *S. mansoni* fumarases and to determine their enzymatic turnover as this could inform future understanding of the redundancy seen in this study.

4.5 Conclusions

This study represents the first time a mitochondrial and cytosolic fumarase has been selectively targeted in a metazoan. This is due to the presence of two biologically distinct fumarases in *S. mansoni*. These results further emphasise the importance of elucidating the localisation of $SmFH_I$ and $SmFH_{II}$ in the cell. A greater understanding of the effects disrupting the translation of these genes or the inhibition of these enzymes has on other metabolic enzymes may provide further insights into how metabolic activity is maintained. This could be achieved by exploring the expression of other genes when these fumarases are silenced.

Data from these experiments informed strategies for enzyme inhibition. The initial exploration of inhibiting only $SmFH_I$ has been shown to potentially not be enough to disrupt adult worms. Other strategies to identify inhibitors of $SmFH_{II}$ were also explored in chapter 5.

5. Drug design and compound screening against $SmFH_I$ and $SmFH_{II}$

5.1 Introduction

In parallel to the RNAi study described in Chapter 4, we sought to investigate whether compounds predicted to bind and affect the activity of $SmFH_I$ (either alone or in combination with inhibition of $SmFH_{II}$) represented a novel strategy for future chemotherapeutic interventions. Here, we describe the identification of compounds predicted to target $SmFH_I$. Further, we describe the testing of these compounds in whole organism phenotypic screens (firstly against larval stage schistosomula, and latterly against adult worms) both individually and in tandem with a compound known to affect the activity of mammalian class II fumarases.

5.2 Aims and Objectives

The primary aim of this chapter is to discover compounds that are predicted to target $SmFH_I$ and to use these compounds in screens of live parasites to determine whether they cause a phenotype after co-culture. A secondary aim of this chapter is to use a known class II fumarase inhibitor, in isolation or tandem with the predicted $SmFH_I$-targeting compounds, to assess phenotypic affects in schistosomula and adults. The objectives to achieve these aims are as follows:

- Computer models of $SmFH_I$ were generated using Molecular Operating Environment (MOE) 2014.09 (Chemical Computing Group ULC). Models were used for docking simulations using a range of programs to form a consensus, targeting the active-site cavity of $SmFH_I$. Virtual screens were carried out against the Specs library of 300,000 compounds.
- Class II fumarase inhibitors were identified in the literature for use in drug screens and were synthesised by colleagues at the University of Dundee.

- Drug screens were performed on *S. mansoni* schistosomula using the Roboworm platform and on adult worms using the WHO-TDR scoring matrix. Screens were performed individually and in tandem with $SmFH_I$ and $SmFH_{II}$ targeting compounds.

5.3 Results

5.3.1 Computer aided drug discovery

5.3.1.1 Homology model of $SmFH_I$

Protein modelling and docking was performed with the assistance of Dr. Salvatore Ferla previously based at Cardiff University. Protein models for $SmFH_I$ were generated using MOE 2014.09. An X-ray crystal structure for SmFHwas not available at the time of this work. Homology modelling of $SmFH_I$ was therefore carried out (Chapter 2.7.2) using the resolved crystal structure of *L. major* class I fumarase, LmFH-2 (5L2R) (Feliciano *et al*., 2016). The amino acid sequences of $SmFH_I$ and 5L2R were aligned: 90% query cover, 60.48% identity (Figure 5.1). The identity was above the 30% cut-off used often in homology modelling for identifying homologs (Pearson, 2013).

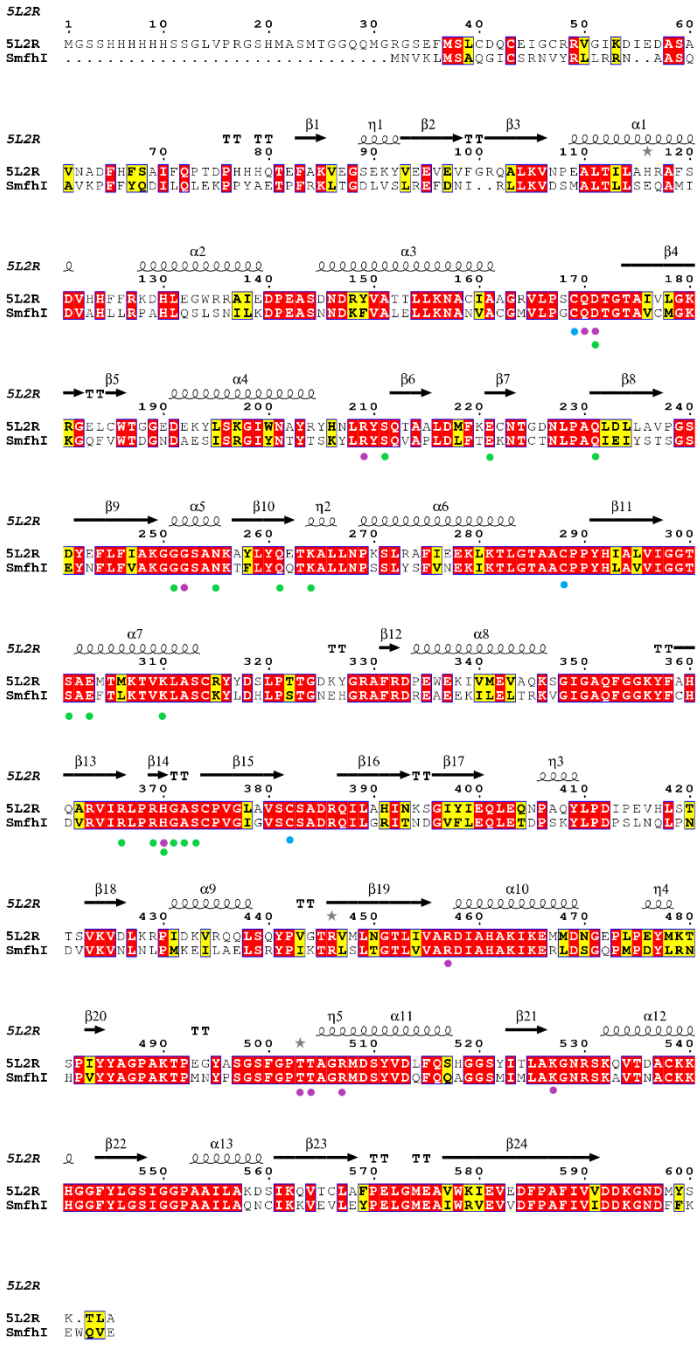

Figure 5.1. Multiple sequence alignment of the sequence of the *L. major* LmFH-2 (5L2R) and SmFHI. α helices indicated by spirals and β pleated sheets indicated by arrow above the sequence tracks. The first 36 residues of 5L2R are residues associated with the 6-His tag and expression vector used to generate this enzyme. Conserved residues are indicated by red boxes. Similar residues are indicated by yellow boxes. Conserved active site residues for class I

fumarases are indicated by purple dots. The three conserved cysteine residues are indicated by blue dots, these interact with the [4Fe-4S] cluster in the active site. The conserved site of dimerisation residues for class I fumarases are indicated by green dots. Alignment was carried out using MUSCLE (EMBL-EBI) and visualised using ESPript 3.0 (https://espript.ibcp.fr).

PDB files of 5L2R were used for induced fit homology modelling in MOE. Crystallisation solvents were kept in the model initially to provide an improved induced fit of $SmFH_I$ to the model. All small molecules and solvents were subsequently removed post-model generation for downstream docking. PDB models of $SmFH_I$ were generated for downstream docking simulations (Figure 5.2.A). Within this enzyme the so-called active site cavity; a positively charged cavity identified in LmFH-2 crystal structures (Feliciano et al., 2016) was identified (Figure 5.2.B). Amino acids that interact with *S*-malate within the positive cavity for transport to the active site: ASN-220 and PHE-223 on one monomer and GLN-226 on the other were highlighted (Figure 5.2.C). LmFH-2 possesses a TYR-222 instead of a PHE-223 in multiple sequence alignments (Figure 5.1). Models contained [4Fe-4S] clusters in the active sites (Figure 5.2.B); these models were simulated with the cluster interacting with malate (Figure 5.2.D).

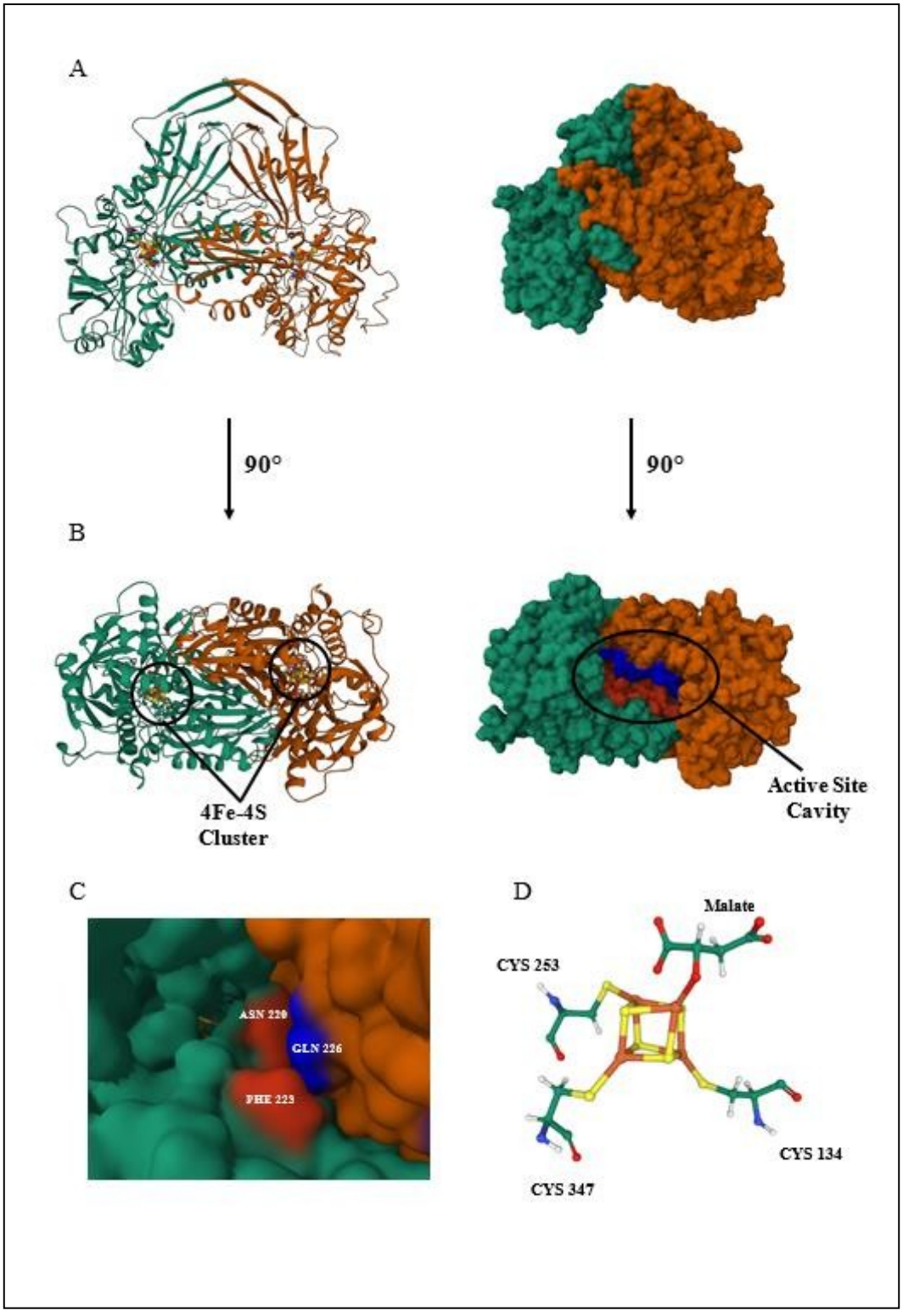

Figure 5.2. Homology model of $SmFH_I$ based on *L. major* LmFH-2 (5L2R) crystal structure. (A) Homo-dimer of $SmFH_I$ shown in cartoon and Gaussian surface representations show the interaction between the two monomers (green and orange). (B) 90° rotation of the homology model to highlight the active site cavity. [4Fe-4S] cluster can be seen on the cartoon

representation within each monomer. Gaussian surface representation shows the formation of the active site cavity between the two monomers (red and blue). (C) Active site cavity amino acids that have been demonstrated to interact with malate during the shuttling of substrates to the active site. ASN-220 and PHE-223 of one monomer (red) and GLN-226 of the other monomer (blue) interact with substrates (Feliciano, *et al.*, 2016). (D) 4FE-4S cluster found within the active site of $SmFH_I$ is linked with CYS-134, -253 and -347 and interacts with malate.

5.3.1.2 Identification of $SmFH_I$ inhibitors using *in silico* docking

5.3.1.2.1 Docking site identification

Structure-based virtual screening was carried out using the homology model of $SmFH_I$. Firstly, a compound library consisting of 300,000 compounds from Specs (www.specs.net; full library including natural compounds and fragment-based library) was accessed using the Cardiff University compound database. Identification of docking sites was performed by uploading the $SmFH_I$ model to Maestro (Schrödinger, 2014). The active site cavity was highlighted as the most appropriate target for *in silico* docking due to its importance in shuttling substrates to the active site and facilitation of enzymatic activity (Feliciano et al., 2019, 2016; Feliciano and Drennan, 2019); and subsequent docking simulations were limited to the active site cavity of $SmFH_I$

5.3.1.2.2 Docking

Structure-based virtual screening is described in detail in chapter 2.3.7.2. The workflow for the docking experiments can be seen in Figure 5.2. Briefly, docking was performed using Glide (Maestro, 2014). High throughput virtual screening (HTVS) was performed on the initial library of 300,000 compounds before being performed with the standard precision (SP)

function. HTVS narrowed the number of unique compounds to 222,000. The Glide SP function tested these predictions more stringently and discarded some false positives before feeding directly into the extra precision docking (XP) function. XP is more stringent than HTVS and SP and applies advanced sampling and scoring matrices to narrow down the number of compounds. These compounds were then rescored using two additional docking programs: FlexX and PLANTS to confirm hits and select only those which were confirmed by Glide, FlexX and PLANTS.

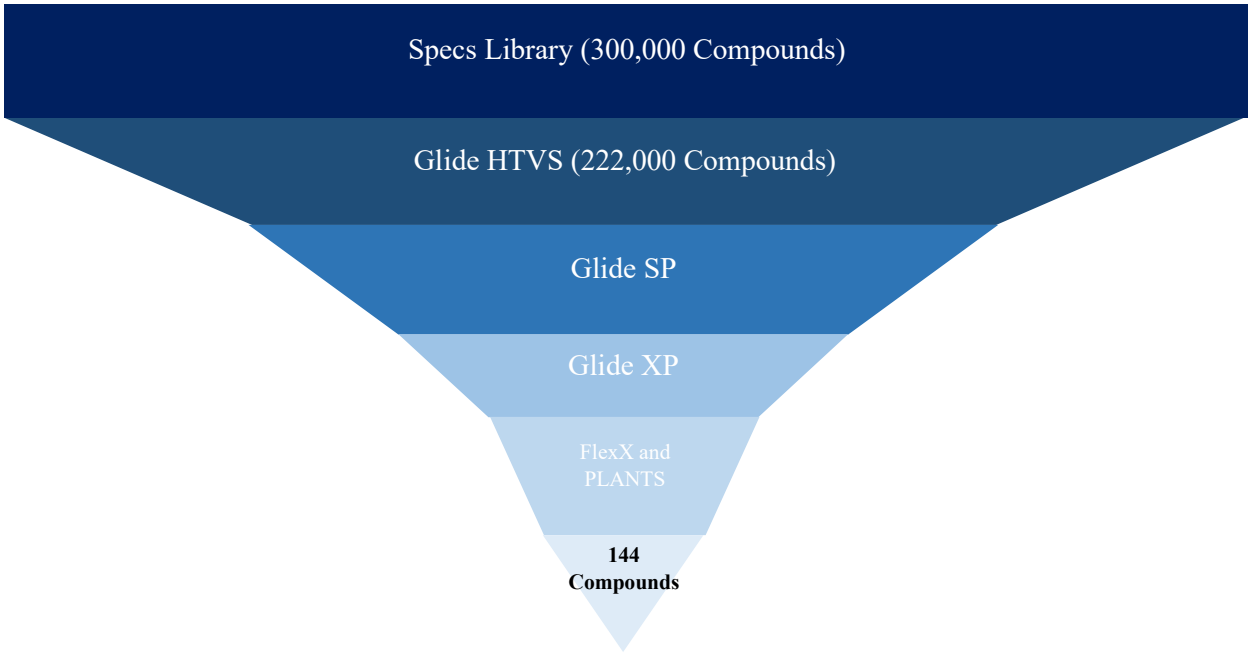

Figure 5.2. Workflow for *in silico* docking of Specs library results in 144 hits. Specs library of 300,000 compounds was screened against homology model of SmFH I through a standard workflow consisting of high throughput virtual screening (HTVS), standard precision screening (SP) and stringent extra precision docking (XP) in the Glide software within Maestro (Schrödinger, 2014). Compounds that passed this screening were confirmed using two additional docking programs FlexX and PLANTS. Only compounds that registered as hits in all three programs were taken forwards.

144 hits were identified through this pipeline and consisted primarily of negatively charged compounds (Appendix, supplementary table. 1). 14 compounds were no longer available from Specs or required synthesis and were therefore not considered for compound screening on live parasites. Of the remaining available 130 compounds, 18 were selected and purchased from Specs with the help of Dr. Gilda Padalino (Table 5.1).

Table 5.1. Putative $SmFH_I$ inhibitors identified in CADD and purchased from Specs

Name	Specs ID	PubChem CID	Chemical Formula	Molecular Weight	LogP (o/w)	Chemical Structure
C1	AN-655/37429001	1768627	$C_{26}H_{20}F_2N_2O_5S$	509.509	6.0407	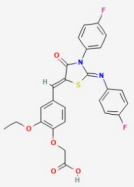
C2	AK-777/12226015	3372165	$C_{22}H_{14}N_2O_2S_3$	433.556	5.891	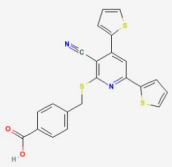
C3	AM-879/40769195	6875320	$C_{24}H_{25}N_3O_4S$	450.539	5.732	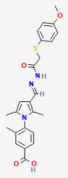
C4	AH-487/40935684	1740193	$C_{22}H_{16}N_2O_3S_2$	419.505	5.651	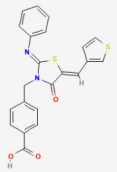
C5	AI-061/33261002	738801	$C_{17}H_{14}N_2O_2S$	309.369	4.067	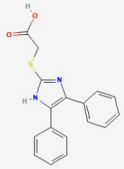

C6	AS-871/13716083	6017359	C17H15ClO4	317.748	4.4267	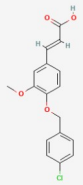
C7	AQ-390/43490637	363328462	$C_{21}H_{18}N_2O_4S$	393.443	4.21	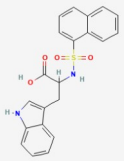
C8	AE-641/05555035	725043	$C_{12}H_8ClNO_2S$	264.712	3.713	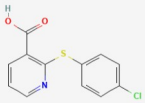
C9	AN-465/43411315	16765663	$C_{22}H_{23}NO_5$	381.428	3.6137	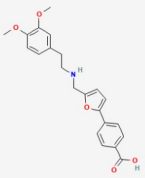
C10	AG-670/36930008	747913	$C_{17}H_{16}N_2O_2S$	311.385	4.139	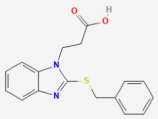
C11	AF-399/15284106	2887123	$C_{20}H_{19}FN_2O_3$	353.373	3.798	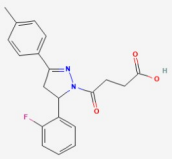
C12	AK-968/37156099	1750068	$C_{12}H_{10}N_2O_3S$	261.281	2.303	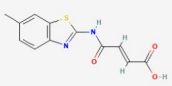
C13	AN-329/40942995	3876194	$C_{22}H_{36}N_2O_6$	422.522	2.176	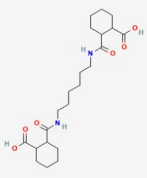

C14	AP-853/43445410	44123244	$C_{17}H_{14}ClN_5O_3S$	402.842	2.531	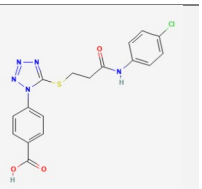
C15	AP-263/43417994	16645330	$C_{15}H_{21}NO_5S$	326.393	1.377	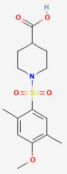
C16	AN-329/11954206	4427060	$C_{17}H_{22}N_2O_5$	333.364	1.781	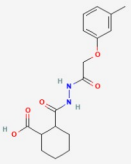
C17	AQ-390/43490690	24319913	$C_{16}H_{23}NO_4S$	324.421	3.132	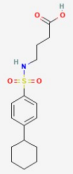
C18	AP-263/43503305	50876604	$C_{15}H_{14}ClNO_6S$	370.789	2.82	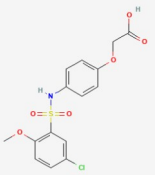

5.3.2 Class II fumarase inhibitors

5.3.2.1 Compound identification using ChEMBL

$SmFH_I$ and $SmFH_{II}$ were BLASTp searched against the ChEMBL database of targets. A single hit was returned for $SmFH_{II}$: ChEMBL target P10173, the class II fumarase of *Sus scorfa*. This target was associated with a single compound: CHEMBL538419. A PubChem search revealed this compound to be 2,3-dicarboxyaziridine (CID:3080847) which has previously been studied and was found to be a competitive inhibitor of class II Fumerase enzymes (Greenhut et al., 1985; Rose, 1998). Synthesis of this compound was required for use in compound screening on live *S. mansoni* due to the lack of commercial suppliers.

5.3.2.2 Synthesis of 2,3-dicarboxyaziridine

All synthesis of 2,3-dicarboxyaziridine was kindly carried out by Dr. Priscilla Mendonca Matos Day at the University of Dundee Drug Discovery Unit, School of Life Sciences.

Synthesis of 2,3-dicarboxyaziridine was carried out as described by Legters *et al*. (1991) and described in chapter 2 (2.8.2), the process yielded 2,3-dicarboxyaziridine in excess of 50mg.

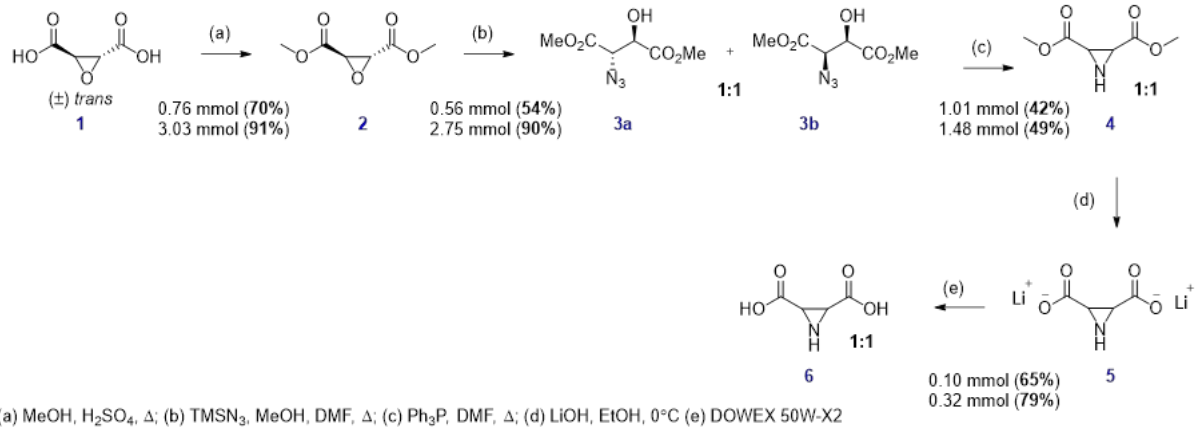

Figure 5.3 Synthesis of 2,3-dicarboxyaziridine. Esterification of commercially available (+/-)-trans-Oxirane-2,3-dicarboxylic acid (1) under acidic conditions in methanol yielded methyl ester (2). A ring opening of the epoxide moiety in compound (2) using trimethylsilyl azide yielded the azido alcohol compounds (3a and 3b), which was then reacted with triphenylphosphine in dimethylformamide to afford the ring closure aziridine motif in compound 4. The subsequent synthetic step was a saponification reaction on compound (4) using lithium hydroxide, and the final step involved the ion-exchange resin using DOWEX 50W-X2 to access 2,3-dicarboxyaziridine (6).

5.3.3 *In vitro* drug screening

Screening of compounds identified in 5.3.1 and 5.3.2 was carried out individually and in tandem (i.e. 2,3-dicarboxyaziridine in combination with each of the 18 Class 1 inhibitors,

separately) against *S .mansoni* parasite life-cycle stages found within the definitive host; Screens were initially performed on larval stage *S. mansoni* using the Roboworm platform. Compounds identified as hits on Roboworm were progressed for screening against adult male and female worms.

5.3.3.1 Schistosomula screens of putative $SmFH_I$ and $SmFH_{II}$ inhibitors individually and in tandem

The Roboworm platform is a bespoke high-throughput, high-content imaging platform that allows the imaging and analysis of 384-well plates harbouring co-incubations of larval stage parasites with compounds of interest. Image analysis is undertaken by a custom-build analysis package written using the software package Pipeline pilot V9.2.

Those compound treatments that result in scores of less than -0.15 for phenotype and -0.35 for motility are considered to be a 'hit' in this assay. As part of this study, compounds were screened individually as dose titrations (0.625 μM, 1.25 μM, 2.5 μM, 5 μM, 10 μM, 25 μM and 50 μM) in duplicate, on three separate occasions. Figure 5.4 shows the results of a representative Roboworm screen for motility and phenotype of schistosomula with corresponding image.

At 72 hours, compounds C2 and C4 were found to be hits in all three screens at 50μM (Appendix, supplementary figure. 3). At 120-hours C2 and C4 were both hits in all replicates of 50 μM (Appendix, supplementary figure. 4). In plate 1053 C2 was a hit at 25 μM in a single replicate however, this was not seen in the other screens. C12 at 50μM was a hit in plate 1036; however, this did not occur in other screens performed.

All putative $SmFH_I$ inhibitors were also screened in tandem with 2,3-dicarboxyaziridine. These screens were performed using a similar workflow to the one outlined above, i.e. as dose titrations (where both compounds were screened at the same concentration) at the same titrations as above and performed three times. All dilutions were performed in

duplicate. In all three screens at 72-hours, C2 and C4 in combination with 2,3-dicarboxyaziridine at 50 µM were hits (Appendix, supplementary figure. 5). No other hits were identified. At 120-hours both C2 and C4 combinations at 50 µM were hits in all screens (Appendix, supplementary figure. 6). C12 in combination with 2,3-dicarboxyaziridine was found to be a hit in plate 1034 in both replicates and in plate 1041 in a single replicate. This was not a hit in plate 1031.

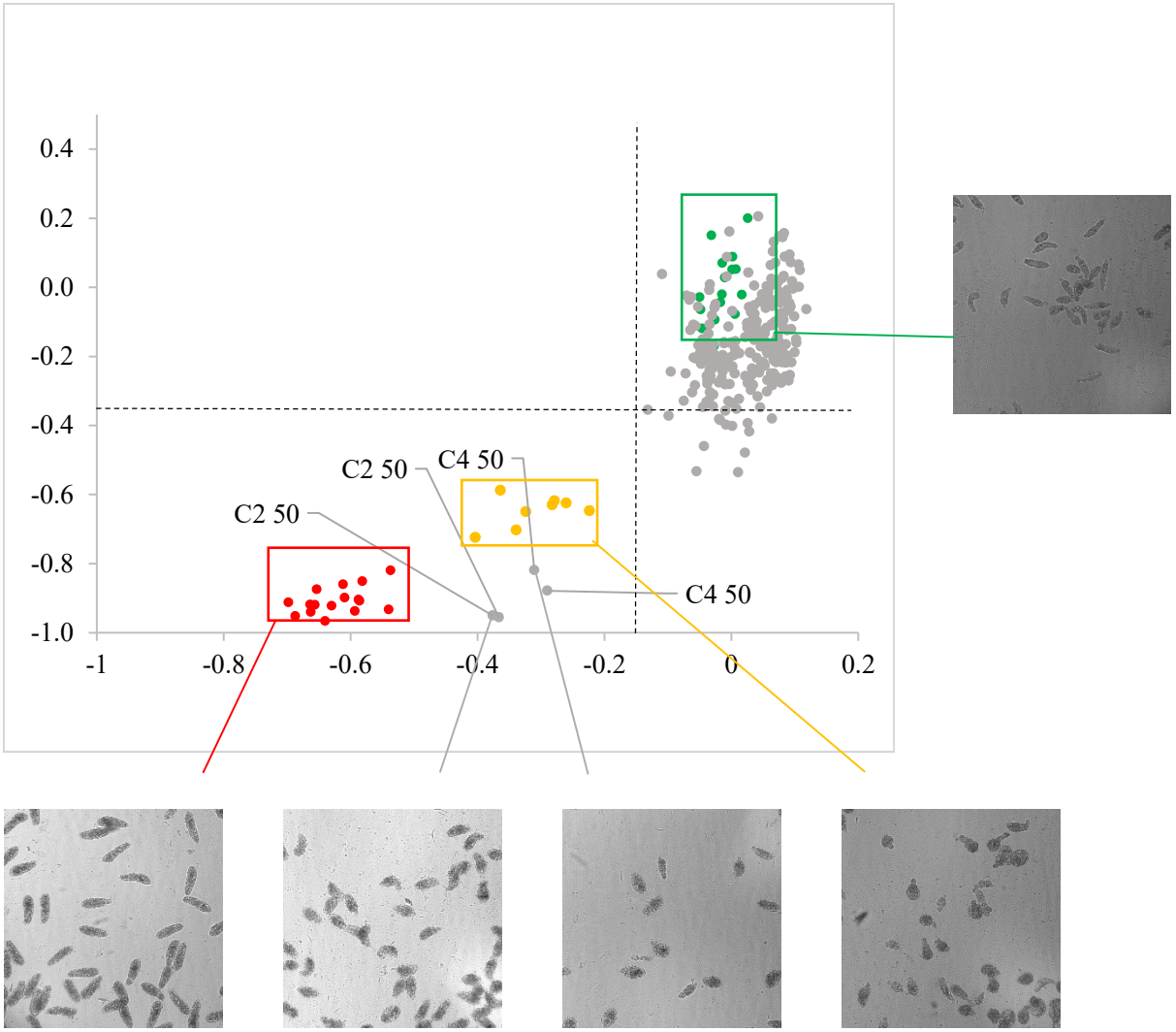

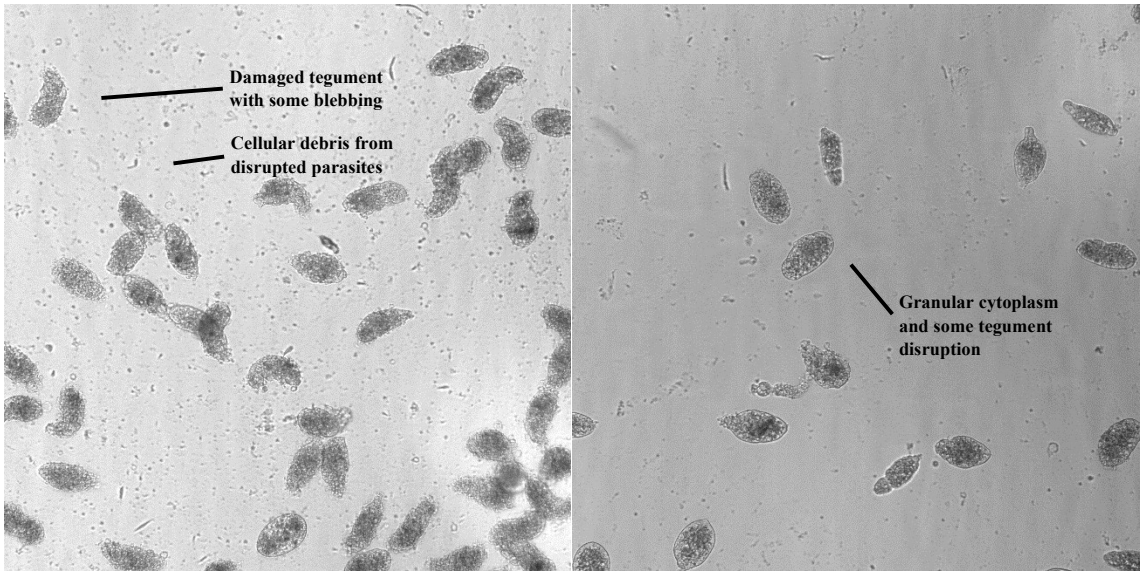

Figure 5.4. Representitive schistosomula screens of putative SmFH$_I$ inhibitors from Specs and 2,3-dicarboxyaziridine shows hits for C2 and C4 at 50 µM. Mechanically transformed schistosomula (n = 120) were incubated at 7 dilutions (0.625 µM, 1.25 µM, 2.5 µM, 5 µM, 10 µM, 25 µM and 50 µM). Parasites were incubated at 37°C and 5% CO_2. Y-axis represents motility score, and X-axis represents phenotype score. Compounds were determined as a hit when motility and phenotype scores were within the 'hit zone' delineated by the dashed lines. Auranofin (●), praziquantel (●), DMSO (●), test compounds (●). Screen taken at 5-days where SmFH$_I$ inhibitors were combined with 2,3-dicarboxyaziridine at equal concentrations. All screens recorded C2 and C4 as hits at 50 µM with or without 2,3-dicarboxyaziridine (See appendix, supplementary figure 3-6). Images show representatives of those used to score the schistosomula taken by the Roboworm platform. Bottom panels show images of C2 50 (left) and C4 50 (right) expanded to show parasite condition and cellular debris from compound disruption.

5.3.3.2 Adult worm screens of C2 and C4

Compounds C2 and C4 were taken forward for testing on adult *S. mansoni*. Given that these compounds were only active in Roboworm screens at 50 µM, worm pairs were dosed with 100 µM, 50 µM and 25 µM (in 1% DMSO) for 72-hours. All screens were compared with a 1% DMSO control. Worms were scored using the WHO-TDR scoring method (4 = normal full-body activity, 3 = slowed full-body activity, 2 = movement only at the head and/or tail, 1 = absence of motility in the body but gut movement present, 0 = total absence of motility in the body and gut) (See Chapter 2.3.5). Screens were performed in triplicate on two separate occasions.

In male worms DMSO controls showed scores of 4 in all replicates across both screens with the exception of one worm at 24-hours scoring 3 (Figure 5.5.A). In males, C2 was found to reduce motility in all replicates after 72-hours at 100 µM with the majority scoring 2 (N = 4) and one scoring 1. In the first screen male worms showed a loss of motility over time at 100µM C2 two worms scoring 3 and above for 24- and 48-hours before scoring a 2. In the second screen both males scored a 2 during this same time period. At 50 µM, C2 showed a slight reduction in motility of male worms over 72-hours with worms scoring 3 in the first screen (N = 3) but no difference between treatment and control in the second screen (N = 3). Similarly for 25 µM C2 there was no loss of motility seen after 72-hours with two male worms scoring 3 at 24-hours and one scoring 3 at 48-hours.

C4 had a greater effect on male worms with 100 µM causing a total loss of motility and death of the worms within the first 24-hours (N = 4) with the exception of one worm that scored a 2 after 24-hours (Figure 5.5). From 48-hours onward, all worms at 100µM scored 0. At 50 µM C4, male worms showed an initial reduction of motility after 24-hours, with one worm scoring 0 in the first screen (Figure 5.5.A. The majority of male worms scored a 1 after 24-hours of 50 µM C4 in both screens (N = 4) with a single worm scoring a 2 in the second screen

(Figure 5.5.B). There was some recovery in both screens after 48- and 72-hours with the first screen showing one individual male returning to a score of 3, one scoring a 2 and the worm that scored 0 scoring a 1 (Figure 5.5.A). In the second screen, all male worms scored a 2 at 48- and 72-hours (N = 3) (Figure 5.5.B). At 25µM C4, male worms showed reduced motility after 24-hours with most male worms scoring 2 (N = 5) and one scoring 3. At 48- and 72-hours motility scores were 4.

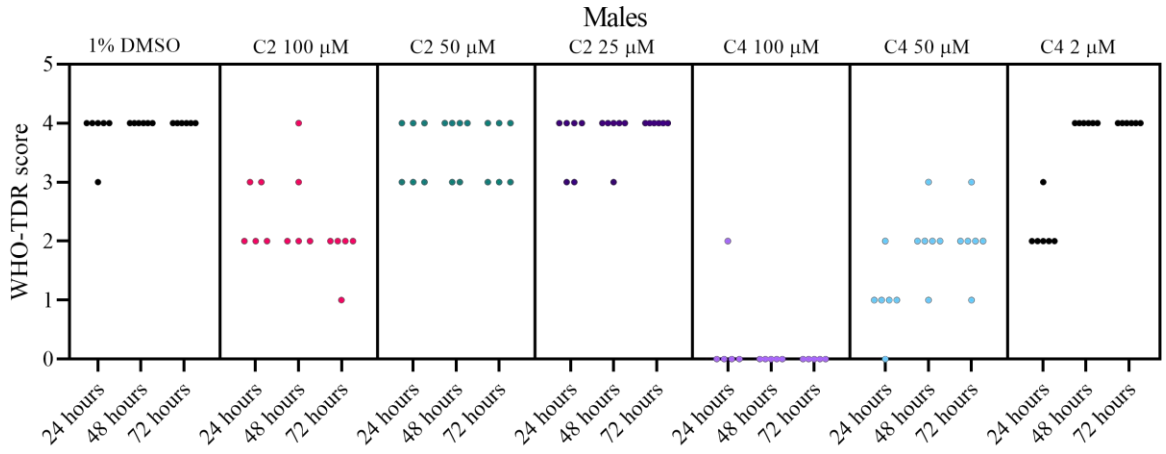

Figure 5.5. Male compound screening of C2 and C4 at 100, 50 and 25 µM. Scores were taken at 24-, 48- and 72- hours based on motility of the male worms.

In female worms both compounds had less of an effect on motility than in males (Figure 5.6). C2 in females showed greatest effect at 100 µM where after 24-hours two worms in the first screen scored 2 and one worm scored 3 (Figure 5.6.A) and in the second screen all worms scored 2 (N = 2, Figure 5.6.B). At 48-hours females recovered to a motility score of 3 in the first screen (N = 3) but remained at a score of 2 in the second screen. At 72-hours one female worm scored 2 in the first screen while the remaining two scored 3 and in the second screen one worm scored 2 and one worm scored 3. At 50 and 25 µM C2, all female worms scored 3 and 4 at all time points (Figure 5.6). Compound C4 at 100µM resulted in all female worms scoring 2 in the first screen (N = 3) at 24- and 48- hours with one female worm scoring 0 at 72-

hours. In the second screen at C4 100 µM (N = 2), one female scored a 2 and one scored a 0 at all time points. At 50 µM C4, all female worms scored 2 at 24-hours in both screens (N = 6). At 48-hours a single female in each screen scored 3. At 72-hours this female remained at a score of 3 in the first screen (Figure 5.6.A) but the female in the second screen scored 2 at 72-hours (Figure 5.6.B). 25 µM C4 showed initial reduction in motility in the first screen where two females scored 2 and one scored 4. At 48-hours all females in the first screen scored 3 and at 72-hours two scored 3 and one scored 4 (Figure 5.6.A). In the second screen a single female scored 2 and two females scored 3 after 24-hours. At 48-hours two females scored 3 and a single female scored 4 and at 72-hours two females scored 4 and a single female scored 3 (Figure 5.6.B).

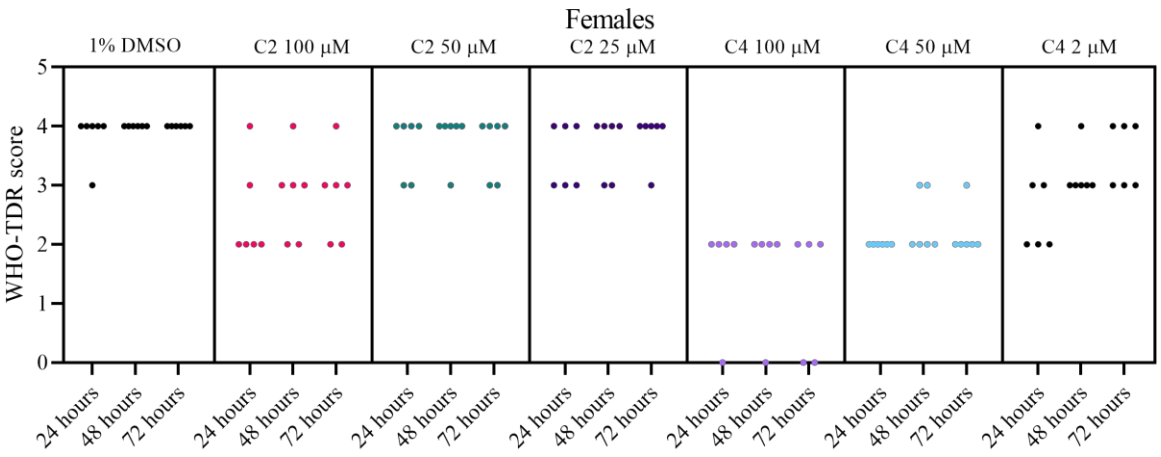

Figure 5.6. Female compound screening of C2 and C4 at 100, 50 and 25 µM. Scores were taken at 24-, 48- and 72- hours based on motility of the female worms.

Data collected from the adult worm screens detailed above were used to generate IC50 curves (Figure 5.7). C4 was calculated to be more potent to both male and female worms than C2.

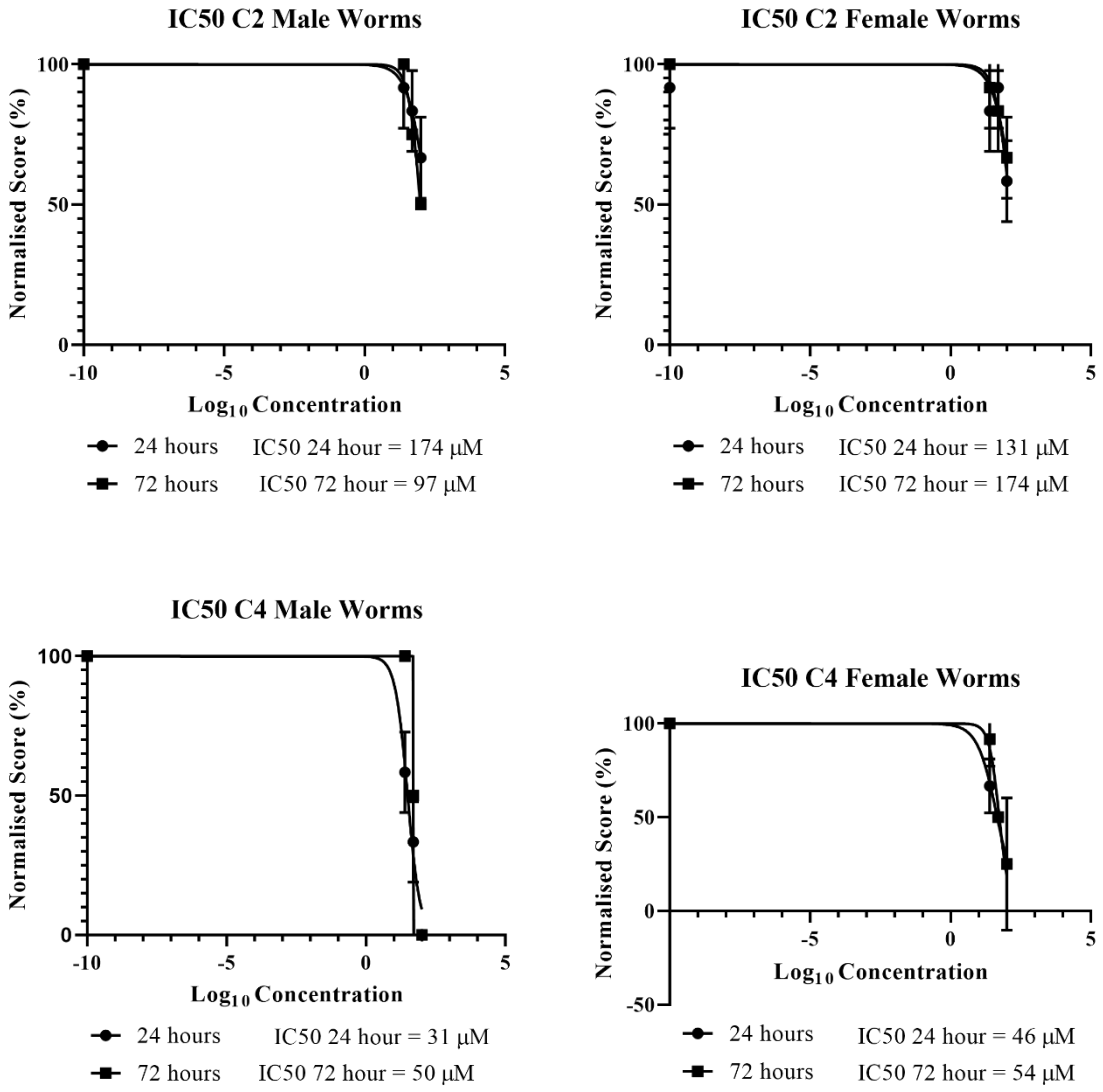

Figure 5.7. IC50 plots of C2 and C4 in adult male and female worms shows that C4 is more potent than C2 in both sexes.

5.3.4 Cytotoxicity of C2 and C4 in HepG2 cell cultures

Cellular cytotoxicity was assessed in C2 and C4 using human HepG2 cell lines as described in chapter 2 (METHODS). MTT assays were performed to calculate percentage cell viability when dosed with C2 and C4. HepG2 cells were incubated in the presence of 100, 75, 50, 25, 10, 5 µM (in 1% DMSO) and compared with a DMSO control. This experiment was performed twice and in both cases, neither compound showed cytotoxicity and there was no correlation shown (Figure 5.8).

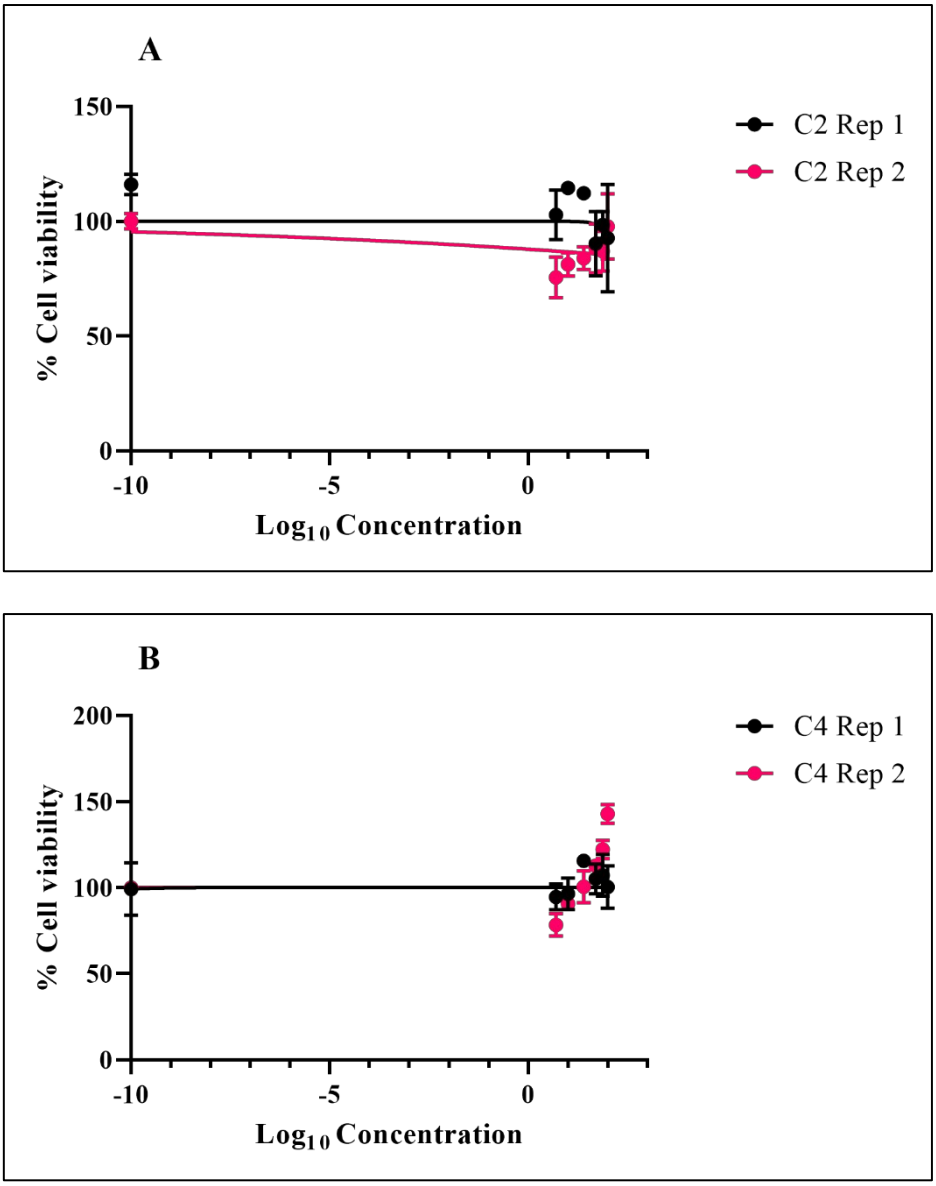

Figure 5.8. Cytotoxicity plots for C2 and C4 using HepG2 cell lines. Cellular cytotoxicity was measured via an MTT cell cytotoxicity assay and visualised using GraphPad Prism 8.14. Plots show mean % cell viability compared with 1% DMSO control with standard deviation (A) Cytotoxicity of C2 shows no correlation between concentration of compound and cell viability when compared with a DMSO control in two independent repetitions. (B) Cytotoxicity of C4 shows no correlation between concentration of compound and cell viability when compared with a DMSO control in two independent repetitions.

5.4 Discussion

5.4.1 Inhibiting class I fumarases

The vast majority of research conducted on fumarases has been on class II enzymes. There are several reasons for this, however, their thermolabile nature and oxygen sensitivity make studying their enzymatic activity and inhibition extremely difficult. Similarly, the class I fumarases of *E. coli*, fumA and fumB, lose 70% of their activity after 30 seconds of exposure to oxygen and after 2 minutes this increases to 90% (van Vugt-Lussenburg *et al*., 2013). Due to this oxygen sensitivity, enzymatic activity experiments must be performed in gloveboxes where atmospheric conditions can be highly controlled. As a result very few inhibitors have been identified for these enzymes with the only known inhibitor being DL-mercaptosuccinic acid (Feliciano *et al*., 2019; Jayaraman *et al*., 2018) which has shown inhibition of *L. major* and *P. falciparum* enzymes. It was also shown to kill *P. falciparum* in *in vitro* cultures at an IC50 >280 μM (Jayaraman *et al*., 2018). With the difficulties of handling these enzymes and a short supply of known inhibitors the CADD approach described herein was undertaken to identify putative inhibitors.

5.4.1.1 $SmFH_I$ homology model provides sites for inhibition

Homology modelling of $SmFH_I$ began with the alignment to the most closely related crystal structure available on PDB, 5L2R, that belongs to LmFH-2 (Feliciano *et al*., 2016). Alignment of these two amino acid sequences revealed that $SmFH_I$ possesses all of the crucial residues for active site formation, [4Fe-4S] cluster binding and enzyme dimerisation (Figure 5.1). One of the key differences was found within the active site cavity which interacts with substrates and transports them into the active site (Feliciano *et al*., 2016). Asn 219, Tyr 222 and Gln 225 were found to interact with malate in the active site cavity of 5L2R. $SmFH_I$ aligned with these amino acids with Asn 220, Phe 223 and Gln 226 (Figure 5.2.C). Tyr 222 has

previously been identified as not being conserved in class I fumarases (Feliciano *et al*., 2016), however phenylalanine is closely related to tyrosine and both belong to the aromatic family of amino acids.

The homology model generated from this alignment using MOE showed the distinctive 'heart-shaped' homo-dimer of class I fumarases (Figure 5.2.A). Exploring this model the positively charged active-site cavity was identified as the best option for inhibitor identification (Figure 5.2.B). DL-mercaptosuccinic acid has been demonstrated to inhibit class I fumarases at high concentrations (Feliciano *et al*., 2019; Jayaraman *et al*., 2018). This molecule is structurally very similar to the fumarase substrate malate (Figure 5.9). Feliciano et al., (2016) showed the interaction between the [4Fe-4S] cluster and malate in their crystal structure of LmFH-2. The cluster interacts with the hydroxyl group of carbon 2 (Figure 5.9.A), which is replaced by a thiol group in DL-mercaptosuccinic acid (Figure 5.9.B). Crystal structures of LmFH-2 interacting with DL-mercaptosuccinic acid show that this thiol group directly interacts with the [4Fe-4S] cluster (Feliciano *et al*., 2019). This interaction was found to be in accordance with hard-soft acid base theory (Pearson, 1969), where a Lewis acid ([4Fe-4S] cluster), binds strongly to a soft base which in this case is the thiol group. This kind of bond is how the [4Fe-4S] cluster is held within the protein thiol groups on the three cysteines (Flint and Allen, 1996). Although very selective, screens performed on live *P. falciparum* show that a very high quantity of DL-mercaptosuccinic acid is required to kill the parasites in culture (Jayaraman *et al*., 2018). Screens using this compound did not show activity in schistosomula or adult worms so further target zones were explored in the positive active-site cavity.

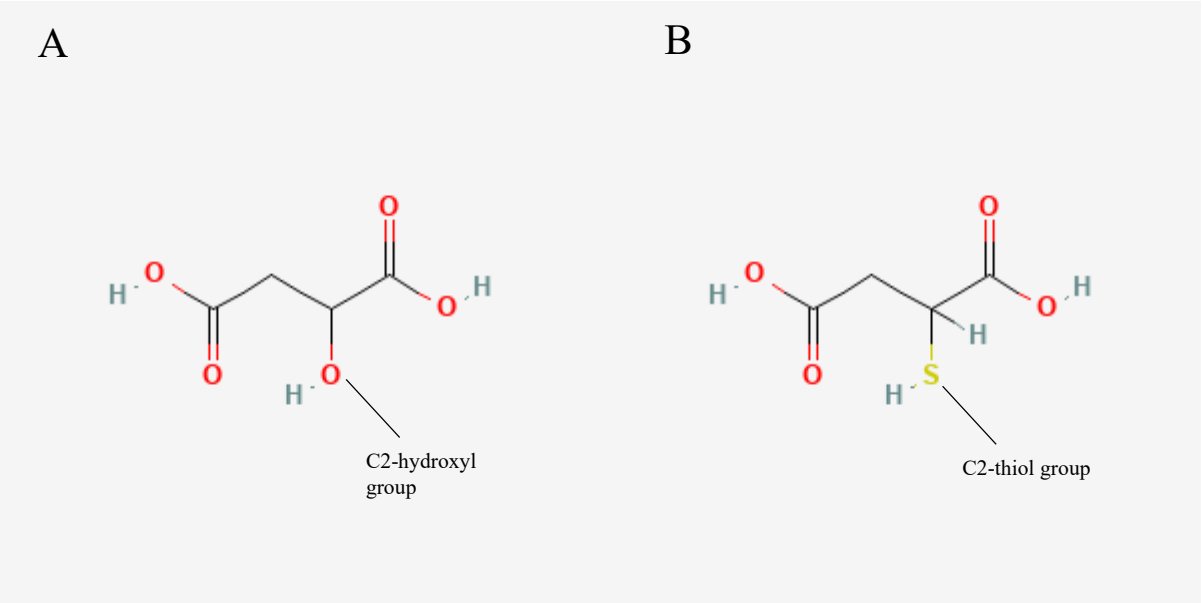

Figure 5.9. Chemical structure depictions of malate and DL-mercaptosuccinate. (A) Malate possesses a hydroxyl group on the second carbon, which interacts with the 4Fe-4S cluster of class I fumarases. (B) A thiol group replaces the hydroxyl group on carbon 2 in DL-mercaptosuccinic acid, which likely forms a strong bond with the [4Fe-4S] cluster, thus preventing enzymatic activity.

The active site cavity of class I fumarases is important for the conformation of substrates and the shuttling of malate to the active site has been shown through X-ray crystallography (Feliciano *et al*., 2016). The active site cavity was identified in the SmFH I homology model and was identified as a site for compound targeting through the CADD pipeline (Figure 5.2.B). This target area increased the number of potential inhibitors as it would allow for larger molecules that could potentially act as a competitive inhibitor. The positive charge of the cavity resulted in the majority of compounds predicted to bind being of a negative charge. The charged nature of these compounds would make it difficult for them to cross lipid membranes and reach the target area of the mitochondria due to the slow diffusion of ionic compounds across hydrophobic lipid bilayers (Alberts et al., 2002b). Additional sites for CADD have been suggested in the literature.

The presence of a 'tunnel cavity' has been observed in the crystal structure of cytosolic (Feliciano *et al*., 2016) and mitochondrial (Feliciano *et al*., 2019) class I fumarases of *L. major*. This cavity runs through the dimer and does not connect to the active site or active site cavity. Weak inhibition by the molecule malonate was observed with binding in this cavity (Feliciano *et al*., 2016). Often such cavities lead to buried active sites (Pravda *et al*., 2014) or the transport of highly reactive or crucial intermediates from one active site to another in the case of tryptophan synthase and others (See: Doukov *et al*., 2008; Raushel *et al*., 2003). The purpose of this cavity has not been identified within class I fumarases and not all residues that form it are conserved across species (Feliciano *et al*., 2016). It was decided that the main focus of this study would be on the active site cavity. However, future work may benefit from exploring the tunnel cavity as a potential site of inhibition. From data presented in chapter 4 it was found that the knockdown of both *S. mansoni* fumarases was required to induce a phenotype consistent with the loss of aerobic metabolism in adult worms. Inhibitors of class II fumarases were therefore explored.

5.4.2 Class II inhibition

5.4.2.1 Class II fumarases show conserved active site residues

Since the discovery of the TCA-cycle (Krebs and Johnson, 1937), a large number of inhibitors of crucial enzymes have been identified (Gasmi *et al*., 2021; Varga *et al.*, 2015). Many marketed compounds often have off-target effects on metabolic cycles involved in cellular respiration, including the TCA-cycle (Varga *et al*., 2015). When looking at the structure of class II fumarases, the enzymatic activity is different to that of class I fumarases. Class II fumarases possess a flexible catalytic loop (SS-loop) within the signature sequence motif: GSSxxPxKxNPxxxE (GUEST et al., 1985; Nast and Muller-Rober, 1996; Puthan Veetil et al., 2012; Suzuki et al., 1989; Woods et al., 1988). The same is true for $SmFH_{II}$ (Cardoso et al., 2021). This SS-loop is involved in the accessibility of the active site by substrates where

class II fumarases are in an open state, accessible to substrates, and closed where the SS-loop covers the active site and enzymatic activity occurs (Mechaly et al., 2012). One of the major difficulties in targeting class II fumarases is the high degree of conservation between different species in the active site (Aleixo et al., 2019).

Class II fumarases range between 20-90% sequence similarity (Aleixo et al., 2019). However, the differences tend to be found distributed across the amino acid sequence and result in changes in the charge distribution of the protein surface as opposed to major differences in the protein structure or active site that can be exploited. It has been suggested that these differences could instead be adaptations to maintain the protein structure in the different chemical environments of species (Aleixo et al., 2019), $SmFH_{II}$ was found to possess a 15 amino acid sequence that wasn't present in the human version (Cardoso et al., 2021). This sequence did not appear to affect the enzymatic activity, it is likely crucial for enzyme stability and could be involved in the recruitment of this enzyme in the DNA-damage repair response Using the ChEMBL database and other literature searches, inhibitors of class II fumarases were identified.

5.4.2.2 Literature searches find few known inhibitors of class II fumarases

Despite a wealth of research into the TCA-cycle and many inhibitors identified for constituent enzymes, only a single compound was identified through ChEMBL in this study. The competitive inhibitor of class II fumarase, 2,3-dicarboxyaziridine (Figure 5.10), belongs to a family of compounds containing aziridine rings (Greenhut et al., 1985). There are 754 compounds containing aziridine rings found in the ChEMBL library as of 2023 (Davies *et al*., 2015). Very few of these compounds are under clinical trials with one in phase 3 testing and one in phase 2. These compounds have been studied with regards to anti-cancer (Naylor et al., 1997; Palmer et al., 1992) and anti-biotic properties (He *et al*., 2018). 2,3-dicarboxyaziridine was found to be a competitive inhibitor of class II fumarases (Greenhut et al., 1985). This

inhibitor has also been demonstrated to affect fumarase activity in both the fumarate → malate and malate → directions (Rose, 1998). No commercial suppliers of this compound were identified so the compound was kindly synthesised by Dr. Priscilla Mendonca Matos. This compound was used in parasite compound screens.

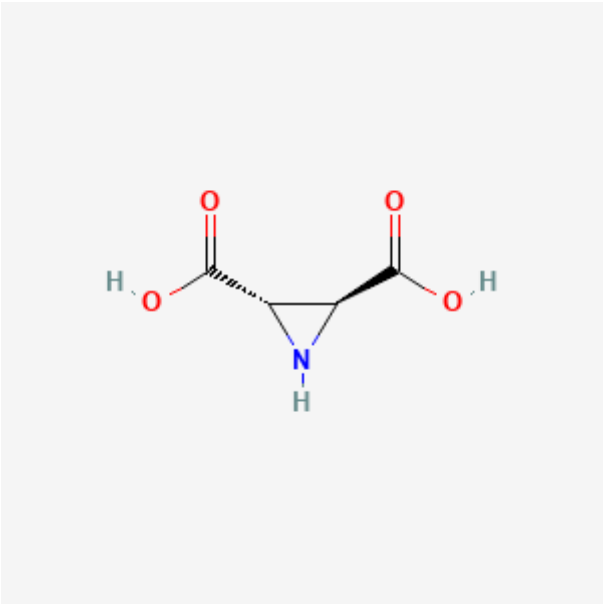

Figure 5.10. Chemical structure of 2,3-dicarboxyaziridine. A competitive inhibitor of class II fumarases that affects both the forward and reverse reaction of these enzymes.

Reports of small molecule class II inhibitors of *M. tuberculosis* were identified in the literature (Kasbekar et al., 2016). Multiple sequence alignments, however, have demonstrated that $SmFH_{II}$ lacks sequence conservation for the target-area of these compounds and further investigation of these compounds was therefore abandoned (Cardoso et al., 2021).

5.4.3 Live parasite screens show hits in two putative class I inhibitors

Loss of motility consistent with the inhibition of aerobic respiration in adult worms (Bossche, 1985) in RNAi experiments was only seen in the knockdown of both *Smfh*$_{I}$ and *Smfh*$_{II}$ (Chapter 4, Figure 4.3). Even with a significant knockdown of these genes when treated with dsRNA individually (Chapter 4, Figure 4.4), no loss of motility was seen. In accordance with

these results, putative inhibitors of SmFH $_1$ and 2,3-dicarboxyaziridine were screened against schistosomula alone and in combination with each other. Curiously, the only consistent hits seen in all screens were that of C2 and C4 (Figure 5.4.A). These hits were not dependent on the co-incubation with 2,3-dicarboxyaziridine (See appendix). Images taken of schistosomula incubated with C2 show disruption of the tegument and no internal structures were visible (Figure 5.4.A). These parasites did show variation in shape, one of the criteria used to score phenotype, suggesting a lower score than auranofin. C4 similarly shows tegument disruption and granularity of the cytoplasm. There appears to be less cellular debris in the medium however, similar to C2, the morphology of the parasites is not uniform (Figure 5.4.B).

Adult worm screens showed a reduction in motility at higher concentrations of both compounds in males (Figure 5.5) and females (Figure 5.6). Female worms showed less of a reduction in motility when compared to males at the same concentrations in both compounds. In both males and females C4 resulted in a greater loss of motility, however the same tegumental damage that occurred in schistosomula did not occur in adult worms. Motility was observed to be lost in one male replicate of C4 at 50 µM at 24 hours in the first screen (Figure 5.5). At 48-hours, gut movement was seen suggesting the worm was not dead and had only lost motility. These results were more consistent with what is expected of aerobic metabolism being inhibited (Bossche, 1985). C2 did show a reduction of motility in male worms but only at 100 µM (Figure 5.5). In female worms the differences in motility between C2 and C4 were more similar. However, in the first screen C2 females at 100µM scored at 3 while at the same concentration when incubated with C4 females scored 2 (Figure 5.6). At 25µM of C4 a slight reduction in motility was observed after 24-hours before returning to normal in both males and females. At lower concentrations in schistosomula screens no significant phenotype or motility scores were observed. When looking at the compounds in question, C2 (Figure 5.11.A) and C4 (Figure 5.11.B) both possess a hydroxyl group, which was predicted to interact with the

positively charged active site cavity. When searching these compounds on PubChem and ChEMBL, no predicted targets were found for either compound. C2 was found to be in a collection of patented antibacterial fabI inhibitors (US-2007027190-A1), however, no study or demonstration of this compound was identified in the literature. Neither C2, nor C4 were present in the ChEMBL database.

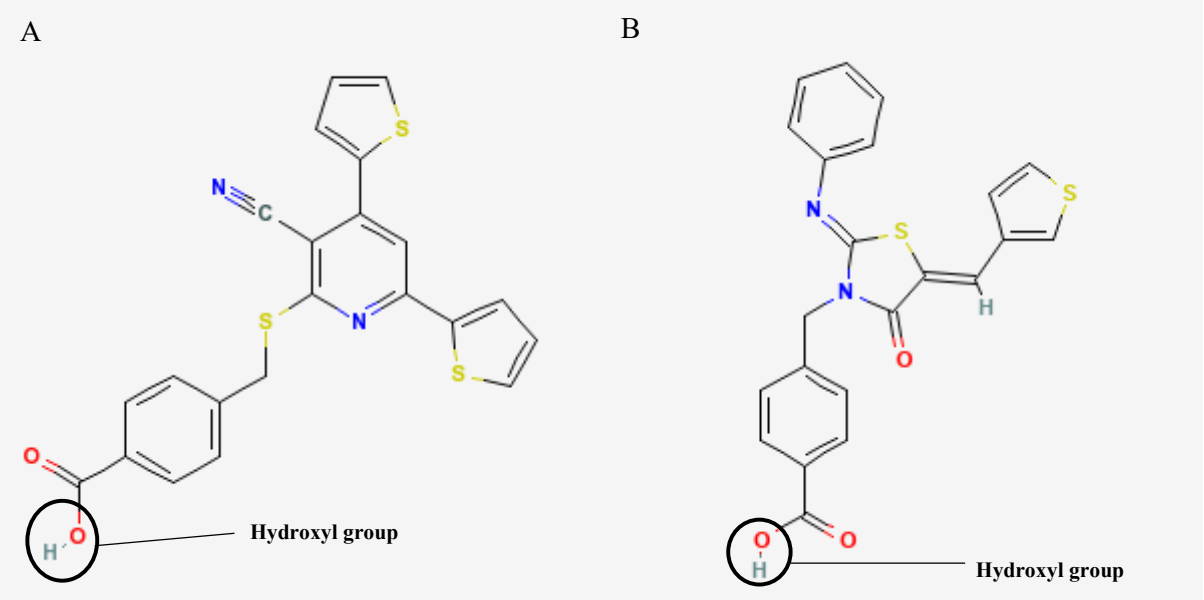

Figure 5.11. Chemical structures of C2 (4-{[(3-Cyano-4,6-dithien-2-ylpyridin-2-yl)thio]methyl}benzoic acid) and C4 (4-{[(2Z,5Z)-4-oxo-2-(phenylimino)-5-(thiophen-3-ylmethylidene)-1,3-thiazolidin-3-yl]methyl}benzoic acid). (A) C2 chemical structure shows hydroxyl group that reacts with the positively charged active site cavity in CADD. (B) C4 chemical structure shows hydroxyl group that is predicted to interact with the positively charged active site cavity.

C2 and C4 showed no cytotoxicity against HEP-G2 cells even at the highest concentration tested 100 µM (Figure 5.7). This suggests that the mechanism of action of these compounds have a limited effect on human cells at concentrations of 100 µM or below. This could be due to compound specificity to the parasite, or the compound may be taken up more readily by parasite cells than by human cells. In order for small molecule compounds to reach

target cellular compartments, they must overcome cellular membranes (Hannesschlaeger et al., 2019; Menichetti et al., 2019; Yang and Hinner, 2015). Permeability of compounds through membranes can depend on multiple factors including membrane composition (Tse et al., 2018), membrane thickness (Frallicciardi et al., 2022), the charge of a compound (Hannesschlaeger et al., 2019) especially regarding hydrogen bond donor and acceptor groups which can hinder permeability across lipid bilayers (Lipinski et al., 2012; Paterson et al., 1994). Lapinski's rule of 5 lays out a framework for identifying drugs that are more likely to be orally active (Lapinski, *et al.*, 2012). These rules are as follows: 1. No more than five hydrogen bond donors, 2. No more than 10 hydrogen bond acceptors (the sum of Ns and Os), 3. Molecular mass less than 500 daltons, 4. Octanol-water partition coefficient (logP) no greater than 5, 5. If the compound is a substrate for transporters, they are an exception to the previous rules. Both C2 and C4 are in violation of rule 4 with logP >5 (Table 5.1), however they are in line with all other rules. Despite the presence of hydroxyl groups and the potential charge they can induce, neither C2 nor C4 exceed 5 donors. Lipinski's rule is broadly a rule of thumb with many exceptions (Lipinski et al., 2012). To elucidate whether cytotoxicity caused by C2 and C4 can be observed in HEP-G2, future studies should test the compounds at higher concentrations. Currently it would appear that the two compounds are affecting a parasite-specific target. Without the generation of a recombinant SmFH $_{I}$ and the appropriate facilities to study this enzyme in an oxygen-free environment, we cannot elucidate whether these compounds are truly inhibitors of $SmFH_I$. Additionally, a recombinant protein could be used to confirm the activity of other putative inhibitors identified in this study.

5.4.4 Mitochondrial targeting of compounds

An area this study was unable to explore was that of targeting compounds to the mitochondria. Mitochondrial targeting of drugs is important for a range of diseases including metabolic, cardiovascular, neurological and inflammatory conditions (see Zinovkin and

Zamyatnin, 2019) and in cancer therapy where high metabolic activity can contribute to rapid cell proliferation (Ghosh et al., 2020). Many anti-cancer compounds have been studied that target the electron transport chain, oxidative phosphorylation and the TCA-cycle (Dong and Neuzil, 2019). One approach to targeting TCA-cycle enzymes has been through targeting unique aspects of the enzymes. In the case of tumours that have mutations in isocitrate dehydrogenases (IDH), selective compounds have been identified for targeting human IDH2 (Quivoron et al., 2014; Yen et al., 2017). Improving target specificity and localisation are crucial in any drug discovery for improving the specificity, potency and the reduction of off-target effects of compounds. The mitochondria possesses cellular machinery that can be taken advantage of for this purpose.

Targeting of drugs can be achieved through the addition of lipophilic cations (Murphy, 2008). Antioxidants have been utilised for prevention of superoxide damage in mitochondria by conjugating them with the lipophilic cation triphenyl phosphonium (TPP). TPP, and other lipophilic cations, are able to cross the lipid bilayers of mitochondria due to their large surface area dispersing charge (Ross et al., 2005) and the membrane potential gradient allows for the accumulation of cations in the mitochondrial matrix where every 61.5 mV of membrane potential increases accumulation 10-fold (Ross et al., 2006). Lipophilic cation probes such as rhodamine and JC-1 are also utilised in other techniques such as the visualisation of mitochondria by fluorescent microscopy (Chen, 1988) or in estimating mitochondrial energy production by flow cytometry (Smith, 1990). There are potentially adverse effects to the accumulation of lipophilic cations in the mitochondria where they can adversely affect mitochondrial function (Millard et al., 2010; Pajuelo et al., 2011; Sancho et al., 2007; Trnka et al., 2015). The accumulation of lipophilic cations can induce changes to the mitochondrial membrane potential; in turn negatively affecting respiration (Trnka et al., 2015). This should be considered for future experiments where off-target accumulation in human cells could lead

to cytotoxicity even if the drug is targeting a schistosome-specific enzyme.

Another technique for small molecule targeting to the mitochondria involves the mitochondrial protein import machinery. This can be achieved by the addition of peptides that can traverse the mitochondrial membranes to deliver compounds to the mitochondrial matrix or inner mitochondrial membrane (Murphy and Smith, 2000). A variety of peptides have been developed for small molecule localisation (Kim et al., 2020). These include Szeto-Schiller (SS) peptides (Zhao et al., 2004), mitochondrial penetrating peptides (MPPs) (Horton et al., 2008) and by using mitochondrial targeting peptides (mTPs) similar to those found on enzymes localised to the mitochondria with the addition of cell penetrating peptides (CPPs) (Lin et al., 2015).

SS peptides have predominantly been researched for the delivery of antioxidants to the inner mitochondrial membrane where they could treat metabolic disorders caused by excessive reactive oxygen species (ROS) (Birk et al., 2014, 2013). Although these peptides do not deliver to the mitochondrial matrix, they are effective at localising to the mitochondria and have been explored for the delivery of small molecule compounds to mitochondria. An example of this is the conjugation of the SS peptide, SS-31, with poly(lactic-co-glycolic acid) nanoparticle for the delivery of the drug cyclosporin A (Zhang et al., 2019). This was found to restore mitochondrial function.

MPPs consist of a library of short peptides that are able to traverse both cellular and mitochondrial membranes through the utilisation of alternating hydrophobic and cationic residues (Horton et al., 2008). Studies into the delivery of anti-cancer drugs have found that MPPs are able to avoid cellular machinery that can remove drugs from the mitochondria. For example some cancers overexpress P-glycoprotein efflux pumps which can remove cytosolic substrates and drugs out of the mitochondrial matrix (Chamberlain et al., 2013). MPPs are able to deliver drugs to the mitochondrial matrix without being recognised by these pumps, thus

allowing for the effective delivery of compounds to their target location (Jean et al., 2015).

The use of shortened mTPs conjugated with CPPs has been utilised broadly as a transfection tool and gene therapy (Lu et al., 2019). The addition of short mTPs to proteins can be highly effective at localisation to the mitochondria. However, they are not necessary for entering cell surface membranes (Lin et al., 2015). By the addition of a CPP at the N-terminus of these mTP-conjugated proteins, uptake by endocytosis can be achieved (Copolovici et al., 2014). Although this strategy is effective for gene therapies and transfection, it has not been utilised for small-molecule compound delivery (Kim et al., 2020).

Another possible delivery system that requires no modification to compounds is the MITO-porter (Yamada et al., 2008). This delivery system consists of liposomes with surface peptides and molecules that allow for the delivery of cargo to the mitochondria by fusion with the mitochondrial membrane. MITO-porters containing all of the previously described peptides have been constructed (Kawamura et al., 2013; Yamada and Harashima, 2012). However, the use of SS peptides has been found to be the highly effective for the localisation of MITO-porters to the mitochondria (Katayama et al., 2019).

Future work exploring fumarase inhibitors in *S. mansoni* would benefit from using mitochondrial targeting methods and could improve the efficiency of putative compounds. More broadly, these techniques could also be utilised in the study of *S. mansoni* metabolism across the lifecycle.

5.5 Conclusion

This study has generated a homology model for SmFH$_{I}$ and identified 144 putative inhibitors using this model. Live parasite screens of 18 of these compounds and a known class II fumarase inhibitor only identified activity in two of these compounds. Without a recombinant or isolated native protein of SmFH$_{I}$ it cannot be determined whether these compounds specifically target SmFH$_{I}$ or if part of/all of their activity is based on off-target effects. The

phenotypes seen in adult worms are similar to those seen when adult worm aerobic respiration is targeted by the compound closantel, where motility of the worms is lost at high concentrations of C2 and C4 in male worms (Bossche, 1985). In schistosomula the phenotype showed damage to the tegument, possibly indicating that there are other mechanisms of action. Effects in both lifecycle stages were seen at high concentrations and in adult worms these motility phenotypes diminished as the concentration decreased. Through the utilisation of mitochondrial targeting modifications described in 5.4.4, compounds could be more effectively targeted to the mitochondria reducing off-target effects and improving the potency of compounds. This would be particularly interesting to study in DL-mercaptosuccinate, which has been demonstrated by X-ray crystallography to interact with class I fumarases and inhibit activity (Feliciano et al., 2019).

6. Final Discussion

At the time of writing this thesis, schistosomiasis remains one of the most significant neglected tropical diseases affecting the worlds poorest people. Praziquantel is the only licensed treatment currently available for this disease. The current strategies for treatment and control of this disease rely on mass drug administration, which could result in the kinds of pressures leading to resistance (Cupit and Cunningham, 2015). Efforts to characterise drug targets are critical to both understand the basic biology of the parasite and can uncover potential vulnerabilities.

Although this PhD has not uncovered any promising drug candidates, it has delivered interesting insights on the basic biology of *S. mansoni*. The work presented in this thesis adds to the growing understanding of energy metabolism in parasitic platyhelminths and on the seldom studied class I fumarases. This work lays the foundations towards understanding how fumarases function within *S. mansoni* and offers a future path towards targeting these enzymes.

6.1 The roles of fumarases in *S. mansoni*

In chapter 3 aspects of class I and class II fumarases were explored in *S. mansoni* and other species. Homolog searches (3.3.1) revealed that *S. mansoni* possesses a single class I and a single class II gene. Analysis of the predicted amino acid sequences revealed that both enzymes possessed the full functional domains (according to Pfam and PANTHER) associated with a class I and a class II fumarase respectively. These searches also identified fumarases in the genomes of many other species. An interesting evolutionary picture was formed revealing that the class I fumarases, an enzyme often remarked as being restricted to prokaryotes and unicellular eukaryotes, is widespread amongst the Lophotrochozoa. These searches have shown that in Metazoa there have been two independent losses of class I fumarases in Chordata and Ecdysozoa. It is proposed (3.4.1.2) that the potential adaptation towards an oxygen- rich environment and the utilisation of iron for the transport of oxygen around the body could have

led to the loss of iron-dependent enzymes where a non-iron-dependent enzyme exists to perform that function. This may explain the loss of class I fumarases in Chordata, however fewer studies surrounding iron metabolism and requirements of Ecdysozoa exist. This makes it more difficult to postulate why class I fumarases were lost in these species. The only example of class II fumarase losses in Metazoa were in Cestoda and Monogenea. Except for these species class I and class II fumarases were found within the Lophotrocozoa (3.4.1.3).

The use of localisation prediction tools TargetP 2.0 (Emanuelsson et al., 2007) and MitoFates (Fukasawa et al., 2015) suggested that not all fumarases possess the capabilities of mitochondrial targeting (3.4.3.3). When looking at the relationship of *S. mansoni* fumarases it was found that $SmFH_I$ possessed a predicted mTP while $SmFH_{II}$ did not. This was also found to be the case in *S. japonicum* but the fumarases of other schistosome species showed no mitochondrial targeting predictions. Without experimental confirmation of localisation, it cannot be said for certain whether $SmFH_I$ localises to the mitochondria. However, these predictions suggest a division of labour between these two genes that has been observed in other Eukaryotic species with two fumarase genes (Feliciano et al., 2012; Pracharoenwattana et al., 2010). When looking at the expression across the lifecycle of *S. mansoni* both $Smfh_I$ and $Smfh_{II}$ are expressed across the human infective lifecycle stages. In DNA-microarray, RNA-seq and qRT-PCR analysis expression was found to be relatively high across all human-infective stages. Work remains to improve our understanding of these two enzymes in *S. mansoni* and to provide greater insight as to why these two classes have remained in the Lophotrochozoa.

6.2 The fumarases of *S. mansoni* buffer the effects of knocking out one gene

Wang et al. (2020) published a large-scale RNAi screen on adult *S. mansoni*. Among this dataset were screens against $Smfh_I$ and $Smfh_{II}$. In the case of both no phenotype change was recorded. In screens carried out in this study it was found that the only condition where a

phenotype was achieved through similar methods was in the case where both fumarase genes were knocked down (4.3.3.3). The phenotype measured was a rapid loss in adult worm motility of both male and female worms from day 7 to day 21. Although significant knockdown was only found in male worms, a reduction in expression of both genes was seen in double knockdowns and single knockdowns. Although no significant increase in the expression of the other fumarase gene was measured when its counterpart was knocked down, the activity of one gene may compensate for the other demonstrating a degree of genetic redundancy.

This study also allowed for the establishment of long-term culturing techniques that improved upon previously used techniques in the lab. In using such techniques further specific RNAi screens or long-term drug screens can be performed routinely in the lab.

6.3 Compound screens of putative inhibitors remain largely inconclusive

Putative compounds that target SmFH1 were identified in this study using CADD approaches. The homology model generated for *in silico* docking can be used in the future for the identification of more compounds through the targeting of different sites. 18 of the 144 identified compounds were screened alongside a known class II inhibitor, however, the only compounds that showed any activity were compounds named C2 and C4. This occurred even when putative inhibitors were screened in tandem with a class II inhibitor. Motility was affected in adult worms by both compounds at higher concentration, however, analysis of schistosomula data showed extensive tegumental damage after 72-hour and 120-hours of incubation with C2 and C4. Whether these compounds have off-target effects could not be determined. However, neither has previously been found or predicted to have activity according to the ChEMBL database. Targeting compounds specifically to the mitochondria can be a difficult task due to the cell layers it is required to transit. Investigation of peptides and modifications that target small molecules to the mitochondria may help in improving the efficacy and specificity of compounds.

6.4 Future work

The work in this thesis represents the foundations of understanding schistosome fumarases and their roles in the development and survival of the parasite. Work needs to be done to elucidate the respective roles of these two enzymes as well as further refinement and improvement of techniques to better identify inhibitors that could be used against these parasites (or in fact other parasitic species) and to better understand the biological role of these enzymes *in vivo*. Summarised below are recommendations for future work:

- **Recombinant expression of SmFH$_{I}$.** A recombinantly expressed SmFH$_{II}$ has already been generated (Cardoso et al., 2021). Having a recombinant SmFH$_{I}$ would improve the identification of inhibitors through *in vitro* activity assays. The handling of these proteins requires specialist facilities and equipment to prevent oxidation of the [4Fe-4S] cluster. Recombinant expression of other class I fumarases have been achieved (e.g. Feliciano et al., 2016).
- **Elucidation of localisation of schistosome fumarases.** Although the SmFH$_{I}$ is predicted to localise to the mitochondria according to mTP prediction tools, this study did not experimentally confirm localisation. Using immunofluorescence or fluorescently labelled SmFH$_{I}$ and SmFH$_{II}$ to determine the localisation of these two enzymes. This would confirm the postulated division of labour between these two proteins.
- **Different approaches to inhibition.** Compounds identified in this study and the homology model generated for SmFH$_{I}$ should be further analysed for their potential use as inhibitors. Coupled with a recombinant protein, modifications could be applied to compounds shown to have effects to improve their efficacy and uptake by the cells. Additionally, techniques should be explored as discussed in chapter 5 to target

compounds directly to the mitochondria through the use of peptides used to target and penetrate the mitochondria.

7. Appendix

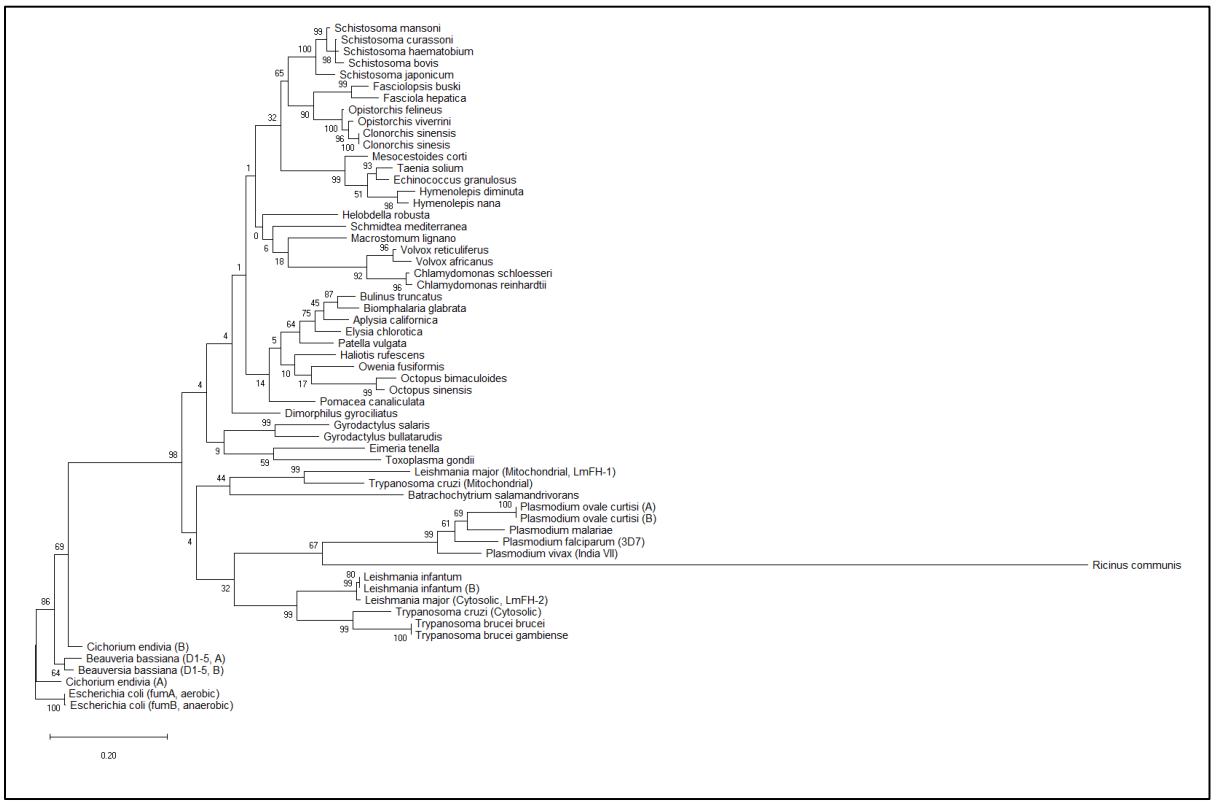

Supplementary Figure 1. Maximum likelihood tree of class I fumarases. Trees were rooted to *E. coli* fumA and fumB. The evolutionary history was inferred by using the Maximum Likelihood method and JTT matrix-based model (Jones et al., 1992). The tree with the highest log likelihood (-11790.49) is shown. The percentage of trees in which the associated taxa clustered together is shown next to the branches. This analysis involved 59 amino acid sequences. Evolutionary analyses were conducted in MEGA X (Kumar et al., 2018).

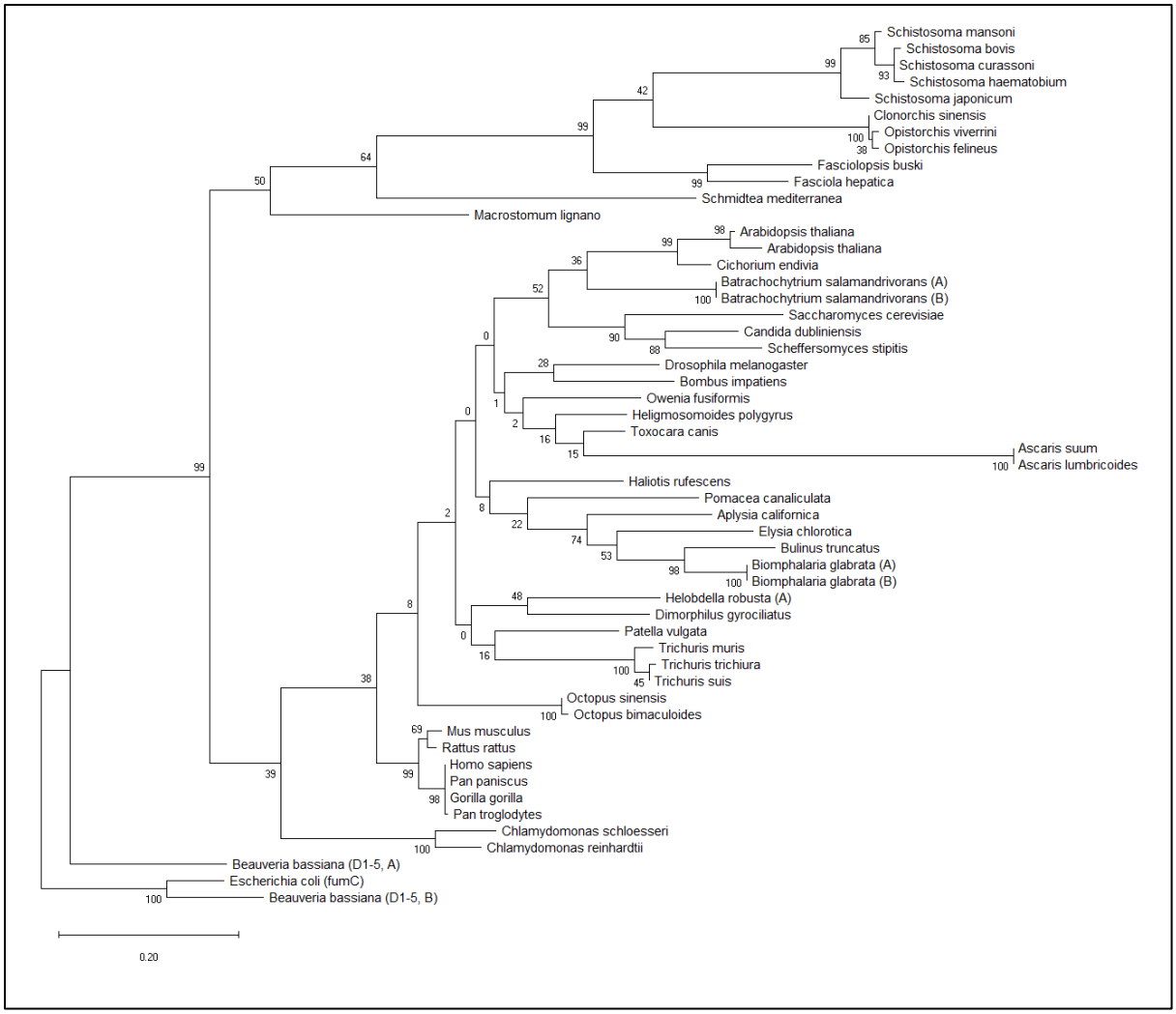

Supplementary Figure 2. Maximum likelihood tree of class II fumarases. Trees were rooted to *E. coli* fumC. The evolutionary history was inferred by using the Maximum Likelihood method and JTT matrix-based model (Jones et al., 1992). The tree with the highest log likelihood (-9206.24) is shown. The percentage of trees in which the associated taxa clustered together is shown next to the branches. This analysis involved 53 amino acid sequences. Evolutionary analyses were conducted in MEGA X (Kumar et al., 2018).

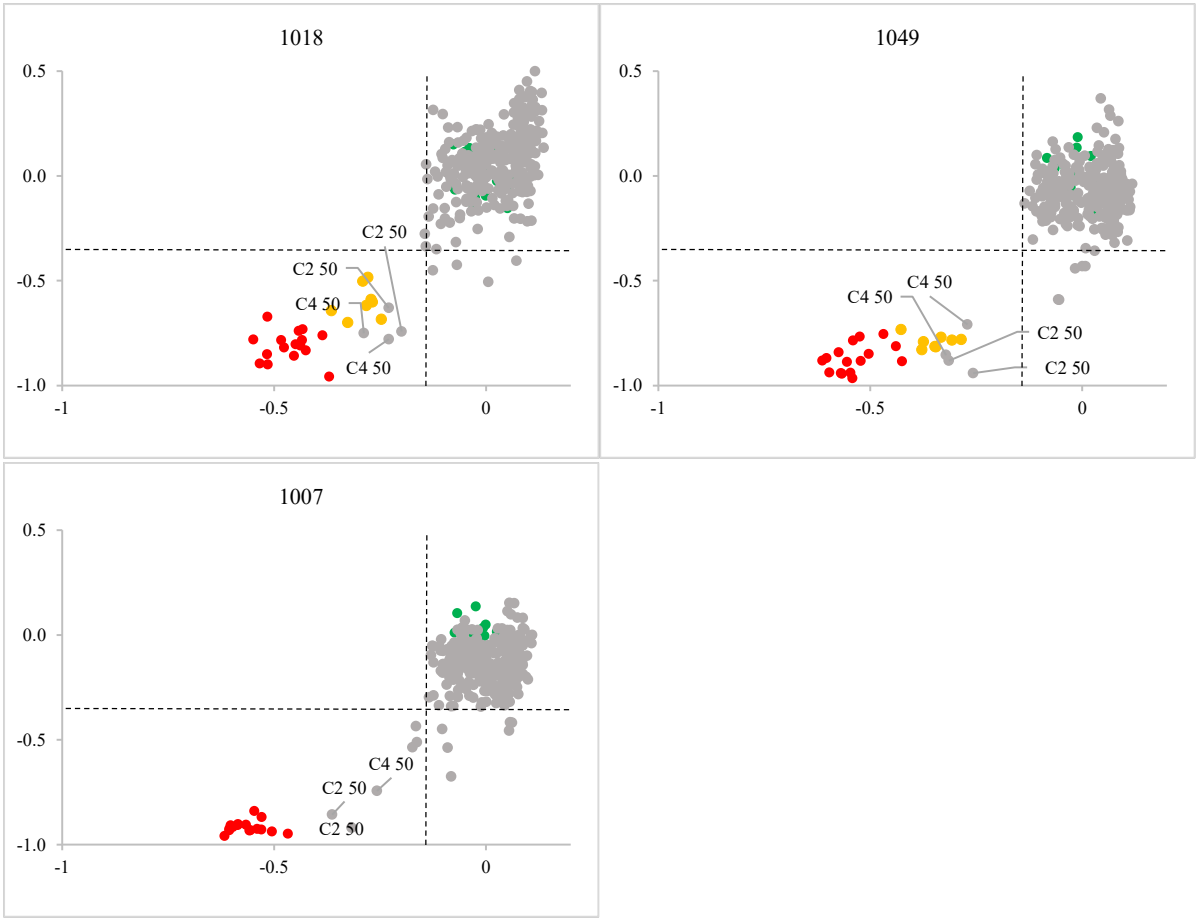

Supplementary Figure 3. Schistosomula screens of putative class I inhibitors and class II inhibitor individually for 72-hours. Mechanically transformed schistosomula (n = 120) were incubated with putative inhibitors of $SmFH_I$ and a known class II inhibitor 2,3-dicarboxyaziridine at 7 dilutions (0.625µM, 1.25µM, 2.5µM, 5µM, 10µM, 25µM and 50µM). Parasites were incubated at 37°C and 5% CO_2. Y-axis represents motility score and X-axis represents phenotype score. Compounds were determined as a hit when motility and phenotype scores were within the 'hit zone' delineated by the dashed lines. Auranofin (●), praziquantel (●), DMSO (●), test compounds (●).

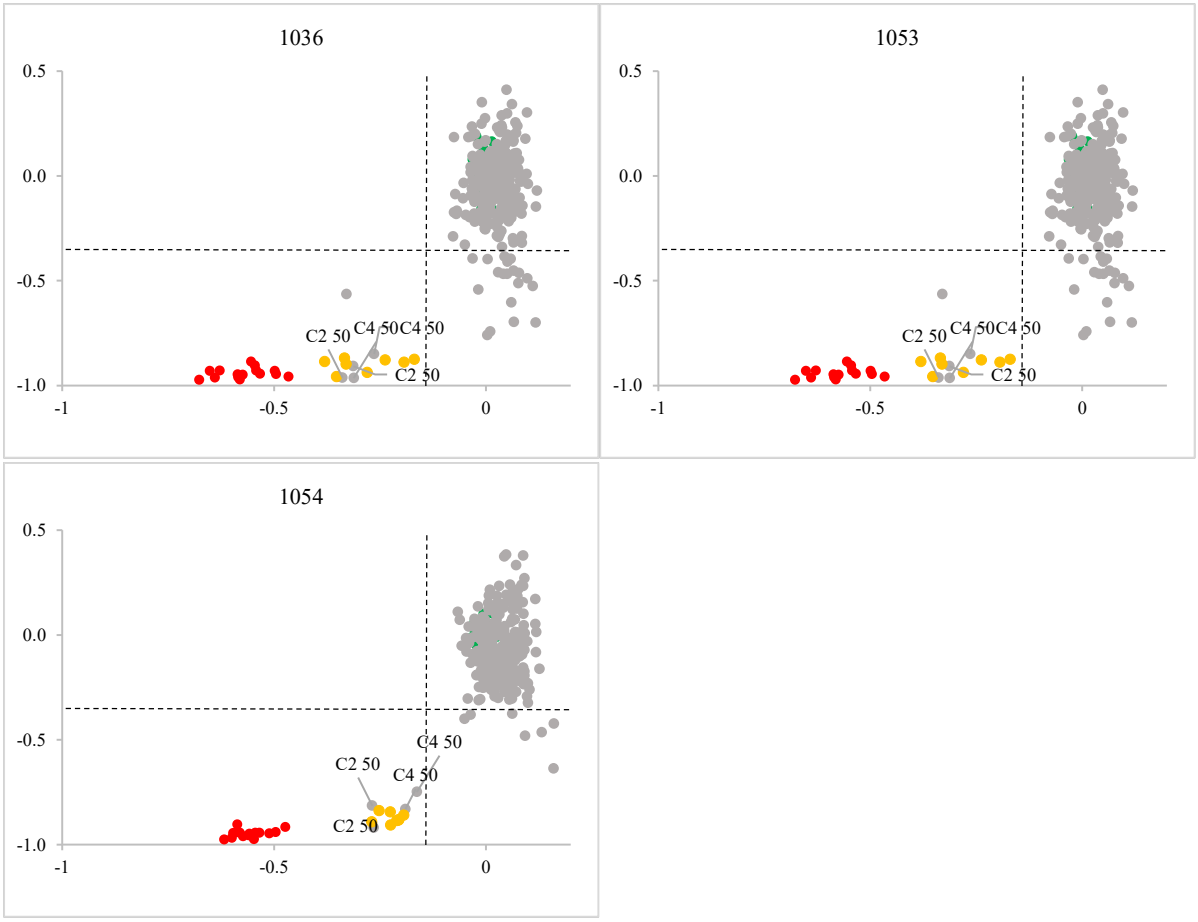

Supplementary Figure 4. Schistosomula screens of putative class I inhibitors and class II inhibitor individually for 120-hours. Mechanically transformed schistosomula (n = 120) were incubated with putative inhibitors of SmFH $_{I}$ and a known class II inhibitor 2,3-dicarboxyaziridine at 7 dilutions (0.625µM, 1.25µM, 2.5µM, 5µM, 10µM, 25µM and 50µM). Parasites were incubated at 37°C and 5% CO_2. Y-axis represents motility score and X-axis represents phenotype score. Compounds were determined as a hit when motility and phenotype scores were within the 'hit zone' delineated by the dashed lines. Auranofin (●), praziquantel (●), DMSO (●), test compounds (●).

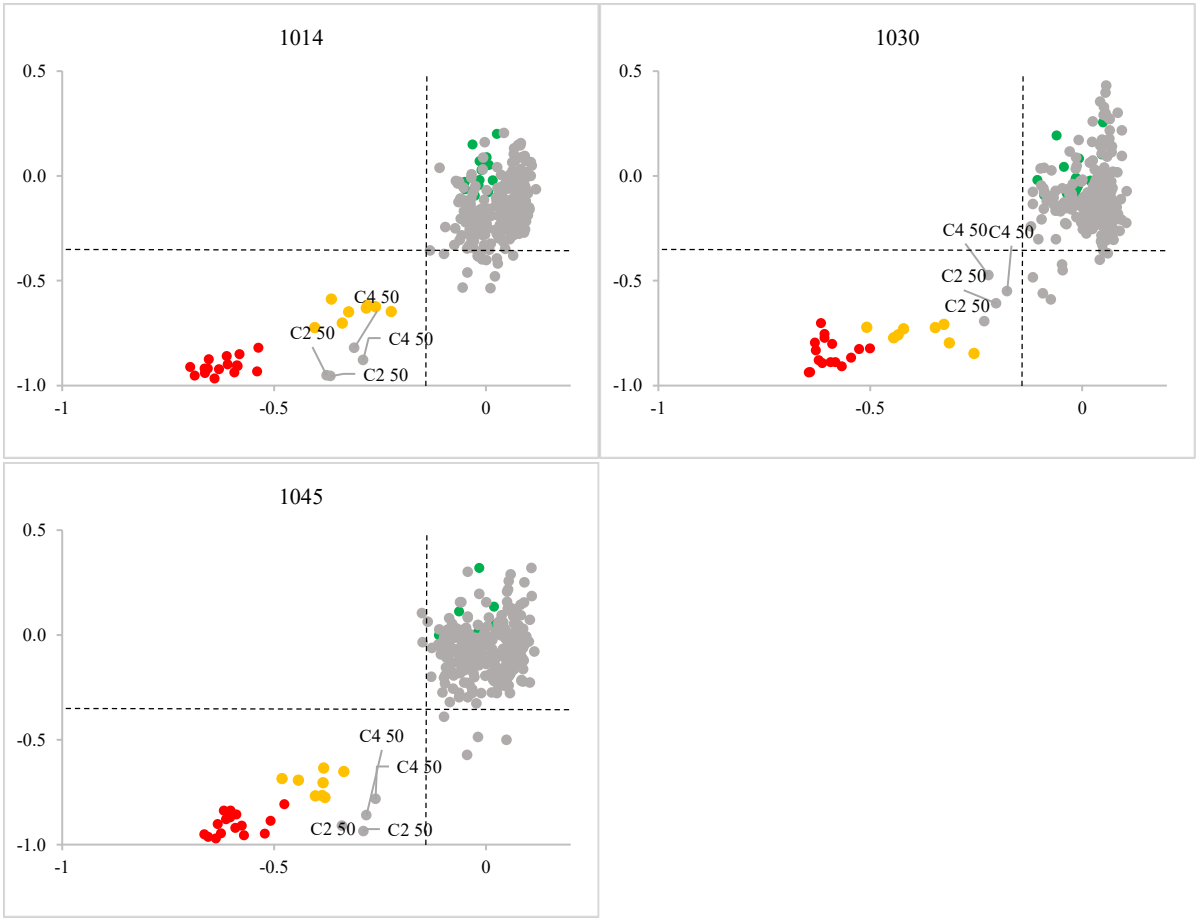

Supplementary Figure 5. Schistosomula screens of putative class I inhibitors and class II inhibitor in tandem for 72-hours. Mechanically transformed schistosomula (n = 120) were incubated with both putative inhibitors of SmFH I and a known class II inhibitor 2,3-dicarboxyaziridine at 7 dilutions (0.625µM, 1.25µM, 2.5µM, 5µM, 10µM, 25µM and 50µM). Parasites were incubated at 37°C and 5% CO_2. Y-axis represents motility score and X-axis represents phenotype score. Compounds were determined as a hit when motility and phenotype scores were within the 'hit zone' delineated by the dashed lines. Auranofin (●), praziquantel (●), DMSO (●), test compounds (●).

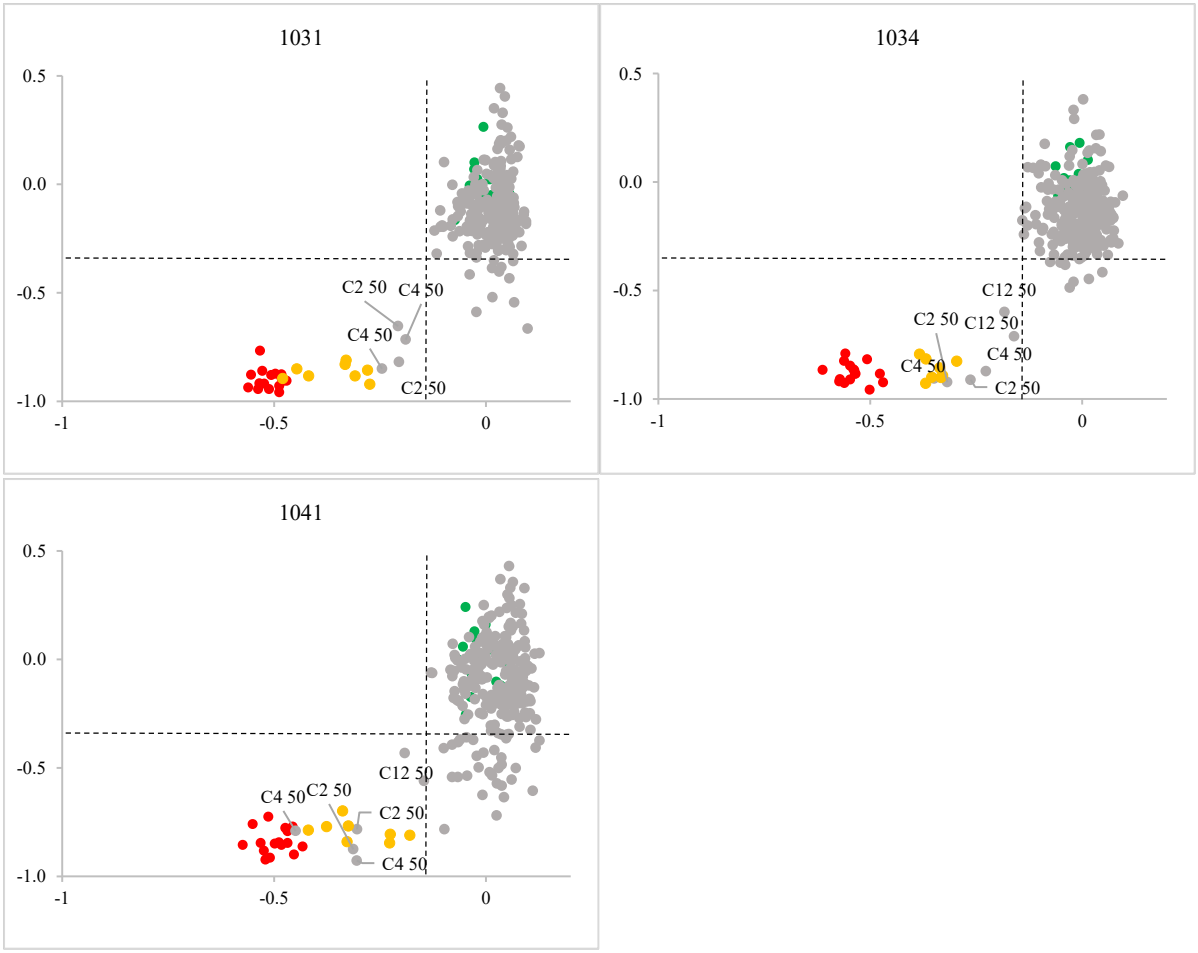

Supplementary Figure 6. Schistosomula screens of putative class I inhibitors and class II inhibitor in tandem for 120-hours. Mechanically transformed schistosomula (n = 120) were incubated with both putative inhibitors of SmFH I and a known class II inhibitor 2,3-dicarboxyaziridine at 7 dilutions (0.625µM, 1.25µM, 2.5µM, 5µM, 10µM, 25µM and 50µM). Parasites were incubated at 37°C and 5% CO_2. Y-axis represents motility score and X-axis represents phenotype score. Compounds were determined as a hit when motility and phenotype scores were within the 'hit zone' delineated by the dashed lines. Auranofin (●), praziquantel (●), DMSO (●), test compounds (●).

Supplementary Table 1. 144 compounds identified in CADD *in silico* docking with homology model of SmFH$_I$

SPECS ID	MOLECULAR WEIGHT	LOGP (O/W)
AH-487/40936239	431.467	6.191
AN-655/37429001	509.509	6.0407
AK-777/12226015	433.556	5.891
AM-879/40769195	450.539	5.732
AH-487/40935684	419.505	5.651
AN-988/14609089	458.898	5.167
AK-968/41171948	310.76	5.159
AP-501/43379908	334.248	4.9848
AN-329/40337445	453.89	4.956
AG-690/33918023	540.496	4.924
AK-968/12100135	445.515	4.792
AK-918/11773521	392.774	4.762
AG-670/11325001	369.465	4.696
AG-690/12871304	276.315	4.493
AP-970/43507379	315.654	4.4638
AS-871/13716083	317.748	4.4267
AN-465/43421753	384.795	4.252
AG-690/37105063	289.379	4.242
AI-204/42001048	261.296	4.237
AQ-390/43490637	393.443	4.21
AG-670/36930008	311.385	4.139
AG-690/11763079	341.411	4.131
AK-918/15589010	368.674	4.121
AI-061/33261002	309.369	4.067
AN-329/13210994	309.128	3.95
AP-970/43507328	289.616	3.8198
AF-399/15284106	353.373	3.798
AS-768/43420458	303.314	3.734
AE-641/05555035	264.712	3.713
AK-918/41450429	334.803	3.711
AN-329/41402680	506.555	3.71
AJ-077/33270055	271.683	3.709
AM-807/42946882	426.472	3.681
AN-465/43411315	381.428	3.6137
AN-329/40826163	525.512	3.5138
AH-487/42922073	308.313	3.4927
AK-918/40894305	367.425	3.368
AN-329/43448289	339.371	3.351
AK-918/41371592	302.737	3.323
AG-205/32983028	266.276	3.301

AG-670/42920053	292.318	3.283
AK-968/13369368	286.09	3.261
AQ-390/42425602	344.367	3.231
AI-942/25034395	266.159	3.203
AK-968/12864498	310.373	3.182
AK-918/11088063	300.677	3.15
AQ-390/43490690	324.421	3.132
AR-009/40188390	285.347	3.065
AO-080/43441800	300.378	3.051
AT-057/42874294	384.368	3.043
AG-690/11311133	330.747	3.015
AH-487/41804513	373.788	2.9117
AQ-086/41476304	252.253	2.872
AI-942/13331753	336.84	2.842
AP-263/43503305	370.789	2.82
AS-871/43477158	314.317	2.814
AN-329/43449094	353.398	2.806
AK-968/41922594	329.356	2.783
AP-263/43371397	350.371	2.77
AK-968/40652827	276.258	2.7688
AK-918/40894329	379.314	2.7568
AK-918/42829283	388.783	2.749
AP-853/42160282	262.289	2.735
AG-667/37281058	371.437	2.614
AK-968/37166220	263.704	2.612
AG-205/12125038	252.677	2.599
AE-848/36311056	291.327	2.588
AN-970/40920811	316.333	2.5785
AQ-086/43457605	268.252	2.562
AN-979/42723452	497.463	2.555
AQ-390/42869320	432.429	2.5437
AN-465/43411617	261.688	2.533
AP-853/43445410	402.842	2.531
AS-871/43476922	296.367	2.512
AP-845/42110292	333.412	2.409
AK-968/10003064	296.302	2.388
AG-690/36924014	352.415	2.382
AP-853/43368051	265.269	2.374
AG-205/12014029	333.182	2.35
AP-853/11334118	265.269	2.335
AN-979/41971667	351.338	2.334
AP-060/40977353	318.305	2.333
AJ-333/25006276	280.348	2.305
AK-968/37156099	261.281	2.303
AJ-333/36117064	317.267	2.2788
AT-057/43469576	283.263	2.276

AL-182/14819025	336.327	2.264
AO-080/43441856	328.3	2.188
AN-329/40942995	422.522	2.176
AN-329/43465286	317.365	2.151
AK-968/41922791	275.284	2.143
AM-807/43303331	360.336	2.0598
AT-057/14534006	347.375	2.051
AM-807/42946864	332.404	2.014
AM-879/37184001	294.331	1.988
AQ-360/42595973	329.307	1.977
AN-329/41583338	353.419	1.947
AS-662/43471422	339.371	1.939
AN-329/43211146	317.267	1.8608
AP-263/41713516	260.191	1.8058
AN-329/43448888	317.365	1.785
AG-205/40776075	282.34	1.782
AN-329/40614851	368.369	1.781
AP-263/13889752	340.291	1.781
AN-329/11954206	333.364	1.781
AF-399/15032590	275.308	1.774
AN-329/42613114	359.382	1.741
AT-057/43232329	294.331	1.732
AN-329/43448559	311.745	1.708
AO-080/41004686	296.298	1.649
AT-057/41290438	323.349	1.633
AK-968/41924758	270.309	1.616
AH-034/33960054	310.35	1.602
AN-329/42682629	367.446	1.598
AK-918/42813845	353.354	1.558
AN-329/12986011	351.403	1.503
AH-262/34336045	298.339	1.487
AA-504/32989012	256.665	1.456
AN-329/43385780	292.311	1.4
AP-263/43417994	326.393	1.377
AP-263/13210752	277.324	1.321
AG-664/25027007	298.339	1.2755
AN-329/43449087	333.364	1.222
AO-990/37423040	277.275	1.214
AK-968/13028424	293.318	1.19
AM-807/42946863	304.35	1.13
AN-329/43448589	277.3	1.046
AO-080/43441855	305.31	1.032
AK-968/41171391	252.2	1.0279
AN-329/43448597	277.3	1.012

8. References

Adam, J., Yang, M., Bauerschmidt, C., Kitagawa, M., O'Flaherty, L., Maheswaran, P., Özkan, G., Sahgal, N., Baban, D., Kato, K., Saito, K., Iino, K., Igarashi, K., Stratford, M., Pugh, C., Tennant, D.A., Ludwig, C., Davies, B., Ratcliffe, P.J., El-Bahrawy, M., Ashrafian, H., Soga, T., Pollard, P.J., 2013. A Role for Cytosolic Fumarate Hydratase in Urea Cycle Metabolism and Renal Neoplasia. Cell Rep 3, 1440–1448. https://doi.org/10.1016/j.celrep.2013.04.006

Adoutte, A., Balavoine, G., Lartillot, N., Lespinet, O., Prud'homme, B., de Rosa, R., 2000. The new animal phylogeny: Reliability and implications. Proceedings of the National Academy of Sciences 97, 4453–4456. https://doi.org/10.1073/pnas.97.9.4453

Ahmed, S.F., Oswald, I.P., Caspar, P., Hieny, S., Keefer, L., Sher, A., James, S.L., 1997. Developmental differences determine larval susceptibility to nitric oxide-mediated killing in a murine model of vaccination against *Schistosoma mansoni*. Infect Immun 65, 219–226.

Ajalla Aleixo, M.A., Rangel, V.L., Rustiguel, J.K., de Pádua, R.A.P., Nonato, M.C., 2019. Structural, biochemical and biophysical characterization of recombinant human fumarate hydratase. The FEBS Journal 286, 1925–1940. https://doi.org/10.1111/febs.14782

Akiba, T., Hiraga, K., Tuboi, S., 1984. Intracellular Distribution of Fumarase in Various Animals. J Biochem 96, 189–195. https://doi.org/10.1093/oxfordjournals.jbchem.a134812

Alberts, B., Johnson, A., Lewis, J., Raff, M., Roberts, K., Walter, P., 2002a. Electron-Transport Chains and Their Proton Pumps. Molecular Biology of the Cell. 4th edition.

Alberts, B., Johnson, A., Lewis, J., Raff, M., Roberts, K., Walter, P., 2002b. Principles of Membrane Transport. Molecular Biology of the Cell. 4th edition.

Alderson, N.L., Wang, Y., Blatnik, M., Frizzell, N., Walla, M.D., Lyons, T.J., Alt, N., Carson, J.A., Nagai, R., Thorpe, S.R., Baynes, J.W., 2006. S-(2-Succinyl)cysteine: A novel chemical modification of tissue proteins by a Krebs cycle intermediate. Archives of Biochemistry and Biophysics 450, 1–8. https://doi.org/10.1016/j.abb.2006.03.005

Aleixo, M.A.A., Rangel, V.L., Rustiguel, J.K., Pádua, R.A.P. de, Nonato, M.C., 2019. Structural, biochemical and biophysical characterization of recombinant human fumarate hydratase [WWW Document]. The FEBS Journal. https://doi.org/10.1111/febs.14782

Anderson, L., Amaral, M.S., Beckedorff, F., Silva, L.F., Dazzani, B., Oliveira, K.C., Almeida, G.T., Gomes, M.R., Pires, D.S., Setubal, J.C., DeMarco, R., Verjovski-Almeida, S., 2015. *Schistosoma mansoni* Egg, Adult Male and Female Comparative Gene Expression Analysis and Identification of Novel Genes by RNA-Seq. PLOS Neglected Tropical Diseases 9, e0004334. https://doi.org/10.1371/journal.pntd.0004334

Angeli, V., Faveeuw, C., Roye, O., Fontaine, J., Teissier, E., Capron, A., Wolowczuk, I., Capron, M., Trottein, F., 2001. Role of the Parasite-Derived Prostaglandin D2 in the Inhibition of Epidermal Langerhans Cell Migration during Schistosomiasis Infection. Journal of Experimental Medicine 193, 1135–1148. https://doi.org/10.1084/jem.193.10.1135

Anraku, Y., 1988. Bacterial Electron Transport Chains. Annual Review of Biochemistry 57, 101–132. https://doi.org/10.1146/annurev.bi.57.070188.000533

Arai, T., 2014. The Development of Animal Nutrition and Metabolism and the Challenges of Our Time. Front Vet Sci 1, 23. https://doi.org/10.3389/fvets.2014.00023

Armenteros, J.J.A., Salvatore, M., Emanuelsson, O., Winther, O., Heijne, G. von, Elofsson, A., Nielsen, H., 2019. Detecting sequence signals in targeting peptides using deep learning. Life Science Alliance 2. https://doi.org/10.26508/lsa.201900429

Atlante, A., Passarella, S., Giannattasio, S., Quagliariello, E., 1985. Fumarate permeation in rat liver mitochondria: Fumarate/malate and fumarate/phosphate translocators. Biochemical and Biophysical Research Communications 132, 8–18. https://doi.org/10.1016/0006-291X(85)90981-7

Barsoum, R.S., 2013. Urinary Schistosomiasis: Review. J Adv Res 4, 453–459. https://doi.org/10.1016/j.jare.2012.08.004

Basyoni, M.M.A., Rizk, E.M.A., 2016. Nematodes ultrastructure: complex systems and processes. J Parasit Dis 40, 1130–1140. https://doi.org/10.1007/s12639-015-0707-8

Bayley, J.-P., Launonen, V., Tomlinson, I.P., 2008. The FH mutation database: an online database of fumarate hydratase mutations involved in the MCUL (HLRCC) tumor syndrome and congenital fumarase deficiency. BMC Medical Genetics 9, 20. https://doi.org/10.1186/1471-2350-9-20

Berriman, M., Haas, B.J., LoVerde, P.T., Wilson, R.A., Dillon, G.P., Cerqueira, G.C., Mashiyama, S.T., Al-Lazikani, B., Andrade, L.F., Ashton, P.D., Aslett, M.A., Bartholomeu, D.C., Blandin, G., Caffrey, C.R., Coghlan, A., Coulson, R., Day, T.A., Delcher, A., DeMarco, R., Djikeng, A., Eyre, T., Gamble, J.A., Ghedin, E., Gu, Y., Hertz-Fowler, C., Hirai, H., Hirai, Y., Houston, R., Ivens, A., Johnston, D.A., Lacerda, D., Macedo, C.D., McVeigh, P., Ning, Z., Oliveira, G., Overington, J.P., Parkhill, J., Pertea, M., Pierce, R.J., Protasio, A.V., Quail, M.A., Rajandream, M.-A., Rogers, J., Sajid, M., Salzberg, S.L., Stanke, M., Tivey, A.R., White, O., Williams, D.L., Wortman, J., Wu, W., Zamanian, M., Zerlotini, A., Fraser-Liggett, C.M., Barrell, B.G., El-Sayed, N.M., 2009. The genome of the blood fluke *Schistosoma mansoni*. Nature 460, 352–358. https://doi.org/10.1038/nature08160

Bexkens, M.L., Mebius, M.M., Houweling, M., Brouwers, J.F., Tielens, A.G.M., van Hellemond, J.J., 2019. *Schistosoma mansoni* does not and cannot oxidise fatty acids,

but these are used for biosynthetic purposes instead. Int J Parasitol 49, 647–656. https://doi.org/10.1016/j.ijpara.2019.03.005

Birk, A.V., Chao, W.M., Bracken, C., Warren, J.D., Szeto, H.H., 2014. Targeting mitochondrial cardiolipin and the cytochrome c/cardiolipin complex to promote electron transport and optimize mitochondrial ATP synthesis. British Journal of Pharmacology 171, 2017–2028. https://doi.org/10.1111/bph.12468

Birk, A.V., Liu, S., Soong, Y., Mills, W., Singh, P., Warren, J.D., Seshan, S.V., Pardee, J.D., Szeto, H.H., 2013. The Mitochondrial-Targeted Compound SS-31 Re-Energizes Ischemic Mitochondria by Interacting with Cardiolipin. Journal of the American Society of Nephrology 24, 1250. https://doi.org/10.1681/ASN.2012121216

Blatnik, M., Thorpe, S.R., Baynes, J.W., 2008. Succination of Proteins by Fumarate: Mechanism of Inactivation of Glyceraldehyde-3-Phosphate Dehydrogenase in Diabetes 6.

Bloch, E.H., 1980. In Vivo Microscopy of Schistosomiasis: II. Migration of Schistosoma mansoni in the Lungs, Liver, and Intestine. The American Journal of Tropical Medicine and Hygiene 29, 62–70. https://doi.org/10.4269/ajtmh.1980.29.62

Boros, D.L., 1989. Immunopathology of Schistosoma mansoni infection. Clinical Microbiology Reviews 2, 250–269. https://doi.org/10.1128/CMR.2.3.250

Bossche, H.V., 1985. How anthelmintics help us to understand helminths. Parasitology 90, 675–685. https://doi.org/10.1017/S0031182000052306

Bourlat, S.J., Nielsen, C., Economou, A.D., Telford, M.J., 2008. Testing the new animal phylogeny: A phylum level molecular analysis of the animal kingdom. Molecular Phylogenetics and Evolution 49, 23–31. https://doi.org/10.1016/j.ympev.2008.07.008

Bowie, J.U., Lüthy, R., Eisenberg, D., 1991. A Method to Identify Protein Sequences That Fold into a Known Three-Dimensional Structure. Science 253, 164–170. https://doi.org/10.1126/science.1853201

Brookfield, J.F.Y., 1997. 3 - Genetic Redundancy, in: Hall, J.C., Dunlap, J.C., Friedmann, T., Giannelli, F. (Eds.), Advances in Genetics. Academic Press, pp. 137–155. https://doi.org/10.1016/S0065-2660(08)60308-9

Bruce, J.I., Weiss, E., Stirewalt, M.A., Lincicome, D.R., 1969. *Schistosoma mansoni*: glycogen content and utilization of glucose, pyruvate, glutamate, and citric acid cycle intermediates by cercariae and schistosomules. Exp Parasitol 26, 29–40. https://doi.org/10.1016/0014-4894(69)90092-7

Bulusu, V., Jayaraman, V., Balaram, H., 2011. Metabolic Fate of Fumarate, a Side Product of the Purine Salvage Pathway in the Intraerythrocytic Stages of Plasmodium falciparum. J Biol Chem 286, 9236–9245. https://doi.org/10.1074/jbc.M110.173328

Burmester, T., Hankeln, T., 2007. The respiratory proteins of insects. Journal of Insect Physiology 53, 285–294. https://doi.org/10.1016/j.jinsphys.2006.12.006

Cardoso, I.A., de Souza, A.K.L., Burgess, A.M.G., Chalmers, I.W., Hoffmann, K.F., Nonato, M.C., 2021. Characterization of class II fumarase from *Schistosoma mansoni* provides the molecular basis for selective inhibition. International Journal of Biological Macromolecules 175, 406–421. https://doi.org/10.1016/j.ijbiomac.2021.01.180

Castresana, J., 2000. Selection of Conserved Blocks from Multiple Alignments for Their Use in Phylogenetic Analysis. Mol Biol Evol 17, 540–552. https://doi.org/10.1093/oxfordjournals.molbev.a026334

CHALMERS, I.W., HOFFMANN, K.F., 2012. Platyhelminth Venom Allergen-Like (VAL) proteins: revealing structural diversity, class-specific features and biological

associations across the phylum. Parasitology 139, 1231–1245. https://doi.org/10.1017/S0031182012000704

Chamberlain, G.R., Tulumello, D.V., Kelley, S.O., 2013. Targeted Delivery of Doxorubicin to Mitochondria. ACS Chem. Biol. 8, 1389–1395. https://doi.org/10.1021/cb400095v

Cheever, A., Macedonia, J., Mosimann, J., Cheever, E., 1994. Kinetics Of Egg Production And Egg Excretion By *Schistosoma mansoni* And *S. japonicum* In Mice Infected With A Single Pair Of Worms. American Journal Of Tropical Medicine And Hygiene 281–295.

Cheever, A.W., Andrade, Z.A., 1967. Pathological lesions associated with schistosoma mansoni infection in man. Transactions of the Royal Society of Tropical Medicine and Hygiene 61, 626–639. https://doi.org/10.1016/0035-9203(67)90125-3

Chen, L.B., 1988. Mitochondrial Membrane Potential in Living Cells. Annual Review of Cell Biology 4, 155–181. https://doi.org/10.1146/annurev.cb.04.110188.001103

Cheng, J., Liu, Y., Yan, J., Zhao, L., Zhou, Y., Shen, X., Chen, Yunan, Chen, Yining, Meng, X., Zhang, X., Jiang, P., 2022. Fumarate suppresses B-cell activation and function through direct inactivation of LYN. Nat Chem Biol 18, 954–962. https://doi.org/10.1038/s41589-022-01052-0

Chernin, E., 1972. Penetrative Activity of *Schistosoma mansoni* Miracidia Stimulated by Exposure to Snail-Conditioned Water. The Journal of Parasitology 58, 209–212. https://doi.org/10.2307/3278071

Chernin, E., 1970. Behavioral Responses of Miracidia of *Schistosoma mansoni* and Other Trematodes to Substances Emitted by Snails. The Journal of Parasitology 56, 287. https://doi.org/10.2307/3277659

Chinopoulos, C., 2013. Which way does the citric acid cycle turn during hypoxia? The critical role of α-ketoglutarate dehydrogenase complex. Journal of Neuroscience Research 91, 1030–1043. https://doi.org/10.1002/jnr.23196

Clegg, J.A., Smithers, S.R., 1968. Death of schistosome cercariae during penetration of the skin: II. Penetration of mammalian skin by *Schistosoma mansoni.* Parasitology 58, 111–128. https://doi.org/10.1017/S0031182000073479

Clumpp, R.K., Slootweg, R., 1997. Chapter 8: Freshwater snails, intermediate hosts of schistosomiasis and foodborne trematode infections, in: Vector Control - Methods for Use by Individuals and Communities. World Health Organization, pp. 337–356.

Cohen, L.M., Neimark, H., Eveland, L.K., 1980. Schistosoma mansoni: Response of Cercariae to a Thermal Gradient. The Journal of Parasitology 66, 362–364. https://doi.org/10.2307/3280843

Collins, J.J., 2017. Platyhelminthes. Current Biology 27, R252–R256. https://doi.org/10.1016/j.cub.2017.02.016

Copolovici, D.M., Langel, K., Eriste, E., Langel, Ü., 2014. Cell-Penetrating Peptides: Design, Synthesis, and Applications. ACS Nano 8, 1972–1994. https://doi.org/10.1021/nn4057269

Corrêa Soares, J.B.R., Maya-Monteiro, C.M., Bittencourt-Cunha, P.R.B., Atella, G.C., Lara, F.A., d'Avila, J.C.P., Menezes, D., Vannier-Santos, M.A., Oliveira, P.L., Egan, T.J., Oliveira, M.F., 2007. Extracellular lipid droplets promote hemozoin crystallization in the gut of the blood fluke *Schistosoma mansoni*. FEBS Letters 581, 1742–1750. https://doi.org/10.1016/j.febslet.2007.03.054

Coutinho, A.D., 1990. A new dynamic approach to the diagnosis of Symmer' fibrosis in schistosomiasis by ultrasound. Revista do Instituto de Medicina Tropical de São Paulo 32, 73–77. https://doi.org/10.1590/S0036-46651990000200001

Cupit, P.M., Cunningham, C., 2015. What is the mechanism of action of praziquantel and how might resistance strike? Future Medicinal Chemistry 7, 701–705. https://doi.org/10.4155/fmc.15.11

da Silva, V.B.R., Campos, B.R.K.L., de Oliveira, J.F., Decout, J.-L., do Carmo Alves de Lima, M., 2017. Medicinal chemistry of antischistosomal drugs: Praziquantel and oxamniquine. Bioorg Med Chem 25, 3259–3277. https://doi.org/10.1016/j.bmc.2017.04.031

Davies, M., Nowotka, M., Papadatos, G., Dedman, N., Gaulton, A., Atkinson, F., Bellis, L., Overington, J.P., 2015. ChEMBL web services: streamlining access to drug discovery data and utilities. Nucleic Acids Research 43, W612–W620. https://doi.org/10.1093/nar/gkv352

Desjardins, C.A., Cerqueira, G.C., Goldberg, J.M., Dunning Hotopp, J.C., Haas, B.J., Zucker, J., Ribeiro, J.M.C., Saif, S., Levin, J.Z., Fan, L., Zeng, Q., Russ, C., Wortman, J.R., Fink, D.L., Birren, B.W., Nutman, T.B., 2013. Genomics of Loa loa, a Wolbachia-free filarial parasite of humans. Nat Genet 45, 495–500. https://doi.org/10.1038/ng.2585

Dietz, J.V., Fox, J.L., Khalimonchuk, O., 2021. Down the Iron Path: Mitochondrial Iron Homeostasis and Beyond. Cells 10, 2198. https://doi.org/10.3390/cells10092198

Dietzel, J., Hirzmann, J., Preis, D., Symmons, P., Kunz, W., 1992. Ferritins of *Schistosoma mansoni*: sequence comparison and expression in female and male worms. Molecular and Biochemical Parasitology 50, 245–254. https://doi.org/10.1016/0166-6851(92)90221-5

Dolan, M.A., Noah, J.W., Hurt, D., 2012. Comparison of Common Homology Modeling Algorithms: Application of User-Defined Alignments, in: Orry, A.J.W., Abagyan, R. (Eds.), Homology Modeling: Methods and Protocols, Methods in Molecular Biology. Humana Press, Totowa, NJ, pp. 399–414. https://doi.org/10.1007/978-1-61779-588-6_18

Dong, L., Neuzil, J., 2019. Targeting mitochondria as an anticancer strategy. Cancer Commun 39, 63. https://doi.org/10.1186/s40880-019-0412-6

Doughty, B.L., 1996. Schistosomes and Other Trematodes, in: Baron, S. (Ed.), Medical Microbiology. University of Texas Medical Branch at Galveston, Galveston (TX).

Doukov, T.I., Blasiak, L.C., Seravalli, J., Ragsdale, S.W., Drennan, C.L., 2008. Xenon in and at the End of the Tunnel of Bifunctional Carbon Monoxide Dehydrogenase/Acetyl-CoA Synthase,. Biochemistry 47, 3474–3483. https://doi.org/10.1021/bi702386t

Drapier, J.C., Hibbs, J.B., 1986. Murine cytotoxic activated macrophages inhibit aconitase in tumor cells. Inhibition involves the iron-sulfur prosthetic group and is reversible. J Clin Invest 78, 790–797.

Duvall, R.H., DeWitt, W.B., 1967. An Improved Perfusion Technique for Recovering Adult Schistosomes from Laboratory Animals. The American Journal of Tropical Medicine and Hygiene 16, 483–486. https://doi.org/10.4269/ajtmh.1967.16.483

Eddy, S.R., 2011. Accelerated Profile HMM Searches. PLoS Comput Biol 7, e1002195. https://doi.org/10.1371/journal.pcbi.1002195

Edgar, R.C., 2004. MUSCLE: multiple sequence alignment with high accuracy and high throughput. Nucleic Acids Res 32, 1792–1797. https://doi.org/10.1093/nar/gkh340

Edwards, Y.H., Hopkinson, D.A., 1979. Further characterization of the human fumarase variant, FH2–1. Annals of Human Genetics 43, 103–108. https://doi.org/10.1111/j.1469-1809.1979.tb02002.x

Egger, B., Lapraz, F., Tomiczek, B., Müller, S., Dessimoz, C., Girstmair, J., Škunca, N., Rawlinson, K.A., Cameron, C.B., Beli, E., Todaro, M.A., Gammoudi, M., Noreña, C., Telford, M.J., 2015. A Transcriptomic-Phylogenomic Analysis of the Evolutionary Relationships of Flatworms. Current Biology 25, 1347–1353. https://doi.org/10.1016/j.cub.2015.03.034

Elbaz, T., Esmat, G., 2013. Hepatic and Intestinal Schistosomiasis: Review. Journal of Advanced Research, Schistosomiasis: Current Status and Recent Updates 4, 445–452. https://doi.org/10.1016/j.jare.2012.12.001

El-Brolosy, M.A., Stainier, D.Y.R., 2017. Genetic compensation: A phenomenon in search of mechanisms. PLOS Genetics 13, e1006780. https://doi.org/10.1371/journal.pgen.1006780

Emanuelsson, O., Brunak, S., von Heijne, G., Nielsen, H., 2007. Locating proteins in the cell using TargetP, SignalP and related tools. Nature Protocols 2, 953–971. https://doi.org/10.1038/nprot.2007.131

Feliciano, P.R., Drennan, C.L., 2019. Structural and Biochemical Investigations of the [4Fe-4S] Cluster-Containing Fumarate Hydratase from *Leishmania major*. Biochemistry. https://doi.org/10.1021/acs.biochem.9b00923

Feliciano, P.R., Drennan, C.L., Nonato, M.C., 2019. Crystal Structures of Fumarate Hydratases from *Leishmania major* in a Complex with Inhibitor 2-Thiomalate. ACS Chem. Biol. 14, 266–275. https://doi.org/10.1021/acschembio.8b00972

Feliciano, P.R., Drennan, C.L., Nonato, M.C., 2016. Crystal structure of an Fe-S cluster-containing fumarate hydratase enzyme from *Leishmania major* reveals a unique protein fold. PNAS 113, 9804–9809. https://doi.org/10.1073/pnas.1605031113

Feliciano, P.R., Gupta, S., Dyszy, F., Dias-Baruffi, M., Costa-Filho, A.J., Michels, P.A.M., Nonato, M.C., 2012. Fumarate hydratase isoforms of *Leishmania major*: Subcellular localization, structural and kinetic properties. International Journal of Biological Macromolecules 51, 25–31. https://doi.org/10.1016/j.ijbiomac.2012.04.025

Felsenstein, J., 1985. CONFIDENCE LIMITS ON PHYLOGENIES: AN APPROACH USING THE BOOTSTRAP. Evolution 39, 783–791. https://doi.org/10.1111/j.1558-5646.1985.tb00420.x

Field, K.G., Olsen, G.J., Lane, D.J., Giovannoni, S.J., Ghiselin, M.T., Raff, E.C., Pace, N.R., Raff, R.A., 1988. Molecular Phylogeny of the Animal Kingdom. Science 239, 748–753. https://doi.org/10.1126/science.3277277

Fiorito, V., Allocco, A.L., Petrillo, S., Gazzano, E., Torretta, S., Marchi, S., Destefanis, F., Pacelli, C., Audrito, V., Provero, P., Medico, E., Chiabrando, D., Porporato, P.E., Cancelliere, C., Bardelli, A., Trusolino, L., Capitanio, N., Deaglio, S., Altruda, F., Pinton, P., Cardaci, S., Riganti, C., Tolosano, E., 2021. The heme synthesis-export system regulates the tricarboxylic acid cycle flux and oxidative phosphorylation. Cell Reports 35, 109252. https://doi.org/10.1016/j.celrep.2021.109252

Fitzpatrick, J.M., Peak, E., Perally, S., Chalmers, I.W., Barrett, J., Yoshino, T.P., Ivens, A.C., Hoffmann, K.F., 2009. Anti-schistosomal Intervention Targets Identified by Lifecycle Transcriptomic Analyses. PLoS Neglected Tropical Diseases 3, e543. https://doi.org/10.1371/journal.pntd.0000543

Flint, D.H., Allen, R.M., 1996. Iron−Sulfur Proteins with Nonredox Functions. Chem. Rev. 96, 2315–2334. https://doi.org/10.1021/cr950041r

Flint, D.H., Emptage, M.H., Guest, J.R., 1992. Fumarase A from *Escherichia coli*: purification and characterization as an iron-sulfur cluster containing enzyme. Biochemistry 31, 10331–10337. https://doi.org/10.1021/bi00157a022

Frallicciardi, J., Melcr, J., Siginou, P., Marrink, S.J., Poolman, B., 2022. Membrane thickness, lipid phase and sterol type are determining factors in the permeability of membranes to small solutes. Nat Commun 13, 1605. https://doi.org/10.1038/s41467-022-29272-x

Friedl, J., Knopp, M.R., Groh, C., Paz, E., Gould, S.B., Herrmann, J.M., Boos, F., 2020. More than just a ticket canceller: the mitochondrial processing peptidase tailors complex precursor proteins at internal cleavage sites. MBoC 31, 2657–2668. https://doi.org/10.1091/mbc.E20-08-0524

Fukasawa, Y., Tsuji, J., Fu, S.-C., Tomii, K., Horton, P., Imai, K., 2015. MitoFates: Improved Prediction of Mitochondrial Targeting Sequences and Their Cleavage Sites*,. Molecular & Cellular Proteomics 14, 1113–1126. https://doi.org/10.1074/mcp.M114.043083

Fukushige, M., Chase-Topping, M., Woolhouse, M.E.J., Mutapi, F., 2021. Efficacy of praziquantel has been maintained over four decades (from 1977 to 2018): A systematic review and meta-analysis of factors influence its efficacy. PLoS Negl Trop Dis 15, e0009189. https://doi.org/10.1371/journal.pntd.0009189

Fuss, J.O., Tsai, C.-L., Ishida, J.P., Tainer, J.A., 2015. Emerging critical roles of Fe–S clusters in DNA replication and repair. Biochimica et Biophysica Acta (BBA) - Molecular Cell Research, SI: Fe/S proteins 1853, 1253–1271. https://doi.org/10.1016/j.bbamcr.2015.01.018

Gasmi, A., Peana, M., Arshad, M., Butnariu, M., Menzel, A., Bjørklund, G., 2021. Krebs cycle: activators, inhibitors and their roles in the modulation of carcinogenesis. Arch Toxicol 95, 1161–1178. https://doi.org/10.1007/s00204-021-02974-9

Gazzinelli, G., Pellegrino, J., 1964. Elastolytic Activity of *Schistosoma mansoni* Cercarial Extract. The Journal of Parasitology 50, 591–592. https://doi.org/10.2307/3275632

GBD 2015 Disease and Injury Incidence and Prevalence Collaborators, 2016. Global, regional, and national incidence, prevalence, and years lived with disability for 310 diseases and injuries, 1990–2015: a systematic analysis for the Global Burden of Disease Study 2015. Lancet 388, 1545–1602. https://doi.org/10.1016/S0140-6736(16)31678-6

Geyer, K.K., López, C.M.R., Chalmers, I.W., Munshi, S.E., Truscott, M., Heald, J., Wilkinson, M.J., Hoffmann, K.F., 2011. Cytosine methylation regulates oviposition in the pathogenic blood fluke *Schistosoma mansoni.* Nat Commun 2, 1–10. https://doi.org/10.1038/ncomms1433

Geyer, K.K., Niazi, U.H., Duval, D., Cosseau, C., Tomlinson, C., Chalmers, I.W., Swain, M.T., Cutress, D.J., Bickham-Wright, U., Munshi, S.E., Grunau, C., Yoshino, T.P., Hoffmann, K.F., 2017. The *Biomphalaria glabrata* DNA methylation machinery displays spatial tissue expression, is differentially active in distinct snail populations and is modulated by interactions with *Schistosoma mansoni*. PLOS Neglected Tropical Diseases 11, e0005246. https://doi.org/10.1371/journal.pntd.0005246

Ghosh, P., Vidal, C., Dey, S., Zhang, L., 2020. Mitochondria Targeting as an Effective Strategy for Cancer Therapy. Int J Mol Sci 21, 3363. https://doi.org/10.3390/ijms21093363

Giacomello, M., Pyakurel, A., Glytsou, C., Scorrano, L., 2020. The cell biology of mitochondrial membrane dynamics. Nat Rev Mol Cell Biol 21, 204–224. https://doi.org/10.1038/s41580-020-0210-7

Giribet, G., 2008. Assembling the lophotrochozoan (=spiralian) tree of life. Philosophical Transactions of the Royal Society B: Biological Sciences 363, 1513–1522. https://doi.org/10.1098/rstb.2007.2241

Golub, T.R., Slonim, D.K., Tamayo, P., Huard, C., Gaasenbeek, M., Mesirov, J.P., Coller, H., Loh, M.L., Downing, J.R., Caligiuri, M.A., Bloomfield, C.D., Lander, E.S., 1999. Molecular classification of cancer: class discovery and class prediction by gene expression monitoring. Science 286, 531–537. https://doi.org/10.1126/science.286.5439.531

Gorman, M.J., 2023. Iron Homeostasis in Insects. Annu Rev Entomol 68, 51–67. https://doi.org/10.1146/annurev-ento-040622-092836

Greenhut, J., Umezawa, H., Rudolph, F.B., 1985. Inhibition of fumarase by S-2,3-dicarboxyaziridine. Journal of Biological Chemistry 260, 6684–6686. https://doi.org/10.1016/S0021-9258(18)88834-2

Grevelding, C.G., Kampkötter, A., Kunz, W., 1997. *Schistosoma mansoni*: Sexing Cercariae by PCR without DNA Extraction. Experimental Parasitology 85, 99–100. https://doi.org/10.1006/expr.1996.4129

Guerrero, J., 1984. Closantel: A review of its antiparasitic activity. Preventive Veterinary Medicine 2, 317–327. https://doi.org/10.1016/0167-5877(84)90075-8

GUEST, J.R., MILES, J.S., ROBERTS, R.E., WOODS, S.A., 1985. The Fumarase Genes of Escherichia coli: Location of the fumB Gene and Discovery of a New Gene (fumC). Microbiology 131, 2971–2984. https://doi.org/10.1099/00221287-131-11-2971

Haas, W., Diekhoff, D., Koch, K., Schmalfuss, G., Loy, C., 1997. *Schistosoma mansoni* Cercariae: Stimulation of Acetabular Gland Secretion Is Adapted to the Chemical Composition of Mammalian Skin. The Journal of Parasitology 83, 1079–1085. https://doi.org/10.2307/3284366

Haas, W., Gui, M., Haberl, B., Ströbel, M., 1991. Miracidia of Schistosoma japonicum: Approach and Attachment to the Snail Host. The Journal of Parasitology 77, 509–513. https://doi.org/10.2307/3283152

Haas, W., Haberl, B., Schmalfuss, G., Khayyal, M.T., 1994. Schistosoma haematobium cercarial host-finding and host-recognition differs from that of S. mansoni. J Parasitol 80, 345–353. https://doi.org/10.2307/3283401

Haberl, B., Kalbe, M., Fuchs, H., Ströbel, M., Schmalfuss, G., Haas, W., 1995. Schistosoma mansoni and S. haematobium: Miracidial host-finding behaviour is stimulated by macromolecules. International Journal for Parasitology 25, 551–560. https://doi.org/10.1016/0020-7519(94)00158-K

Hahn, U.K., Bender, R.C., Bayne, C.J., 2001. Involvement of Nitric Oxide in Killing of *Schistosoma mansoni* Sporocysts by Hemocytes from Resistant *Biomphalaria glabrata*. The Journal of Parasitology 87, 778–785. https://doi.org/10.2307/3285134

Hannesschlaeger, C., Horner, A., Pohl, P., 2019. Intrinsic Membrane Permeability to Small Molecules. Chem. Rev. 119, 5922–5953. https://doi.org/10.1021/acs.chemrev.8b00560

Hansell, E., Braschi, S., Medzihradszky, K.F., Sajid, M., Debnath, M., Ingram, J., Lim, K.C., McKerrow, J.H., 2008. Proteomic Analysis of Skin Invasion by Blood Fluke Larvae. PLoS Neglected Tropical Diseases 2, e262. https://doi.org/10.1371/journal.pntd.0000262

He, X., Li, M., Song, Shuting, Wu, X., Zhang, J., Wu, G., Yue, R., Cui, H., Song, Siqing, Ma, C., Lu, F., Zhang, H., 2018. Ficellomycin: an aziridine alkaloid antibiotic with potential therapeutic capacity. Appl Microbiol Biotechnol 102, 4345–4354. https://doi.org/10.1007/s00253-018-8934-4

Hellemans, J., Mortier, G., De Paepe, A., Speleman, F., Vandesompele, J., 2007. qBase relative quantification framework and software for management and automated analysis of real-time quantitative PCR data. Genome Biology 8, R19. https://doi.org/10.1186/gb-2007-8-2-r19

Hockley, D.J., McLaren, D.J., 1973. *Schistosoma mansoni*: Changes in the outer membrane of the tegument during development from cercaria to adult worm. International Journal for Parasitology 3, 13–20. https://doi.org/10.1016/0020-7519(73)90004-0

Horton, K.L., Stewart, K.M., Fonseca, S.B., Guo, Q., Kelley, S.O., 2008. Mitochondria-Penetrating Peptides. Chemistry & Biology 15, 375–382. https://doi.org/10.1016/j.chembiol.2008.03.015

Hotez, P.J., Fenwick, A., Kjetland, E.F., 2009. Africa's 32 Cents Solution for HIV/AIDS. PLOS Neglected Tropical Diseases 3, e430. https://doi.org/10.1371/journal.pntd.0000430

Huelsenbeck, J.P., Ronquist, F., 2001. MRBAYES: Bayesian inference of phylogenetic trees. Bioinformatics 17, 754–755. https://doi.org/10.1093/bioinformatics/17.8.754

Hulme, B.J., Geyer, K.K., Forde-Thomas, J.E., Padalino, G., Phillips, D.W., Ittiprasert, W., Karinshak, S.E., Mann, V.H., Chalmers, I.W., Brindley, P.J., Hokke, C.H., Hoffmann, K.F., 2022. *Schistosoma mansoni* α-N-acetylgalactosaminidase (SmNAGAL) regulates coordinated parasite movement and egg production. PLOS Pathogens 18, e1009828. https://doi.org/10.1371/journal.ppat.1009828

Iii, J.J.C., Hou, X., Romanova, E.V., Lambrus, B.G., Miller, C.M., Saberi, A., Sweedler, J.V., Newmark, P.A., 2010. Genome-Wide Analyses Reveal a Role for Peptide Hormones in Planarian Germline Development. PLOS Biology 8, e1000509. https://doi.org/10.1371/journal.pbio.1000509

James, S.L., 1995. Role of Nitric Oxide in Parasitic Infections. MICROBIOL. REV. 59, 15.

Janse, J.J., Langenberg, M.C.C., Kos-Van Oosterhoud, J., Ozir-Fazalalikhan, A., Brienen, E.A.T., Winkel, B.M.F., Erkens, M.A.A., van der Beek, M.T., van Lieshout, L., Smits, H.H., Webster, B.L., Zandvliet, M.L., Verbeek, R., Westra, I.M., Meij, P., Visser, L.G., van Diepen, A., Hokke, C.H., Yazdanbakhsh, M., Roestenberg, M., 2018. Establishing the Production of Male *Schistosoma mansoni* Cercariae for a Controlled Human Infection Model. J Infect Dis 218, 1142–1146. https://doi.org/10.1093/infdis/jiy275

Janssens, P.A., Bryant, C., 1969. The ornithine-urea cycle in some parasitic helminths. Comparative Biochemistry and Physiology 30, 261–272. https://doi.org/10.1016/0010-406X(69)90809-3

Jayaraman, V., Suryavanshi, A., Kalale, P., Kunala, J., Balaram, H., 2018. Biochemical characterization and essentiality of Plasmodium fumarate hydratase. J. Biol. Chem. 293, 5878–5894. https://doi.org/10.1074/jbc.M117.816298

Jean, S.R., Tulumello, D.V., Riganti, C., Liyanage, S.U., Schimmer, A.D., Kelley, S.O., 2015. Mitochondrial Targeting of Doxorubicin Eliminates Nuclear Effects Associated with

Cardiotoxicity. ACS Chem. Biol. 10, 2007–2015. https://doi.org/10.1021/acschembio.5b00268

Jiang, Y., Qian, X., Shen, J., Wang, Y., Li, X., Liu, R., Xia, Y., Chen, Q., Peng, G., Lin, S.-Y., Lu, Z., 2015. Local generation of fumarate promotes DNA repair through inhibition of histone H3 demethylation. Nat Cell Biol 17, 1158–1168. https://doi.org/10.1038/ncb3209

Jones, D.T., Taylor, W.R., Thornton, J.M., 1992. The rapid generation of mutation data matrices from protein sequences. Comput Appl Biosci 8, 275–282. https://doi.org/10.1093/bioinformatics/8.3.275

Jones, M.K., McManus, D.P., Sivadorai, P., Glanfield, A., Moertel, L., Belli, S.I., Gobert, G.N., 2007. Tracking the fate of iron in early development of human blood flukes. The International Journal of Biochemistry & Cell Biology 39, 1646–1658. https://doi.org/10.1016/j.biocel.2007.04.017

Jourdane, J., Theron, A., Combes, C., 1980. Demonstration of several sporocysts generations as a normal pattern of reproduction of *Schistosoma mansoni.* Acta Trop 37, 177–182.

Kasbekar, M., Fischer, G., Mott, B.T., Yasgar, A., Hyvönen, M., Boshoff, H.I.M., Abell, C., Barry, C.E., Thomas, C.J., 2016. Selective small molecule inhibitor of the Mycobacterium tuberculosis fumarate hydratase reveals an allosteric regulatory site. PNAS 113, 7503–7508. https://doi.org/10.1073/pnas.1600630113

Katayama, T., Kinugawa, S., Takada, S., Furihata, T., Fukushima, A., Yokota, T., Anzai, T., Hibino, M., Harashima, H., Yamada, Y., 2019. A mitochondrial delivery system using liposome-based nanocarriers that target myoblast cells. Mitochondrion 49, 66–72. https://doi.org/10.1016/j.mito.2019.07.005

Kawamura, E., Yamada, Y., Harashima, H., 2013. Mitochondrial targeting functional peptides as potential devices for the mitochondrial delivery of a DF-MITO-Porter. Mitochondrion 13, 610–614. https://doi.org/10.1016/j.mito.2013.08.010

Kerrigan, J.F., Aleck, K.A., Tarby, T.J., Bird, C.R., Heidenreich, R.A., 2000. Fumaric aciduria: clinical and imaging features. Ann Neurol 47, 583–588.

Kim, H.J., Khalimonchuk, O., Smith, P.M., Winge, D.R., 2012. Structure, function, and assembly of heme centers in mitochondrial respiratory complexes. Biochimica et Biophysica Acta (BBA) - Molecular Cell Research, Cell Biology of Metals 1823, 1604–1616. https://doi.org/10.1016/j.bbamcr.2012.04.008

Kim, J.-H., O'Brien, K.M., Sharma, R., Boshoff, H.I.M., Rehren, G., Chakraborty, S., Wallach, J.B., Monteleone, M., Wilson, D.J., Aldrich, C.C., Barry, C.E., Rhee, K.Y., Ehrt, S., Schnappinger, D., 2013. A genetic strategy to identify targets for the development of drugs that prevent bacterial persistence. Proceedings of the National Academy of Sciences 110, 19095–19100. https://doi.org/10.1073/pnas.1315860110

Kim, O.B., Lux, S., Unden, G., 2007. Anaerobic growth of Escherichia coli on d-tartrate depends on the fumarate carrier DcuB and fumarase, rather than the l-tartrate carrier TtdT and l-tartrate dehydratase. Arch Microbiol 188, 583–589. https://doi.org/10.1007/s00203-007-0279-9

Kim, S., Nam, H.Y., Lee, J., Seo, J., 2020. Mitochondrion-Targeting Peptides and Peptidomimetics: Recent Progress and Design Principles. Biochemistry 59, 270–284. https://doi.org/10.1021/acs.biochem.9b00857

Kinch, L., Grishin, N.V., Brugarolas, J., 2011. Succination of Keap1 and Activation of Nrf2-Dependent Antioxidant Pathways in FH-Deficient Papillary Renal Cell Carcinoma Type 2. Cancer Cell 20, 418–420. https://doi.org/10.1016/j.ccr.2011.10.005

Kjetland, E.F., Kurewa, E.N., Ndhlovu, P.D., Midzi, N., Gwanzura, L., Mason, P.R., Gomo, E., Sandvik, L., Mduluza, T., Friis, H., Gundersen, S.G., 2008. Female genital schistosomiasis – a differential diagnosis to sexually transmitted disease: genital itch and vaginal discharge as indicators of genital *Schistosoma haematobium* morbidity in a cross-sectional study in endemic rural Zimbabwe. Tropical Medicine & International Health 13, 1509–1517. https://doi.org/10.1111/j.1365-3156.2008.02161.x

Kobayashi, K., Tuboi, S., 1983. End Group Analysis of the Cytosolic and Mitochondrial Fumarases from Rat Liver. J Biochem 94, 707–713. https://doi.org/10.1093/oxfordjournals.jbchem.a134410

Korb, O., Stützle, T., Exner, T.E., 2009. Empirical scoring functions for advanced protein-ligand docking with PLANTS. J Chem Inf Model 49, 84–96. https://doi.org/10.1021/ci800298z

Krautz-Peterson, G., Simoes, M., Faghiri, Z., Ndegwa, D., Oliveira, G., Shoemaker, C.B., Skelly, P.J., 2010. Suppressing Glucose Transporter Gene Expression in Schistosomes Impairs Parasite Feeding and Decreases Survival in the Mammalian Host. PLOS Pathogens 6, e1000932. https://doi.org/10.1371/journal.ppat.1000932

Krebs, H.A., 1940. The citric acid cycle and the Szent-Györgyi cycle in pigeon breast muscle. Biochem J 34, 775–779.

Krebs, H.A., Johnson, W.A., 1980. The role of citric acid in intermediate metabolism in animal tissues. FEBS LETTERS 117, 9.

Krebs, H.A., Johnson, W.A., 1937. Metabolism of ketonic acids in animal tissues. Biochemical Journal 31, 645–660. https://doi.org/10.1042/bj0310645

Kumar, S., Stecher, G., Li, M., Knyaz, C., Tamura, K., 2018. MEGA X: Molecular Evolutionary Genetics Analysis across Computing Platforms. Mol Biol Evol 35, 1547–1549. https://doi.org/10.1093/molbev/msy096

Kura, K., Hardwick, R.J., Truscott, J.E., Toor, J., Hollingsworth, T.D., Anderson, R.M., 2020. The impact of mass drug administration on *Schistosoma haematobium* infection: what is required to achieve morbidity control and elimination? Parasites & Vectors 13, 554. https://doi.org/10.1186/s13071-020-04409-3

Latif, B., Heo, C.C., Razuin, R., Shamalaa, D.V., Tappe, D., 2013. Autochthonous Human Schistosomiasis, Malaysia. Emerg Infect Dis 19, 1340–1341. https://doi.org/10.3201/eid1908.121710

Laumer, C.E., Hejnol, A., Giribet, G., 2015. Nuclear genomic signals of the 'microturbellarian' roots of platyhelminth evolutionary innovation. eLife 4, e05503. https://doi.org/10.7554/eLife.05503

Lee, C.-L., Lewert, R.M., 1956. The Maintenance of *Schistosoma mansoni* in the Laboratory. J Infect Dis 99, 15–20. https://doi.org/10.1093/infdis/99.1.15

Legters, J., Thijs, L., Zwanenburg, B., 1991. Synthesis of naturally occurring (2S,3S)-(+)-aziridine-2,3-dicarboxylic acid. Tetrahedron 47, 5287–5294. https://doi.org/10.1016/S0040-4020(01)87140-4

Leshets, M., Silas, Y.B.H., Lehming, N., Pines, O., 2018. Fumarase: From the TCA Cycle to DNA Damage Response and Tumor Suppression. Front Mol Biosci 5. https://doi.org/10.3389/fmolb.2018.00068

Leutscher, P.D.C., Ramarokoto, C.-E., Hoffmann, S., Jensen, J.S., Ramaniraka, V., Randrianasolo, B., Raharisolo, C., Migliani, R., Christensen, N., 2008. Coexistence of Urogenital Schistosomiasis and Sexually Transmitted Infection in Women and Men Living in an Area Where *Schistosoma haematobium* is Endemic. Clin Infect Dis 47, 775–782. https://doi.org/10.1086/591127

Lin, R., Zhang, P., Cheetham, Andrew.G., Walston, J., Abadir, P., Cui, H., 2015. Dual Peptide Conjugation Strategy for Improved Cellular Uptake and Mitochondria Targeting. Bioconjugate Chem. 26, 71–77. https://doi.org/10.1021/bc500408p

Lipinski, C.A., Lombardo, F., Dominy, B.W., Feeney, P.J., 2012. Experimental and computational approaches to estimate solubility and permeability in drug discovery and development settings. Advanced Drug Delivery Reviews, MOST CITED PAPERS IN THE HISTORY OF ADVANCED DRUG DELIVERY REVIEWS: A TRIBUTE TO THE 25TH ANNIVERSARY OF THE JOURNAL 64, 4–17. https://doi.org/10.1016/j.addr.2012.09.019

Littlewood, D.T.J., Rohde, K., Bray, R.A., Herniou, E.A., 1999. Phylogeny of the Platyhelminthes and the evolution of parasitism. Biological Journal of the Linnean Society 68, 257–287. https://doi.org/10.1111/j.1095-8312.1999.tb01169.x

Lloyd, G.M., 1986. Energy metabolism and its regulation in the adult liver fluke Fasciola hepatica. Parasitology 93, 217. https://doi.org/10.1017/S0031182000049957

Lorenzato, A., Olivero, M., Perro, M., Brière, J.J., Rustin, P., Renzo, M.F.D., 2008. A cancer-predisposing “hot spot” mutation of the fumarase gene creates a dominant negative protein. International Journal of Cancer 122, 947–951. https://doi.org/10.1002/ijc.23209

Lovell, S.C., Davis, I.W., Arendall III, W.B., de Bakker, P.I.W., Word, J.M., Prisant, M.G., Richardson, J.S., Richardson, D.C., 2003. Structure validation by Cα geometry: ϕ,ψ and Cβ deviation. Proteins: Structure, Function, and Bioinformatics 50, 437–450. https://doi.org/10.1002/prot.10286

Lu, P., Redd Bowman, K.E., Brown, S.M., Joklik-Mcleod, M., Vander Mause, E.R., Nguyen, H.T.N., Lim, C.S., 2019. p53-Bad: A Novel Tumor Suppressor/Proapoptotic Factor

Hybrid Directed to the Mitochondria for Ovarian Cancer Gene Therapy. Mol. Pharmaceutics 16, 3386–3398. https://doi.org/10.1021/acs.molpharmaceut.9b00136

Lu, Z., Berriman, M., 2018. Meta-analysis of RNA-seq studies reveals genes responsible for life stage-dominant functions in Schistosoma mansoni. bioRxiv 308189. https://doi.org/10.1101/308189

Lu, Z., Sessler, F., Holroyd, N., Hahnel, S., Quack, T., Berriman, M., Grevelding, C.G., 2016. Schistosome sex matters: a deep view into gonad-specific and pairing-dependent transcriptomes reveals a complex gender interplay. Scientific Reports 6. https://doi.org/10.1038/srep31150

Mann, P.J.G., Woolf, B., 1930. The action of salts on fumarase. I. Biochemical Journal 24, 427–434. https://doi.org/10.1042/bj0240427

Marelja, Z., Leimkühler, S., Missirlis, F., 2018. Iron Sulfur and Molybdenum Cofactor Enzymes Regulate the *Drosophila* Life Cycle by Controlling Cell Metabolism. Front Physiol 9, 50. https://doi.org/10.3389/fphys.2018.00050

Martínez-Reyes, I., Chandel, N.S., 2020. Mitochondrial TCA cycle metabolites control physiology and disease. Nat Commun 11. https://doi.org/10.1038/s41467-019-13668-3

Mas-Coma, S., Bargues, M.D., Valero, M.A., 2005. Fascioliasis and other plant-borne trematode zoonoses. International Journal for Parasitology, Parasitic Zoonoses - Emerging Issues 35, 1255–1278. https://doi.org/10.1016/j.ijpara.2005.07.010

McKerrow, J.H., Salter, J., 2002. Invasion of skin by Schistosoma cercariae. Trends Parasitol 18, 193–195. https://doi.org/10.1016/s1471-4922(02)02309-7

Mechaly, A.E., Haouz, A., Miras, I., Barilone, N., Weber, P., Shepard, W., Alzari, P.M., Bellinzoni, M., 2012. Conformational changes upon ligand binding in the essential

class II fumarase Rv1098c from Mycobacterium tuberculosis. FEBS Letters 586, 1606–1611. https://doi.org/10.1016/j.febslet.2012.04.034

Menichetti, R., Kanekal, K.H., Bereau, T., 2019. Drug–Membrane Permeability across Chemical Space. ACS Cent Sci 5, 290–298. https://doi.org/10.1021/acscentsci.8b00718

Menko, F.H., Maher, E.R., Schmidt, L.S., Middelton, L.A., Aittomäki, K., Tomlinson, I., Richard, S., Linehan, W.M., 2014. Hereditary leiomyomatosis and renal cell cancer (HLRCC): renal cancer risk, surveillance and treatment. Familial Cancer 13, 637–644. https://doi.org/10.1007/s10689-014-9735-2

Meuleman, E.A., 1971. Host-Parasite Interrelationships Between the Freshwater Pulmonate Biomphalaria Pfeifferi and the Trematode *Schistosoma mansoni*. Netherlands Journal of Zoology 22, 355–427. https://doi.org/10.1163/002829672X00013

Meuleman, E.A., Holzmann, P.J., Peet, R.C., 1980. The development of daughter sporocysts inside the mother sporocyst of *Schistosoma mansoni* with special reference to the ultrastructure of the body wall. Zeitschrift für Parasitenkunde Parasitology Research 61, 201–212. https://doi.org/10.1007/BF00925512

Millard, M., Pathania, D., Shabaik, Y., Taheri, L., Deng, J., Neamati, N., 2010. Preclinical Evaluation of Novel Triphenylphosphonium Salts with Broad-Spectrum Activity. PLOS ONE 5, e13131. https://doi.org/10.1371/journal.pone.0013131

Miller, P., Wilson, R.A., 1978. Migration of the schistosomula of *Schistosoma mansoni* from skin to lungs. Parasitology 77, 281–302. https://doi.org/10.1017/S0031182000050253

Mohamed-Ali, Q., Elwali, N.-E.M.A., Abdelhameed, A.A., Mergani, A., Rahoud, S., Elagib, K.E., Saeed, O.K., Abel, L., Magzoub, M.M.A., Dessein, A.J., 1999. Susceptibility to Periportal (Symmers) Fibrosis in Human *Schistosoma mansoni* Infections: Evidence

That Intensity and Duration of Infection, Gender, and Inherited Factors Are Critical in Disease Progression. J Infect Dis 180, 1298–1306. https://doi.org/10.1086/314999

Molehin, A.J., 2020. Schistosomiasis vaccine development: update on human clinical trials. Journal of Biomedical Science 27, 28. https://doi.org/10.1186/s12929-020-0621-y

Moss, G.D., 1970. The excretory metabolism of the endoparasitic digenean Fasciola hepatica and its relationship to its respiratory metabolism. Parasitology 60, 1–19. https://doi.org/10.1017/S0031182000077209

Mostafa, M.H., Sheweita, S.A., O'Connor, P.J., 1999. Relationship between Schistosomiasis and Bladder Cancer. Clin Microbiol Rev 12, 97–111.

Murphy, M.P., 2008. Targeting lipophilic cations to mitochondria. Biochimica et Biophysica Acta (BBA) - Bioenergetics, 15th European Bioenergetics Conference 2008 1777, 1028–1031. https://doi.org/10.1016/j.bbabio.2008.03.029

Murphy, M.P., Smith, R.A.J., 2000. Drug delivery to mitochondria: the key to mitochondrial medicine. Advanced Drug Delivery Reviews, Recent Advances in Cellular, Subcellular and Molecular Targeting 41, 235–250. https://doi.org/10.1016/S0169-409X(99)00069-1

Nast, G., Muller-Rober, B., 1996. Molecular Characterization of Potato Fumarate Hydratase and Functional Expression in Escherichia coli. Plant Physiology 112, 1219–1227. https://doi.org/10.1104/pp.112.3.1219

Nation, C.S., Da'dara, A.A., Marchant, J.K., Skelly, P.J., 2020. Schistosome migration in the definitive host. PLOS Neglected Tropical Diseases 14, e0007951. https://doi.org/10.1371/journal.pntd.0007951

Naylor, M.A., Jaffar, M., Nolan, J., Stephens, M.A., Butler, S., Patel, K.B., Everett, S.A., Adams, G.E., Stratford, I.J., 1997. 2-Cyclopropylindoloquinones and Their Analogues

as Bioreductively Activated Antitumor Agents: Structure−Activity in Vitro and Efficacy in Vivo. J. Med. Chem. 40, 2335–2346. https://doi.org/10.1021/jm9608422

Netz, D.J.A., Stith, C.M., Stümpfig, M., Köpf, G., Vogel, D., Genau, H.M., Stodola, J.L., Lill, R., Burgers, P.M.J., Pierik, A.J., 2012. Eukaryotic DNA polymerases require an iron-sulfur cluster for the formation of active complexes. Nat Chem Biol 8, 125–132. https://doi.org/10.1038/nchembio.721

Nowak, M.A., Boerlijst, M.C., Cooke, J., Smith, J.M., 1997. Evolution of genetic redundancy. Nature 388, 167–171. https://doi.org/10.1038/40618

O'Hare, M.C., Doonan, S., 1985. Purification and structural comparisons of the cytosolic and mitochondrial isoenzymes of fumarase from pig liver. Biochim Biophys Acta 827, 127–134. https://doi.org/10.1016/0167-4838(85)90080-9

Oliveira, M.F., Kycia, S.W., Gomez, A., Kosar, A.J., Bohle, D.S., Hempelmann, E., Menezes, D., Vannier-Santos, M.A., Oliveira, P.L., Ferreira, S.T., 2005. Structural and morphological characterization of hemozoin produced by Schistosoma mansoni and Rhodnius prolixus. FEBS Letters 579, 6010–6016. https://doi.org/10.1016/j.febslet.2005.09.035

Olivier, L., Mao, C.P., 1949. The Early Larval Stages of Schistosoma mansoni Sambon, 1907 in the Snail Host, Australorbis glabratus (Say, 1818). The Journal of Parasitology 35, 267–275. https://doi.org/10.2307/3273302

Pajuelo, L., Calviño, E., Diez, J.C., Boyano-Adánez, M. del C., Gil, J., Sancho, P., 2011. Dequalinium induces apoptosis in peripheral blood mononuclear cells isolated from human chronic lymphocytic leukemia. Invest New Drugs 29, 1156–1163. https://doi.org/10.1007/s10637-010-9454-y

Palmer, B.D., Wilson, W.R., Cliffe, S., Denny, W.A., 1992. Hypoxia-selective antitumor agents. 5. Synthesis of water-soluble nitroaniline mustards with selective cytotoxicity

for hypoxic mammalian cells. J. Med. Chem. 35, 3214–3222. https://doi.org/10.1021/jm00095a018

Pantopoulos, K., Porwal, S.K., Tartakoff, A., Devireddy, L., 2012. Mechanisms of mammalian iron homeostasis. Biochemistry 51, 5705–5724. https://doi.org/10.1021/bi300752r

Paps, J., Baguñà, J., Riutort, M., 2009. Lophotrochozoa internal phylogeny: new insights from an up-to-date analysis of nuclear ribosomal genes. Proc Biol Sci 276, 1245–1254. https://doi.org/10.1098/rspb.2008.1574

Passador-Gurgel, G., Hsieh, W.-P., Hunt, P., Deighton, N., Gibson, G., 2007. Quantitative trait transcripts for nicotine resistance in *Drosophila melanogaster*. Nat Genet 39, 264–268. https://doi.org/10.1038/ng1944

Passarella, S., Schurr, A., Portincasa, P., 2021. Mitochondrial Transport in Glycolysis and Gluconeogenesis: Achievements and Perspectives. Int J Mol Sci 22, 12620. https://doi.org/10.3390/ijms222312620

Paterson, D.A., Conradi, R.A., Hilgers, A.R., Vidmar, T.J., Burton, P.S., 1994. A Non-aqueous Partitioning System for Predicting the Oral Absorption Potential of Peptides. Quantitative Structure-Activity Relationships 13, 4–10. https://doi.org/10.1002/qsar.19940130103

Paveley, R.A., Bickle, Q.D., 2013. Automated Imaging and other developments in whole-organism anthelmintic screening. Parasite Immunology 35, 302–313. https://doi.org/10.1111/pim.12037

Pearson, R.G., 1969. Hard and Soft Acids and Bases, in: Scott, A.F. (Ed.), Survey of Progress in Chemistry, Survey of Progress in Chemistry. Elsevier, pp. 1–52. https://doi.org/10.1016/B978-0-12-395706-1.50007-8

Pearson, W.R., 2013. An Introduction to Sequence Similarity ("Homology") Searching. Curr Protoc Bioinformatics 0 3, 10.1002/0471250953.bi0301s42. https://doi.org/10.1002/0471250953.bi0301s42

Pfaffl, M.W., 2001. A new mathematical model for relative quantification in real-time RT–PCR. Nucleic Acids Res 29, e45.

Poggensee, G., Kiwelu, I., Weger, V., Göppner, D., Diedrich, T., Krantz, I., Feldmeier, H., 2000. Female Genital Schistosomiasis of the Lower Genital Tract: Prevalence and Disease-Associated Morbidity in Northern Tanzania. J Infect Dis 181, 1210–1213. https://doi.org/10.1086/315345

Pollard, P.J., Brière, J.J., Alam, N.A., Barwell, J., Barclay, E., Wortham, N.C., Hunt, T., Mitchell, M., Olpin, S., Moat, S.J., Hargreaves, I.P., Heales, S.J., Chung, Y.L., Griffiths, J.R., Dalgleish, A., McGrath, J.A., Gleeson, M.J., Hodgson, S.V., Poulsom, R., Rustin, P., Tomlinson, I.P.M., 2005. Accumulation of Krebs cycle intermediates and over-expression of HIF1α in tumours which result from germline FH and SDH mutations. Human Molecular Genetics 14, 2231–2239. https://doi.org/10.1093/hmg/ddi227

Pracharoenwattana, I., Zhou, W., Keech, O., Francisco, P.B., Udomchalothorn, T., Tschoep, H., Stitt, M., Gibon, Y., Smith, S.M., 2010. Arabidopsis has a cytosolic fumarase required for the massive allocation of photosynthate into fumaric acid and for rapid plant growth on high nitrogen: Cytosolic fumarase and growth on nitrogen. The Plant Journal 62, 785–795. https://doi.org/10.1111/j.1365-313X.2010.04189.x

Pravda, L., Berka, K., Svobodová Vařeková, R., Sehnal, D., Banáš, P., Laskowski, R.A., Koča, J., Otyepka, M., 2014. Anatomy of enzyme channels. BMC Bioinformatics 15, 379. https://doi.org/10.1186/s12859-014-0379-x

Protasio, A.V., Tsai, I.J., Babbage, A., Nichol, S., Hunt, M., Aslett, M.A., De Silva, N., Velarde, G.S., Anderson, T.J.C., Clark, R.C., Davidson, C., Dillon, G.P., Holroyd, N.E., LoVerde, P.T., Lloyd, C., McQuillan, J., Oliveira, G., Otto, T.D., Parker-Manuel, S.J., Quail, M.A., Wilson, R.A., Zerlotini, A., Dunne, D.W., Berriman, M., 2012. A Systematically Improved High Quality Genome and Transcriptome of the Human Blood Fluke *Schistosoma mansoni*. PLoS Neglected Tropical Diseases 6, e1455. https://doi.org/10.1371/journal.pntd.0001455

Punta, M., Coggill, P.C., Eberhardt, R.Y., Mistry, J., Tate, J., Boursnell, C., Pang, N., Forslund, K., Ceric, G., Clements, J., Heger, A., Holm, L., Sonnhammer, E.L.L., Eddy, S.R., Bateman, A., Finn, R.D., 2012. The Pfam protein families database. Nucleic Acids Research 40, D290–D301. https://doi.org/10.1093/nar/gkr1065

Puthan Veetil, V., Fibriansah, G., Raj, H., Thunnissen, A.-M.W.H., Poelarends, G.J., 2012. Aspartase/Fumarase Superfamily: A Common Catalytic Strategy Involving General Base-Catalyzed Formation of a Highly Stabilized aci-Carboxylate Intermediate. Biochemistry 51, 4237–4243. https://doi.org/10.1021/bi300430j

Qiu, P., 2020. Embracing the dropouts in single-cell RNA-seq analysis. Nat Commun 11, 1169. https://doi.org/10.1038/s41467-020-14976-9

Quivoron, C., David, M., Straley, K., Travins, J., Kim, H., Chen, Y., Zhu, D., Saada, V., Bawa, O., Opolon, P., Polrot, M., Micol, J.-B., Willekens, C., Bernard, O., Yang, H., Agresta, S., de Botton, S., Yen, K., Penard-Lacronique, V., 2014. AG-221, an Oral, Selective, First-in-Class, Potent IDH2-R140Q Mutant Inhibitor, Induces Differentiation in a Xenotransplant Model. Blood 124, 3735. https://doi.org/10.1182/blood.V124.21.3735.3735

Ramaswamy, K., Kumar, P., He, Y.-X., 2000. A Role for Parasite-Induced PGE2 in IL-10-Mediated Host Immunoregulation by Skin Stage Schistosomula of *Schistosoma*

mansoni. The Journal of Immunology 165, 4567–4574. https://doi.org/10.4049/jimmunol.165.8.4567

Ramaswamy, K., Salafsky, B., Potluri, S., He, Y.X., Li, J.W., Shibuya, T., 1995. Secretion of an anti-inflammatory, immunomodulatory factor by Schistosomulae of *Schistosoma mansoni*. J Inflamm 46, 13–22.

Ramirez, B., Bickle, Q., Yousif, F., Fakorede, F., Mouries, M.-A., Nwaka, S., 2007. Schistosomes: challenges in compound screening. Expert Opin Drug Discov 2, S53-61. https://doi.org/10.1517/17460441.2.S1.S53

Rao, A.U., Carta, L.K., Lesuisse, E., Hamza, I., 2005. Lack of heme synthesis in a free-living eukaryote. Proc Natl Acad Sci U S A 102, 4270–4275. https://doi.org/10.1073/pnas.0500877102

Raushel, F.M., Thoden, J.B., Holden, H.M., 2003. Enzymes with Molecular Tunnels. Acc. Chem. Res. 36, 539–548. https://doi.org/10.1021/ar020047k

Rognstad, R., Katz, J., 1973. Malate exchange between the cytosol and mitochondria. Biochem J 132, 349–352.

Romano, A.H., Conway, T., 1996. Evolution of carbohydrate metabolic pathways. Research in Microbiology 147, 448–455. https://doi.org/10.1016/0923-2508(96)83998-2

Rose, I.A., 1998. How fumarase recycles after the malate --> fumarate reaction. Insights into the reaction mechanism. Biochemistry 37, 17651–17658. https://doi.org/10.1021/bi9821521

Rosencrans, W.M., Rajendran, M., Bezrukov, S.M., Rostovtseva, T.K., 2021. VDAC regulation of mitochondrial calcium flux: From channel biophysics to disease. Cell Calcium 94, 102356. https://doi.org/10.1016/j.ceca.2021.102356

Ross, M.F., Da Ros, T., Blaikie, F.H., Prime, T.A., Porteous, C.M., Severina, I.I., Skulachev, V.P., Kjaergaard, H.G., Smith, R.A.J., Murphy, M.P., 2006. Accumulation of lipophilic

dications by mitochondria and cells. Biochemical Journal 400, 199–208. https://doi.org/10.1042/BJ20060919

Ross, M.F., Kelso, G.F., Blaikie, F.H., James, A.M., Cochemé, H.M., Filipovska, A., Da Ros, T., Hurd, T.R., Smith, R.A.J., Murphy, M.P., 2005. Lipophilic triphenylphosphonium cations as tools in mitochondrial bioenergetics and free radical biology. Biochemistry (Moscow) 70, 222–230. https://doi.org/10.1007/s10541-005-0104-5

Ruecker, N., Jansen, R., Trujillo, C., Puckett, S., Jayachandran, P., Piroli, G.G., Frizzell, N., Molina, H., Rhee, K.Y., Ehrt, S., 2017. Fumarase Deficiency Causes Protein and Metabolite Succination and Intoxicates Mycobacterium tuberculosis. Cell Chemical Biology 24, 306–315. https://doi.org/10.1016/j.chembiol.2017.01.005

Ryder, B., Moore, F., Mitchell, A., Thompson, S., Christodoulou, J., Balasubramaniam, S., 2018. Fumarase Deficiency: A Safe and Potentially Disease Modifying Effect of High Fat/Low Carbohydrate Diet. JIMD Rep 40, 77–83. https://doi.org/10.1007/8904_2017_65

Safran, M., Kim, W.Y., O'Connell, F., Flippin, L., Günzler, V., Horner, J.W., DePinho, R.A., Kaelin, W.G., 2006. Mouse model for noninvasive imaging of HIF prolyl hydroxylase activity: Assessment of an oral agent that stimulates erythropoietin production. PNAS 103, 105–110. https://doi.org/10.1073/pnas.0509459103

Salter, J.P., Lim, K.-C., Hansell, E., Hsieh, I., McKerrow, J.H., 2000. Schistosome Invasion of Human Skin and Degradation of Dermal Elastin Are Mediated by a Single Serine Protease. J. Biol. Chem. 275, 38667–38673. https://doi.org/10.1074/jbc.M006997200

Samuelson, J.C., Quinn, J.J., Caulfield, J.P., 1984. Hatching, Chemokinesis, and Transformation of Miracidia of Schistosoma mansoni. The Journal of Parasitology 70, 321–331. https://doi.org/10.2307/3281558

Sancho, P., Galeano, E., Nieto, E., Delgado, M.D., García-Pérez, A.I., 2007. Dequalinium induces cell death in human leukemia cells by early mitochondrial alterations which enhance ROS production. Leukemia Research 31, 969–978. https://doi.org/10.1016/j.leukres.2006.11.018

Sanin, D.E., Mountford, A.P., 2015. Sm16, a major component of *Schistosoma mansoni* cercarial excretory/secretory products, prevents macrophage classical activation and delays antigen processing. Parasites Vectors 8, 1. https://doi.org/10.1186/s13071-014-0608-1

Sass, E., Blachinsky, E., Karniely, S., Pines, O., 2001. Mitochondrial and cytosolic isoforms of yeast fumarase are derivatives of a single translation product and have identical amino termini. J Biol Chem 276, 46111–46117. https://doi.org/10.1074/jbc.M106061200

Satija, R., Farrell, J.A., Gennert, D., Schier, A.F., Regev, A., 2015. Spatial reconstruction of single-cell gene expression data. Nat Biotechnol 33, 495–502. https://doi.org/10.1038/nbt.3192

Saunders, H.A., Calzadilla, P.I., Schwartz, J.-M., Johnson, G.N., 2022. Cytosolic fumarase acts as a metabolic fail-safe for both high and low temperature acclimation of Arabidopsis thaliana. J Exp Bot 73, 2112–2124. https://doi.org/10.1093/jxb/erab560

Saz, H.J., Hubbard, J.A., 1957. THE OXIDATIVE DECARBOXYLATION OF MALATE BY ASCARIS LUMBRICOIDES. Journal of Biological Chemistry 225, 921–933. https://doi.org/10.1016/S0021-9258(18)64890-2

Schüßler, P., Pötters, E., Winnen, R., Bottke, W., Kunz, W., 1995. An isoform of ferritin as a component of protein yolk platelets in *Schistosoma mansoni*. Molecular Reproduction and Development 41, 325–330. https://doi.org/10.1002/mrd.1080410307

Schwartz, C., Fallon, P.G., 2018. *Schistosoma* "Eggs-Iting" the Host: Granuloma Formation and Egg Excretion. Frontiers in Immunology 9, 2492. https://doi.org/10.3389/fimmu.2018.02492

Shen, J., Lai, D.-H., Wilson, R.A., Chen, Y.-F., Wang, L.-F., Yu, Z.-L., Li, M.-Y., He, P., Hide, G., Sun, X., Yang, T.-B., Wu, Z.-D., Ayala, F.J., Lun, Z.-R., 2017. Nitric oxide blocks the development of the human parasite *Schistosoma japonicum*. PNAS 114, 10214–10219. https://doi.org/10.1073/pnas.1708578114

Silas, Y., Singer, E., Das, K., Lehming, N., Pines, O., 2021. A combination of Class-I fumarases and metabolites (α-ketoglutarate and fumarate) signal the DNA damage response in Escherichia coli. Proc Natl Acad Sci U S A 118, e2026595118. https://doi.org/10.1073/pnas.2026595118

Silveira, G.O., Amaral, M.S., Coelho, H.S., Maciel, L.F., Pereira, A.S.A., Olberg, G.G.O., Miyasato, P.A., Nakano, E., Verjovski-Almeida, S., 2021. Assessment of reference genes at six different developmental stages of *Schistosoma mansoni* for quantitative RT-PCR. Sci Rep 11, 16816. https://doi.org/10.1038/s41598-021-96055-7

Skelly, P.J., Shoemaker, C.B., Skelly, P.J., Shoemaker, C.B., 1995. A molecular genetic study of the variations in metabolic function during schistosome development. Memórias do Instituto Oswaldo Cruz 90, 281–284. https://doi.org/10.1590/S0074-02761995000200027

Skelly, P.J., Stein, L.D., Shoemaker, C.B., 1993. Expression of Schistosoma mansoni genes involved in anaerobic and oxidative glucose metabolism during the cercaria to adult transformation. Molecular and Biochemical Parasitology 60, 93–104. https://doi.org/10.1016/0166-6851(93)90032-S

Small, I., Peeters, N., Legeai, F., Lurin, C., 2004. Predotar: A tool for rapidly screening proteomes for N-terminal targeting sequences. Proteomics 4, 1581–1590. https://doi.org/10.1002/pmic.200300776

Smith, J.C., 1990. Potential-sensitive molecular probes in membranes of bioenergetic relevance. Biochimica et Biophysica Acta (BBA) - Bioenergetics 1016, 1–28. https://doi.org/10.1016/0005-2728(90)90002-L

Stamler, J.S., Singel, D.J., Loscalzo, J., 1992. Biochemistry of nitric oxide and its redox-activated forms. Science 258, 1898–1902. https://doi.org/10.1126/science.1281928

Struck, T.H., Wey-Fabrizius, A.R., Golombek, A., Hering, L., Weigert, A., Bleidorn, C., Klebow, S., Iakovenko, N., Hausdorf, B., Petersen, M., Kück, P., Herlyn, H., Hankeln, T., 2014. Platyzoan Paraphyly Based on Phylogenomic Data Supports a Noncoelomate Ancestry of Spiralia. Mol Biol Evol 31, 1833–1849. https://doi.org/10.1093/molbev/msu143

Suzuki, T., Sato, M., Yoshida, T., Tuboi, S., 1989. Rat liver mitochondrial and cytosolic fumarases with identical amino acid sequences are encoded from a single gene. Journal of Biological Chemistry 264, 2581–2586. https://doi.org/10.1016/S0021-9258(19)81652-6

Tautz, D., 1992. Problems and paradigms: Redundancies, development and the flow of information. BioEssays 14, 263–266. https://doi.org/10.1002/bies.950140410

Ternette, N., Yang, M., Laroyia, M., Kitagawa, M., O'Flaherty, L., Wolhulter, K., Igarashi, K., Saito, K., Kato, K., Fischer, R., Berquand, A., Kessler, B.M., Lappin, T., Frizzell, N., Soga, T., Adam, J., Pollard, P.J., 2013. Inhibition of Mitochondrial Aconitase by Succination in Fumarate Hydratase Deficiency. Cell Rep 3, 689–700. https://doi.org/10.1016/j.celrep.2013.02.013

Thomas, P.D., Ebert, D., Muruganujan, A., Mushayahama, T., Albou, L.-P., Mi, H., 2022. PANTHER: Making genome-scale phylogenetics accessible to all. Protein Science 31, 8–22. https://doi.org/10.1002/pro.4218

Tielens, A.G.M., van Hellemond, J.J., 2005. Unusual Aspects of Metabolism in Flatworm Parasites, in: Maule, A.G., Marks, N.J. (Eds.), Parasitic Flatworms: Molecular Biology, Biochemistry, Immunology and Physiology. CABI, Wallingford, pp. 387–407. https://doi.org/10.1079/9780851990279.0327

Tolley, E., Craig, I., 1975. Presence of two forms of fumarase (fumarate hydratase E.C. 4.2.1.2) in mammalian cells: Immunological characterization and genetic analysis in somatic cell hybrids. Confirmation of the assignment of a gene necessary for the enzyme expression to human chromosome 1. Biochemical Genetics 13, 867–883. https://doi.org/10.1007/BF00484417

Tomlinson, I.P.M., Alam, N.A., Rowan, A.J., Barclay, E., Jaeger, E.E.M., Kelsell, D., Leigh, I., Gorman, P., Lamlum, H., Rahman, S., Roylance, R.R., Olpin, S., Bevan, S., Barker, K., Hearle, N., Houlston, R.S., Kiuru, M., Lehtonen, R., Karhu, A., Vilkki, S., Laiho, P., Eklund, C., Vierimaa, O., Aittomäki, K., Hietala, M., Sistonen, P., Paetau, A., Salovaara, R., Herva, R., Launonen, V., Aaltonen, L.A., The Multiple Leiomyoma Consortium, Group 1, Group 2, Group 3, 2002. Germline mutations in FH predispose to dominantly inherited uterine fibroids, skin leiomyomata and papillary renal cell cancer. Nat Genet 30, 406–410. https://doi.org/10.1038/ng849

Toro, J.R., Nickerson, M.L., Wei, M.-H., Warren, M.B., Glenn, G.M., Turner, M.L., Stewart, L., Duray, P., Tourre, O., Sharma, N., Choyke, P., Stratton, P., Merino, M., Walther, M.M., Linehan, W.M., Schmidt, L.S., Zbar, B., 2003. Mutations in the Fumarate Hydratase Gene Cause Hereditary Leiomyomatosis and Renal Cell Cancer in Families

in North America. The American Journal of Human Genetics 73, 95–106. https://doi.org/10.1086/376435

Trnka, J., Elkalaf, M., Anděl, M., 2015. Lipophilic Triphenylphosphonium Cations Inhibit Mitochondrial Electron Transport Chain and Induce Mitochondrial Proton Leak. PLOS ONE 10, e0121837. https://doi.org/10.1371/journal.pone.0121837

Tsai, I.J., Zarowiecki, M., Holroyd, N., Garciarrubio, A., Sanchez-Flores, A., Brooks, K.L., Tracey, A., Bobes, R.J., Fragoso, G., Sciutto, E., Aslett, M., Beasley, H., Bennett, H.M., Cai, J., Camicia, F., Clark, R., Cucher, M., De Silva, N., Day, T.A., Deplazes, P., Estrada, K., Fernández, C., Holland, P.W.H., Hou, J., Hu, S., Huckvale, T., Hung, S.S., Kamenetzky, L., Keane, J.A., Kiss, F., Koziol, U., Lambert, O., Liu, K., Luo, X., Luo, Y., Macchiaroli, N., Nichol, S., Paps, J., Parkinson, J., Pouchkina-Stantcheva, N., Riddiford, N., Rosenzvit, M., Salinas, G., Wasmuth, J.D., Zamanian, M., Zheng, Y., Cai, X., Soberón, X., Olson, P.D., Laclette, J.P., Brehm, K., Berriman, M., 2013. The genomes of four tapeworm species reveal adaptations to parasitism. Nature 496, 57–63. https://doi.org/10.1038/nature12031

Tse, C.H., Comer, J., Wang, Y., Chipot, C., 2018. Link between Membrane Composition and Permeability to Drugs. J. Chem. Theory Comput. 14, 2895–2909. https://doi.org/10.1021/acs.jctc.8b00272

Tzeng, S., McKerrow, J.H., Fukuyama, K., Jeong, K., Epstein, W.L., 1983. Degradation of Purified Skin Keratin by a Proteinase Secreted from *Schistosoma mansoni* Cercariae. The Journal of Parasitology 69, 992–994. https://doi.org/10.2307/3281072

Umeh, J.C., Amali, O., Umeh, E.U., 2004. The socio-economic effects of tropical diseases in Nigeria. Economics & Human Biology 2, 245–263. https://doi.org/10.1016/j.ehb.2004.04.001

Unger, R., Harel, D., Wherland, S., Sussman, J.L., 1989. A 3D building blocks approach to analyzing and predicting structure of proteins. Proteins: Structure, Function, and Bioinformatics 5, 355–373. https://doi.org/10.1002/prot.340050410

Utzinger, J., N'Goran, E.K., Caffrey, C.R., Keiser, J., 2011. From innovation to application: Social–ecological context, diagnostics, drugs and integrated control of schistosomiasis. Acta Tropica, The Diagnostics and Control of Neglected Tropical Helminth Diseases 120, S121–S137. https://doi.org/10.1016/j.actatropica.2010.08.020

Valentine, J.W., Collins, A.G., 2000. The significance of moulting in Ecdysozoan evolution. Evolution & Development 2, 152–156. https://doi.org/10.1046/j.1525-142x.2000.00043.x

Van Oordt, B.E.P., Tielens, A.G.M., Van Den Bergh, S.G., 1989. Aerobic to anaerobic transition in the carbohydrate metabolism of Schistosoma mansoni cercariae during transformation in vitro. Parasitology 98, 409. https://doi.org/10.1017/S0031182000061497

van Oordt, B.E.P., Tielens, A.G.M., van den Bergh, S.G., 1988. The energy metabolism of *Schistosoma mansoni* during its development in the hamster. Parasitol Res 75, 31–35. https://doi.org/10.1007/BF00931187

van Oordt, B.E.P., van den Heuvel, J.M., Tielens, A.G.M., van den Bergh, S.G., 1985. The energy production of the adult *Schistosoma mansoni* is for a large part aerobic. Molecular and Biochemical Parasitology 16, 117–126. https://doi.org/10.1016/0166-6851(85)90080-5

van Vugt-Lussenburg, B.M.A., van der Weel, L., Hagen, W.R., Hagedoorn, P.-L., 2013. Biochemical Similarities and Differences between the Catalytic [4Fe-4S] Cluster Containing Fumarases FumA and FumB from *Escherichia coli*. PLoS ONE 8, e55549. https://doi.org/10.1371/journal.pone.0055549

Vanden Bossche, H., 1990. Studies of the mode of action of anthelmintic drugs: tools to investigate the biochemical pecularities of helminths. Annales de Parasitologie Humaine et Comparée 65, 99–102. https://doi.org/10.1051/parasite/1990651099

Vandesompele, J., De Preter, K., Pattyn, F., Poppe, B., Van Roy, N., De Paepe, A., Speleman, F., 2002. Accurate normalization of real-time quantitative RT-PCR data by geometric averaging of multiple internal control genes. Genome Biology 3, research0034.1. https://doi.org/10.1186/gb-2002-3-7-research0034

Varga, Z.V., Ferdinandy, P., Liaudet, L., Pacher, P., 2015. Drug-induced mitochondrial dysfunction and cardiotoxicity. Am J Physiol Heart Circ Physiol 309, H1453–H1467. https://doi.org/10.1152/ajpheart.00554.2015

Voge, M., Seidel, J.S., 1972. Transformation In vitro of Miracidia of *Schistosoma mansoni* and *S. japonicum* into Young Sporocysts. The Journal of Parasitology 58, 699–704. https://doi.org/10.2307/3278294

Vos, T., Flaxman, A.D., Naghavi, M., Lozano, R., Michaud, C., Ezzati, M., Shibuya, K., Salomon, J.A., Abdalla, S., Aboyans, V., Abraham, jerry, Ackerman, I., Aggarwal, R., Ahn, S.Y., Ali, M.K., AlMazroa, M.A., Alvarado, M., Anderson, H.R., Anderson, L.M., Andrews, K.G., Atkinson, C., Baddour, L.M., Bahalim, A.N., Barker-Collo, S., Barrero, L.H., Bartels, D.H., Basáñez, M.-G., Baxter, A., Bell, M.L., Benjamin, E.J., Bennett, D., Bernabé, E., Bhalla, K., Bhandari, B., Bikbov, B., Abdulhak, A.B., Birbeck, G., Black, J.A., Blencowe, H., Blore, J.D., Blyth, F., Bolliger, I., Bonaventure, A., Boufous, S., Bourne, R., Boussinesq, M., Braithwaite, T., Brayne, C., Bridgett, L., Brooker, S., Brooks, P., Brugha, T.S., Bryan-Hancock, C., Bucello, C., Buchbinder, R., Buckle, G., Budke, C.M., Burch, M., Burney, P., Burstein, R., Calabria, B., Campbell, B., Canter, C.E., Carabin, H., Carapetis, J., Carmona, L., Cella, C., Charlson, F., Chen, H., Cheng, A.T.-A., Chou, D., Chugh, S.S., Coffeng, L.E., Colan, S.D., Colquhoun, S.,

Colson, K.E., Condon, J., Connor, M.D., Cooper, L.T., Corriere, M., Cortinovis, M., de Vaccaro, K.C., Couser, W., Cowie, B.C., Criqui, M.H., Cross, M., Dabhadkar, K.C., Dahiya, M., Dahodwala, N., Damsere-Derry, J., Danaei, G., Davis, A., De Leo, D., Degenhardt, L., Dellavalle, R., Delossantos, A., Denenberg, J., Derrett, S., Jarlais, D.Cd., Dharmaratne, S.D., Dherani, M., Diaz-Torne, C., Dolk, H., Dorsey, E.R., Driscoll, T., Duber, H., Ebel, B., Edmond, K., Elbaz, A., Ali, S.E., Erskine, H., Erwin, P.J., Espindola, P., Ewoigbokhan, S.E., Farzadfar, F., Feigin, V., Felson, D.T., Ferrari, A., Ferri, C.P., Fèvre, E.M., Finucane, M.M., Flaxman, S., Flood, L., Foreman, K., Forouzanfar, M.H., Fowkes, F.G.R., Franklin, R., Fransen, M., Freeman, M.K., Gabbe, B.J., Gabriel, S.E., Gakidou, E., Ganatra, H.A., Garcia, B., Gaspari, F., Gillum, R.F., Gmel, G., Gosselin, R., Grainger, R., Groeger, J., Guillemin, F., Gunnell, D., Gupta, R., Haagsma, J., Hagan, H., Halasa, Y.A., Hall, W., Haring, D., Haro, J.M., Harrison, J.E., Havmoeller, R., Hay, R.J., Higashi, H., Hill, C., Hoen, B., Hoffman, H., Hotez, P.J., Hoy, D., Huang, J.J., Ibeanusi, S.E., Jacobsen, K.H., James, S.L., Jarvis, D., Jasrasaria, R., Jayaraman, S., Johns, N., Jonas, J.B., Karthikeyan, G., Kassebaum, N., Kawakami, N., Keren, A., Khoo, J.-P., King, C.H., Knowlton, L.M., Kobusingye, O., Koranteng, A., Krishnamurthi, R., Lalloo, R., Laslett, L.L., Lathlean, T., Leasher, J.L., Lee, Y.Y., Leigh, J., Lim, S.S., Limb, E., Lin, J.K., Lipnick, M., Lipshultz, S.E., Liu, W., Loane, M., Ohno, S.L., Lyons, R., Ma, J., Mabweijano, J., MacIntyre, M.F., Malekzadeh, R., Mallinger, L., Manivannan, S., Marcenes, W., March, L., Margolis, D.J., Marks, G.B., Marks, R., Matsumori, A., Matzopoulos, R., Mayosi, B.M., McAnulty, J.H., McDermott, M.M., McGill, N., McGrath, J., Medina-Mora, M.E., Meltzer, M., Memish, Z.A., Mensah, G.A., Merriman, T.R., Meyer, A.-C., Miglioli, V., Miller, M., Miller, T.R., Mitchell, P.B., Mocumbi, A.O., Moffitt, T.E., Mokdad, A.A., Monasta, L., Montico, M., Moradi-Lakeh, M., Moran, A., Morawska, L., Mori, R.,

Murdoch, M.E., Mwaniki, M.K., Naidoo, K., Nair, M.N., Naldi, L., Narayan, K.V., Nelson, P.K., Nelson, R.G., Nevitt, M.C., Newton, C.R., Nolte, S., Norman, P., Norman, R., O'Donnell, M., O'Hanlon, S., Olives, C., Omer, S.B., Ortblad, K., Osborne, R., Ozgediz, D., Page, A., Pahari, B., Pandian, J.D., Rivero, A.P., Patten, S.B., Pearce, N., Padilla, R.P., Perez-Ruiz, F., Perico, N., Pesudovs, K., Phillips, D., Phillips, M.R., Pierce, K., Pion, S., Polanczyk, G.V., Polinder, S., Pope, C.A., Popova, S., Porrini, E., Pourmalek, F., Prince, M., Pullan, R.L., Ramaiah, K.D., Ranganathan, D., Razavi, H., Regan, M., Rehm, J.T., Rein, D.B., Remuzzi, G., Richardson, K., Rivara, F.P., Roberts, T., Robinson, C., De Leòn, F.R., Ronfani, L., Room, R., Rosenfeld, L.C., Rushton, L., Sacco, R.L., Saha, S., Sampson, U., Sanchez-Riera, L., Sanman, E., Schwebel, D.C., Scott, J.G., Segui-Gomez, M., Shahraz, S., Shepard, D.S., Shin, H., Shivakoti, R., Silberberg, D., Singh, D., Singh, G.M., Singh, J.A., Singleton, J., Sleet, D.A., Sliwa, K., Smith, E., Smith, J.L., Stapelberg, N.J.C., Steer, A., Steiner, T., Stolk, W.A., Stovner, L.J., Sudfeld, C., Syed, S., Tamburlini, G., Tavakkoli, M., Taylor, H.R., Taylor, J.A., Taylor, W.J., Thomas, B., Thomson, W.M., Thurston, G.D., Tleyjeh, I.M., Tonelli, M., Towbin, J.A., Truelsen, T., Tsilimbaris, M.K., Ubeda, C., Undurraga, E.A., van der Werf, M.J., va nOs, J., Vavilala, M.S., Venketasubramanian, N., Wang, M., Wang, W., Watt, K., Weatherall, D.J., Weinstock, M.A., Weintraub, R., Weisskopf, M.G., Weissman, M.M., White, R.A., Whiteford, H., Wiersma, S.T., Wilkinson, J.D., Williams, H.C., Williams, S.R.M., Witt, E., Wolfe, F., Woolf, A.D., Wulf, S., Yeh, P.-H., Zaidi, A.K.M., Zheng, Z.-J., Zonies, D., Lopez, A.D., Murray, C.J.L., 2012. Years lived with disability (YLDs) for 1160 sequelae of 289 diseases and injuries 1990-2010: a systematic analysis for the Global Burden of Disease Study 2010. Lancet 380, 2163–2196. https://doi.org/10.1016/S0140-6736(12)61729-2

Wang, B., Collins, J.J., III, Newmark, P.A., 2013. Functional genomic characterization of neoblast-like stem cells in larval *Schistosoma mansoni*. eLife 2, e00768. https://doi.org/10.7554/eLife.00768

Wang, J., Chen, R., Iii, J.J.C., 2019. Systematically improved in vitro culture conditions reveal new insights into the reproductive biology of the human parasite *Schistosoma mansoni*. PLOS Biology 17, e3000254. https://doi.org/10.1371/journal.pbio.3000254

Wang, J., Pantopoulos, K., 2011. Regulation of cellular iron metabolism. Biochem J 434, 365–381. https://doi.org/10.1042/BJ20101825

Wang, J., Paz, C., Padalino, G., Coghlan, A., Lu, Z., Gradinaru, I., Collins, J.N.R., Berriman, M., Hoffman, K.F., Collins, J., 2020. Large-scale RNAi screening uncovers new therapeutic targets in the human parasite *Schistosoma mansoni*. bioRxiv 2020.02.05.935833. https://doi.org/10.1101/2020.02.05.935833

Wang, S., Zhu, X., Cai, X., 2017. Gene Duplication Analysis Reveals No Ancient Whole Genome Duplication but Extensive Small-Scale Duplications during Genome Evolution and Adaptation of *Schistosoma mansoni*. Front Cell Infect Microbiol 7, 412. https://doi.org/10.3389/fcimb.2017.00412

Waterhouse, A.M., Procter, J.B., Martin, D.M.A., Clamp, M., Barton, G.J., 2009. Jalview Version 2—a multiple sequence alignment editor and analysis workbench. Bioinformatics 25, 1189–1191. https://doi.org/10.1093/bioinformatics/btp033

Wendt, G., Zhao, L., Chen, R., Liu, C., O'Donoghue, A.J., Caffrey, C.R., Collins, J.J., 2020. A single-cell RNAseq atlas of the pathogenic stage of *Schistosoma mansoni* identifies a key regulator of blood feeding. bioRxiv 2020.02.03.932004. https://doi.org/10.1101/2020.02.03.932004

Wendt, G.R., Reese, M.L., Collins, J.J., 2021. SchistoCyte Atlas: A Single-Cell Transcriptome Resource for Adult Schistosomes. Trends in Parasitology 37, 585–587. https://doi.org/10.1016/j.pt.2021.04.010

WHO, 2016. Schistosomiasis: number of people treated worldwide in 2014. Wkly Epidemiol Rec 91, 53–60.

Wiederstein, M., Sippl, M.J., 2007. ProSA-web: interactive web service for the recognition of errors in three-dimensional structures of proteins. Nucleic Acids Research 35, W407–W410. https://doi.org/10.1093/nar/gkm290

Wilson, R.A., Draskau, T., Miller, P., Lawson, J.R., 1978. Schistosoma mansoni: the activity and development of the schistosomulum during migration from the skin to the hepatic portal system. Parasitology 77, 57–73. https://doi.org/10.1017/S0031182000048721

Wilson, S., Vennervald, B.J., Dunne, D.W., 2011. Chronic Hepatosplenomegaly in African School Children: A Common but Neglected Morbidity Associated with Schistosomiasis and Malaria. PLOS Neglected Tropical Diseases 5, e1149. https://doi.org/10.1371/journal.pntd.0001149

WoldeMussie, E., Bennett, J.L., 1982. Plasma Spectrometric Analysis for Na, K, Ca, Mg, Fe, and Cu in *Schistosoma mansoni* and *S. japonicum*. The Journal of Parasitology 68, 48–52. https://doi.org/10.2307/3281324

Wolmarans, C.T., Kock, K.N. de, Strauss, H.D., Bornman, M., 2002. Daily emergence of *Schistosoma mansoni* and *S. haematobium* cercariae from naturally infected snails under field conditions. Journal of Helminthology 76, 273–277. https://doi.org/10.1079/JOH2002122

Woods, S.A., Miles, J.S., Roberts, R.E., Guest, J.R., 1986. Structural and functional relationships between fumarase and aspartase. Nucleotide sequences of the fumarase

(fumC) and aspartase (aspA) genes of Escherichia coli K12. Biochemical Journal 237, 547–557. https://doi.org/10.1042/bj2370547

Woods, S.A., Schwartzbach, S.D., Guest, J.R., 1988. Two biochemically distinct classes of fumarase in Escherichia coli. Biochimica et Biophysica Acta (BBA) - Protein Structure and Molecular Enzymology 954, 14–26. https://doi.org/10.1016/0167-4838(88)90050-7

Wu, M., Tzagoloff, A., 1987. Mitochondrial and cytoplasmic fumarases in *Saccharomyces cerevisiae* are encoded by a single nuclear gene FUM1. J. Biol. Chem. 262, 12275–12282.

Xiao, M., Yang, H., Xu, W., Ma, S., Lin, H., Zhu, H., Liu, L., Liu, Y., Yang, C., Xu, Y., Zhao, S., Ye, D., Xiong, Y., Guan, K.-L., 2012. Inhibition of α-KG-dependent histone and DNA demethylases by fumarate and succinate that are accumulated in mutations of FH and SDH tumor suppressors. Genes Dev. 26, 1326–1338. https://doi.org/10.1101/gad.191056.112

Yamada, Y., Akita, H., Kamiya, H., Kogure, K., Yamamoto, T., Shinohara, Y., Yamashita, K., Kobayashi, H., Kikuchi, H., Harashima, H., 2008. MITO-Porter: A liposome-based carrier system for delivery of macromolecules into mitochondria via membrane fusion. Biochimica et Biophysica Acta (BBA) - Biomembranes 1778, 423–432. https://doi.org/10.1016/j.bbamem.2007.11.002

Yamada, Y., Harashima, H., 2012. Delivery of bioactive molecules to the mitochondrial genome using a membrane-fusing, liposome-based carrier, DF-MITO-Porter. Biomaterials 33, 1589–1595. https://doi.org/10.1016/j.biomaterials.2011.10.082

Yang, N.J., Hinner, M.J., 2015. Getting Across the Cell Membrane: An Overview for Small Molecules, Peptides, and Proteins. Methods Mol Biol 1266, 29–53. https://doi.org/10.1007/978-1-4939-2272-7_3

Yen, K., Travins, J., Wang, F., David, M.D., Artin, E., Straley, K., Padyana, A., Gross, S., DeLaBarre, B., Tobin, E., Chen, Y., Nagaraja, R., Choe, S., Jin, L., Konteatis, Z., Cianchetta, G., Saunders, J.O., Salituro, F.G., Quivoron, C., Opolon, P., Bawa, O., Saada, V., Paci, A., Broutin, S., Bernard, O.A., de Botton, S., Marteyn, B.S., Pilichowska, M., Xu, Y., Fang, C., Jiang, F., Wei, W., Jin, S., Silverman, L., Liu, W., Yang, H., Dang, L., Dorsch, M., Penard-Lacronique, V., Biller, S.A., Su, S.-S.M., 2017. AG-221, a First-in-Class Therapy Targeting Acute Myeloid Leukemia Harboring Oncogenic IDH2 Mutations. Cancer Discovery 7, 478–493. https://doi.org/10.1158/2159-8290.CD-16-1034

Yip, J., Wang, S., Tan, J., Lim, T.K., Lin, Q., Yu, Z., Karmon, O., Pines, O., Lehming, N., 2021. Fumarase affects the deoxyribonucleic acid damage response by protecting the mitochondrial desulfurase Nfs1p from modification and inactivation. iScience 24, 103354. https://doi.org/10.1016/j.isci.2021.103354

Yogev, O., Naamati, A., Pines, O., 2011. Fumarase: a paradigm of dual targeting and dual localized functions: Fumarase: dual targeting and dual localized functions. FEBS Journal 278, 4230–4242. https://doi.org/10.1111/j.1742-4658.2011.08359.x

Yogev, O., Pines, O., 2011. Dual targeting of mitochondrial proteins: Mechanism, regulation and function. Biochimica et Biophysica Acta (BBA) - Biomembranes, Including the Special Section: Protein translocation across or insertion into membranes 1808, 1012–1020. https://doi.org/10.1016/j.bbamem.2010.07.004

Yogev, Ohad, Yogev, Orli, Singer, E., Shaulian, E., Goldberg, M., Fox, T.D., Pines, O., 2010. Fumarase: A Mitochondrial Metabolic Enzyme and a Cytosolic/Nuclear Component of the DNA Damage Response. PLOS Biology 8, e1000328. https://doi.org/10.1371/journal.pbio.1000328

Zecchini, V., Paupe, V., Herranz-Montoya, I., Janssen, J., Wortel, I.M.N., Morris, J.L., Ferguson, A., Chowdury, S.R., Segarra-Mondejar, M., Costa, A.S.H., Pereira, G.C., Tronci, L., Young, T., Nikitopoulou, E., Yang, M., Bihary, D., Caicci, F., Nagashima, S., Speed, A., Bokea, K., Baig, Z., Samarajiwa, S., Tran, M., Mitchell, T., Johnson, M., Prudent, J., Frezza, C., 2023. Fumarate induces vesicular release of mtDNA to drive innate immunity. Nature 615, 499–506. https://doi.org/10.1038/s41586-023-05770-w

Zhang, C., Cheng, Y., Liu, D., Liu, M., Cui, H., Zhang, B., Mei, Q., Zhou, S., 2019. Mitochondria-targeted cyclosporin A delivery system to treat myocardial ischemia reperfusion injury of rats. J Nanobiotechnol 17, 18. https://doi.org/10.1186/s12951-019-0451-9

Zhao, K., Zhao, G.-M., Wu, D., Soong, Y., Birk, A.V., Schiller, P.W., Szeto, H.H., 2004. Cell-permeable Peptide Antioxidants Targeted to Inner Mitochondrial Membrane inhibit Mitochondrial Swelling, Oxidative Cell Death, and Reperfusion Injury *. Journal of Biological Chemistry 279, 34682–34690. https://doi.org/10.1074/jbc.M402999200

Zhao, S., Fung-Leung, W.-P., Bittner, A., Ngo, K., Liu, X., 2014. Comparison of RNA-Seq and microarray in transcriptome profiling of activated T cells. PLoS One 9, e78644. https://doi.org/10.1371/journal.pone.0078644

Zinovkin, R.A., Zamyatnin, A.A., 2019. Mitochondria-Targeted Drugs. Curr Mol Pharmacol 12, 202–214. https://doi.org/10.2174/1874467212666181127151059